

RILEM State-of-the-Art Reports

Lars-Olof Nilsson *Editor*

# Methods of Measuring Moisture in Building Materials and Structures

State-of-the-Art Report of the RILEM  
Technical Committee 248-MMB



 Springer

The Springer logo features a white chess knight piece on a blue square background, positioned to the left of the word "Springer" in a white, serif font.

# **RILEM State-of-the-Art Reports**

# RILEM STATE-OF-THE-ART REPORTS

Volume 26

---

RILEM, The International Union of Laboratories and Experts in Construction Materials, Systems and Structures, founded in 1947, is a non-governmental scientific association whose goal is to contribute to progress in the construction sciences, techniques and industries, essentially by means of the communication it fosters between research and practice. RILEM's focus is on construction materials and their use in building and civil engineering structures, covering all phases of the building process from manufacture to use and recycling of materials. More information on RILEM and its previous publications can be found on [www.RILEM.net](http://www.RILEM.net).

The RILEM State-of-the-Art Reports (STAR) are produced by the Technical Committees. They represent one of the most important outputs that RILEM generates—high level scientific and engineering reports that provide cutting edge knowledge in a given field. The work of the TCs is one of RILEM's key functions.

Members of a TC are experts in their field and give their time freely to share their expertise. As a result, the broader scientific community benefits greatly from RILEM's activities.

RILEM's stated objective is to disseminate this information as widely as possible to the scientific community. RILEM therefore considers the STAR reports of its TCs as of highest importance, and encourages their publication whenever possible.

The information in this and similar reports is mostly pre-normative in the sense that it provides the underlying scientific fundamentals on which standards and codes of practice are based. Without such a solid scientific basis, construction practice will be less than efficient or economical.

It is RILEM's hope that this information will be of wide use to the scientific community.



More information about this series at <http://www.springer.com/series/8780>

Lars-Olof Nilsson  
Editor

# Methods of Measuring Moisture in Building Materials and Structures

State-of-the-Art Report of the RILEM  
Technical Committee 248-MMB



 Springer

The Springer logo, which consists of a stylized chess knight (horse) facing left, positioned above the word 'Springer' in a serif font.

*Editor*  
Lars-Olof Nilsson  
Division of Building Materials  
Lund University  
Lund  
Sweden

ISSN 2213-204X                      ISSN 2213-2031 (electronic)  
RILEM State-of-the-Art Reports  
ISBN 978-3-319-74230-4              ISBN 978-3-319-74231-1 (eBook)  
<https://doi.org/10.1007/978-3-319-74231-1>

Library of Congress Control Number: 2017963841

© RILEM 2018

No part of this work may be reproduced, stored in a retrieval system, or transmitted in any form or by any means, electronic, mechanical, photocopying, microfilming, recording or otherwise, without written permission from the Publisher, with the exception of any material supplied specifically for the purpose of being entered and executed on a computer system, for exclusive use by the purchaser of the work. Permission for use must always be obtained from the owner of the copyright: RILEM.

Printed on acid-free paper

This Springer imprint is published by the registered company Springer International Publishing AG  
part of Springer Nature  
The registered company address is: Gewerbestrasse 11, 6330 Cham, Switzerland

# Preface

Properties and performance of building materials and structures are to a large extent influenced by the moisture conditions in the materials. Obvious examples are heat conductivity, shrinkage and creep, transport properties, most types of deterioration, discolouration, etc. For research and applications, the moisture conditions must be quantified, by measurements in the laboratory or under field conditions. The methods being used today are very different in different countries, very different for different materials and very different for different applications. Also, researchers within the same topic use different methods. No consensus whatsoever does exist. For the construction industry, it is important to be able to quantify the moisture conditions in an accurate way in various applications.

RILEM TC 248-MMB was established in 2012 with the main aim to improve and distribute knowledge related to moisture measurement in construction materials in various scientific and industrial applications. The scope of the TC was concentrated on publishing a state-of-the-art report.

The committee came together for the first time in Lund, Sweden, in July 2012 with subsequent meetings held in Cape Town, Dresden, Paris, Alicante, Minho, Bordeaux, Bologna, Munich, Lille and Kongens Lyngby. A small Round Robin Test series on specimens for calibrating moisture measurements was organized. The final TC-meeting in Kongens Lyngby, Denmark, was accompanied by a two-week PhD course on Moisture in Materials and Structures and a three-day conference on Moisture in Materials and Structures, which was attended by delegates from around the world.

The main outcome of RILEM TC 248-MMB is this state-of-the-art report, which is divided into two parts, A Principles and B Applications, with altogether 28 chapters on various moisture measuring principles and a number of applications. Each chapter had a main author. All TC members who made contributions to a chapter were made co-authors of that chapter, in alphabetic order. The final structure and layout of the chapters were discussed and approved in the last meeting and via email correspondence.

The editor thanks all TC members who have actively contributed to this report through meeting attendance, direct input to the various chapters and participating in the discussions.

Lund, Sweden

Lars-Olof Nilsson

# RILEM Publications

The following list is presenting the global offer of RILEM Publications, sorted by series. Each publication is available in printed version and/or in online version.

## RILEM PROCEEDINGS (PRO)

**PRO 1:** Durability of High Performance Concrete (ISBN: 2-912143-03-9; e-ISBN: 2-351580-12-5; e-ISBN: 2351580125); *Ed. H. Sommer*

**PRO 2:** Chloride Penetration into Concrete (ISBN: 2-912143-00-04; e-ISBN: 2912143454); *Eds. L.-O. Nilsson and J.-P. Ollivier*

**PRO 3:** Evaluation and Strengthening of Existing Masonry Structures (ISBN: 2-912143-02-0; e-ISBN: 2351580141); *Eds. L. Binda and C. Modena*

**PRO 4:** Concrete: From Material to Structure (ISBN: 2-912143-04-7; e-ISBN: 2351580206); *Eds. J.-P. Bournazel and Y. Malier*

**PRO 5:** The Role of Admixtures in High Performance Concrete (ISBN: 2-912143-05-5; e-ISBN: 2351580214); *Eds. J. G. Cabrera and R. Rivera-Villarreal*

**PRO 6:** High Performance Fiber Reinforced Cement Composites—HPFRCC 3 (ISBN: 2-912143-06-3; e-ISBN: 2351580222); *Eds. H. W. Reinhardt and A. E. Naaman*

**PRO 7:** 1st International RILEM Symposium on Self-Compacting Concrete (ISBN: 2-912143-09-8; e-ISBN: 2912143721); *Eds. Å. Skarendahl and Ö. Petersson*

**PRO 8:** International RILEM Symposium on Timber Engineering (ISBN: 2-912143-10-1; e-ISBN: 2351580230); *Ed. L. Boström*

**PRO 9:** 2nd International RILEM Symposium on Adhesion between Polymers and Concrete ISAP '99 (ISBN: 2-912143-11-X; e-ISBN: 2351580249); *Eds. Y. Ohama and M. Puterman*

**PRO 10:** 3rd International RILEM Symposium on Durability of Building and Construction Sealants (ISBN: 2-912143-13-6; e-ISBN: 2351580257); *Ed. A. T. Wolf*

**PRO 11:** 4th International RILEM Conference on Reflective Cracking in Pavements (ISBN: 2-912143-14-4; e-ISBN: 2351580265); *Eds. A. O. Abd El Halim, D. A. Taylor and El H. H. Mohamed*

**PRO 12:** International RILEM Workshop on Historic Mortars: Characteristics and Tests (ISBN: 2-912143-15-2; e-ISBN: 2351580273); *Eds. P. Bartos, C. Groot and J. J. Hughes*

**PRO 13:** 2nd International RILEM Symposium on Hydration and Setting (ISBN: 2-912143-16-0; e-ISBN: 2351580281); *Ed. A. Nonat*

**PRO 14:** Integrated Life-Cycle Design of Materials and Structures—ILCDES 2000 (ISBN: 951-758-408-3; e-ISBN: 235158029X); (ISSN: 0356-9403); *Ed. S. Sarja*

**PRO 15:** Fifth RILEM Symposium on Fibre-Reinforced Concretes (FRC)—BEFIB'2000 (ISBN: 2-912143-18-7; e-ISBN: 291214373X); *Eds. P. Rossi and G. Chanvillard*

**PRO 16:** Life Prediction and Management of Concrete Structures (ISBN: 2-912143-19-5; e-ISBN: 2351580303); *Ed. D. Naus*

**PRO 17:** Shrinkage of Concrete—Shrinkage 2000 (ISBN: 2-912143-20-9; e-ISBN: 2351580311); *Eds. V. Baroghel-Bouny and P.-C. Aïtcin*

**PRO 18:** Measurement and Interpretation of the On-Site Corrosion Rate (ISBN: 2-912143-21-7; e-ISBN: 235158032X); *Eds. C. Andrade, C. Alonso, J. Fullea, J. Polimon and J. Rodriguez*

**PRO 19:** Testing and Modelling the Chloride Ingress into Concrete (ISBN: 2-912143-22-5; e-ISBN: 2351580338); *Eds. C. Andrade and J. Kropp*

**PRO 20:** 1st International RILEM Workshop on Microbial Impacts on Building Materials (CD 02) (e-ISBN 978-2-35158-013-4); *Ed. M. Ribas Silva*

**PRO 21:** International RILEM Symposium on Connections between Steel and Concrete (ISBN: 2-912143-25-X; e-ISBN: 2351580346); *Ed. R. Eligehausen*

**PRO 22:** International RILEM Symposium on Joints in Timber Structures (ISBN: 2-912143-28-4; e-ISBN: 2351580354); *Eds. S. Aicher and H.-W. Reinhardt*

**PRO 23:** International RILEM Conference on Early Age Cracking in Cementitious Systems (ISBN: 2-912143-29-2; e-ISBN: 2351580362); *Eds. K. Kovler and A. Bentur*

**PRO 24:** 2nd International RILEM Workshop on Frost Resistance of Concrete (ISBN: 2-912143-30-6; e-ISBN: 2351580370); *Eds. M. J. Setzer, R. Auberg and H.-J. Keck*

**PRO 25:** International RILEM Workshop on Frost Damage in Concrete (ISBN: 2-912143-31-4; e-ISBN: 2351580389); *Eds. D. J. Janssen, M. J. Setzer and M. B. Snyder*

**PRO 26:** International RILEM Workshop on On-Site Control and Evaluation of Masonry Structures (ISBN: 2-912143-34-9; e-ISBN: 2351580141); *Eds. L. Binda and R. C. de Vekey*

**PRO 27:** International RILEM Symposium on Building Joint Sealants (CD03; e-ISBN: 235158015X); *Ed. A. T. Wolf*

**PRO 28:** 6th International RILEM Symposium on Performance Testing and Evaluation of Bituminous Materials—PTEBM'03 (ISBN: 2-912143-35-7; e-ISBN: 978-2-912143-77-8); *Ed. M. N. Partl*

**PRO 29:** 2nd International RILEM Workshop on Life Prediction and Ageing Management of Concrete Structures (ISBN: 2-912143-36-5; e-ISBN: 2912143780); *Ed. D. J. Naus*

**PRO 30:** 4th International RILEM Workshop on High Performance Fiber Reinforced Cement Composites—HPFRCC 4 (ISBN: 2-912143-37-3; e-ISBN: 2912143799); *Eds. A. E. Naaman and H. W. Reinhardt*

**PRO 31:** International RILEM Workshop on Test and Design Methods for Steel Fibre Reinforced Concrete: Background and Experiences (ISBN: 2-912143-38-1; e-ISBN: 2351580168); *Eds. B. Schnütgen and L. Vandewalle*

**PRO 32:** International Conference on Advances in Concrete and Structures 2 vol. (ISBN (set): 2-912143-41-1; e-ISBN: 2351580176); *Eds. Ying-shu Yuan, Surendra P. Shah and Heng-lin Lü*

**PRO 33:** 3rd International Symposium on Self-Compacting Concrete (ISBN: 2-912143-42-X; e-ISBN: 2912143713); *Eds. Ó. Wallevik and I. Nielsson*

**PRO 34:** International RILEM Conference on Microbial Impact on Building Materials (ISBN: 2-912143-43-8; e-ISBN: 2351580184); *Ed. M. Ribas Silva*

**PRO 35:** International RILEM TC 186-ISA on Internal Sulfate Attack and Delayed Ettringite Formation (ISBN: 2-912143-44-6; e-ISBN: 2912143802); *Eds. K. Scrivener and J. Skalny*

**PRO 36:** International RILEM Symposium on Concrete Science and Engineering—A Tribute to Arnon Bentur (ISBN: 2-912143-46-2; e-ISBN: 2912143586); *Eds. K. Kovler, J. Marchand, S. Mindess and J. Weiss*

**PRO 37:** 5th International RILEM Conference on Cracking in Pavements—Mitigation, Risk Assessment and Prevention (ISBN: 2-912143-47-0; e-ISBN: 2912143764); *Eds. C. Petit, I. Al-Qadi and A. Millien*

**PRO 38:** 3rd International RILEM Workshop on Testing and Modelling the Chloride Ingress into Concrete (ISBN: 2-912143-48-9; e-ISBN: 2912143578); *Eds. C. Andrade and J. Kropp*

**PRO 39:** 6th International RILEM Symposium on Fibre-Reinforced Concretes—BEFIB 2004 (ISBN: 2-912143-51-9; e-ISBN: 2912143748); *Eds. M. Di Prisco, R. Felicetti and G. A. Plizzari*

**PRO 40:** International RILEM Conference on the Use of Recycled Materials in Buildings and Structures (ISBN: 2-912143-52-7; e-ISBN: 2912143756); *Eds. E. Vázquez, Ch. F. Hendriks and G. M. T. Janssen*

**PRO 41:** RILEM International Symposium on Environment-Conscious Materials and Systems for Sustainable Development (ISBN: 2-912143-55-1; e-ISBN: 2912143640); *Eds. N. Kashino and Y. Ohama*

**PRO 42:** SCC'2005—China: 1st International Symposium on Design, Performance and Use of Self-Consolidating Concrete (ISBN: 2-912143-61-6; e-ISBN: 2912143624); *Eds. Zhiwu Yu, Caijun Shi, Kamal Henri Khayat and Youjun Xie*

**PRO 43:** International RILEM Workshop on Bonded Concrete Overlays (e-ISBN: 2-912143-83-7); *Eds. J. L. Granju and J. Silfwerbrand*

**PRO 44:** 2nd International RILEM Workshop on Microbial Impacts on Building Materials (CD11) (e-ISBN: 2-912143-84-5); *Ed. M. Ribas Silva*

**PRO 45:** 2nd International Symposium on Nanotechnology in Construction, Bilbao (ISBN: 2-912143-87-X; e-ISBN: 2912143888); *Eds. Peter J. M. Bartos, Yolanda de Miguel and Antonio Porro*

**PRO 46:** ConcreteLife'06—International RILEM-JCI Seminar on Concrete Durability and Service Life Planning: Curing, Crack Control, Performance in Harsh Environments (ISBN: 2-912143-89-6; e-ISBN: 291214390X); *Ed. K. Kovler*

**PRO 47:** International RILEM Workshop on Performance Based Evaluation and Indicators for Concrete Durability (ISBN: 978-2-912143-95-2; e-ISBN: 9782912143969); *Eds. V. Baroghel-Bouny, C. Andrade, R. Torrent and K. Scrivener*

**PRO 48:** 1st International RILEM Symposium on Advances in Concrete through Science and Engineering (e-ISBN: 2-912143-92-6); *Eds. J. Weiss, K. Kovler, J. Marchand, and S. Mindess*

**PRO 49:** International RILEM Workshop on High Performance Fiber Reinforced Cementitious Composites in Structural Applications (ISBN: 2-912143-93-4; e-ISBN: 2912143942); *Eds. G. Fischer and V. C. Li*

**PRO 50:** 1st International RILEM Symposium on Textile Reinforced Concrete (ISBN: 2-912143-97-7; e-ISBN: 2351580087); *Eds. Josef Hegger, Wolfgang Brameshuber and Norbert Will*

**PRO 51:** 2nd International Symposium on Advances in Concrete through Science and Engineering (ISBN: 2-35158-003-6; e-ISBN: 2-35158-002-8); *Eds. J. Marchand, B. Bissonnette, R. Gagné, M. Jolin and F. Paradis*

**PRO 52:** Volume Changes of Hardening Concrete: Testing and Mitigation (ISBN: 2-35158-004-4; e-ISBN: 2-35158-005-2); *Eds. O. M. Jensen, P. Lura and K. Kovler*

**PRO 53:** High Performance Fiber Reinforced Cement Composites—HPFRCC5 (ISBN: 978-2-35158-046-2; e-ISBN: 978-2-35158-089-9); *Eds. H. W. Reinhardt and A. E. Naaman*

**PRO 54:** 5th International RILEM Symposium on Self-Compacting Concrete (ISBN: 978-2-35158-047-9; e-ISBN: 978-2-35158-088-2); *Eds. G. De Schutter and V. Boel*

**PRO 55:** International RILEM Symposium Photocatalysis, Environment and Construction Materials (ISBN: 978-2-35158-056-1; e-ISBN: 978-2-35158-057-8); *Eds. P. Baglioni and L. Cassar*

**PRO 56:** International RILEM Workshop on Integral Service Life Modelling of Concrete Structures (ISBN 978-2-35158-058-5; e-ISBN: 978-2-35158-090-5); *Eds. R. M. Ferreira, J. Gulikers and C. Andrade*

**PRO 57:** RILEM Workshop on Performance of cement-based materials in aggressive aqueous environments (e-ISBN: 978-2-35158-059-2); *Ed. N. De Belie*

**PRO 58:** International RILEM Symposium on Concrete Modelling—CONMOD'08 (ISBN: 978-2-35158-060-8; e-ISBN: 978-2-35158-076-9); *Eds. E. Schlangen and G. De Schutter*

**PRO 59:** International RILEM Conference on On Site Assessment of Concrete, Masonry and Timber Structures—SACoMaTiS 2008 (ISBN set: 978-2-35158-061-5; e-ISBN: 978-2-35158-075-2); *Eds. L. Binda, M. di Prisco and R. Felicetti*

**PRO 60:** Seventh RILEM International Symposium on Fibre Reinforced Concrete: Design and Applications—BEFIB 2008 (ISBN: 978-2-35158-064-6; e-ISBN: 978-2-35158-086-8); *Ed. R. Gettu*

**PRO 61:** 1st International Conference on Microstructure Related Durability of Cementitious Composites 2 vol., (ISBN: 978-2-35158-065-3; e-ISBN: 978-2-35158-084-4); *Eds. W. Sun, K. van Breugel, C. Miao, G. Ye and H. Chen*

**PRO 62:** NSF/ RILEM Workshop: In-situ Evaluation of Historic Wood and Masonry Structures (e-ISBN: 978-2-35158-068-4); *Eds. B. Kasal, R. Anthony and M. Drdác'ky*

**PRO 63:** Concrete in Aggressive Aqueous Environments: Performance, Testing and Modelling, 2 vol., (ISBN: 978-2-35158-071-4; e-ISBN: 978-2-35158-082-0); *Eds. M. G. Alexander and A. Bertron*

**PRO 64:** Long Term Performance of Cementitious Barriers and Reinforced Concrete in Nuclear Power Plants and Waste Management—NUCPERF 2009 (ISBN: 978-2-35158-072-1; e-ISBN: 978-2-35158-087-5); *Eds. V. L'Hostis, R. Gens, C. Gallé*

**PRO 65:** Design Performance and Use of Self-consolidating Concrete—SCC'2009 (ISBN: 978-2-35158-073-8; e-ISBN: 978-2-35158-093-6); *Eds. C. Shi, Z. Yu, K. H. Khayat and P. Yan*

**PRO 66:** 2nd International RILEM Workshop on Concrete Durability and Service Life Planning—ConcreteLife'09 (ISBN: 978-2-35158-074-5); *Ed. K. Kovler*

**PRO 67:** Repairs Mortars for Historic Masonry (e-ISBN: 978-2-35158-083-7); *Ed. C. Groot*

**PRO 68:** Proceedings of the 3rd International RILEM Symposium on 'Rheology of Cement Suspensions such as Fresh Concrete (ISBN 978-2-35158-091-2; e-ISBN: 978-2-35158-092-9); *Eds. O. H. Wallevik, S. Kubens and S. Oesterheld*

**PRO 69:** 3rd International PhD Student Workshop on 'Modelling the Durability of Reinforced Concrete (ISBN: 978-2-35158-095-0); *Eds. R. M. Ferreira, J. Gulikers and C. Andrade*

**PRO 70:** 2nd International Conference on 'Service Life Design for Infrastructure' (ISBN set: 978-2-35158-096-7; e-ISBN: 978-2-35158-097-4); *Ed. K. van Breugel, G. Ye and Y. Yuan*

**PRO 71:** Advances in Civil Engineering Materials—The 50-year Teaching Anniversary of Prof. Sun Wei' (ISBN: 978-2-35158-098-1; e-ISBN: 978-2-35158-099-8); *Eds. C. Miao, G. Ye, and H. Chen*

**PRO 72:** First International Conference on 'Advances in Chemically-Activated Materials—CAM'2010' (2010), 264 pp., ISBN: 978-2-35158-101-8; e-ISBN: 978-2-35158-115-5; *Eds. Caijun Shi and Xiaodong Shen*

**PRO 73:** 2nd International Conference on 'Waste Engineering and Management—ICWEM 2010' (2010), 894 pp., ISBN: 978-2-35158-102-5; e-ISBN: 978-2-35158-103-2; *Eds. J. Zh. Xiao, Y. Zhang, M. S. Cheung and R. Chu*

**PRO 74:** International RILEM Conference on 'Use of Superabsorbent Polymers and Other New Additives in Concrete' (2010) 374 pp., ISBN: 978-2-35158-104-9; e-ISBN: 978-2-35158-105-6; *Eds. O. M. Jensen, M. T. Hasholt, and S. Laustsen*

**PRO 75:** International Conference on ‘Material Science—2nd ICTRC—Textile Reinforced Concrete—Theme 1’ (2010) 436 pp., ISBN: 978-2-35158-106-3; e-ISBN: 978-2-35158-107-0; *Ed. W. Brameshuber*

**PRO 76:** International Conference on ‘Material Science—HetMat—Modelling of Heterogeneous Materials—Theme 2’ (2010) 255 pp., ISBN: 978-2-35158-108-7; e-ISBN: 978-2-35158-109-4; *Ed. W. Brameshuber*

**PRO 77:** International Conference on ‘Material Science—AdIPoC—Additions Improving Properties of Concrete—Theme 3’ (2010) 459 pp., ISBN: 978-2-35158-110-0; e-ISBN: 978-2-35158-111-7; *Ed. W. Brameshuber*

**PRO 78:** 2nd Historic Mortars Conference and RILEM TC 203-RHM Final Workshop—HMC2010 (2010) 1416 pp., e-ISBN: 978-2-35158-112-4; *Eds. J. Válek, C. Groot, and J. J. Hughes*

**PRO 79:** International RILEM Conference on Advances in Construction Materials Through Science and Engineering (2011) 213 pp., ISBN: 978-2-35158-116-2; e-ISBN: 978-2-35158-117-9; *Eds. Christopher Leung and K. T. Wan*

**PRO 80:** 2nd International RILEM Conference on Concrete Spalling due to Fire Exposure (2011) 453 pp., ISBN: 978-2-35158-118-6; e-ISBN: 978-2-35158-119-3; *Eds. E. A. B. Koenders and F. Dehn*

**PRO 81:** 2nd International RILEM Conference on Strain Hardening Cementitious Composites (SHCC2-Rio) (2011) 451 pp., ISBN: 978-2-35158-120-9; e-ISBN: 978-2-35158-121-6; *Eds. R. D. Toledo Filho, F. A. Silva, E. A. B. Koenders and E. M. R. Fairbairn*

**PRO 82:** 2nd International RILEM Conference on Progress of Recycling in the Built Environment (2011) 507 pp., e-ISBN: 978-2-35158-122-3; *Eds. V. M. John, E. Vazquez, S. C. Angulo and C. Ulsen*

**PRO 83:** 2nd International Conference on Microstructural-related Durability of Cementitious Composites (2012) 250 pp., ISBN: 978-2-35158-129-2; e-ISBN: 978-2-35158-123-0; *Eds. G. Ye, K. van Breugel, W. Sun and C. Miao*

**PRO 84:** CONSEC13—Seventh International Conference on Concrete under Severe Conditions—Environment and Loading (2013) 1930 pp., ISBN: 978-2-35158-124-7; e-ISBN: 978-2-35158-134-6; *Eds. Z. J. Li, W. Sun, C. W. Miao, K. Sakai, O. E. Gjorv & N. Banthia*

**PRO 85:** RILEM-JCI International Workshop on Crack Control of Mass Concrete and Related issues concerning Early-Age of Concrete Structures—ConCrack 3—Control of Cracking in Concrete Structures 3 (2012) 237 pp., ISBN: 978-2-35158-125-4; e-ISBN: 978-2-35158-126-1; *Eds. F. Toutlemonde and J.-M. Torrenti*

**PRO 86:** International Symposium on Life Cycle Assessment and Construction (2012) 414 pp., ISBN: 978-2-35158-127-8; e-ISBN: 978-2-35158-128-5; *Eds. A. Ventura and C. de la Roche*

**PRO 87:** UHPFRC 2013—RILEM-fib-AFGC International Symposium on Ultra-High Performance Fibre-Reinforced Concrete (2013), ISBN: 978-2-35158-130-8; e-ISBN: 978-2-35158-131-5; *Eds. F. Toutlemonde*

**PRO 88:** 8th RILEM International Symposium on Fibre Reinforced Concrete (2012) 344 pp., ISBN: 978-2-35158-132-2; e-ISBN: 978-2-35158-133-9; *Eds. Joaquim A. O. Barros*

**PRO 89:** RILEM International workshop on performance-based specification and control of concrete durability (2014) 678 pp., ISBN: 978-2-35158-135-3; e-ISBN: 978-2-35158-136-0; *Eds. D. Bjegović, H. Beushausen and M. Serdar*

**PRO 90:** 7th RILEM International Conference on Self-Compacting Concrete and of the 1st RILEM International Conference on Rheology and Processing of Construction Materials (2013) 396 pp., ISBN: 978-2-35158-137-7; e-ISBN: 978-2-35158-138-4; *Eds. Nicolas Roussel and Hela Bessaies-Bey*

**PRO 91:** CONMOD 2014—RILEM International Symposium on Concrete Modelling (2014), ISBN: 978-2-35158-139-1; e-ISBN: 978-2-35158-140-7; *Eds. Kefei Li, Peiyu Yan and Rongwei Yang*

**PRO 92:** CAM 2014—2nd International Conference on advances in chemically-activated materials (2014) 392 pp., ISBN: 978-2-35158-141-4; e-ISBN: 978-2-35158-142-1; *Eds. Caijun Shi and Xiadong Shen*

**PRO 93:** SCC 2014—3rd International Symposium on Design, Performance and Use of Self-Consolidating Concrete (2014) 438 pp., ISBN: 978-2-35158-143-8; e-ISBN: 978-2-35158-144-5; *Eds. Caijun Shi, Zhihua Ou, Kamal H. Khayat*

**PRO 94 (online version):** HPRCC-7—7th RILEM conference on High performance fiber reinforced cement composites (2015), e-ISBN: 978-2-35158-146-9; *Eds. H. W. Reinhardt, G. J. Parra-Montesinos, H. Garrecht*

**PRO 95:** International RILEM Conference on Application of superabsorbent polymers and other new admixtures in concrete construction (2014), ISBN: 978-2-35158-147-6; e-ISBN: 978-2-35158-148-3; *Eds. Viktor Mechtcherine, Christof Schroefl*

**PRO 96 (online version):** XIII DBMC: XIII International Conference on Durability of Building Materials and Components (2015), e-ISBN: 978-2-35158-149-0; *Eds. M. Quattrone, V. M. John*

**PRO 97:** SHCC3—3rd International RILEM Conference on Strain Hardening Cementitious Composites (2014), ISBN: 978-2-35158-150-6; e-ISBN: 978-2-35158-151-3; *Eds. E. Schlangen, M. G. Sierra Beltran, M. Lukovic, G. Ye*

**PRO 98:** FERRO-11—11th International Symposium on Ferrocement and 3rd ICTRC—International Conference on Textile Reinforced Concrete (2015), ISBN: 978-2-35158-152-0; e-ISBN: 978-2-35158-153-7; *Ed. W. Bramshuber*

**PRO 99 (online version):** ICBBM 2015—1st International Conference on Bio-Based Building Materials (2015), e-ISBN: 978-2-35158-154-4; *Eds. S. Amziane, M. Sonebi*

**PRO 100:** SCC16—RILEM Self-Consolidating Concrete Conference (2016), ISBN: 978-2-35158-156-8; e-ISBN: 978-2-35158-157-5; *Ed. Kamal H. Kayat*

**PRO 101 (online version):** III Progress of Recycling in the Built Environment (2015), e-ISBN: 978-2-35158-158-2; *Eds. M. Quattrone, V. M. John*

**PRO 102 (online version):** RILEM Conference on Microorganisms-Cementitious Materials Interactions (2016), e-ISBN: 978-2-35158-160-5; *Eds. Alexandra Bertron, Henk Jonkers, Virginie Wiktor*

**PRO 103 (online version):** ACESC'16—Advances in Civil Engineering and Sustainable Construction (2016), e-ISBN: 978-2-35158-161-2; *Eds. T. Ch. Madhavi, G. Prabhakar, Santhosh Ram, and P. M. Rameshwaran*

**PRO 104 (online version):** SSCS'2015—Numerical Modeling—Strategies for Sustainable Concrete Structures (2015), e-ISBN: 978-2-35158-162-9

**PRO 105:** 1st International Conference on UHPC Materials and Structures (2016), ISBN: 978-2-35158-164-3; e-ISBN: 978-2-35158-165-0

**PRO 106:** AFGC-ACI-fib-RILEM International Conference on Ultra-High-Performance Fibre-Reinforced Concrete—UHPFRC 2017 (2017), ISBN: 978-2-35158-166-7; e-ISBN: 978-2-35158-167-4; *Eds. François Toutlemonde & Jacques Resplendino*

**PRO 107 (online version):** XIV DBMC—14th International Conference on Durability of Building Materials and Components (2017), e-ISBN: 978-2-35158-159-9; *Eds. Geert De Schutter, Nele De Belie, Arnold Janssens, Nathan Van Den Bossche*

**PRO 108:** MSSCE 2016—Innovation of Teaching in Materials and Structures (2016), ISBN: 978-2-35158-178-0; e-ISBN: 978-2-35158-179-7; *Ed. Per Goltermann*

**PRO 109 (2 volumes):** MSSCE 2016—Service Life of Cement-Based Materials and Structures (2016), ISBN Vol. 1: 978-2-35158-170-4, Vol. 2: 978-2-35158-171-4, Set Vol. 1&2: 978-2-35158-172-8; e-ISBN: 978-2-35158-173-5; *Eds. Miguel Azenha, Ivan Gabrijel, Dirk Schlicke, Terje Kanstad and Ole Mejlhede Jensen*

**PRO 110:** MSSCE 2016—Historical Masonry (2016), ISBN: 978-2-35158-178-0; e-ISBN: 978-2-35158-179-7; *Eds. Inge Rörig-Dalgaard and Ioannis Ioannou*

**PRO 111:** MSSCE 2016—Electrochemistry in Civil Engineering (2016), ISBN: 978-2-35158-176-6; e-ISBN: 978-2-35158-177-3; *Ed. Lisbeth M. Ottosen*

**PRO 112:** MSSCE 2016—Moisture in Materials and Structures (2016), ISBN: 978-2-35158-178-0; e-ISBN: 978-2-35158-179-7; *Eds. Kurt Kielsgaard Hansen, Carsten Rode and Lars-Olof Nilsson*

**PRO 113:** MSSCE 2016—Concrete with Supplementary Cementitious Materials (2016), ISBN: 978-2-35158-178-0; e-ISBN: 978-2-35158-179-7; *Eds. Ole Mejlhede Jensen, Konstantin Kovler and Nele De Belie*

**PRO 114:** MSSCE 2016—Frost Action in Concrete (2016), ISBN: 978-2-35158-182-7; e-ISBN: 978-2-35158-183-4; *Eds. Marianne Tange Hasholt, Katja Fridh and R. Doug Hooton*

**PRO 115:** MSSCE 2016—Fresh Concrete (2016), ISBN: 978-2-35158-184-1; e-ISBN: 978-2-35158-185-8; *Eds. Lars N. Thrane, Claus Pade, Oldrich Svec and Nicolas Roussel*

**PRO 116:** BEFIB 2016—9th RILEM International Symposium on Fiber Reinforced Concrete (2016), ISBN: 978-2-35158-187-2; e-ISBN: 978-2-35158-186-5; *Eds. N. Banthia, M. di Prisco and S. Soleimani-Dashtaki*

**PRO 117:** 3rd International RILEM Conference on Microstructure Related Durability of Cementitious Composites (2016), ISBN: 978-2-35158-188-9; e-ISBN: 978-2-35158-189-6; *Eds. Changwen Miao, Wei Sun, Jiaping Liu, Huisu Chen, Guang Ye and Klaas van Breugel*

**PRO 118 (4 volumes):** International Conference on Advances in Construction Materials and Systems (2017), ISBN Set: 978-2-35158-190-2, Vol. 1: 978-2-35158-193-3, Vol. 2: 978-2-35158-194-0, Vol. 3: ISBN:978-2-35158-195-7, Vol. 4: ISBN:978-2-35158-196-4; e-ISBN: 978-2-35158-191-9; *Ed. Manu Santhanam*

**PRO 119 (online version):** ICBBM 2017—Second International RILEM Conference on Bio-based Building Materials, (2017), e-ISBN: 978-2-35158-192-6; *Ed. Sofiane Amziane*

**PRO 120:** 2nd International RILEM/COST Conference on Early Age Cracking and Serviceability in Cement-based Materials and Structures (EAC-02), 2017, ISBN: 978-2-35158-197-1; e-ISBN: 978-2-35158-198-8; *Eds. Dimitrios Aggelis and Stéphanie Staquet*

**PRO 121:** SynerCrete18, Interdisciplinary Approaches for Cement-based Materials and Structural Concrete: Synergizing Expertise and Bridging Scales of Space and Time, (2018), ISBN: 978-2-35158-202-2; e-ISBN: 978-2-35158-203-9; *Eds. Miguel Azenha, Dirk Schlicke, Farid Benboudjema, Agnieszka Knoppik*

## RILEM REPORTS (REP)

**Report 19:** Considerations for Use in Managing the Aging of Nuclear Power Plant Concrete Structures (ISBN: 2-912143-07-1); *Ed. D. J. Naus*

**Report 20:** Engineering and Transport Properties of the Interfacial Transition Zone in Cementitious Composites (ISBN: 2-912143-08-X); *Eds. M. G. Alexander, G. Arliguie, G. Ballivy, A. Bentur and J. Marchand*

**Report 21:** Durability of Building Sealants (ISBN: 2-912143-12-8); *Ed. A. T. Wolf*

**Report 22:** Sustainable Raw Materials—Construction and Demolition Waste (ISBN: 2-912143-17-9); *Eds. C. F. Hendriks and H. S. Pietersen*

**Report 23:** Self-Compacting Concrete state-of-the-art report (ISBN: 2-912143-23-3); *Eds. Å. Skarendahl and Ö. Petersson*

**Report 24:** Workability and Rheology of Fresh Concrete: Compendium of Tests (ISBN: 2-912143-32-2); *Eds. P. J. M. Bartos, M. Sonebi and A. K. Tamimi*

**Report 25:** Early Age Cracking in Cementitious Systems (ISBN: 2-912143-33-0); *Ed. A. Bentur*

**Report 26:** Towards Sustainable Roofing (Joint Committee CIB/RILEM) (CD 07) (e-ISBN 978-2-912143-65-5); *Eds. Thomas W. Hutchinson and Keith Roberts*

**Report 27:** Condition Assessment of Roofs (Joint Committee CIB/RILEM) (CD 08) (e-ISBN 978-2-912143-66-2); *Ed. CIB W 83/RILEM TC166-RMS*

**Report 28:** Final report of RILEM TC 167-COM ‘Characterisation of Old Mortars with Respect to Their Repair (ISBN: 978-2-912143-56-3); *Eds. C. Groot, G. Ashall and J. Hughes*

**Report 29:** Pavement Performance Prediction and Evaluation (PPPE): Interlaboratory Tests (e-ISBN: 2-912143-68-3); *Eds. M. Partl and H. Piber*

**Report 30:** Final Report of RILEM TC 198-URM ‘Use of Recycled Materials’ (ISBN: 2-912143-82-9; e-ISBN: 2-912143-69-1); *Eds. Ch. F. Hendriks, G. M. T. Janssen and E. Vázquez*

**Report 31:** Final Report of RILEM TC 185-ATC ‘Advanced testing of cement-based materials during setting and hardening’ (ISBN: 2-912143-81-0; e-ISBN: 2-912143-70-5); *Eds. H. W. Reinhardt and C. U. Grosse*

**Report 32:** Probabilistic Assessment of Existing Structures. A JCSS publication (ISBN 2-912143-24-1); *Ed. D. Diamantidis*

**Report 33:** State-of-the-Art Report of RILEM Technical Committee TC 184-IFE ‘Industrial Floors’ (ISBN 2-35158-006-0); *Ed. P. Seidler*

**Report 34:** Report of RILEM Technical Committee TC 147-FMB ‘Fracture mechanics applications to anchorage and bond’ Tension of Reinforced Concrete Prisms—Round Robin Analysis and Tests on Bond (e-ISBN 2-912143-91-8); *Eds. L. Elfgren and K. Noghabai*

**Report 35:** Final Report of RILEM Technical Committee TC 188-CSC ‘Casting of Self Compacting Concrete’ (ISBN 2-35158-001-X; e-ISBN: 2-912143-98-5); *Eds. Å. Skarendahl and P. Billberg*

**Report 36:** State-of-the-Art Report of RILEM Technical Committee TC 201-TRC ‘Textile Reinforced Concrete’ (ISBN 2-912143-99-3); *Ed. W. Brameshuber*

**Report 37:** State-of-the-Art Report of RILEM Technical Committee TC 192-ECM ‘Environment-conscious construction materials and systems’ (ISBN: 978-2-35158-053-0); *Eds. N. Kashino, D. Van Gemert and K. Imamoto*

**Report 38:** State-of-the-Art Report of RILEM Technical Committee TC 205-DSC ‘Durability of Self-Compacting Concrete’ (ISBN: 978-2-35158-048-6); *Eds. G. De Schutter and K. Audenaert*

**Report 39:** Final Report of RILEM Technical Committee TC 187-SOC ‘Experimental determination of the stress-crack opening curve for concrete in tension’ (ISBN 978-2-35158-049-3); *Ed. J. Planas*

**Report 40:** State-of-the-Art Report of RILEM Technical Committee TC 189-NEC ‘Non-Destructive Evaluation of the Penetrability and Thickness of the Concrete Cover’ (ISBN 978-2-35158-054-7); *Eds. R. Torrent and L. Fernández Luco*

**Report 41:** State-of-the-Art Report of RILEM Technical Committee TC 196-ICC ‘Internal Curing of Concrete’ (ISBN 978-2-35158-009-7); *Eds. K. Kovler and O. M. Jensen*

**Report 42:** ‘Acoustic Emission and Related Non-destructive Evaluation Techniques for Crack Detection and Damage Evaluation in Concrete’—Final Report of RILEM Technical Committee 212-ACD (e-ISBN: 978-2-35158-100-1); *Ed. M. Ohtsu*

**Report 45:** Repair Mortars for Historic Masonry—State-of-the-Art Report of RILEM Technical Committee TC 203-RHM (e-ISBN: 978-2-35158-163-6); *Eds. Paul Maurenbrecher and Caspar Groot*

**Report 46:** Surface delamination of concrete industrial floors and other durability related aspects guide—Report of RILEM Technical Committee TC 268-SIF (e-ISBN: 978-2-35158-201-5); *Ed. Valerie Pollet*

# Contents

<b>1</b>	<b>Introduction</b> .....	1
	Lars-Olof Nilsson, Elisa Franzoni and Hemming Paroll	
<b>2</b>	<b>Definitions</b> .....	9
	Lars-Olof Nilsson, Elisa Franzoni and Olivier Weichold	
<b>Part I Moisture Measuring Principles</b>		
<b>3</b>	<b>Drying Methods</b> .....	17
	Kurt Kielsgaard Hansen, Sture Lindmark, Lars-Olof Nilsson and Oliver Weichold	
<b>4</b>	<b>Calibration Techniques</b> .....	27
	Miguel-Ángel Climent, Sture Lindmark and Lars-Olof Nilsson	
<b>5</b>	<b>Gravimetry</b> .....	39
	Lars-Olof Nilsson	
<b>6</b>	<b>Chemical Reaction</b> .....	43
	Lars-Olof Nilsson, Miguel-Ángel Climent and Oliver Weichold	
<b>7</b>	<b>Infrared Thermography</b> .....	49
	Jean-François Lataste and Lars-Olof Nilsson	
<b>8</b>	<b>Electrical Resistance</b> .....	55
	Jean-François Lataste, Charlotte Thiel and Elisa Franzoni	
<b>9</b>	<b>Gas Permeability</b> .....	67
	Franck Agostini	
<b>10</b>	<b>Hygrometry</b> .....	73
	Lars-Olof Nilsson, Kurt Kielsgaard Hansen and Miguel Azenha	
<b>11</b>	<b>Pore Water Pressure</b> .....	87
	Lars-Olof Nilsson	

**12 Introduction to Electromagnetic Radiation . . . . . 93**  
 Oliver Weichold

**13 Nuclear Magnetic Resonance and Magnetic Resonance Imaging . . . . . 99**  
 Charlotte Thiel and Christoph Gehlen

**14 Capacimetry . . . . . 109**  
 Jean-François Lataste, Walter Denzel and Hemming Paroll

**15 Time Domain Reflectometry . . . . . 115**  
 Alexander Michel, Henryk Sobczuk and Kurt Kielsgaard Hansen

**16 Microwave Reflection . . . . . 123**  
 Jean-François Lataste and Arndt Göller

**17 Neutron Radiography . . . . . 141**  
 Zhang Peng and Zhao Tiejun

**18 X-Ray and Gamma-Ray . . . . . 157**  
 Owe Lindgren and Lars-Olof Nilsson

**Part II Applications**

**19 Spatial Distributions . . . . . 173**  
 Jean-François Lataste, Kurt Kielsgaard Hansen, Lars-Olof Nilsson,  
 Charlotte Thiel, Angelika Schießl-Pecka, Arndt Göller  
 and Christoph Gehlen

**20 Moisture Distribution in a Structure/Specimen—General . . . . . 191**  
 Lars-Olof Nilsson

**21 ND-Methods—From a Surface . . . . . 193**  
 Kurt Kielsgaard Hansen, Jean-François Lataste and Charlotte Thiel

**22 Coring, Drilling and Sampling Techniques . . . . . 199**  
 Lars-Olof Nilsson and Elisa Franzoni

**23 Installation of Probes . . . . . 207**  
 Lars-Olof Nilsson, Franck Agostini and Charlotte Thiel

**24 Specimen or Core; In the Laboratory (Sides Available) . . . . . 221**  
 Kurt Kielsgaard Hansen, Jean-Francois Lataste, Lars-Olof Nilsson,  
 Charlotte Thiel and Alexander Michel

**25 Moisture in a Substrate Before Surface Covering . . . . . 229**  
 Lars-Olof Nilsson

**26 Monitoring, Remote Measurements . . . . . 237**  
 Franck Agostini, Elisa Franzoni, Kurt Kielsgaard Hansen,  
 Hemming Paroll and Lars-Olof Nilsson

<b>27 Heterogeneous Materials</b> .....	251
Lars-Olof Nilsson and Elisa Franzoni	
<b>Part III Conclusions</b>	
<b>28 Conclusions</b> .....	261
Lars-Olof Nilsson	
<b>References</b> .....	263

## Members of RILEM TC 248-MMB

Prof. Lars-Olof Nilsson (SE)—*TC-chairman*, Lund University & Moistenginst AB, Sweden  
Associate Prof. Kurt Kielsgaard Hansen (DK)—*TC-secretary*, Technical University of Denmark, Denmark  
Dr. Franck Agostini (FR), École Centrale de Lille, France  
Dr. Ing. Udo Antons (DE) Technical University of Dortmund, Germany  
Dr. Miguel Azenha (PT), University of Minho, Portugal  
Prof. Miguel-Ángel Climent (ES), University of Alicante, Spain  
Mr. Walter Denzel (DE), DNS-Denzel, Börtlingen, Germany  
Dr. Elisa Franzoni (IT), University of Bologna, Italy  
Prof. Christoph Gehlen (DE), Technical University of Munich, Germany  
Dr. Arndt Göller (DE), hf sensor GmbH, Leipzig, Germany  
Howard Kanare (USA), KOSTER American Corporation, Virginia Beach, USA  
Prof. Krüger, Markus (AT), Graz University of Technology, Austria  
Dr. Alexander Michel (DK), Technical University of Denmark, Denmark  
Hemming Paroll, M.Sc. (FI), Fuktcom AB, Espoo, Finland  
Prof. Rudolf Plagge (DE) Technical University of Dresden, Germany  
Prof. Henryk Sobczuk (PL), Lublin University of Technology, Poland  
Prof. Thomas Tannert (CA), University of Northern British Columbia, Canada  
Dipl.-Ing. Charlotte Thiel (DE), Technical University of Munich, Germany  
Roberto Torrent (AR), Materials Advanced Services Ltd., Buenos Aires, Argentina  
Dr. Jeanette Visser (NL), TNO, Delft, The Netherlands  
Prof. Oliver Weichold (DE), IBAC, Aachen, Germany  
Prof. Jason Weiss (USA), Oregon State University, Corvallis, USA  
Prof. Folker Wittmann (DE), Aedificat Institut Freiburg, Germany  
Prof. Peng Zhang (PRC & DE), Qingdao University of Technology, China, and Karlsruhe Institute of Technology, Germany  
Dr. Peihua Zhang (PRC), Southeast University, Nanjing, China

# Chapter 1

## Introduction



Lars-Olof Nilsson, Elisa Franzoni and Hemming Paroll

### 1.1 Significance of Moisture in Building Materials

The amount of moisture and the state of water in porous materials are decisive for the properties and the behaviour of the materials and structures. Thermal and mechanical properties of a material are directly affected by the moisture content. Moisture content variations in a material cause dimensional changes; swelling, shrinkage and other deformations.

Moisture contents in a material above certain critical limits may cause deterioration of the material itself due to physical-mechanical (e.g. freezing, salts crystallization), biological (root decay, aggressive substances, rot), chemical (various reactions) and electro-chemical (metal corrosion) deterioration processes.

An example of the relevance of measuring moisture can be found in concrete flooring finishes. Indeed, there are critical levels of concrete moisture that need to be reached before applying impermeable finishes, to avoid delamination, emissions etc. associated with moisture imprisonment (Fig. 1.1).

Most deterioration processes involve transport of gases, liquids and ions and the moisture level is decisive for these transport processes. Some examples are shown in Figs. 1.2 and 1.3.

---

L.-O. Nilsson (✉)  
Lund University, Lund, Sweden  
e-mail: lars-olof.nilsson@byggtek.lth.se

L.-O. Nilsson  
Moistenginst AB, Trelleborg, Sweden

E. Franzoni  
University of Bologna, Bologna, Italy

H. Paroll  
Fuktcom AB, Espoo, Finland

**Fig. 1.1** An example of a deteriorated floor covering, a PVC-flooring attached to a concrete slab, due to high levels of moisture and alkali in the substrate (*Photo Leif Erlandsson*)



**Fig. 1.2** An example of a deteriorated concrete structure due to internal expansion from alkali-aggregate reactions that require a certain moisture level for the alkalis to reach the reactive aggregate. The structure is covered to protect against rain (*Photo Lars-Olof Nilsson*)





**Fig. 1.3** Examples of damages due to rising damp in a sandstone column (left) and a brick masonry (right). The deterioration patterns are due to a combination of salt crystallisation cycles and frost damage, both to be ascribed to the presence of moisture in the materials pores (*Photos Elisa Franzoni*)

Wooden based materials are sensitive to too high, or too low, moisture contents. Moisture contents above a certain limit may cause root decay. Surface humidity and temperature conditions above a critical limit,  $RH_{crit}(T, t)$ , may cause mould growth at wooden surfaces. Moisture content changes will cause swelling and shrinkage and if they are too large may cause curling, cracking, too large gaps between boards etc. Two examples are shown in Fig. 1.4.

Chemical and biological processes that cause emissions to indoor air, bad odour or uncomfortable indoor conditions require moisture levels above a certain limit. In fact the EU Regulation 305/2011 ‘Construction Products Directive’ requires to avoid “dampness in parts of the construction works or on surfaces within the construction works” for inhabitants’ hygiene and health.

The traditions to quantify the moisture conditions in research and in various applications are very different in different research areas, for different materials, in different industrial applications and in different countries for the same application. This state-of-the-art report is meant to describe the present state of knowledge and application traditions when it comes to moisture measurements in building materials and structures.

## 1.2 Why Measure Moisture?

There are numerous reasons for quantifying the moisture conditions in research and applications. Since a number of material properties and processes in materials are significantly affected by the level of moisture and moisture changes, experimental



**Fig. 1.4** Examples of damages in wood structures due to too high moisture contents. Root decay in an outdoor timber structure with a non-suitable paint system (left) (*Photo Stefan Hjort*) and large gaps between floor tiles (right) (*Photo Lars-Olof Nilsson*). The board in the bottom centre has been compressed by swelling too much. The two marks show the width of the other tiles that were not compressed but shrank reversible after swelling

research requires a thorough quantification of the absolute level of moisture conditions and the spatial distribution of moisture in specimens and setups and how they change with time. For the construction industry it is important to be able to quantify the moisture conditions in an accurate way in various applications.

During production of building materials, during construction and during the use of buildings there are many reasons why the moisture conditions must be controlled and determined. Some examples are:

- delivery checks at a construction site,
- controls during construction,
- control of required level of drying,
- conditions in a substrate before applying a surface material,
- comparison with acceptable moisture levels,
- long-term performance controls of structures,
- quantifying the direction of moisture flow to find the cause of moisture damage.

### 1.3 What Moisture to Measure?

Methods for measuring moisture in materials determine the amount of moisture, the moisture content, or the state of moisture, the pore humidity or pore water pressure.

These two concepts are of course related to each other. The relationship is shown by a sorption isotherm for each individual material, a curve showing the moisture content at equilibrium with a certain relative humidity RH, cf. Fig. 1.5.

The methods for measuring moisture are suitable for different ranges of moisture conditions. Some methods are only used in the “hygroscopic range”, at relative humidities below some 95–98%, while special methods are applicable in the “capillary range”, at RH above 98%. Methods that determine the moisture content are more suitable in the capillary range.

In theory, a measured moisture content  $u$  may be translated into a relative humidity RH, if the sorption isotherm is known. In practice, however, the uncertainty of such a translation usually is very large, for two reasons: (1) the sorption isotherm is not known for exactly the material quality in question and (2) the relation between  $u$  and RH is not a unique curve but a series of desorption, absorption and scanning curves that are relevant depending on the “moisture history”, i.e. in what way the present moisture conditions have been achieved; by drying, wetting or series of drying/wetting.

One exception is wooden based materials. If the moisture content is expressed in % by weight “all” wooden based materials have approximately the same sorption

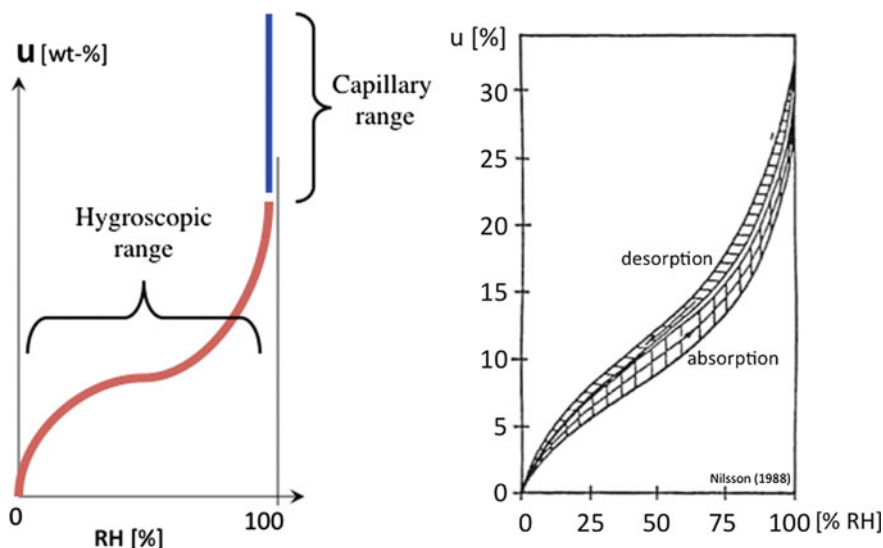


**Fig. 1.5** A sorption isotherm, in principle; the moisture content  $u$  as a function of the state of moisture, the relative humidity RH (left) and a sorption isotherm for spruce and pine at +20 °C, Nilsson (1988)

isotherm. An example for spruce and pine of various densities is shown in Fig. 1.5. If it is known that a point in a timber structure has dried and never was rewetted, the relationship would follow the desorption isotherm. The variation of desorption isotherms is then very small in Fig. 1.5, a few % RH. A direct measurement of the RH would, however, have a much smaller uncertainty.

A moisture content of a particular material says very little in comparison with a moisture content of another material. If a comparison is required it is better to measure the RH. RH of two different materials can be compared, if they have the same temperature. It is possible to say which one of the two materials are more humid and will moisten the other one. This is not possible if only the moisture contents are available. An obvious application where this is relevant is when moisture is measured in a substrate before a surface covering is to be applied.

The magnitude of a moisture content of a particular material does not give any relevant information without knowledge of the sorption isotherm for that material. Likewise, to be able to say whether a material is dry enough, from a measured moisture content, the sorption isotherm must be known, except for cases where the drying requirements are expressed in terms of moisture contents. The magnitude of a moisture content does also depend on the drying method used to define “moisture”.

In some cases the concept of “degree of saturation” is used. The measured moisture content is then compared to the moisture content of the same material, or sample, after saturation of the pore system. The saturation could be done by vacuum or by capillary suction, the latter giving the “degree of capillary saturation”. One example where the degree of saturation is relevant is when dealing with the frost resistance of a material. The degree of capillary saturation is especially used for heterogeneous materials.

The objectives of methods to measure moisture may be to quantify the level of moisture in a sample or in a point in a material or structure. In a number of cases the spatial distribution of moisture is targeted, to determine moisture gradients and how they change with time. Some other applications require methods to measure surface moisture or to scan large surfaces for moisture variations.

In some cases moisture measurements are done to check whether certain requirements are fulfilled, i.e. before applying a moisture sensitive material to a substrate. The formulation of the requirement will then decide what moisture to measure.

## 1.4 Limitations

The report concentrates on measurement of moisture content and moisture conditions and do not deal with all other aspects of moisture! The applications are laboratory experiments on materials and material combinations and quantification of conditions in buildings during construction and use. The methods dealt with are methods for measurements in materials and at material surfaces, on samples, specimens and in building components and structures.

## **1.5 Structure of the Report**

The report is structured in such a way that the chapters in a Part I deals with moisture measuring principles. The chapters in Part II are describing various applications, with references to the principles in Part I.

# Chapter 2

## Definitions



Lars-Olof Nilsson, Elisa Franzoni and Olivier Weichold

For the various sections of the report a number of common expressions and symbols are used. Most of them are defined here. Most of the definitions and symbols are the same as in CIB-W40(2012), with some minor revisions.

### 2.1 Expressions

**Adsorption of water:** binding of water molecules at a (pore) surface.

More general: *An increase in the concentration of a dissolved substance at the interface of a condensed and a liquid phase due to the operation of surface forces. Adsorption can also occur at the interface of a condensed and a gaseous phase, IUPAC (1990).*

**Absorption of water:** uptake of water by a material.

More general: *The process of one material (absorbate) being retained by another (absorbent); this may be the physical solution of a gas, liquid, or solid in a liquid, attachment of molecules of a gas, vapour, liquid, or dissolved substance to a solid surface by physical forces, etc., IUPAC (1990).*

---

L.-O. Nilsson (✉)  
Lund University, Lund, Sweden  
e-mail: lars-olof.nilsson@byggtek.lth.se

L.-O. Nilsson  
Moistenginst AB, Trelleborg, Sweden

E. Franzoni  
University of Bologna, Bologna, Italy

O. Weichold  
IBAC, Aachen, Germany

© RILEM 2018

L.-O. Nilsson (ed.), *Methods of Measuring Moisture in Building Materials and Structures*, RILEM State-of-the-Art Reports 26,  
[https://doi.org/10.1007/978-3-319-74231-1\\_2](https://doi.org/10.1007/978-3-319-74231-1_2)

**Attenuation:** weakening of radiation when passing through a substance.

**Desorption of water:** release of water from a material or a material's (pore) surface. It should be noted that the term **desorption** is used as the converse of adsorption and of absorption.

**Drying:** process that decrease the moisture content of a material, i.e. changing from a less dry state to a drier state. Drying is a term used as opposed to "wetting".

**Hygro:** moisture in air.

(Hygro from greek is simply an adjective meaning moist or wet).

**Hygroscopy:** the property of a porous material to absorb moisture from the air. The common definition is "*The property of a substance to absorb or adsorb water from its surroundings.*"

**Hygroscopic range:** the range of relative humidity in a material between 0 and 98% RH.

**Moisture:** the evaporable water in a material, i.e. the physically bound water, adsorbed at internal surfaces or capillary absorbed in pores; has to be defined by a drying method.

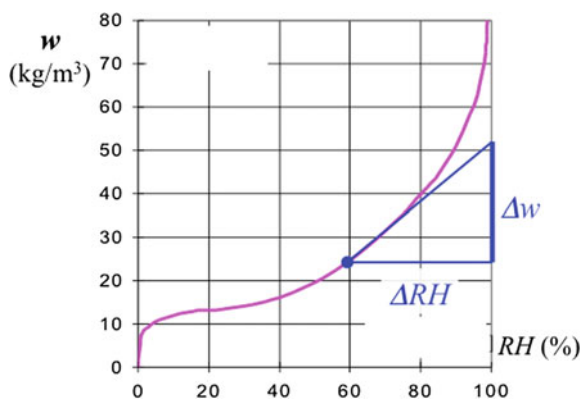
**Moisture content:** the amount of moisture, in a unit volume, per weight of dry material or in per cent by dry mass.

**Moisture content at complete saturation:** moisture content when all open pores are water-filled.

**Moisture content at capillary saturation:** moisture content when the pores are filled with water after capillary suction.

**Moisture capacity:** the slope of the sorption isotherm; a material's ability to bind or loose moisture when RH changes (Fig. 2.1).

**Fig. 2.1** An example of the moisture capacity; at 60% RH:  $\Delta w/\Delta RH$



**Moisture sorption isotherm:** the relationship, at a certain temperature, between the moisture content of a material and the relative humidity.

More general: *The concentration of a sorbed species (=moisture content), expressed as a function of its concentration in its surrounding medium (=RH) under specified conditions and at constant temperature, IUPAC (1993).*

**Sorption:** *the process by which a substance (sorbate) is sorbed (adsorbed or absorbed) on or in another substance (sorbent), IUPAC (1990).*

**Suction curve:** the relationship, at a certain temperature, between the moisture content of a material and the pore water pressure.

**Scanning curve** (sorption scanning curve): a part of the sorption isotherm where drying is followed by wetting or vice versa.

**Wetting:** Process that increase the moisture content of a material, i.e. changing from a drier state to a less dry state.

More general: Process by which an interface between a solid and a gas is replaced by an interface between the same solid and a liquid, IUPAC (2004).

Wetting is a term used as opposed to “drying”.

## 2.2 Symbols

These symbols are used in the report:

Mass:  $m$  (kg)

Dry mass:  $m_{dry}$  (kg)

Volume:  $V$  (m<sup>3</sup>)

Density:  $\rho$  (kg/m<sup>3</sup>) =  $m/V$

Dry density:  $\rho_o$  (kg/m<sup>3</sup>) =  $m_{dry}/V$

Water vapour pressure:  $p_v$  (Pa)

Water vapour concentration/content:  $v$  (kg/m<sup>3</sup>)

Pressure of water or air:  $P$  (Pa)

Moisture content, mass per volume:  $w$  (kg/m<sup>3</sup>) =  $m_{moisture}/V$

Moisture content, at complete saturation:  $w_{sat}$  (kg/m<sup>3</sup>)

Moisture content, at capillary saturation:  $w_{cap}$  (kg/m<sup>3</sup>)

Moisture ratio, mass by dry weight:  $u$  (kg/kg; %) =  $m_{moisture}/m_{dry}$

Moisture ratio, mass by wet weight:  $u_{wet}$  (kg/kg; %) =  $m_{moisture}/m_{wet} = m_{moisture}/(m_{dry} + m_{moisture})$

Moisture content by volume:  $\psi$  (m<sup>3</sup>/m<sup>3</sup>)

Degree of saturation:  $S$  (-) =  $w/w_{sat}$

Degree of capillary saturation:  $DCS$  or  $S_{cap} = w/w_{cap}$  (-)

Relative humidity:  $RH$  or  $\phi$  (-; %)

Moisture capacity:  $dw/d\phi$  (kg/m<sup>3</sup>)

Porosity:  $\xi$  (-)  
 Effective porosity:  $\xi_{\text{eff}}$  (-)  
 Total porosity:  $\xi_{\text{tot}}$  (-)  
 Resistivity:  $\rho_{\Omega}$  (ohms/m) ( $\rho$  also for density!)

## 2.3 Abbreviations

1D, 2D	One, two-dimensional
ASTM	American Society for Testing Materials
BS	British standard
CEM-x	Cement type, where x can be I to III and V
CM	Calcium carbide method
CT	Computed tomography
DCS	Degree of capillary saturation
DVS	Dynamic Vapour Sorption (balance)
EM	Electromagnetic
EMR	Electromagnetic radiation
EN	European Standard
ERT	Electrical resistivity tomography
eV	Electronvolt
FSP	Fiber saturation point (for wood)
GGBF	Ground granulated blast furnace
GPR	Ground penetrating radar
HSC	High-strength concrete
IR	Infrared
ISO	International Organization for Standardization
KFT	Karl Fischer titration
MB	Moisture balance
MC	Moisture content
MRE	Multi ring electrodes
MRI	Magnetic resonance imaging
ND	Non-destructive
NDT	Non-destructive technique
NIH	National Institute of Health
NIR	Near-infrared
nm	Nanometer
NMR	Nuclear magnetic resonance
OPC	Ordinary Portland cement
PFA	Pulverized fuel ash, also called fly ash
PID	Proportional–integral–derivative (regulator)
RBK	The Swedish Council for Building Control (Rådet för byggkontroll)
RFID	Radio frequency identification

RILEM	International union of laboratories and experts in construction materials, systems and structures (Réunion Internationale des Laboratoires et Experts des Matériaux)
RH	Relative humidity
SFRC	Steel fibre reinforced concrete
SRPC	Sulphate resistant Portland cement
TDR	Time domain reflectometry
TGA	Thermogravimetric analysis
WST	Wedge split test.

# Part I

## Moisture Measuring Principles

The moisture content of a material or the state of water inside a material may be determined by a large number of alternative measuring principles. In this part of the report the state of art of these principles are described, in Chaps. 5–19. Applications where these measuring principles are used are dealt with in the next part (II), Chaps. 20–27.

An essential part of measuring the moisture content of a material is the definition of “moisture”. This is always done by a drying method since there is no other way to separate e.g. “physically bound water” from “chemically bound water”. Different drying methods and the relationship between them are described in Chap. 3.

Most measuring principles are indirect, i.e. the reading from a measuring principle must be translated into moisture content or state of water in some way, usually with a calibration. Methods and processes used to perform calibration of moisture measuring principles are, therefore, described in Chap. 4.

# Chapter 3

## Drying Methods



**Kurt Kielsgaard Hansen, Sture Lindmark, Lars-Olof Nilsson  
and Oliver Weichold**

### 3.1 Introduction

When measuring the moisture content of a material by gravimetry, or when another method for measuring moisture content is to be calibrated, it is of course essential to be able to determine the exact amount of water in a sample. This may be done for instance by radioactive methods or by some technique in which the water is removed from a representative sample of the material. The latter technique is simply known as drying.

Drying, though, is not easily defined and can be done in several different ways, and the removal of water may have negative consequences for the material. This text provides a survey of ways to dry material samples. Only methods based on removal of water vapour are considered. Methods based on removal of liquid water, e.g. centrifugation, are excluded, as are radioactive techniques, in which water or its vapour are not removed from the sample.

The scientific field of drying is vast. Commercially, there are hundreds of apparatuses available to carry out drying of grains, pharmaceuticals, etc. This text is concerned only with small-scale laboratory drying of relatively small samples of building materials.

---

K. K. Hansen  
Technical University of Denmark, Kongens Lyngby, Denmark

S. Lindmark  
FuktCom, Lund, Sweden

L.-O. Nilsson (✉)  
Lund University, Lund, Sweden  
e-mail: lars-olof.nilsson@byggttek.lth.se

L.-O. Nilsson  
Moistenginst AB, Trelleborg, Sweden

O. Weichold  
IBAC, Aachen, Germany

© RILEM 2018

L.-O. Nilsson (ed.), *Methods of Measuring Moisture in Building Materials and Structures*, RILEM State-of-the-Art Reports 26,  
[https://doi.org/10.1007/978-3-319-74231-1\\_3](https://doi.org/10.1007/978-3-319-74231-1_3)

## 3.2 Evaporable Water—“Moisture”

The water content of interest is the non-chemically bound water, i.e. not the water that is a structural part of the material itself. This water is often referred to as the evaporable water, or the physically absorbed water. The evaporable water may be defined as the difference between the water content at a state of interest and the water content when the sample is in a “dry” state. Consequently, the definition of “dry” is decisive for the determination of water content. This means that what is to be regarded as evaporable water is dependent on the drying technique used. Consequently, what is to be regarded as chemically bound water is also dependent on the drying technique. An insufficiently effective drying method will leave some water in the sample which leads to an underestimation of the water content and thus the pore volume, etc. On the other hand, a too harsh drying technique will remove chemically bound water and will thus lead to an over-estimation of the water content, the pore volume and, for many materials, to a destruction of the material.

Finally, it is important that the drying technique produces repeatable results, i.e. the technique must produce the same result irrespective of where, when and by whom the drying is done.

For ordinary building materials, it is often implicitly understood that evaporable water is the water lost on drying at 105 °C. It is then also understood that the drying is done in ordinary air at the prevailing atmospheric pressure. In practice, this means that the drying is done by equilibrating the water content to the state of the water vapour in the oven, i.e. to a low relative vapour pressure. As will be seen below, this may be an insufficiently well-defined point of reference.

## 3.3 Basic Principles

The basic principle of a drying process is to bring forth a phase change from liquid to vapour and then to remove the vapour from the sample. The phase change may also occur as sublimation, i.e. a direct change from the solid state to vapour. This is done in freeze-drying.

The potential for phase change is the difference in vapour pressure between the water in the sample, and the vapour in its surroundings. Such a difference may be brought about by reducing the vapour pressure of the surroundings or by heating the sample, thus increasing the vapour pressure exerted by its water content. The removal of vapour may be arranged either with an air stream (convective transport) or via a vacuum system.

The most common drying technique is to heat the sample with a stream of warm air, which serves both to heat the sample (thereby raising the vapour pressure of the pore water) and to remove the vapour that is released from the sample. The high temperature also accelerates the rate of vapour removal.

By exposing the sample to a low pressure, like in a vacuum system, water vapour may be removed without raising the sample temperature. This is beneficial when handling heat sensitive materials like cellular plastics, etc. Another way of maintaining a low vapour pressure around the sample is to expose it to ice at a very low temperature, or to expose it to a powerful desiccant, like some salt.

Heating a sample may be done in several ways: Convective heating with hot air, conductive heating via a hot surface, microwave heating, and heating via infrared radiation.

The moisture content determined by any method for measuring moisture depends on, and is defined by, the drying method used. The sample or the specimen is exposed to a surrounding climate where the RH is low, preferably close to zero. As said above, this is done with one of two drying principles: lowering the vapour content  $v$  (or vapour pressure  $p$ ) of the surroundings or raising its vapour content  $v_s(T)$  at saturation by using a high temperature.

$$\text{RH}(v, T) = v/v_s(T)(-)$$
 (3.3.1)

Various methods to perform drying of a sample are described in the next sections. Korpa and Trettin (2006) and Fagerlund (2009) have given a survey of ways to establish a dry climate for drying material samples. According to these references there are four main methods for determining the dry weight. These are drying in a ventilated oven at an elevated temperature, P-drying, D-drying and freeze-drying.

The “problem” of measuring the moisture content of heterogeneous materials is dealt with elsewhere, see Part II Applications. It is a special form of application with several different problems and solutions.

### 3.4 Drying in an Oven

In this method, the sample is exposed to hot air. The heat serves to vaporize the water in the sample and to raise its the vapour pressure, and also to lower the relative humidity of the air in the oven. Most frequently, the temperature is set to be 105 °C. Since the air in the oven is the same air as in the laboratory, the vapour pressure in the oven will be dependent on the climate in the laboratory.

In a ventilated oven the vapour content of the air is equal to the vapour content  $v_{\text{room}}$  of the surrounding air. By raising the temperature of the sample to  $T_{\text{oven}}$  the RH of the sample will, eventually, reach

$$\text{RH} = v_{\text{room}}/v_s(T_{\text{oven}})(-)$$
 (3.4.1)

This means that the equilibrium RH of the dry sample depends on the climate in the laboratory. In winter time the vapour content may be, for example, 7 g/m<sup>3</sup> and in summertime the vapour content may be 14 g/m<sup>3</sup>. If the oven temperature is +105 °C the vapour content at saturation is  $v_s(+105\text{ °C}) \approx 600\text{ g/m}^3$  which gives

$$RH_{\text{winter}}(+105\text{ }^{\circ}\text{C}) = 0.01 \text{ or } 1\%$$

$$RH_{\text{summer}}(+105\text{ }^{\circ}\text{C}) = 0.02 \text{ or } 2\%.$$

While oven-drying at 105 °C is very rapid, the material might be damaged by this technique. For example, in hardened cement pastes oven-drying at temperatures  $\geq 60$  °C damages pores and degrades ettringite and monosulphate. In addition, stresses in the C-S-H-phases are generated, Collier et al. (2008).

For some materials the drying is done at lower temperatures: gypsum, wood, materials with presence of organic fractions (consolidating and protective treatments, traces of paints, etc.) or with presence of high amount of salts (efflorescence). In this case the drying-RH is much higher and the annual variations are large.

Using +50 °C as a drying temperature gives:

$$RH_{\text{winter}}(+50\text{ }^{\circ}\text{C}) = 0.08 \text{ or } 8\%$$

$$RH_{\text{summer}}(+50\text{ }^{\circ}\text{C}) = 0.15 \text{ or } 15\%.$$

Drying in an oven is described in EN-ISO12570. The standard prescribes that the temperature should be set to 40, 70 or 105 °C depending on type of material. The standard says constant mass is reached when the weight change between two consecutive weightings made 24 h apart is less than 0.1% of the total mass. [Note: This value may need to be changed depending on the sample composition. For instance, for a concrete sample containing a small amount of cement paste and a large amount of large aggregate, the weight change relative to the total weight may be less than 0.1% although drying is not completed. One way of handling this is to check the weight change versus the weight of that part of the sample that is capable of absorbing water, Fagerlund (2009).] The standard says samples should be cooled in a desiccator to between 30° and 40 °C before the weighing is done. Specimens are weighed before completely coming back to room temperature in order to minimize any re-absorption of moisture from the air.

Sample drying by exposure to elevated temperature can be achieved also on-site, by the use of portable thermo-balances. These instruments are balances of suitable accuracy equipped with a cover in which a heating source is integrated (infrared heating element or a halogen lamp). The powdered sample (e.g. extracted from building structures by drilling) is put on the weighing pan and then the cover is put on to start the drying procedure. Automatic stop usually occurs when the difference between two subsequent weights is less than a set percentage. Possibly, errors might arise from on-site disturbing factors (wind, slope and vibrations).

Thermogravimetry (TGA) is an experimental technique that consists in subjecting a sample of known mass in a controlled atmosphere to temperature variations and evaluating the weight changes along the experiment. The temperature variations are normally monotonically growing from room temperature until values as high as 1500 °C. Based on the weight losses along the experiment, it is possible to infer many compositional or behavioural features such as: loss of water, loss of

solvent, loss of plasticizer, decarboxylation, dehydroxilation, pyrolysis, oxidation, decomposition, weight percentage of filler, etc.

This experimental technique is normally conducted on very small samples, and on specialized equipment that comprises a pan/crucible to hold the sample, which in turn is held inside a furnace. The pan/crucible with its content is continuously weighted during the controlled temperature programmed experiment. The environment around the sample can be controlled with an inert or reactive gas.

The moisture content in a given sample can be assessed through TGA in the same way that is applied in oven drying. However, as mentioned above, TGA testing has the potential to bring about much additional information by heating up to temperatures well above 105 °C.

Several DVS devices are also able to control the internal relative humidity of the controlled environment around the sample, and allow automatic sorption isotherm testing. Such test is merely conducted by keeping the testing temperature constant, and successively changing the environmental humidity upon successive attainment of hygric equilibrium (i.e. constant weight) between the sample and the environment. The DVS devices with such capability are often called 'sorption analyzers'.

### 3.5 D-drying Using Dry Ice

By circulating the air around the sample over dry ice at  $-78$  °C the vapour pressure of the air can be reduced to 0.07 Pa, Brunauer et al. (1970). This gives a drying at an RH of  $p/p_s(20\text{ °C}) = 0.07/2346 = 0.003\%$ .

The D-drying apparatus consists of a vacuum desiccator attached to a vacuum pump through a side arm of a cold trap, which is cooled by a mixture of solid CO<sub>2</sub> and alcohol at a temperature of  $-79$  °C. The partial pressure of water vapour over dry ice is 0.07 Pa. The vacuum applied to facilitate the drying process should keep the pressure in the system below 4 Pa. Under these conditions, removal of water inside the porous system of a sample is very slow, Korpa and Trettin (2006). The time needed to reach constant sample weight depends on many factors, such as the vacuum level maintained by the vacuum pump used, the sample weight being evacuated, and the sample size; for millimetre-sized samples, it takes at least 14 days.

### 3.6 P-drying Using a Drying Agent

By circulating the air around the sample over an effective drying agent the vapour content of the air can be significantly reduced. One effective drying agent is magnesium perchlorate hydrates (di-hydrate and tetra hydrate) (Mg(ClO<sub>4</sub>)<sub>2</sub>·2H<sub>2</sub>O – Mg(ClO<sub>4</sub>)<sub>2</sub>·4H<sub>2</sub>O) of analytical grade purity to obtain a partial pressure of water of 1.1 Pa at 25 °C, Copeland and Hayes (1953).

( $\text{Mg}(\text{ClO}_4)_2 \cdot 2\text{H}_2\text{O}$ ) maintains a water vapour pressure of about 1.067 Pa, Brunauer (1957). Thus, at 20 °C, it maintains a relative humidity of  $1.06/2346 = 0.045\%$ . Magnesium perchlorate is a very strong oxidant (hazardous). It is therefore recommended that it is not used.

Commercial sources are an anhydrous  $\text{Mg}(\text{ClO}_4)_2$  (CAS 10034-81-8), a dihydrate (CAS 18716-62-6), a hexahydrate (CAS 13446-19-0) and an unspecified hydrate  $\text{Mg}(\text{ClO}_4)_2 \cdot \text{H}_2\text{O}$  (CAS 64010-42-0). No reference has been found for tetrahydrate.

As a desiccant, usually the anhydrous compounds are used, because they give rise to the lowest residual water vapour pressures. For example: anhydrous magnesium perchlorate gives rise to a residual atmospheric water concentration of approx. 5 ppb (approx. 0.012% RH at 20 °C), while the “trihydrate” (This comes from an old reference, so I presume it’s the unspecified hydrate) as well as silica gel (which is mostly used in chemistry nowadays) give rise to a residual atmospheric water concentration of approx. 75 ppb (approx. 0.18% RH at 20 °C), Bower (1934).

In terms of reactivation, the hexahydrate decomposes at 190 °C. References do not say if that is dehydration, but it seems likely since the anhydrous compound decomposes at 250 °C liberating oxygen. In order to regenerate silica gel, it is usually kept in a 120–150 °C oven over night. It comes with a colour indicator, from which one can see when it is dry.

The use of magnesium perchlorate is not recommended anymore, since it can form, even with small amounts of flammable compounds, explosive mixtures which can be shock sensitive.

P-drying is the type of drying that Powers and Brownyard (1948) used in their studies of adsorption of water vapour on hardened Portland cement paste. Powers and Brownyard mention that although the drying is commenced over a mix of  $\text{Mg}(\text{ClO}_4)_2 \cdot \text{H}_2\text{O}$  and  $\text{Mg}(\text{ClO}_4)_2 \cdot 2\text{H}_2\text{O}$ , it may end over a mix of  $\text{Mg}(\text{ClO}_4)_2 \cdot 2\text{H}_2\text{O}$  and  $\text{Mg}(\text{ClO}_4)_2 \cdot 4\text{H}_2\text{O}$ , simply because the  $\text{Mg}(\text{ClO}_4)_2$  reacts with the water given off from the samples.

Powers and Brownyard also used other types of chemicals to dry out “evaporable” water. These were  $\text{P}_2\text{O}_5$ , the magnesium chlorides mentioned above and  $\text{H}_2\text{SO}_4$ . The drying was done in an evacuated desiccator. The amount of water lost on drying was approximately 20–25% by weight of original cement in the samples. The relative amounts of water lost with the different drying agents are given in the Table 3.1.

Powers and Brownyard also compared drying over  $\text{Mg}(\text{ClO}_4)_2$  to drying in an oven at 105 °C. The results are given in the table below. As seen, the drying in a ventilated oven causes further loss of water. Powers and Brownyard comment that no attempt was made to determine the actual water vapour pressure in the oven, and that “This is the incorrect procedure that has frequently been used in studies of this kind.” (Table 3.2).

**Table 3.1** Amount of water retained relative to that retained by  $\text{Mg}(\text{ClO}_4)_2 \cdot 2\text{H}_2\text{O}$ 

Paste No.	$\text{P}_2\text{O}_5^{\text{b}}$	$\text{Mg}(\text{ClO}_4)_2^{\text{c}}$	$\text{Mg}(\text{ClO}_4)_2 \cdot 2\text{H}_2\text{O}$	$\text{H}_2\text{SO}_4$ conc.
1	0.80	0.94	1.00	0.98 <sup>a</sup>
2	0.79	0.94	1.00	1.03
3	0.80	0.95	1.00	1.02
4	0.80	0.95	1.00	1.02
5	0.79	0.95	1.00	1.02
6	0.79	0.94	1.00	1.02

<sup>a</sup>According to Powers and Brownard, this value was probably erroneous

<sup>b</sup> $\text{P}_2\text{O}_5$  is phosphorpentoxide

<sup>c</sup> $\text{Mg}(\text{ClO}_4)_2$  can be reused by drying at 160 °C under continuous vacuum during 16 h

**Table 3.2** Loss in weight in oven as found by isothermal drying over  $\text{Mg}(\text{ClO}_4)_2 \cdot 2\text{H}_2\text{O} + \text{Mg}(\text{ClO}_4)_2 \cdot 4\text{H}_2\text{O}$ 

Sample Nr.	Loss in weight (% of non-evaporable water content)
1	10
2	11
3	10
4	13

### 3.7 Freeze-Drying Using Liquid Nitrogen

In this method a first freezing (at  $-195$  °C) is done by the immersion of the sample in liquid nitrogen for 5 min. Then a freeze-dryer is used in which temperature and vacuum are kept constant (varying literature data from  $-80$  to  $-10$  °C and from  $10^{-1}$  to 6 Pa) i.e. temperature  $-20$  °C and vacuum 6 Pa.

Fagerlund (2009) emphasizes that a sufficient drying time is very important for the results. In his work, he has chosen to consider a weight change of less than 0.001 g per gram of cement paste (i.e. 1‰) over 24 h as sufficient. This is the same relative amount as given in the standard SS/EN-ISO 12570, but in Fagerlund's case, the weight loss is compared to that part of the sample which is able to hold water (the paste); not the total weight of the sample (as in the standard). The most natural procedure would be to compare the rate of weight loss to the determined total content of water. This can be done repeatedly during the measurement procedure.

Freeze-drying is controversially discussed in literature. Gallé (2001) reported freeze-drying as effective with regard to microstructure preservation due to the softening of capillary stress effects at solid-water-vapour boundaries during oven drying. Collier et al. (2008) found that freeze-drying caused more cracking of the microstructure than solvent replacement, vacuum drying and oven drying.

### 3.8 Solvent Replacement

Solvent replacement is a drying method used to be able to dry hydrating cement paste specimens at room temperature to avoid increasing the rate of hydration.

Thin (approximately 3 mm) water saturated cement paste specimens are placed in a sealed container with relatively large volume of technical grade methanol. The methanol is replaced by fresh methanol each second day for two weeks. Finally, the methanol-replaced specimens are dried in a ventilated oven at 105 °C until constant mass.

### 3.9 Distillation

For materials for which a drying procedure may drive off other components than water (e.g. extractive components in wood), one may collect the vapours (by condensation) and determine the water content by distillation, Shmulsky and Jones (2011).

### 3.10 Consequences of Drying—Reasons for Choosing a Specific Drying Technique

At least two major non-desired effects may occur as a consequence of the drying process:

1. The pore volume may change.
2. The pore size distribution may change.

The change in pore volume is due to physical as well as chemical effects. On the physical side, the material structure may be damaged by the strong tensions that occur in the remaining pore water during the drying process. This may lead to collapse of pore walls, and also to an overall net shrinkage. On the chemical side, the material may start to de-compose when the water vapour pressure becomes very low. For instance, gypsum will start losing its crystal water already at about 45 °C. Consequently, materials containing gypsum will lose weight that should not be regarded as evaporable water, but rather as loosely, chemically bound water. Other materials may behave similarly, and thus it is important to have good information on the material composition before drawing any conclusions based on the registered weight losses.

When the matrix is exposed to the high tensions that occur in the remaining pore water, pore walls may collapse causing changes of the pore size distribution. Pores are coarsened, and may open up new ways for moisture transport. Thus a material

that has been dried must be expected to have other properties with regard to moisture than before the drying.

In order to minimize these negative effects of drying:

- Avoid high vapour pressures inside the material
- Avoid steep gradients in temperature
- Avoid steep gradients in pore water pressure
- Reduce the surface tension of the remaining water
- Avoid temperatures that will cause vaporization, melting or decomposition of the solid material.

The first three of these necessitate slow changes in sample temperature and slow changes in the drying climate (from start of drying until drying is completed).

It may be possible to reduce the amount of pressures occurring in a sample during drying by carrying out the drying process in a balanced way. The water inside the material must not be allowed to turn into steam too early or at a too high pressure, moisture gradients should be kept as small as possible, and temperature gradients too should be kept small. All of these call for a slow drying process.

Gradients (in moisture content and in temperature) are affected by the relation of sample size to heating rate and vapour pressure potential. A smaller sample will be less sensitive to harsh drying methods.

Spray-drying is another way of reducing the negative effects of drying: By spraying the surface of the sample with water, extremely low moisture content in the surface zone is avoided. This will facilitate drying since the coefficient of moisture transport may be kept at a reasonably high level at the surface. This is in contrast to ordinary drying in which the surface zone may become dry quickly, which leads to a reduction in moisture transport coefficient, thus hindering the transport from the inner parts of the sample.

Some examples of materials that have to be dried carefully are discussed here.

### **Gypsum**

Gypsum contains crystal water;  $\text{Ca}_2\text{SO}_4 \cdot 2\text{H}_2\text{O}$ . In air at normal vapour pressure, the crystal water will start to decompose when the gypsum is heated to a temperature of some 40–50 °C. The determination of evaporable water can thus be carried out by drying in a desiccator at room temperature, as suggested by ASTM D2216, namely at 23 °C and ~0.5% RH as recommended by Wilkes et al. (2004).

### **Wood**

The major components of wood (cellulose, hemicellulose and lignin) are not known to be decomposed by drying at 105 °C. Extractive components (non-cell wall components) are relatively small and may be vaporized at <105 °C, thus contributing to the weight loss. Wood normally contains about 1–5% of extractive components, heartwood is richer in extractive components, and tropical wood may contain as much as 15%. Standard test methods for moisture determination in wood (ISO 3130:1985) and wood-based panels (EN 322:1994) provides for the oven

drying of the specimens at  $103 \pm 2$  °C. Ringpores connecting adjacent wood cells may be permanently closed during drying. This may change the rate of moisture absorption and moisture transport in the wood. When studying such properties of wood, it may thus be essential to keep in mind the “moisture content history” of the samples when evaluating the results. If drying at 105 °C is not considered suitable, Karl Fischer titration may be used, see Chap. 5.

Shmulsky and Jones (2011), said that “*In most cases, the dry weight is calculated by oven-drying the sample, as would be done for moisture content calculation. Because high temperatures may drive off some of the extractives in addition to the water, it is sometimes desirable to determine the moisture content by distillation, a process that involves condensing and weighing the collected vapour.*”

### **Portland cement paste**

Powers and Brownyard (1948) found that permeability to water flow would increase by a factor 70 if the sample was dried at 70% RH prior to the permeability test.

Brunauer (1957), referring to Copeland and Hayes (1953), says the true value of  $w_n$  is found after drying at a water vapour pressure between that obtained by D-drying and P-drying, i.e. somewhere in the interval 0.0067 Pa and 1.067 Pa. Both Brunauer and Copeland & Hayes concluded that the correct value lies closer to that obtained at 0.0067 Pa than that obtained at 1.067 Pa.

For hardened Portland cement paste, Fagerlund (2009) describes how an erroneous determination of the evaporable water leads to erroneous determinations of chemically bound water. This in turn leads to miscalculation of the porosity and other properties which depend on the amount of hydrated cement.

# Chapter 4

## Calibration Techniques



Miguel-Ángel Climent, Sture Lindmark and Lars-Olof Nilsson

Many moisture-measuring principles have to be calibrated against a sample with known moisture content. The preparation of samples with a well-defined, and evenly distributed, moisture content requires a thorough procedure. This is dealt with in Sect. 4.1. The measuring principles where the state of water is measured in a material need calibration against well-known and well-defined humidity conditions. This is described in Sect. 4.2.

### 4.1 Preparation of Samples for Calibration with Defined Moisture Content

The methods for measuring moisture in building materials and structures are based on a wide range of physical-chemical properties, and some of them can be considered as indirect methods since they make use of a property that is more or less dependent on the moisture content. However, such a property may also be dependent on several other physical variables. For instance, the electrical resistance of concrete is a good indicator of the presence of moisture since the inner electrolyte is the only phase able to conduct current in normal concrete; but the

---

M.-Á. Climent  
University of Alicante, Alicante, Spain

S. Lindmark  
FuktCom, Lund, Sweden

L.-O. Nilsson (✉)  
Lund University, Lund, Sweden  
e-mail: lars-olof.nilsson@byggtek.lth.se

L.-O. Nilsson  
Moistenginst AB, Trelleborg, Sweden

resistance is also dependent on the nature of the porous network and of the chemical composition of the pore solution.

All indirect measuring methods need calibration. In the abovementioned case of measurement of the electrical resistance of concrete, the result in ohms does not provide information on moisture unless we have previously performed an adequate calibration.

#### ***4.1.1 Sample Preparation***

When preparing calibration samples we first need to identify the appropriate requirements of these samples, which, in the case of measuring moisture in concrete, can be listed as:

- (a) Taking into account the composite nature of concrete, (composed of hardened cement paste, aggregates and pore space), the size of the samples must be large enough to ensure representativity. Many test methods of concrete define the minimum size of samples taking into account the size of the large aggregates.
- (b) For each type of measuring method, we must consider its own requirements regarding shape and size of the concrete samples.
- (c) The samples must have a known, well characterized, moisture content.
- (d) The spatial distribution of moisture within the calibration samples must be homogeneous.
- (e) There is a need for a system for keeping unaltered the moisture state of the samples during manipulation, and for ensuring the possibility of repeated measurement on the same sample. It must be considered that, depending on the environmental conditions; concrete can easily dry or absorb water vapour from the atmosphere. The optimum condition would be represented by a system that, in case of small perturbation of the moisture state of the samples (by slight drying or absorption of water vapour), could restore the moisture state through quasi-equilibrium interactions.

To the abovementioned requirements we can add, from the practical point of view, the necessity that the procedures of preparation of the calibration samples should be not excessively time consuming. This is relevant taking into account that the drying of concrete members of a certain size or thickness, by interaction with the atmosphere, may be very lengthy.

In the field of mass transport testing in concrete it has been found that an important influential condition on the transport properties of concrete is its moisture content and distribution, especially at the exposed surfaces of the specimens or structures, Ollivier et al. (1995), Parrott and Chen (1990), Romer (2005), Nokken and Hooton (2002). These facts have led to the conclusion that test methods, for gas permeability and capillary absorption of water, must include a standardized preconditioning, which must result in a controlled average moisture concentration with a uniform distribution, RILEM TC-116-PCD (1999a). The recommended

preconditioning installs a defined intermediate moisture concentration in concrete, which is in equilibrium with the ambient air at 75% relative humidity (RH) and a temperature of 20 °C. The preconditioning procedure consists of a pre-drying step at a temperature of 50 °C, followed by a redistribution phase also performed at 50 °C, RILEM TC-116-PCD (1999b). This last redistribution step was shown to be necessary for obtaining, within reasonable conditioning times, a uniform moisture distribution into the concrete specimens, Parrott (1994). Another preconditioning procedure has been proposed, Carcassès (2002), which includes pre-drying and redistribution of moisture at 80 °C, and allows obtaining two levels of water saturation in concrete: 0.70 and 0.30.

In the case of tests aimed at determining the ionic diffusivity properties through non-saturated concrete, Climent et al. (2002), Nielsen and Geiker (2003), de Vera et al. (2007), Guimarães et al. (2011), Olsson et al. (2013), Antón et al. (2013), there appears another specific requirement of avoiding modifications of the moisture state of the concrete specimen during the diffusion test, which may be rather lengthy. For this reason these type of tests need preconditioning procedures for obtaining concrete samples with known and homogeneously distributed moisture content, requirements (c) and (d); and also they need systems for keeping the moisture state of the sample during the diffusion test, requirement (e).

### ***4.1.2 Proposed Procedure***

Recently, Antón et al. (2013) proposed an experimental procedure for obtaining, (within reasonable conditioning times), and maintaining selected well characterized water contents, which can cover a sufficiently broad and significant range of saturation degrees of the concrete specimens. The protocol also allows determining the ambient relative humidity (RH) value in equilibrium with the preconditioned concrete specimens, in order to define the conditions ensuring the maintenance of the hygric state during the diffusion tests through non-saturated concrete. The proposed procedure has the following steps:

- Obtaining basic drying data at 50 °C (water absorption capacity and drying curves).
- Unidirectional drying of the specimens at 50 °C until reaching the target values for the degree of saturation.
- Redistribution phase in closed containers at 50 °C (with measurement of the quasi-equilibrium RH).
- Storage into controlled RH chambers until and during mass transport tests. This last step allows fulfilling the abovementioned requirement (e), i.e. the samples can be kept during long time without alteration of their moisture state. In the case of small perturbation of the moisture content of the samples, evidenced by mass checking, the quasi-equilibrium water vapour exchanges with the RH controlled environment of the chamber can restore the moisture state of the samples.

There is a possibility that the proposed preconditioning procedures, RILEM TC 116-PCD (1999b), Carcassès et al. (2002), Antón et al. (2013), may be useful for the preparation of calibration samples for some of the methods of measuring moisture described during the work of the RILEM TC 248-MMB committee.

### 4.1.3 Uneven Moisture Content Profiles

A sample with defined moisture content as prepared by the procedure described in Sect. 4.1.2 will get moisture profiles with lower moisture contents closer to the surfaces and higher in the centre. This is due to the procedure of drying and the subsequent redistributing the remaining moisture. The surface regions will first follow the desorption isotherm on drying but when the redistribution starts the surfaces are following scanning curves. When finally equilibrium is reached, the moisture content close to the surfaces will be lower than the average value across the specimen volume, see Fig. 4.1.

A possible way to avoid this uneven moisture content distribution is to dry the sample at the intended RH at equilibrium. In such a way all points in the sample are following the desorption isotherm to equilibrium. This will of course take a long time but drying at elevated temperature can shorten the procedure.

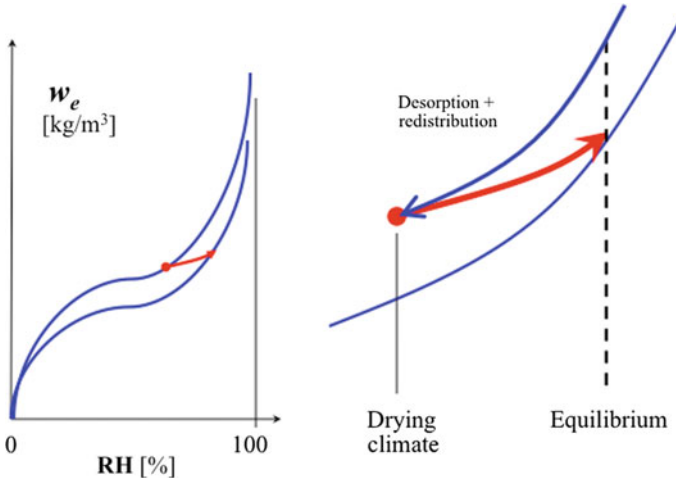


**Fig. 4.1** The moisture history of the surfaces of a sample that is conditioned to a defined average moisture content by drying and redistribution. The right picture is a detail of the left

## 4.2 Preparing Calibration Conditions with a Defined RH by Saturated Salt Solutions

The most common way to prepare calibrating conditions with a well-defined RH is to use saturated salt solutions. Alternative ways are several, e.g. solutions with a defined concentration of an acid, but are not as frequently used. Here, a short description is made of how to prepare saturated salt solutions in order to generate a certain level of relative humidity.

The basic principle is to prepare a solution that is well oversaturated so that an amount of non-dissolved salt is visible in the solution. For further information, the reader is referred to the European standard EN 12571, the Nordic standard Nordtest 340, Nordtest (1988), and the American standard ASTM E104-02.

### 4.2.1 Warnings

Some saturated solutions may be corrosive and/or harmful to health, and thus care should be taken when handling them. Even the vapours may have those properties. Some salts are harmful to life in water, and thus such salts must be taken care of in an appropriate way.

### 4.2.2 Container

The container in which the salt solution is kept must be of a quality which is not affected by the salt solution (e.g. glass is often suitable). Make sure the container has a tight lid so that there are no air leakages. In some cases though, it may be necessary to have a container with a small ventilation in order to avoid any pressure changes inside the container. Such a vent must be made small in order not to affect the relative humidity in the container. If the container is ventilated, carbon dioxide will be present in the container, and thus materials containing  $\text{Ca}(\text{OH})_2$  will become altered during the conditioning process.

According to the American standard, the container should have such proportions that there is not more than  $25 \text{ cm}^3$  of air per  $\text{cm}^2$  of salt solution surface. Generally though, the container should be made as small as possible. A small fan may be installed in the container to make the air circulate. This requires that the heat released by the fan motor does not disturb the temperature inside the container. To exclude this possibility, the motor may be mounted outside the container.

### ***4.2.3 Quality of Salt and Water***

Both standards prescribe the use of reagent grade chemicals (salts). The European standard prescribes distilled water. The American standard prescribes water produced by distillation, ion exchange or reverse osmosis followed by distillation.

### ***4.2.4 Mixing Salt Solutions***

In the European standard, it is said that the solution should be prepared by mixing the correct amounts of water and salt (as given in a table in the standard) and then heating the mixture to a given temperature, and then the solution shall be let to cool slowly under constant stirring.

According to the American standard, the solution shall be prepared by covering the bottom of the container with a sufficient amount of salt (a layer with a thickness of a few centimetres), and then adding water until the mixture becomes a thick slurry.

If the solution will lose or gain moisture during its use, the concentration will change. Thus it is important to prepare the solution in such a way that it does not go dry, nor becomes diluted during use (also see below).

### ***4.2.5 Temperature Stability***

The relative humidity exerted by saturated salt solutions is temperature dependent. Thus, it is necessary to maintain constant temperature in the test chamber. Temperature fluctuation of  $\pm 0.1$  °C may change the RH by some  $\pm 0.5\%$ . (The relative humidity exerted by various salt solutions at different temperatures are given in both standards.)

### ***4.2.6 Preferred Salts***

Many salts are available for generating fixed relative humidities, for instance see Greenspan (1977). According to the American standard, not all of these are truly suitable though, because they are not sufficiently accurate, or may change their properties too easily. The standard specifies 11 salt solutions that are said to be stable for at least one year. These salts generate relative humidities in a range from 3 through 98%RH, see Table 4.1.

**Table 4.1** Equilibrium Relative humidity values for saturated aqueous salt solutions as given in ASTM E104

Temp (°C)	Caesium- fluoride <b>HFP4</b>	Lithium- bromide <b>HFP7</b>	Lithium- chloride <b>HFP12</b>	Potassium- acetate <b>HFP23</b>	Magnesium- chloride <b>HFP33</b>	Potassium- carbonate <b>HFP43</b>	Sodium- bromide <b>HFP59</b>	Potassium- iodide <b>HFP70</b>	Sodium- chloride <b>HFP75</b>	Potassium- chloride <b>HFP85</b>	Potassium- sulfate <b>HFP98</b>
5	–	7.4 ± 0.8	13 (11.2– 14.0)	–	33.6 ± 0.3	43.1 ± 0.5	63.5 ± 0.8	73.3 ± 0.4	75.7 ± 0.3	87.7 ± 0.5	98.5 ± 1.0
10	–	7.1 ± 0.7	13 (11.3– 14.3)	23.4 ± 0.6	33.5 ± 0.3	43.1 ± 0.4	62.2 ± 0.6	72.1 ± 0.4	75.7 ± 0.3	86.8 ± 0.4	98.2 ± 0.8
15	4.3 ± 1.4	6.9 ± 0.7	12 (11.3– 13.8)	23.4 ± 0.4	33.3 ± 0.3	43.2 ± 0.4	60.7 ± 0.6	71.0 ± 0.3	75.6 ± 0.2	85.9 ± 0.4	97.9 ± 0.7
20	3.8 ± 1.1	6.6 ± 0.6	12 (11.1– 12.6)	23.1 ± 0.3	33.1 ± 0.2	43.2 ± 0.4	59.1 ± 0.5	69.9 ± 0.3	75.5 ± 0.2	85.1 ± 0.3	97.6 ± 0.6
25	3.4 ± 1.1	6.4 ± 0.6	11.3 ± 0.3	22.5 ± 0.4	32.8 ± 0.2	43.2 ± 0.4	57.6 ± 0.4	68.9 ± 0.3	75.3 ± 0.2	84.2 ± 0.3	97.3 ± 0.5
30	3.0 ± 0.8	6.2 ± 0.5	11.3 ± 0.3	21.6 ± 0.6	32.4 ± 0.2	43.2 ± 0.5	56.0 ± 0.4	67.9 ± 0.3	75.1 ± 0.2	83.6 ± 0.3	97.0 ± 0.4
35	2.7 ± 0.7	6.0 ± 0.5	11.3 ± 0.3	–	32.1 ± 0.2	–	54.6 ± 0.4	67.0 ± 0.3	74.9 ± 0.2	83.0 ± 0.3	96.7 ± 0.4
40	2.4 ± 0.6	5.8 ± 0.4	11.2 ± 0.3	–	31.6 ± 0.2	–	53.2 ± 0.5	66.1 ± 0.3	74.7 ± 0.2	82.3 ± 0.3	96.4 ± 0.4
45	2.2 ± 0.5	5.7 ± 0.4	11.2 ± 0.3	–	31.1 ± 0.2	–	52.0 ± 0.5	65.3 ± 0.3	74.5 ± 0.2	81.7 ± 0.3	96.1 ± 0.4
50	2.1 ± 0.4	5.5 ± 0.4	11.1 ± 0.3	–	30.5 ± 0.2	–	50.9 ± 0.6	64.5 ± 0.3	74.5 ± 0.9	81.2 ± 0.4	95.8 ± 0.5
55	2.0 ± 0.4	5.4 ± 0.3	11.0 ± 0.3	–	29.9 ± 0.2	–	50.2 ± 0.7	63.8 ± 0.3	74.5 ± 0.9	80.7 ± 0.4	–
60	2.0 ± 0.4	5.3 ± 0.3	11.0 ± 0.3	–	29.3 ± 0.3	–	49.7 ± 0.8	63.1 ± 0.4	74.4 ± 0.9	80.3 ± 0.5	–
65	2.1 ± 0.5	5.3 ± 0.3	10.9 ± 0.3	–	28.5 ± 0.3	–	49.5 ± 1.0	62.5 ± 0.4	74.2 ± 0.9	79.9 ± 0.5	–
70	2.2 ± 0.6	5.2 ± 0.3	10.8 ± 0.4	–	27.8 ± 0.3	–	49.7 ± 1.1	61.9 ± 0.3	74.1 ± 0.9	79.5 ± 0.6	–
75	2.4 ± 0.7	5.2 ± 0.3	10.6 ± 0.4	–	26.9 ± 0.3	–	50.3 ± 1.3	61.4 ± 0.5	74.0 ± 0.9	79.2 ± 0.7	–
80	2.6 ± 0.8	5.2 ± 0.3	10.5 ± 0.5	–	26.1 ± 0.4	–	51.4 ± 1.5	61.0 ± 0.5	73.9 ± 0.9	78.9 ± 0.8	–

### 4.2.7 *Things to Think About*

If the solution is to be used in order to dry out a material sample, care should be taken to make sure that the solution remains (over-)saturated throughout the drying process. This means that the solution should be prepared with a sufficient excess of salt. If samples are to be moistened, the opposite applies. Thus, the exact mixing techniques described in the two standards may need to be modified according to the user's needs. It is recommended that solutions are checked regularly (with a separate RH-instrument) to make sure the intended relative humidity is attained (there is always the risk of using the wrong salt, and some salt solutions change their properties due to hydrolysis or through reaction with environmental components, such as carbon dioxide).

Some salt solutions release large amounts of heat during mixing. Add reagents slowly to keep temperature under control.

There must always be an amount of undissolved salt left in the salt solution. Otherwise, the balance between absorption of water by the salt, and evaporation of water from the solution will not balance each other, and then the intended relative humidity will not be reached.

## 4.3 **Preparing Calibration Conditions with a Defined RH by Climate Chambers**

Hygrometric equipment can be calibrated by placing the equipment, or more frequently the probe, inside a climate chamber. The RH of the climate chamber can be controlled in different ways.

### 4.3.1 *Two-Pressure Chambers*

A common technique to create a precise RH in a chamber is the two-pressure technique where a pressurized air stream is saturated with water vapour and then let into a chamber with another air pressure. The two air pressures control the RH in the chamber

$$\frac{RH_1}{RH_{sat}} = \frac{B + P_1}{B + P_{sat}} \quad (4.3.1)$$

where  $RH_1$  is the RH in the chamber,  $RH_{sat}$  is the RH (100%) of the saturated air stream,  $B$  is the barometric air pressure,  $P_1$  is the air pressure in the chamber and  $P_{sat}$  is the air pressure of the saturated air stream before the chamber. The equation assumes that the temperature in the air stream is constant.

Ahlgren (1972) built a two-pressure apparatus for precise controlling RH in a chamber, see Fig. 4.2. The whole apparatus, including the pipes with the air stream, was placed in a large container with a liquid to maintain a constant temperature of the air stream.

Today two-pressure apparatuses are commercially available, cf. e.g. Fig. 4.3 from [www.thunderscientific.com](http://www.thunderscientific.com). They do not include the large temperature controlling volume of a liquid. Consequently, the equipment must be placed in a climate room with small temperature variations.

### 4.3.2 Mixing Air Streams

By mixing two air streams, one that is saturated with water vapour and one that is dry, any RH can be obtained in a chamber. Commercially available sorption balances, e.g. a Dynamic Vapour Sorption (DVS) balance, can be used for this purpose.

The RH is regulated by a PID (proportional–integral–derivative) regulator, which shortly opens the magnetic valves for the saturated air stream and the dry air stream, respectively. The RH signal for the PID comes from a calibrated Rotronic sensor, which can also regulate the temperature inside the climate chamber by use of another PID regulator (Fig. 4.4).

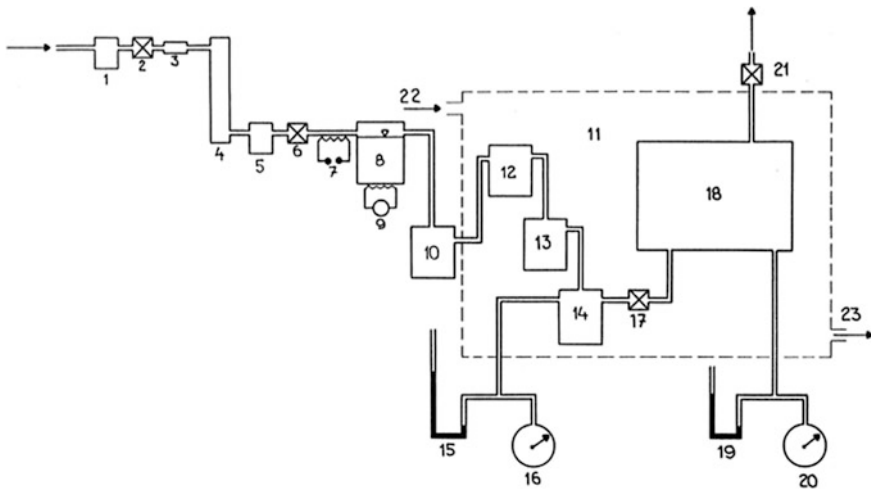


**Fig. 4.2** The two-pressure apparatus by Ahlgren (1972). 18 is the chamber and 11 is the volume of liquid. The air pressures are measured in points 16 and 20

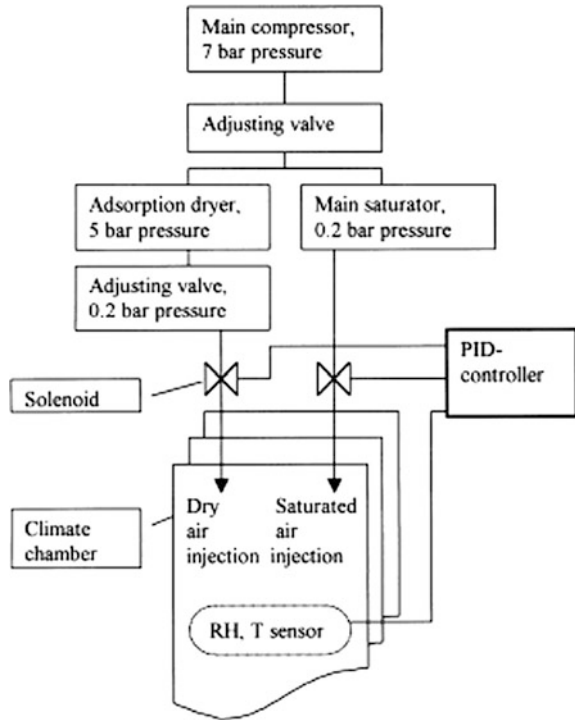


**Fig. 4.3** A two-pressure apparatus by Thunder Scientific Corporation at the Laboratory of Building Materials at Lund University (photo L.-O. Nilsson)

#### 4.4 Calibration Issues in Measuring Moisture in Old Masonries

Calibration is a key feature of most non-destructive surveys, McCann and Forde (2001). Apart from calibration issues connected to the different non-destructive techniques, discussed in the relevant chapters of Part I, moisture measurement in old masonries raises additional problems connected to the heterogeneity of historical building materials (fired clay bricks, stones, etc.). Even adjacent bricks or stone ashlar may exhibit extremely different mass transport properties due to their far different porosity and pore size distribution. In Fig. 27.1, the pore size distribution curves of nine brick samples from a single masonry in the *SS. Crocefisso* Church in the Monumental Cemetery of Ravenna (1817) are reported as an example in Sandrolini and Franzoni (2006). Their impressive difference is due to the pre-industrial bricks technology, involving variable firing temperatures. The frequent re-use of bricks taken from older demolished buildings further contributes to the heterogeneity of historic masonry materials. Significant microstructural heterogeneity may be found also in stone ashlar, due to their different location in the quarries, different sedimentary members, etc.

**Fig. 4.4** The principle of the dry and saturated air streams, Strømdahl (2000)



Due to this heterogeneity, calibration should be theoretically performed for each single brick element or stone ashlar, which of course would cancel the advantages of non-destructive survey. In any case, a significant number of samples should be considered for a suitable calibration.

When monitoring moisture in historic masonry it is highly recommended that moisture measurements always be made in the same points.

# Chapter 5 Gravimetry



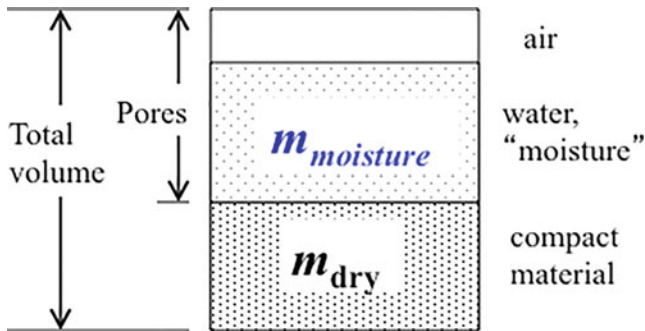
Lars-Olof Nilsson

The principle of using gravimetry to measure the moisture content of a sample or a specimen is to determine the weight by a balance before and after drying.

$$m_{\text{wet}} = \text{weight of the wet sample (kg)}$$

$$m_{\text{dry}} = \text{weight of the dry sample (kg)}$$

where  $m_{\text{wet}}$  equals  $m_{\text{moisture}} + m_{\text{dry}}$ .



From these two weights the moisture ratio can be presented as by dry weight

$$u = (m_{\text{wet}} - m_{\text{dry}}) / m_{\text{dry}} (-) \tag{5a}$$

---

L.-O. Nilsson (✉)  
Lund University, Lund, Sweden  
e-mail: lars-olof.nilsson@byggtek.lth.se

L.-O. Nilsson  
Moistenginst AB, Trelleborg, Sweden

or by wet weight

$$u_{\text{wet}} = (m_{\text{wet}} - m_{\text{dry}}) / m_{\text{wet}}(-) \quad (5b)$$

In most cases these moisture ratios are given as per cent by dry or wet weight.

The dry weight depends of course on the drying procedure being used. This is described in Chap. 3.

## 5.1 Errors and Uncertainties

The main errors when using gravimetry to determine the moisture ratio of a sample are five, in principle:

- drying of the sample during sampling and handling, before the wet weight is determined
- loss of material from the sample during handling
- wrong temperature or vapour content in the drying chamber
- incomplete drying
- lack of representativity of a sample of a heterogeneous material.

The moisture loss before the wet weigh determination is mainly connected to the procedure for sampling. This is further described in Chap. 22.

Errors connected to an incomplete drying are possible mostly when drying is carried out directly on-site, as in the case of portable thermo-balances. Here the weight measurement is performed very frequently (intervals of some minutes) and complete drying is not necessarily achieved when measurement stops; moreover weight measurement might be affected by wind, vibrations, etc.

The error connected to lack of representativity can be reduced by taking a larger sample, whose size must be determined on the basis of the nature of the material. Another alternative is to determine the degree of capillary saturation DCS, see Sect. 5.2 and Chap. 27.

## 5.2 Uncertainty Due to Sample Inhomogeneity

If a composite material consists of a mix of a porous part that can contain moisture and a non-porous part that has no moisture content, the determination of the moisture ratio of such a material depends on the representativity of the sample taken. With small samples from a material with large non-porous parts the representativity might be extremely bad. An obvious example is a small sample from a concrete with large aggregate particles.

The error  $E$  of the representativity can be expressed by

$$E = \Delta m_{\text{dry}} / m_{\text{dry}} (-) \quad (5.2.1)$$

where  $m_{\text{dry}}$  is the dry weight of a perfectly representative sample and  $\Delta m_{\text{dry}}$  is the weight of the “additional” amount of non-porous parts making the sample non-representative.

The moisture ratio  $u$  of such a sample would be

$$u = (m_{\text{wet}} - m_{\text{dry}}) / (m_{\text{dry}} + \Delta m_{\text{dry}}) \quad (5.2.2)$$

which is equal to

$$u = (m_{\text{wet}} - m_{\text{dry}}) / (m_{\text{dry}}(1 + E)) = u_0 / (1 + E) \quad (5.2.3)$$

where  $u_0$  is the moisture ratio of a perfectly representative sample. The error in the moisture ratio is a factor of  $1/(1 + E)$ .

The error is of course smaller the larger sample (larger  $m_{\text{dry}}$ ) that is taken. To overcome the drawback when it is essential to take small samples from a heterogeneous material the degree of capillary saturation can be determined, see Chap. 27.

# Chapter 6

## Chemical Reaction



Lars-Olof Nilsson, Miguel-Ángel Climent and Oliver Weichold

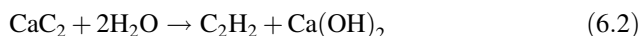
### 6.1 Measuring Principle

The principle of using chemical reactions to measure the moisture content of a sample is to determine the consumption of a reactant A that reacts chemically with water or to determine the amount of a reaction product B from such a reaction



### 6.2 The Carbide Method

The only commercially available chemical method for measuring moisture is the calcium carbide method (“CM-gerät” in German). The principle is based on the chemical reaction between calcium carbide and water that produces acetylene gas



---

L.-O. Nilsson (✉)  
Lund University, Lund, Sweden  
e-mail: lars-olof.nilsson@byggtek.lth.se

L.-O. Nilsson  
Moistenginst AB, Trelleborg, Sweden

M.-Á. Climent  
University of Alicante, Alicante, Spain

O. Weichold  
IBAC, Aachen, Germany

© RILEM 2018

L.-O. Nilsson (ed.), *Methods of Measuring Moisture in Building Materials and Structures*, RILEM State-of-the-Art Reports 26,  
[https://doi.org/10.1007/978-3-319-74231-1\\_6](https://doi.org/10.1007/978-3-319-74231-1_6)

For each two moles of water one mole of acetylene gas is produced. The amount of gas is determined by measuring the gas pressure in a steel container (Fig. 6.1).

A certain amount of wet sample is put into a steel container. Pieces of a material may need to be crushed before put into the container. Steel balls are then placed in the container, a glass ampoule containing calcium carbide is placed on top and the container is closed. The container is shaken so the glass ampoule is crushed and the carbide is mixed with the moist sample. The chemical reaction between water in the sample and the carbide produces acetylene gas and the gas pressure is determined with a manometer.

The gas pressure is translated into an amount of water in a table. For a certain weight of the wet sample the moisture ratio can be read in such a table.

Since the amount of water is proportional to the amount of gas and the wet weight of the sample is used, the output is the moisture ratio  $u_{\text{wet}}$  by wet weight.

### 6.3 The Carbide Method Versus Oven Drying

Since a material sample might have to be crushed before the moisture ratio is determined some water might evaporate before the initial weight is determined. This is especially relevant for concrete samples. A comparison is shown in Fig. 6.2.

Figure 6.2 shows that the carbide method could not detect moisture contents larger than some five per cent by weight, most probably due to drying of the crushed samples.

In addition, the very small samples used cause very large variations when samples are taken from heterogeneous materials, cf. Fig. 27.6.

**Fig. 6.1** The equipment for the calcium carbide method, in principle

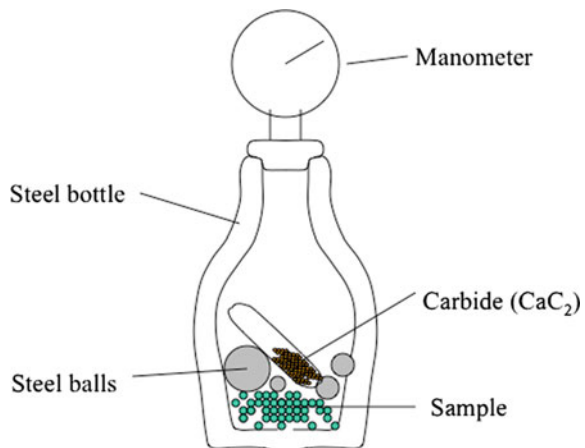
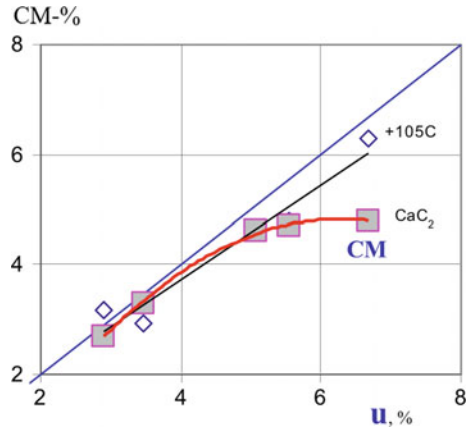
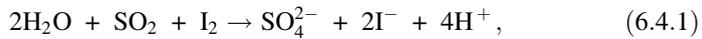


**Fig. 6.2** An example of a comparison between the moisture ratio ( $u$ ) determined by oven drying of samples and determined by the calcium carbide method (CM) on small crushed concrete samples. Data from Nilsson (1980)

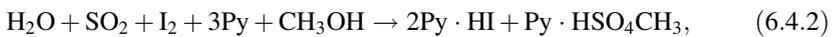


## 6.4 The Karl Fischer Titration Method

The Karl-Fischer-Titration (KFT) is a method for the quantitative determination of water based on the chemical reaction between sulphur dioxide and iodine



which only works in the presence of water and is known as the Bunsen reaction, Scholz (1984). However, using this reaction as an analytical tool requires the presence of a solvent, usually an alcohol such as methanol, and a base. This modification was introduced by Fischer in 1935 for the method that today bears his name, Fischer (1935). In the presence of an alcohol and a base, the reaction becomes



where Py denotes the base pyridine ( $\text{C}_5\text{H}_5\text{N}$ ) and  $\text{Py} \cdot \text{HI}$  is the pyridinium iodide  $\text{C}_5\text{H}_6\text{N}^+\text{I}^-$ , Smith et al. (1939). For practical and health reasons pyridine is normally substituted by another suitable nitrogen-containing base  $\text{R}_3\text{N}$ , e.g. imidazole, Scholz (1984), which then forms the adduct  $\text{R}_3\text{N} \cdot \text{HSO}_4\text{CH}_3$ .

Equations 6.4.1 and 6.4.2 clearly show that the reaction consumes water and only proceeds as long as water is present. For each molecule of water, one molecule of iodine is consumed, although several circumstances may modify the stoichiometry of the reaction. The iodine can be added as solution or generated electrochemically in the reaction mixture. However, the KF reagent must be standardized against a standard solution of water in methanol, Bassett et al. (1978). The end-point of the titration is detected when the water is completely consumed and the added iodine is no longer reduced causing the reaction medium to turn brown.

The end point detection of the titration may be performed through one of the following methods, Bruttel and Schlink (2006):

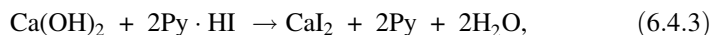
- (a) Visual or photometric indication. This method is not convenient for coloured sample solutions.
- (b) Bi-amperometric indication. In this case two polarizable electrodes (usually platinum) are used. A constant potential difference is established between them and the resulting current is measured. It is a method conceptually similar to polarography. The end point of the titration and, thus, the water content, can be obtained by plotting the recorded current against volume of added reagent and determining the turning point of the curve.
- (c) Bi-voltammetric indication. In this case a small direct or alternating current is applied between electrodes and the resulting potential is measured. The determination of the water content is similar to the bi-amperometric indication.

Equation 6.4.2 also shows that the titration works in solution and the KFT can, thus, only detect water that is dissolved in the solvent. Suspending a solid sample in a dry alcohol causes the physically adsorbed surface water to be released into the solution. However, there is not enough information to ensure that this methodology can quantitatively extract the water contained in the capillary and gel pores of hardened cement paste.

Some details are important for ensuring reliability of results:

- The KF reagent must be added as precisely, accurately and reproducibly and with as high a resolution as possible. This is readily accomplished through the actual automatic titration systems.
- The titration cell must be as impervious as possible to atmospheric water vapour.
- The water adhering to the walls of the titration cell (surface water film) must be removed.

In addition to this, a number of compounds interfere with the chemical reaction in Eq. 6.4.2. Despite the presence of a base, the KFT produces an acidic environment during the reaction. Thus, the most problematic compounds for the determination of water in cement and concrete materials are hydroxides, carbonates, and silicates, which can liberate water upon contact with acidic compounds, e.g.



and thus give a higher water content. Similarly, in acidic media, silanol and silanolate groups can undergo intermolecular condensation to form siloxane bridges or react with the alcohol to form alkoxy silanes liberating water in the process. Furthermore, iron salts can react with either iodine or sulphur dioxide and falsify the result.

As a consequence, it is generally not recommended to run the KFT in the presence of the cement sample, but rather heat it in an external oven and transport the evaporated water to the liquid medium in a stream of dry carrier gas,

Smith et al. (1939). This, of course, raises the question of how to heat the sample without causing structural damages or detect water that was bound in the CSH phases, cf. Chap. 3. One reference recommends heating the sample to 1000 °C in order to determine the true water content and claims this method to be more accurate than the loss on ignition, since the simultaneously expelled CO<sub>2</sub> from carbonated samples is not considered in the KFT, Rechenberg (1976).

Another report compares the differences in water content when heating Portland cement to 107 and to 160 °C and finds essentially the same values, Margolis et al. (2004). Although it is not discussed which type of water is liberated, a contribution from the decomposition reaction of Portlandite according to  $\text{Ca}(\text{OH})_2 \rightarrow \text{CaO} + \text{H}_2\text{O}$ , which occurs at 580 °C, could be excluded.

Despite this, the KFT method is probably the most accurate method and the method of choice for the determination of water that is or can be brought into solution. There exist a number of published procedures and standards for analyzing samples of very different nature: liquids, solids, and even gases. It is used as a common analytical method in the food, pharmaceutical, petrochemical, and many other industries. Regarding the field of solid building materials it has not been used much, although there are applications for gypsum (plaster of Paris), regulated set cement, and wood, Bruttel and Schlink (2006). It has been applied for other solid materials like minerals, carbon powder, etc. However, to the best of our knowledge, the application of the KF method to hardened cement paste, mortar, or concrete has not been reported. One of the problems with solid samples is that they need to be thoroughly comminuted and homogenized, which implies an intense manipulation of the samples. Another fact with solids is that the amount of sample usually tested is in the range of 0.2–1 g, which may be also a problem with inhomogeneous materials like concrete.

In conclusion we must state that the KF method can be used to determine the water content in various construction materials. There even exist proven procedures for wood, gypsum and regulated set cement. In the case of concrete, even though in principle the method can be applied, it seems that several inconveniences may arise from the preceding necessary handling of the sample. The crushing and grinding or milling of the sample to the adequate grain size could modify the water content. The representativeness of the concrete samples may also be inadequate with the usual size of the analysed samples, which is in the range 0.2–1 g. Furthermore, since the oven method should be used for concrete samples, the water released will be dependent on the temperature imposed in the oven. So, a careful selection of the heating regime would be necessary in connection with the fraction of water of interest.

# Chapter 7

## Infrared Thermography



Jean-François Lataste and Lars-Olof Nilsson

### 7.1 Introduction

The infrared thermography is a non-destructive technique (NDT) allowing the evaluation of the material surface temperature. It is a non-contact technique, particularly adapted for high yield investigation. The method records the electromagnetic ray in the infrared spectrum, emitted from the external surface. The surface temperature of a material is influenced by the moisture conditions in some cases; this could be detected by IR-thermography.

Thermal radiations are functions of a material's internal properties (composition, rates for various phases, as also condition, and possible damage), as well as external conditions (sunlight, artificial or natural heat source), Maldague (2001). The infrared thermography allows assessing the luminance, which can be translated in term of surface temperature, through the radiometric equation, Sirieix et al. (2005). The principle is then to assess the effect resulting on the surface of the material's internal characteristic, influenced by surroundings conditions.

Measurement is generally done with a numeric thermal camera that records 2D the thermal field on the investigated surface, cf. Fig. 7.1. The interpretation is essentially qualitative aiming at flaws detection or extension (for zoning).

---

J.-F. Lataste  
Université de Bordeaux, Bordeaux, France  
e-mail: jean-francois.lataste@u-bordeaux.fr

L.-O. Nilsson (✉)  
Lund University, Lund, Sweden  
e-mail: lars-olof.nilsson@byggtek.lth.se

L.-O. Nilsson  
Moistenginst AB, Trelleborg, Sweden

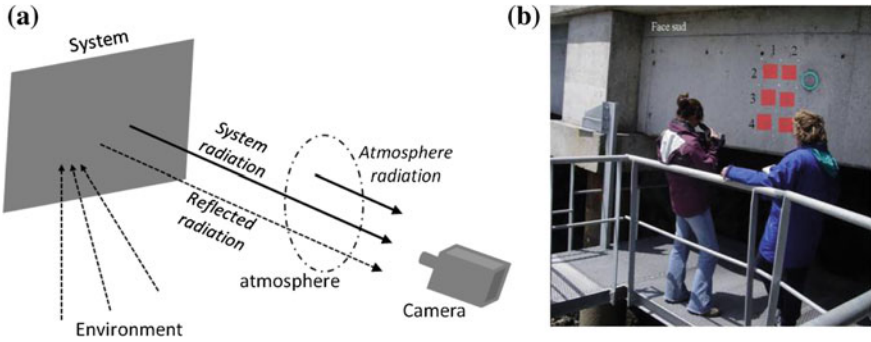


**Fig. 7.1** **a** Composition of the ray recorded by the thermal sensor, Sirieix and Defer (2005); **b** view of an acquisition

## 7.2 Physical Principle and Measurement

Thermal transfer within isotropic materials is essentially a conductive process. It depends mainly on thermal conductivity and the specific heat, as explain by Fourier's equation:

$$\lambda \nabla^2 T_{(x,y,z,t)} = \rho \cdot C_p \cdot \frac{\partial T_{(x,y,z,t)}}{\partial t}. \quad (7.2)$$

where  $T$  is the temperature ( $^{\circ}\text{C}$ ),  $t$  is the time (s),  $\lambda$  is the thermal conductivity ( $\text{W}/(\text{m}\cdot\text{K})$ ),  $\rho$  the volumetric mass ( $\text{kg}/\text{m}^3$ ),  $C_p$  the specific heat ( $\text{J}/(\text{kg}\cdot\text{K})$ ),  $x$ ,  $y$ ,  $z$  the coordinates of points (m). Others thermal properties, as thermal diffusivity, effusivity and inertia, are mainly associated with dynamic thermal behaviour and will not be considered here.

The question of heat transfer in concrete is complex due to the material's heterogeneity: composed by cement, fine and coarse aggregates, water and voids to make finally a three-phase material. To simplify the problem, one can subdivide the conduction process as the sum of conduction process through each component, Larget (2011).

## 7.3 Influence of Moisture on Thermal Conductivity

Free water in concrete porosity has a significant effect on its thermal properties. Even if water is less conductive than concrete, its properties appear higher than air (more than 20 times higher). Thermal conductivity increases with water content. The increase ratio could reach up to 70% between dry concrete and totally saturated concrete, Campbell-Allen et al. (1963). Table 7.1 gives some values for concretes with various saturation levels.

**Table 7.1** Thermal conductivity measured on several concretes with various type of sands, on dry or saturated conditions, Khan (2002)

Type of sand	Conductivity (W/(m·K))			
	Quartz sands (from red soils)		Sands with mica (grey river sands)	
Saturation rate	Dry	Saturated	Dry	Saturated
Basalt	2.26	3.52	1.97	3.24
Limestone	2.03	2.92	1.60	2.71
Sandstone	2.21	3.61	1.91	2.90

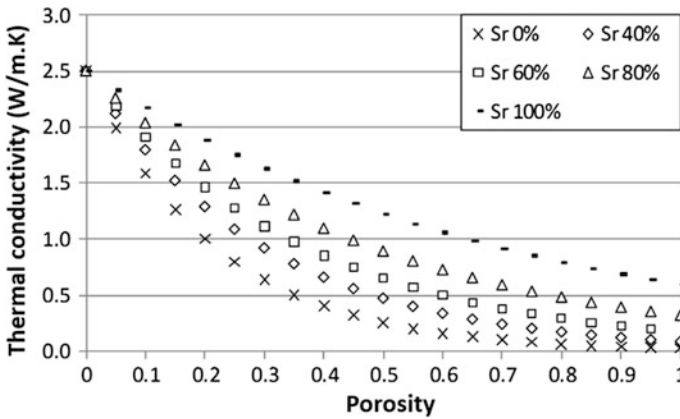


**Fig. 7.2** Thermal conductivity for concretes in function of porosity and saturation rate, Larget (2011)

An empirical model allows assessment of the water content effect, Beziat (1987). It considers that thermal conductivity of a porous material equals the geometrical average of the conductivity of each component, weighted by their volumetric ratios. This equation is illustrated in Fig. 7.2.

### 7.4 Influence of Moisture on Specific Heat

The specific heat of water is far higher than for concrete or air voids. The concrete specific heat is significantly influenced by its saturation, dos Santos (2003), Neville (2000).

The specific heat of a multiphasic material could be assessed according to the Newmann-Kropp equation, which is like a law of mix. It considers the specific heat of each phase weighted by its mass proportion.

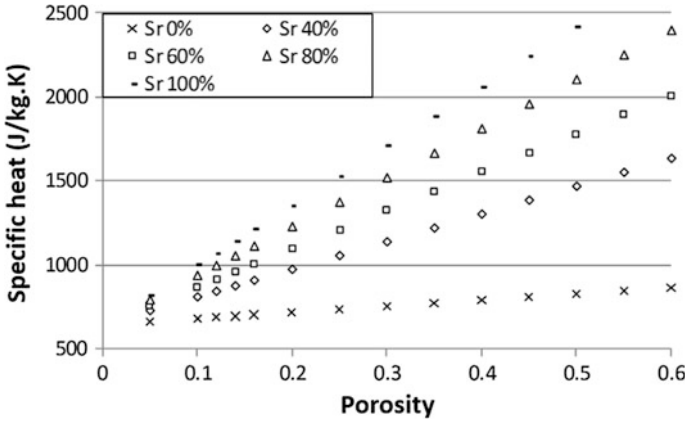


**Fig. 7.3** Specific heat for concretes as function of porosity and saturation degree (Sr), Target (2011)

An illustration of this law to assess specific mass of concretes is given in Fig. 7.3. The specific heat is proportional to porosity and the influence of water saturation increases for more porous materials.

## 7.5 Influence of Moisture on Surface Temperature Due to Evaporation

Evaporation from a wet surface depends on the water vapour content (or pressure) at the surface  $v_{surf}$  and in the surrounding air  $v_{air}$ , the “wetness” of the surface and the air velocity  $u$  over the surface. The rate of evaporation  $J_{evap}$  can be described by

$$J_{evap} = \beta(u)(v_{surf} - v_{air}) \text{ or}$$

$$J_{evap} = \frac{(v_{surf} - v_{air})}{Z_{surf}(u)} (\text{kg}/(\text{m}^2\text{s})) \quad (7.5)$$

where  $\beta(u)$  is the surface vapour transfer coefficient and  $Z_{surf}$  is the resistance to moisture flow of the surface.

For the evaporation of water a certain amount of energy is required per unit weight. This energy is “taken” from the surface, which means that the surface is cooled down. The resulting surface temperature depends on the energy balance at the surface, cf. Eq. (7.2), i.e. the required energy for the evaporation, the heat flow to the surface from the material and the heat flow from the surface to the surrounding air. This surface temperature can be detected by IR-technique and quantify the magnitude of the evaporation and, in turn, the water vapour content  $v_{surf}$  and the surface “wetness”.

### 7.6 Examples

The use of infrared thermography in civil engineering for moisture content assessment is limited to the detection and the limitation of sectors on a structure. An example could be given through an investigation done in a metro station in Montreal (Quebec, Canada) where the infrared thermography highlights the moisture ingress through a concrete wall, cf. Fig. 7.4.

The investigation shows the water table level behind the wall. The measures allow zonation of the more moistened part of the wall (more cold than the part of the wall above the water table level). On the figure we could also see the influence of surface condition of the wall. Locally, some water flows on the wall led to moss deposit on the surface. The surface characteristics changed by this, explains the darker part of the wall which is not directly linked to a colder sector. This illustrates the difficulty to inverse the results for quantification of water content, even if this technique appears adapted for detection.

Johansson (2005) used IR-thermography at laboratory conditions to determine moisture profiles in specimens that been exposed to capillary suction from one end. The surface temperature profile was measured by an IR-camera and the surface temperature was then translated into moisture contents by calibration. An example is shown in Fig. 7.5.

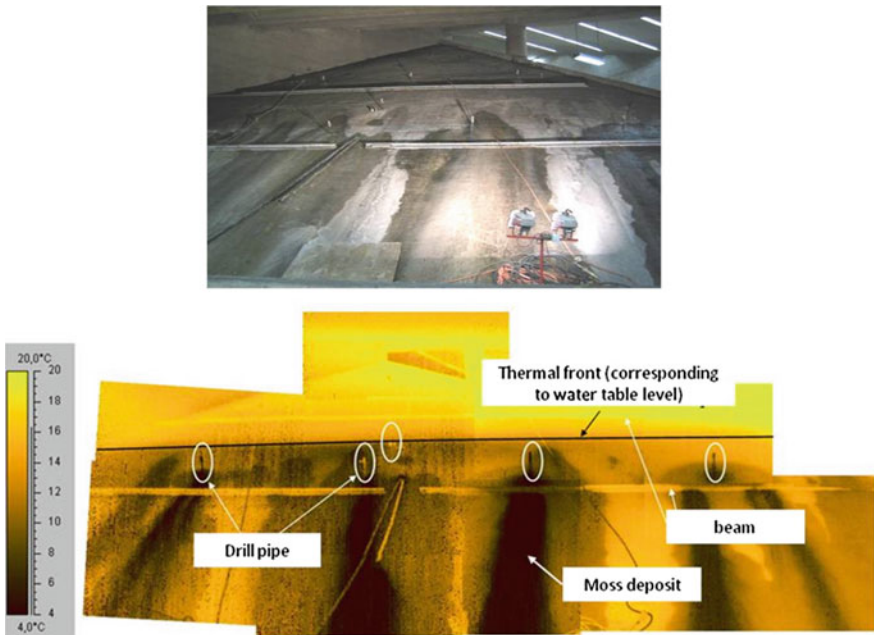
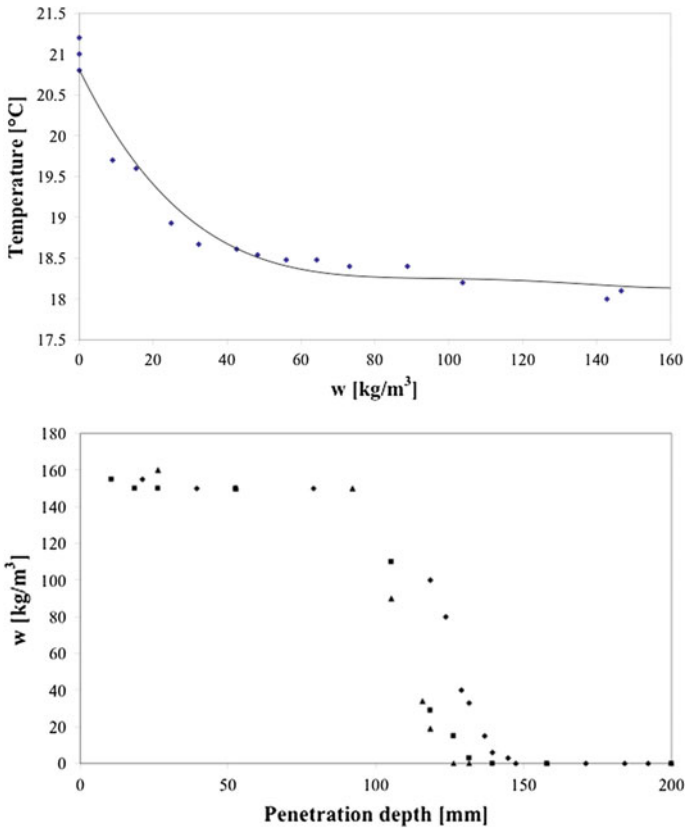


Fig. 7.4 Infrared thermogram on a wall in assumption metro station (Quebec, Canada). Courtesy of Samuel Naar



**Fig. 7.5** A calibration curve (top) between surface temperature and moisture content for three specimens of a Gotland sandstone and a moisture profile (bottom) after one hour of capillary suction from the left, determined by IR-thermography and this calibration curve, Johansson (2005)

The calibration procedure is of course extremely delicate since the conditions must be the same as during the later measurements. A major disadvantage is the low resolution in the high moisture content range, Johansson (2005).

# Chapter 8

## Electrical Resistance



Jean-François Lataste, Charlotte Thiel and Elisa Franzoni

### 8.1 Physical Principle

Electrical resistance is the ability for a material to impede the flow of electrical current. The resistance ( $R$ ) is expressed in ohm (Ohm), its inverse is the conductance ( $C$ ) is expressed in siemens (S). The resistance is function of geometry of tested body and measurement device. So one generally prefers the resistivity ( $\rho_{\Omega}$ ) expressed in ohm-meter (Ohm·m), or its inverse the conductivity ( $\sigma$ ) in siemens per meter (S/m), representing the intrinsic material's property.

The resistance is assessed by injecting a known electrical current intensity ( $I$  in A) between two electrodes, and measuring the difference of potential resulting ( $U$  in V) between two electrodes. Ohm's law (8.1.1) allows the calculation of  $R$ .

$$U = R \cdot I \tag{8.1.1}$$

Electrical resistivity is deducted multiplying  $R$  with a geometric factor (also called cell factor)  $k$  (in m), and linked to the sample shape or the geometrical characteristics of the measurement device (8.1.2):

$$\rho_{\Omega} = k \cdot R \tag{8.1.2}$$

---

J.-F. Lataste (✉)  
Université de Bordeaux, Bordeaux, France  
e-mail: jean-francois.lataste@u-bordeaux.fr

C. Thiel  
Technical University of Munich, Munich, Germany  
e-mail: charlotte.thiel@tum.de

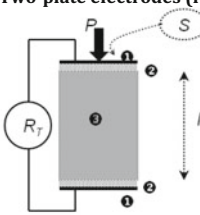
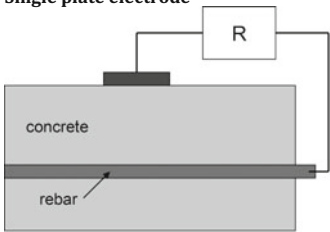
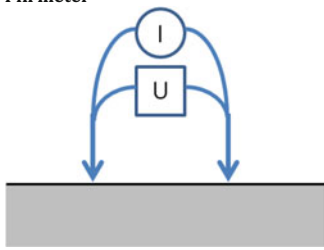
E. Franzoni  
University of Bologna, Bologna, Italy

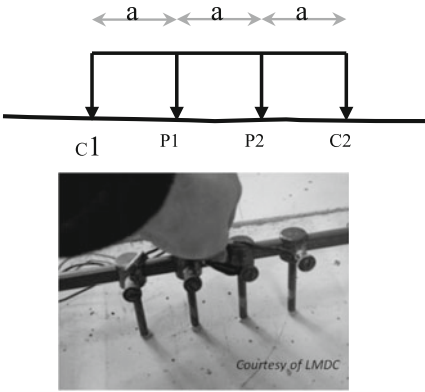
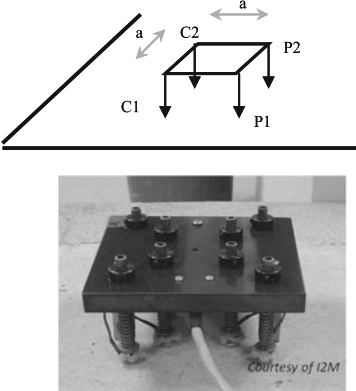
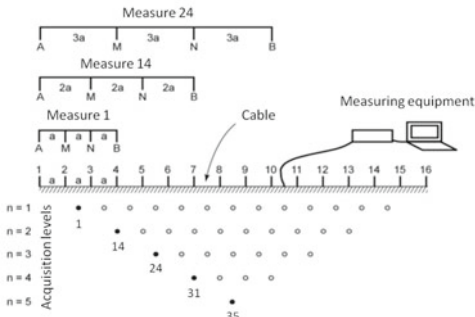
## 8.2 Measurement Devices

Several devices are possible, varying in their characteristics and interpretation modes (Table 8.1):

- (i) The two-plate-electrodes technique consists in the circulation of a current tube (as by transparency) between the two probes put on the two opposite faces of the tested material. This technique is adapted for in laboratory measurement, on cores or samples with plane surfaces, Lataste (2010). Some case on site is also known, Weydert and Gehlen (1999). From resistance, the calculation of resistivity is possible, knowing the distance between electrodes and their surfaces. The assessed resistivity is representative of the average material's behaviour, without being able to consider a gradient for instance. A variation of this device is the single-plate-electrode. The second electrode is then a conductive body within the material (as a reinforcement for instance in the case of reinforced concrete, Polder et al. (2001). In this case too, any evaluation of a gradient is impossible. The lack of knowledge of the surface of the second electrode forbids the calculation of resistivity. The result is then only in term of resistance, very influenced by the cover depth, and higher resistances.
- (ii) The two-point electrode (or pin meter) consists in the injection of electrical current and measurement of difference of potential between the two same electrodes, Kasal and Lear (2010). This method allows to rapidly assessing the electrical resistance, but not the resistivity. The value measured is in fact very influenced by the resistance at the contact electrode-material. The potential drop mainly corresponds to the electrical coupling at the contact between electrodes and surface material. Its distribution between the two probes (with 2 cm between probes and 1 mm for the probe diameter) shows that the potential drop is 25% of the total difference of potential at a distance of one electrode diameter from the electrode axis (in other words at half a diameter from the edge of the electrode). This potential drop is 40% of the total difference of potential at a distance equals to two diameters from the electrode axis (Fig. 8.1). Thus, the measurement is very influenced by the materials properties in the vicinity of electrodes, more than by properties in depth.
- (iii) The four probes electrodes method consists in the injection of intensity between two probes, and measurement of the difference of potential between two others electrodes. The most known device is the Wenner configuration, where the electrodes are aligned and equidistant, Polder et al. (2001). Another geometry is the square, where electrodes are located at each corner of a square, Lataste (2010). More generally, a variation (from geophysics fields) is the electrical resistivity tomography (ERT), This method combines several four-electrodes devices, through a multi-electrodes line Chouteau et al. (2002). All these measurements allow to cover a larger surface, and to increase the investigation depth. From resistance, the resistivity is deduced using the geometrical factor. This value is representative of a global behaviour of the material in the investigated volume, so one speaks about

**Table 8.1** Measurement devices

Device	k (m)	Result
<p><b>Two-plate electrodes (resistivity cell)</b></p>  <ul style="list-style-type: none"> <li>1 Probes</li> <li>2 Wet sponges</li> <li>3 Concrete sample</li> </ul> <p><i>P</i> the contact pressure  <i>l</i> the sample length  <i>S</i> the sample surface connected with probe</p> 	$S/l$	$\rho_a$ (global value)
<p><b>Single plate electrode</b></p> 	-	$R$ (influence of cover depth)
<p><b>Pin meter</b></p> 	-	$R$

<p><b>Four-electrodes Wenner</b></p>  <p>Courtesy of LMDC</p>	$2\pi a$	$\rho_{\Omega a}$
<p><b>Square configuration</b></p>  <p>Courtesy of I2M</p>	$\frac{2\pi \cdot a}{2 - \sqrt{2}}$	$\rho_{\Omega a}$
<p><b>ERT (electrical resistivity tomography)</b></p> 	<p>Function of configuration</p>	<p><math>\rho_{\Omega t}</math> (adapted for assessment of gradient in depth)</p>

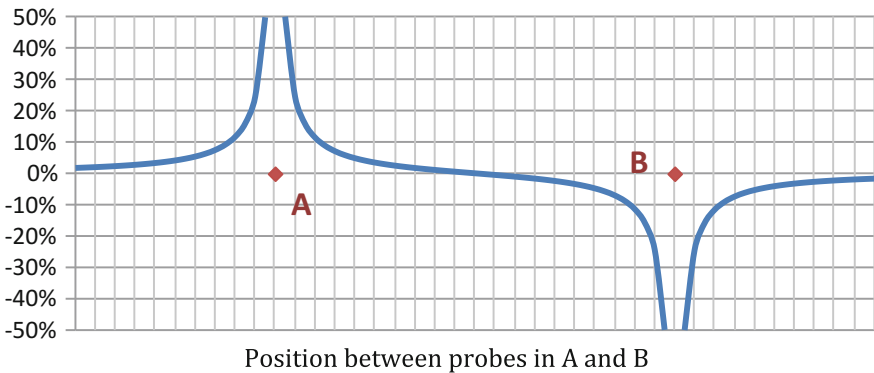
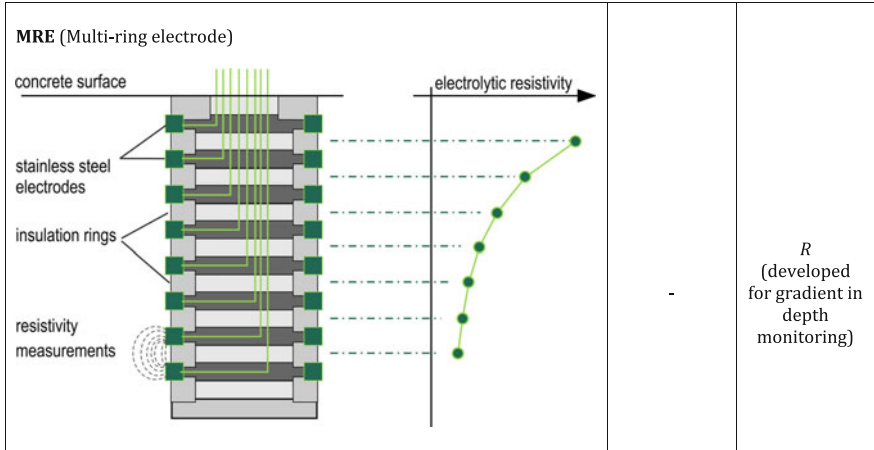


**Fig. 8.1** Relative electrical potential on the surface linked to electrical current injected between two points (A and B), expressed in term of rate. The values consider a probe diameter corresponding to 5% of distance AB

apparent resistivity ( $\rho_{\Omega a}$ ). Classically, the relative variations of  $\rho_{\Omega a}$  are interpreted for investigations. In the case of ERT, apparent resistivity can be inverted to reach a 2D model of true resistivities’ ( $\rho_{\Omega t}$ ) distribution.

- (iv) The development of sensors for resistivity or resistance is done to assess gradients in depth. For instance the multi ring electrodes (MRE) allow the measure of resistance in several materials “slices”. The device is made with several metallic rings (electrodes) separated by insulating rings, Schießl and Breit (1995). The intensity injection and the measurement of the difference of potential are done successively between these various rings, to investigate several depths within the material.

All these methods are done in the range of continuous current, or with low frequency alternative current (<300 Hz). In these ranges, the material is purely resistive. Some works are nevertheless done with a larger range of frequency for alternative current (mHz to GHz). In this case, the material presents also capacitive behaviours, McCarter and Garvin (1989). One speaks about AC impedance spectroscopy (ACIS) or else electrical impedance spectroscopy (EIS). These approaches are few used on site due to the ergonomics of apparatus needed (more adapted for laboratory studies) and due to the time needed for each measurement point. These techniques are not developed in this chapter.

### 8.3 Electrical Resistance Versus Moisture

In building materials (stone, concrete, wood) the electrical conduction is essentially an electrolytical phenomenon, linked to the fluid phase in porosity. For instance, the resistivity of concrete can evolve between less than 100  $\Omega\text{m}$  (in the semiconductor range) when it is saturated, to  $10^9$  when it is dry (in the insulator range), Monfore (1968). Actually, the water volume influences the ability for ions to move through porous network.

For porous material, the Archie's law, Archie (1942), established empirically on geological material, allow to highlight the influence of water, on resistive properties (8.3.1). With  $\rho_{\Omega}$  the rock resistivity,  $\xi$  its porosity,  $\rho_{\Omega_w}$  the resistivity of pore fluid, then a, m, and n three parameters linked to the material. S is the saturation rate.

$$\rho_{\Omega} = a \cdot \xi^{-m} \cdot \rho_{\Omega_w} \cdot S^{-n} \quad (8.3.1)$$

Thus, for a given material, a, m and n are fixed, if one neglects porosity variations and water salinity variations (in the context of the investigated material), the resistivity is linked to water saturation according a power relation. Another shape to express the relation between resistivity and saturation is:

$$\text{Log}(\rho_{\Omega}) = -n \cdot \text{Log}(S) + \text{Cst} \quad \text{with} \quad \text{Cst} = \text{Log}(a \cdot \xi^{-m} \cdot \rho_{\Omega_w}) \quad (8.3.2)$$

#### 8.3.1 Electrical Conduction and Moisture—Concrete

Electrical resistivity measurement is developed, notably to the fact that rebar corrosion in reinforced concrete is an electrochemical phenomenon. Thus, numerous works show that corrosion is “driven” by moisture and the ability to corrosion currents to flow through concrete. So, resistivity appears as an adapted tool to monitor corrosion activity, Lopez et al. (1993), Andrade and Martinez (2009).

Other works focused on the non-destructive assessment of concrete alteration. Moisture can appear as a bias for several techniques, so developments are also done to assess moisture, to de-combine its effects on non-destructive techniques (NDT), Breyse et al. (2012). This is also the case for commercial device as “Permeametre” where electrical resistivity is a data that allows the assessment of concrete moisture, for the complete interpretation of permeates, Torrent and Frenzer (1995).

The link between resistivity and water saturation has been largely presented in various publications (Fig. 8.2). Lopez et al. (1993) present a study on mortar evaluated with a laboratory device, Laurens et al. (2005) on a concrete slab on site investigated with a Wenner probe, Lataste (2010) through a study on various concretes conditioned in laboratory and investigated with a square four probes device.

These various studies highlight that the link between saturation rate (S) and resistivity is shaped as a power function. It appears that the sensibility of the relation is better for saturation rate in the range of 40–80%. Below 30–40% for S (dry material), the hydraulic continuity within pores is disrupted, Marty (1999), so the conduction is no longer mainly electrolytical, and Archie’s law cannot describe the link. For S higher than to 80–90% (for very saturated material) the resistivity is no more very sensitive to variations, Marty (1999).

The resistivity ranges are different along the three presented cases. This shows the influence of material’s composition (binder, water/cement ratio, ...), of the age and condition of the material (degree of hydration, ...), Weydert and Gehlen (1999), Hunkeler (1996), Monfore (1968). This point excluded the use of the absolute resistivity value as an indicator of moisture. The interpretation of resistivity is done by the analysis of the relative variation, sometimes completed with a calibration.

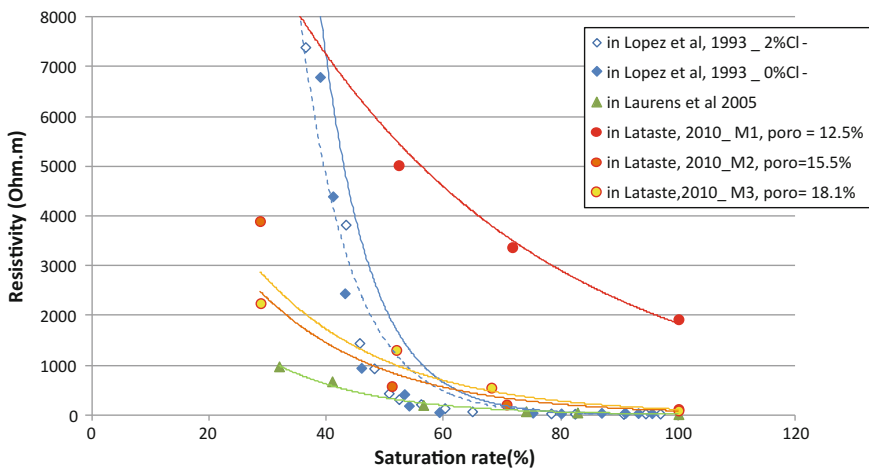


**Fig. 8.2** Saturation rate versus electrical resistivity (according to various authors)

In any case, electrical resistivity is identified as a tool allowing the moisture cartography on concrete building, Polder et al. (2001), and several work presents this use. For instance, Klysz et al. (2006) present the case of moisture zoning along a profile, investigated with the square four electrodes device, on a bridge partially damaged by alkali silica reaction (ASR). Another case is presented by Karasthatis et al. (2011) with the use of ERT, to identify water ingress in the Marathon concrete dam.

The technique is also used to follow temporal variations of material's property, due to water ingress. thus, ERT can be used as showed by Buettner et al. (1995a, b) through laboratory tests. With ERT, recent works are also presented in du Plooy et al. (2013), measurements on concrete are completed by a calibration process to quantify saturation rate in depth.

The assessment of moisture gradient from the surface is a real stake for NDT. A solution is proposed through monitoring, and the development of the MRE then appears as an interesting tool, Schießl and Breit (1995). This device, if calibration on sample is possible, allows the assessment of the saturation gradient in depth, and its variation in time.

### **8.3.2 *Electrical Conduction and Moisture—Brick and Stone Masonry***

The application of electrical resistivity methods to moisture determination in masonry has been attempted and investigated several times, with the main scope of monitoring the wetting and/or drying processes of masonry after rainfall or flooding events, e.g. Sass and Viles (2010) and Kruschwitz et al. (2012). Electrodes of course cannot be cast-in as in concrete; hence they consist in either nails inserted in the materials or plates positioned on the masonry surface with the aid of a couplant (self-adhesive, agar gel, etc.), Sass and Viles (2010) and Kruschwitz et al. (2012) or electrodes simply pushed against the surface with constant pressure, Martinho et al. (2012). Both 2D and 3D measurements have been carried out.

Some development of new sensors has been done, ONSITEFORMASONRY (2006), viewing the geophysical electrical resistivity tomography tools as interesting in the frame of NDT on masonry (Fig. 8.3). The adaptation to micro geophysical techniques offers many advantages as the cost, the non-pervasiveness and the relative velocity of execution.

From a qualitative point of view this approach allowed to follow the wetting/drying behaviour of different kinds of masonry quite well, but the quantitative conversion from resistivity to absolute moisture values gave much more scattered and controversial results. The main factors making this determination so complex are the following:

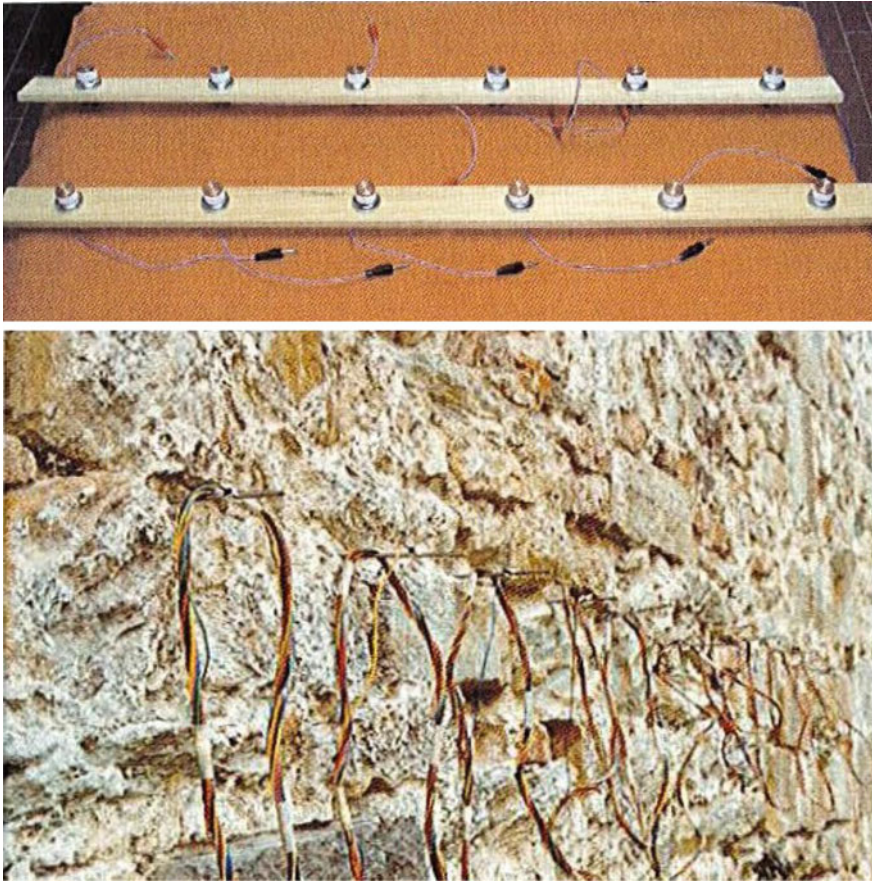


**Fig. 8.3** Two devices for ERT on masonry: above, the HeP\_El\_01 prototype, at the bottom electrical array consisting of small metallic bars on an external wall (on site for masonry)

- The presence of discontinuity surfaces, namely mortar layers  
 In some stone masonries, the Wenner-four-points measurements performed across mortar layers gave unacceptably erratic results, due to major differences between stone and mortars properties, hence measurement within single stone blocks was preferred, Valek et al. (2010).
- The presence of soluble salts;  
 Electrical properties of porous materials strongly depend, among the others, on the salinity of the water inside the pores that can be very high in real masonries. Soluble salts may be supplied to masonry materials mainly by rising damp from ground, marine spray, reaction products between materials and atmospheric pollutants (sulphates contained in black crusts) and building materials themselves (gypsum presence in mortars, etc.). When comparing the saturation levels determined by electrical resistivity and the gravimetric procedure, a significant

overestimation was found in the first one due to salts presence (values approximately 5 times higher), although the use of a complex resistivity approach is expected to partially overcome this limitation, Kruschwitz et al. (2012).

- The heterogeneity of brick units and stone ashlar (especially in historic masonries). This heterogeneity is typical of old masonries and can be ascribed to ‘natural’ variability of stone properties, manufacturing technology of pre-industrial bricks, and reuse of materials from previous demolished structures. Besides this, non-linear effects due to sedimentary planes orientation and/or clay minerals might occur in natural stones, which may cause an anisotropic geometry of the electrical field (Sass et al. 2005). For all these reasons, different calibration curves should be virtually determined for each single stone or brick unit, which is of course impossible to achieve in practice. Such aspect represent a strong limitation towards the qualitative determination of moisture content, and the results obtained using a limited number of sampling points for calibration or pre-existing databases, Kruschwitz et al. (2012) and Sass and Viles (2010) may be affected by significant errors and their reliability should be evaluated case by case, on the basis of the features of the specific masonry structure under testing.

### **8.3.3 *Electrical Conduction and Moisture—Wood***

In wood the moisture is generally expressed in moisture content (kg/kg). A classical tool to assess moisture is the two pin methods, Kasal and Lear (2010). Measurement can be done in two pre drilled hole for contact or simply pushing the pins on the wood surface up to a penetration about 1–3 mm. By varying their depths between measures, operator can assess a gradient. The technique allows to easily assessing relative moisture distribution on a structures, with calibration the results can be also quantified. This calibration should be done carefully since that technique is influenced by the wood species its provenances and others intrinsic parameters (listed in Fredriksson et al. (2013a), as well as and the orientation of the device relatively to fibres, Fredriksson et al. 2013a, b).

Given the absence of salts in most of timber structures and the good electrical continuity achieved by inserting the pins in the wood, good results were obtained in terms of accuracy, as in the example, Fig. 8.4.

## **8.4 Limits and Perspectives**

Resistance and resistivity methods are adapted to assess moisture in building material. The limits still existing are clearly identified:



Measurement point	Moisture content (wt./wt.%) obtained by the gravimetric method (oven drying)	Moisture content (wt./wt.%) obtained by two pins resistivity method (calibration supplied by the manufacturer)
A	7.0	7.8
B	8.7	8.6
C	8.9	8.2

**Fig. 8.4** Comparison between the moisture content measured by the gravimetric method (oven drying at  $70 \pm 2 \text{ }^\circ\text{C}$ ) and a 2-pin resistivity analyzer in three different timber trusses of the Ebe Stignati Theatre in Imola (Italy, XIX Cent.) (Courtesy of Elisa Franzoni)

- It appears that whatever the material, the techniques can only be interpreted in relative variations.
- The influence of composition and age for concrete, nature and origin for stone, or species and density for wood, forbids the direct evaluation of the water content.
- Only the calibration on each new material seems the solution to improve investigation.
- The presence of soluble salts (especially in buildings affected by marine spray and/or rising damp) may influence the results to a great extent.

The range of variation of electrical properties only due to intrinsic properties appears larger than the measurement noises identified for each techniques and material, Lataste and Breyse (2011), Kasal and Lear (2010). For instance a concrete composition casted 20 times along a year shows variability about 15% in resistivity. It is larger than the reproducibility, assessed below 4%, Lataste and Breyse (2011). So it appears that developments are needed to better control influencing factor than on the measurement technique itself.

Some biases have known effects and can be easily corrected if the initial data (the right temperature for instance) is evaluated. Some others biases are less studied and they need further developments for their corrections: as for instance geometrical effects on pin meter, Fredriksson et al. (2013b), or on rebar effect in concrete.

The new developments in term of device, Schießl and Breit (1995), Fredriksson et al. (2013a), du Plooy et al. (2013) deal with the assessment of gradient in depth. The knowledge of this effect, which is always present on real structures, needs to be reached for the method to be pertinent in the frame of NDT. But one of the main

question relatively to gradient, is the decoupling of the different gradients sitting on the material surface (moisture, alteration, temperature etc.).

The interpretation of electrical measurement is associated to calibration for the complete interpretation of water content. The optimization of its step and the definition of a calibration process could also appear as a solution to be able later to objectively compare data among various studies, leading to the building of a common database across materials.

# Chapter 9

## Gas Permeability



Franck Agostini

### 9.1 Measurement Principle

The effective, or relative, gas permeability of a partially saturated porous media depends on the amount of available porosity for gas percolation, its connectivity, tortuosity and pore throat diameter. It is well known that gas permeability varies significantly with the distribution and the amount of moisture present in the porous network Abbas et al. (1999), Dana and Skoczylas (2002). As illustrated in Fig. 9.1, existing literature (Chen et al. (2012)) shows that in a first approach, for a given cementitious material, gas relative permeability can be seen as depending on the water concrete saturation only.

Following these results it was thought that an efficient measurement method of in situ concrete water content could be designed and based on gas permeability evaluation and variation. This method has been applied in a recent publication by Liu et al. (2013) and is designated as “Pulse Test Protocol”. The moisture content measurement protocol lies in three steps:

- Defining the characteristic  $K_{r,g}(S_w)$ -curve of the tested material,
- Measuring in situ effective gas permeability  $k_{eff}$ ,
- Deducing the moisture content of the material  $S_w$ .

---

F. Agostini (✉)

CNRS, Centrale Lille, FRE 2016 - LaMCUBE - Laboratoire de Mécanique Multiphysique et Multi-échelle, Univ. Lille, Lille F-59000, France  
e-mail: franck.agostini@centralelille.fr

© RILEM 2018

L.-O. Nilsson (ed.), *Methods of Measuring Moisture in Building Materials and Structures*, RILEM State-of-the-Art Reports 26,  
[https://doi.org/10.1007/978-3-319-74231-1\\_9](https://doi.org/10.1007/978-3-319-74231-1_9)

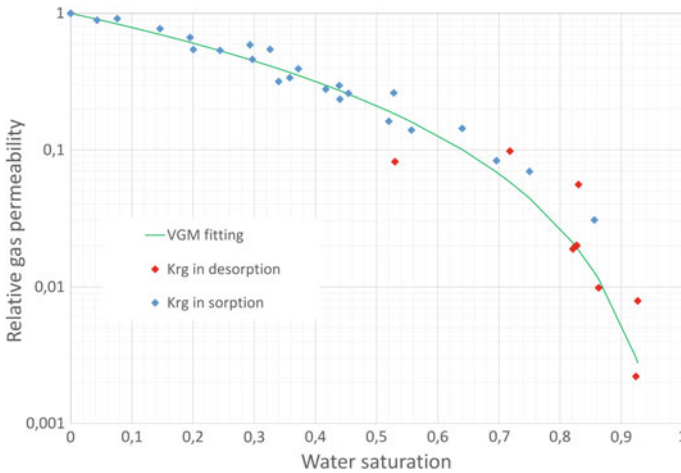


**Fig. 9.1** Relative gas permeability  $K_{r,g}$  versus degree of water saturation  $S_w$  for CEM-V concrete: during desorption and sorption paths, Chen et al. (2012)

## 9.2 Need for Calibration

The characteristic  $K_{r,g}(S_w)$ -curve of the tested material is an essential data. Those curves can either be obtained using predictive models (based on Mercury Intrusion Porosimetry for example) or through direct experimental characterization. Predictive models can be successfully employed to fit experimental points to obtain a complete  $K_{r,g}(S_w)$ -curve useful for simulation purpose, but an experimental characterization campaign is strongly recommended to ensure acceptable moisture measurement accuracy.

## 9.3 Calibration Techniques

To obtain the  $K_{r,g}(S_w)$ -curve, routine laboratory gas permeability measurement have to be realized on samples with various homogenous moisture content. The range of studied moisture content can be adapted to the expected in situ range of moisture content. Various existing experimental apparatus can be used for this purpose, with various sample size, geometry and accuracy Martin (1986), Lydon (1993), Skoczylas and Henry (1995), AFREM (1996), RILEM (1999b), Meziani and Skoczylas (1999), Loosveldt et al. (2002), Lion et al. (2004), Choinska et al. (2007) and Gardner et al. (2008). Kaczmarek (2008) and Kaczmarek (2010) have proposed schematic views of the most frequent experimental conditions, cf. Fig. 9.2.

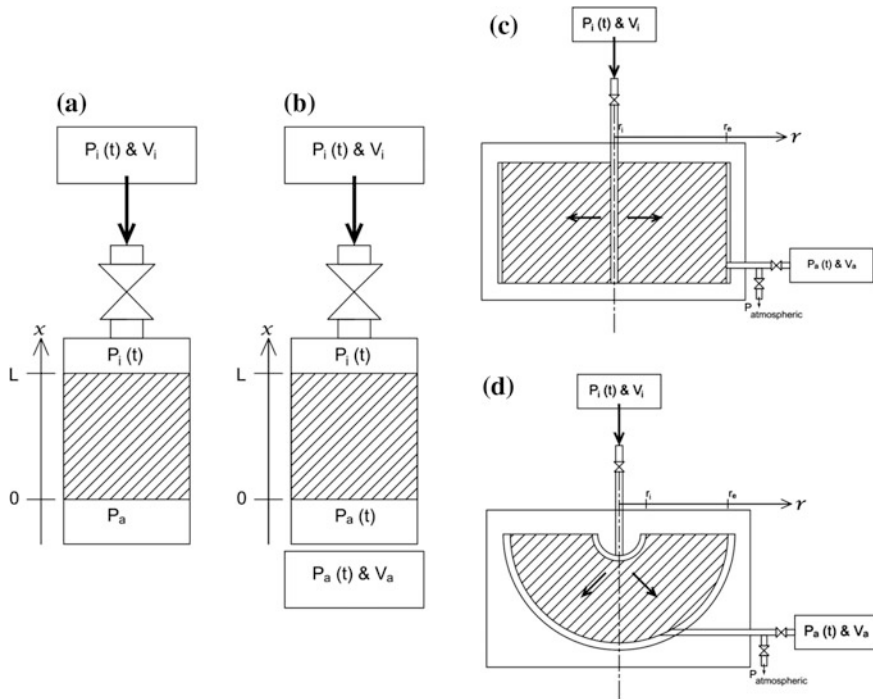


**Fig. 9.2** Schematic configurations of single-reservoir (a) and double-reservoir (b) methods for uniaxial flow, Kaczmarek (2008), and reservoir tests for cylindrical (c) and spherical (d) geometry of samples, Kaczmarek (2010)

### 9.4 Parameters Measured

Once obtained the  $K_{r,g}(S_w)$ -curve, a sole parameters has to be measured in order to obtain the moisture content: it is the effective gas permeability. The effective gas permeability is measured by applying one of the existing measurement techniques that can be found in literature. Among numerous available tests to assess the permeation properties of the concrete cover on site, we can cite, the “Vacuum Permeability Test” Claisse et al. (2003), the Torrent permeability test, Torrent (1992) and Romer (2005), the “Autoclam Water and Air Permeability Test” (see Fig. 9.3), the “Figg Air Permeability Test”, the “Schönlin Air Permeability Test” or the “Surface Air Flow Test”, all reported by Henderson et al. (2004).

More recently, a test has been developed to measure gas permeability in the core of concrete structures by Liu et al. (2013), see Fig. 9.4.

For a more detailed overview of existing tests see previous RILEM TC publications RILEM (1999a), Paulmann and Molin (1995) and RILEM (2007).

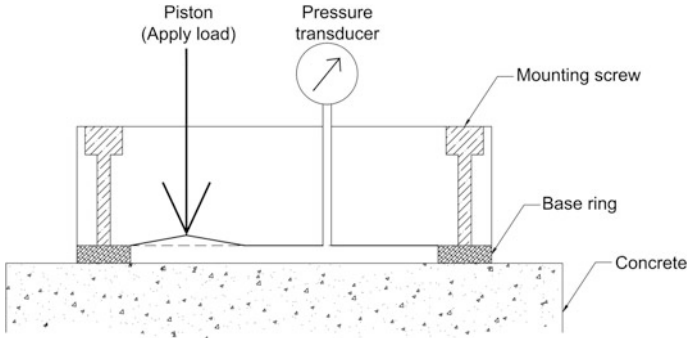


Fig. 9.3 Schematic of Autoclam test for air permeability, Henderson et al. (2004)

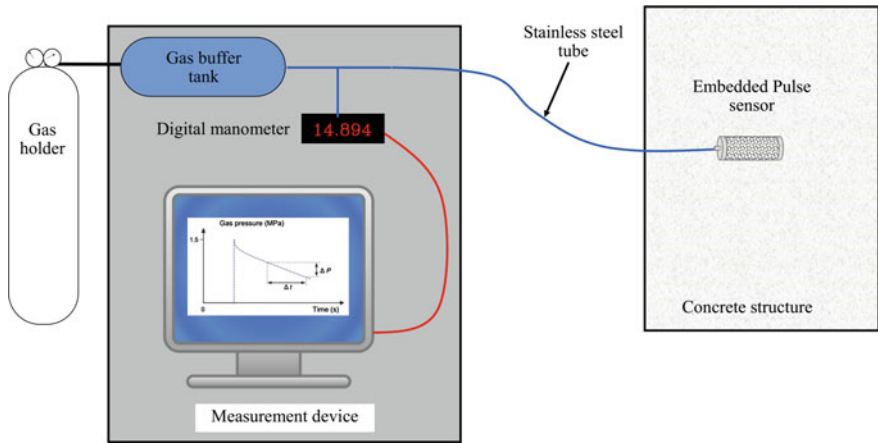


Fig. 9.4 Schematic view of the pulse measurement protocol, Liu et al. (2013)

### 9.5 Measuring Range

The measuring range mainly depends on the accuracy of the volumetric flow rate measurement. The effective gas permeability of concrete can vary from  $10^{-16} \text{ m}^2$  [equivalent to 0.1 mD ( $D = \text{Darcy}$ )] for a dry low quality concrete to  $10^{-19}$ – $10^{-20} \text{ m}^2$  (0.1–0.01  $\mu\text{D}$ ) for medium to high quality concrete with relatively high moisture content. In fact there is no lower limit for effective gas permeability as a fully water saturated concrete has a null gas permeability. In theory, with the appropriate measurement apparatus the whole moisture range can be measured. In practice, for classical structural concretes, when using available in situ gas permeability measurement apparatus, moisture contents ranging from 0 to 80–90% can be measured.

## 9.6 Required Time

The required time depend on the test duration necessary to obtain a sufficiently accurate evaluation of the gas flow rate. For high flow rate, a few minutes can be sufficient, while one hour or more can be necessary when testing low gas permeability materials, i.e. high quality concrete or with high moisture content.

## 9.7 Representative Volume

The investigated volume depends on:

- the chosen gas permeability measurement apparatus,
- the duration of the test: the longer is the measurement the larger is the investigated volume,
- the effective gas permeability of the material: the more permeable is the material, the larger the investigated volume (for a given test duration).

The approximate size of the investigated volume can then range from a few  $\text{cm}^3$  to several  $\text{dm}^3$ .

## 9.8 Sources of Errors

The main source of error is an inappropriate characteristic  $K_{r,g}(S_w)$ -curve. This may be due to:

- the use of an unsuitable predictive model,
- an inaccurate gas permeability apparatus,
- a laboratory characterization performed on a material which is not representative of in situ material: unsuitable storing conditions, concrete sampled from a different batch, casting defects in the area where gas permeability is measured, etc.

For surface measurement using vacuum methods, high water saturation can lead to overestimation of the intrinsic permeability, Romer (2005).

Furthermore, the existence of gradients of relative humidity in the near surface concrete can lead to misleading results for surface measurement devices, Basheer and Nolan (2001). Methods have been investigated to deal with those gradients. Coupling together surface permeability measure with NDT-methods giving information on the existence and shape of relative humidity gradients, may significantly improve the quality of the measurement.

Micro-cracking can also lead to important differences between the  $K_{r,g}(S_w)$ -curve of a sound laboratory sample and the one of the in situ concrete. The influence of micro-cracking on the mass transport properties of concrete has been

largely studied Abbas et al. (1999), Burlion et al. (2003), Jacobs (1998), Picandet et al. (2001, 2009), Samaha and Hover (1992) and Wu et al. (2015). A large increase of apparent gas permeability is then observed when micro-cracking occurs, and the  $K_{r,g}(S_w)$ -curve obtained on sound concrete is no more valid. This micro-cracking may be caused by drying shrinkage, de Sa et al. (2008), Burlion et al. (2003), or mechanical loading, Picandet et al. (2001). Furthermore, other studies have shown that the effect of cracks on gas permeability is not reversible even when a mechanical loading is applied in order to reduce cracks opening, Chen et al. (2013), and Wang et al. (2014).

Other sources of error strongly depend on the chosen in situ gas permeability apparatus and its flow rate measurement accuracy.

## 9.9 Commercial Availability

In theory, once an appropriate characteristic  $K_{r,g}(S_w)$ -curve of the material is available, any gas permeability device is suitable as long as its flow rate measurement range match with expected effective permeability.

In practice, the “Pulse Test” apparatus presented by Liu et al. (2013), is the only gas permeability measurement device which has been used to determine the in situ moisture content of a concrete structure.

# Chapter 10

## Hygrometry



Lars-Olof Nilsson, Kurt Kielsgaard Hansen and Miguel Azenha

### 10.1 General Principles

The humidity of air can be measured with a number of various methods, i.e. psychrometers, dew-point sensors, mechanical hygrometers and electronic RH-probes (RH = Relative Humidity).

In most cases when measuring RH in materials a number of electronic RH-probes are used. The sensors in these probes are, in most cases, capacitive or resistive where a small piece of a sensor material (typically a polymer) has two electrodes between which the electrical capacitance or resistance is measured. The capacitance or the resistance between the electrodes is a measure of the moisture content of the sensor material. The readings must be translated to RH with a calibration. It is noted however that capacitance-based sensors are more disseminated, Rittersma (2002), probably because of their improved performance in harsh environments as compared to resistive sensors.

Some RH-probes have dew-point sensors where a small mirror is chilled until the temperature reaches the dew point of the surrounding air and condensation occurs at the mirror. The detection of condensation is done in different ways.

---

L.-O. Nilsson (✉)  
Lund University, Lund, Sweden  
e-mail: lars-olof.nilsson@byggtek.lth.se

L.-O. Nilsson  
Moistenginst AB, Trelleborg, Sweden

K. K. Hansen  
Technical University of Denmark, Kongens Lyngby, Denmark  
e-mail: kkh@byg.dtu.dk

M. Azenha  
University of Minho, Braga, Portugal

© RILEM 2018

L.-O. Nilsson (ed.), *Methods of Measuring Moisture in Building Materials and Structures*, RILEM State-of-the-Art Reports 26,  
[https://doi.org/10.1007/978-3-319-74231-1\\_10](https://doi.org/10.1007/978-3-319-74231-1_10)

The thermoelement psychrometer works by use of the thermoelectric effect, the Peltier effect, that cools down the welded junction below the dew point and water from the surrounding condenses on the welded junction. When stopping the cooling process the condensed water evaporates from the welded junction and creates a thermoelectric effect (i.e. voltage). The voltage is measured as function of time and the nick point when stopping the cooling process is determined from which the RH can be determined. This measurement principle was introduced by Spanner (1951) and further developed by Wiebe (1971) and is today commercialized, see Table 10.1.

Some RH-indicators are using a hygroscopic salt that is coloured. When RH is reaching a certain threshold level, determined by the type of salt, the salt is accumulating water and is spread. By containing the salt in a cloth, the movement of the coloured salt can be observed. The movement itself says that RH has reached a level above the threshold. The magnitude of the movement can say something about for how long time RH has been above the threshold. Alfasensor AB has commercialized this technique, see Alfasensor (2016).

The swelling and shrinkage due to moisture changes is used in some humidity meters like in traditional hair hygrometers. A bundle of hair whiskers is mechanically connected to a hand that moves when the bundle is shrinking and swelling. This phenomenon was used by Monfore (1963) who connected a thread of Dacron (a polymer) to a very thin nickel-copper wire. Humidity changes caused the Dacron thread to swell and shrink and that changed stretched the nickel-copper wire more or less. This change in elongation could be measured as electrical resistance changes. The arrangement of the polymer thread and the nickel-copper wire was done inside a long, perforated tube with a diameter of 2.5 mm that constituted an RH-probe that could be inserted into small, long holes in concrete specimens.

A polymer optical fibre sensor is a single-mode optical fibre with a Fiber Bragg Grating (FBG) inscribed into the fibre close to the tip of the fibre. A FBG is a periodic series of perturbations in the refractive index of the optical fibre. The FBG reflects a specific wavelength portion of the light impinged on it; the wavelength of the reflected portion is changed when the FBG is exposed to changes in strain, temperature or humidity. The change in reflection is due to the expansion or contraction of the FBG, which changes the periodicity of the perturbations.

## 10.2 Principles for Measuring in Materials

The principle of using hygrometry to measure the moisture condition of a material is to utilize an instrument that can measure the RH of air and place it in a closed “space” in contact with the material. The “space” can be

**Table 10.1** Information on some frequently used RH-probes and their sensors

Sensor	Sensor material	Principle	Size probe/sensor (mm)/(mm <sup>3</sup> )	Electrodes	dw/dRH (mg/% RH) <sup>a</sup>	Range (% RH)	Ref
Humi-guard	Woven polymer + salt solution	Resistive		Two straight metallic wires	0.02–0.06		(1)
Sahlén	Birch	Resistive	Φ12 × 45/	Two parallel nails		64–98	(2)
Sensirion SHTW2	“Some kind of polymer”	Capacitive	1.3 × 0.7 × 0.5 2 × 2 × 0.8 7.5 × 4.9 × 2.6 3 × 3 × 1.1 2.5 × 2.5 × 0.9 19.5 × 5.1 × 3.1	Confidential			(3)
SHTC1							
SHT1x							
SHT2x							
SHT3x							
SHT7x							
Testo 605-H1		Capacitive	Φ12 × 125/		0.07		(4)
Vaisala	Polymer	Capacitive	1 × 4 × 4	Two metal sheets; one porous	0.07		(5)
Hygropin							(6)
Shute	Optical fiber		Φ5				(7)
Wescor PCT/PST-55	Thermo couple	Thermo electric				93–99.5	(8)

<sup>a</sup>[www.rbk.nu](http://www.rbk.nu)

- [www.industrifysik.se](http://www.industrifysik.se) and private communication
- <http://www.fuktbitken.se/sv/ef-matare/sahlengivaren-inkl-05m-kabel.html>
- <https://www.sensirion.com/products/digital-humidity-sensors-for-reliable-measurements/> and private communication
- <http://www.testolimited.com> and private communication
- [www.vaisala.com](http://www.vaisala.com) and private communication
- <http://www.proceq.com>
- <http://shute.dk/> and private communication
- <http://water.wescor.com/pct55.html>

- a container with a sample of the material,
- a “cup” at a surface of the material,
- a space in a material or between two materials in a structure,
- a drilled hole in a material,
- a cast hole in a concrete specimen.

A few examples of “spaces” where the RH of a material is measured are shown in Figs. 10.1, 10.2 and 10.3.

The sample or the surface of the material gives off a small amount of moisture that is enough to humidify the enclosed air volume and the RH-probe, with its sensor and its filter. The RH-probe must have a low moisture capacity so this gain of moisture does not cause too large an error. This is further analysed in Sect. 10.6.2.

A certain time is needed to reach equilibrium conditions in the measuring situation. The time required depends on the geometry, the properties of the material and the properties of the RH-probe. The traditional way to handle this is to simply wait until a steady reading is obtained.

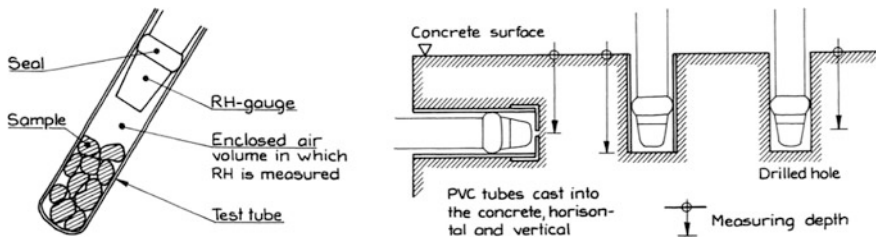


**Fig. 10.1** Examples of “spaces” where the RH of a material can be measured. From Nilsson (1980)

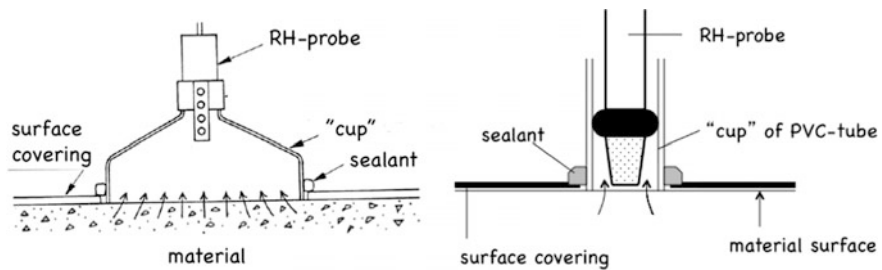
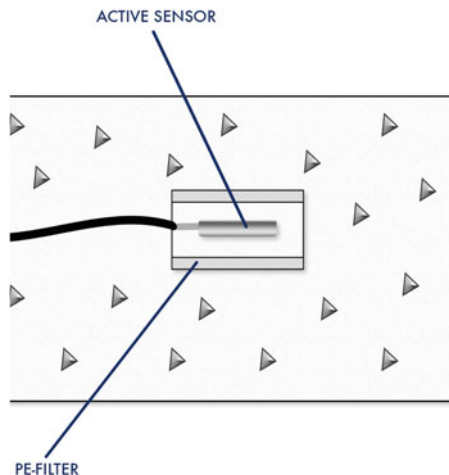


**Fig. 10.2** Examples of “spaces” where the RH at the surface of a material can be measured. From Nilsson (1979)

**Fig. 10.3** Example of “space” where RH is measured by a wooden sensor, inside an embedded, porous polyethylene cylinder, Sahlén (2016)



### 10.3 Sensors for Hygrometric Measurements with RH-Probes

Today, most measurements of humidity in materials are done with a small electronic probe that reacts to the humidity in the surroundings of the probe. The decisive part of such probes is the sensor and the sensor material.

As said in Sect. 10.1, the principles of sensors used for measuring RH in a material are

- small size to be able to measure in a defined, local point,
- equilibrium between the sensor material and its immediate surroundings,
- a measure of the moisture content in the sensor itself is obtained with one of several techniques:
  - electrical resistivity
  - electrical capacity
  - length change
- alternatively, the vapour content of the immediate surrounding air is determined by chilling the sensor and detect at what (dew-point) temperature condensation occurs; together with a temperature measurement the RH can be quantified.

A large number of probes are available on the market. In many cases it is not always clear what the principles are behind each type of probe. The manufacturers are of course hiding information that is company secrets but some general information should be available to make it possible for the user to understand what is happening during a measurement.

In Table 10.1 frequently used probes and sensors are described in more detail. The information is what could be obtained from open sources and directly

from the manufacturers. Some information is missing because it is a company secret.

A very important property of an RH-probe is the moisture capacity  $dw/dRH$ , i.e. the amount of moisture (from the surroundings) that is required for the RH-reading to change. It should be quantified as e.g.  $mg/\%RH$ . All probes have a sensor that has a more or less significant moisture capacity. Additionally, a number of probes have a filter protecting the sensor and it is that filter that has the large moisture capacity. Some systematic errors are directly linked to the moisture capacity of the probe. Consequently, information about the moisture capacity of the sensor and the filter must be available.

## 10.4 Temperature Effects

The temperature conditions are crucial when using a hygrometric method. A couple of different temperature effects are affecting the measurements.

### 10.4.1 *Temperature Difference, Sensor—Material*

Any temperature difference between the surface of the material and the sensor of the RH-probe will cause a systematic error. A rough estimation of this error is, Nilsson (1988),

$$\Delta RH_{T_{diff-a}} \approx 5 \cdot \Delta T = 5 \cdot (T_{mtrl} - T_{sensor})(\%) \quad (10.4.1)$$

A temperature difference of 1 °C gives an error of about 5% RH.

### 10.4.2 *Temperature Difference, Measurement—Sampling*

If the measurement is made at another temperature than where the sample was taken, the measured RH will be different from what the RH was where the sample was taken. The effect of this temperature difference can be calculated, with some uncertainty, if required.

The “correction” of the measured RH is done by

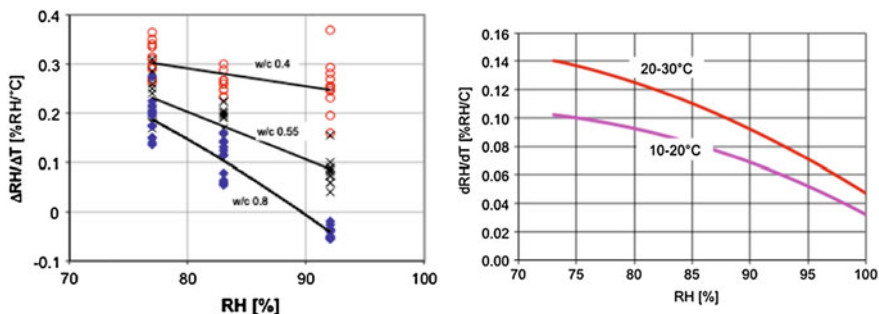


Fig. 10.4 Examples of the temperature dependency of the sorption isotherms for concretes at +5 to +20 °C (left), Sjöberg et al. (2002), and wood (right), Nilsson et al. (2006), expressed as  $dRH/dT$

$$\Delta RH_{T_{diff-b}} \approx -dRH/dT \cdot \Delta T = -dRH/dT \cdot (T_{in\ situ} - T_{measure})(\%) \quad (10.4.2)$$

where  $dRH/dT$  follows from the temperature dependency of the sorption isotherm. The correction factor  $dRH/dT$  depends on the material, the RH-level and the temperature level. Two examples are given in Fig. 10.4.

Temperature effects when the temperature is varying in time in on-site measurements, creating temperature differences between the sensor and the material, are dealt with in Chap. 27.

## 10.5 Calibration

The principle of calibrating a hygrometric probe or sensor is to create a known RH, at a certain temperature, in an air volume and read the signal from the sensor/probe after equilibrium is achieved. The ways to create a known RH are several and are described in Sect. 4.3.

A calibration must include test for linearity, drift over time, hysteresis and repeatability, that all affect the result of the RH-reading. These four phenomena are described briefly in the following and selected results are shown.

### 10.5.1 Tests by Use of Saturated Salt Solutions

The tests are all performed in a box to prevent disturbances from wind, etc. The calibration vessels in the box are placed in a piece of rigid insulation material to secure a constant temperature and to prevent direct exposure of light. The calibration vessel is shown in Fig. 10.5.

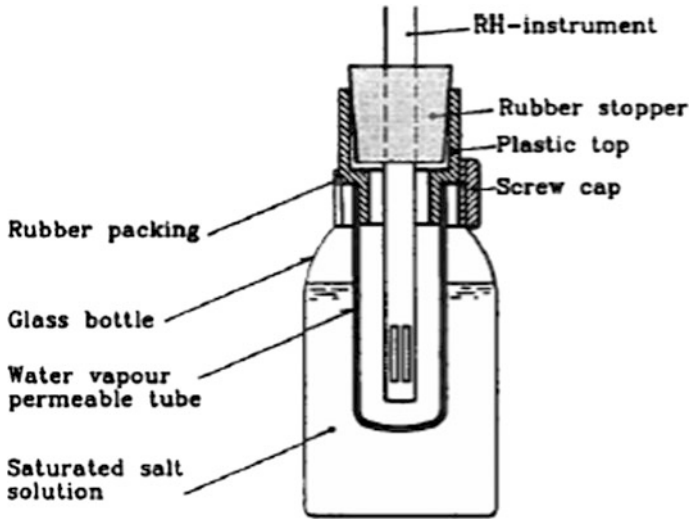


**Fig. 10.5** A calibration vessel with a saturated salt solution separated from the air around the RH-probe by a semi-permeable membrane, Hansen and Christensen (1998)

### 10.5.2 Linearity of the Calibration Curve

Linearity of the calibration curve is important to ensure a precise determination of a RH-reading between two calibration points on the calibration curve. Increasing the number of salt solutions in the calibration process can minimize this factor. The linearity is evaluated according to calibration curves applied to the measured RH-readings found under desorption by a linear curve fit or a 2nd order polynomial curve fit, respectively. Figure 10.6 shows an example of non-linearity of the calibration curve for an RH-instrument. It is seen that at 87.8% RH the difference between the linear curve fit and the 2nd order polynomial fit is 1.2% RH. As the 2nd order polynomial curve fits the measuring points very well a polynomial curve should normally be used. In Fig. 10.6 (right) the maximum deviation from linearity for four types of RH-instruments is compared.

### 10.5.3 Drift Over Time

Drift causes changes in the RH-reading of an instrument even at constant RH. Having drift in an instrument the RH-reading changes as time goes for the same RH. The drift might vary from time to time. In Fig. 10.7 an example of drift over time for a RH-instrument through a 55 days period is shown. It is seen that the

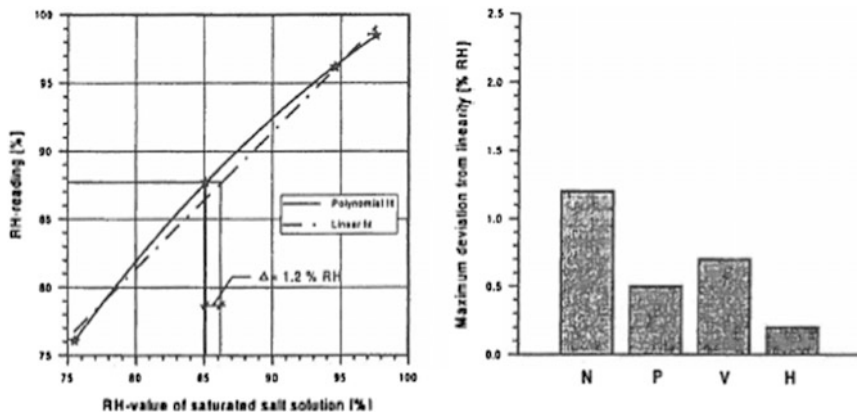


**Fig. 10.6** An example of non-linearity of the calibration curve for an RH-instrument (left). Maximum deviation from linearity for four types of RH-instruments (right). From Hansen and Christensen (1998)

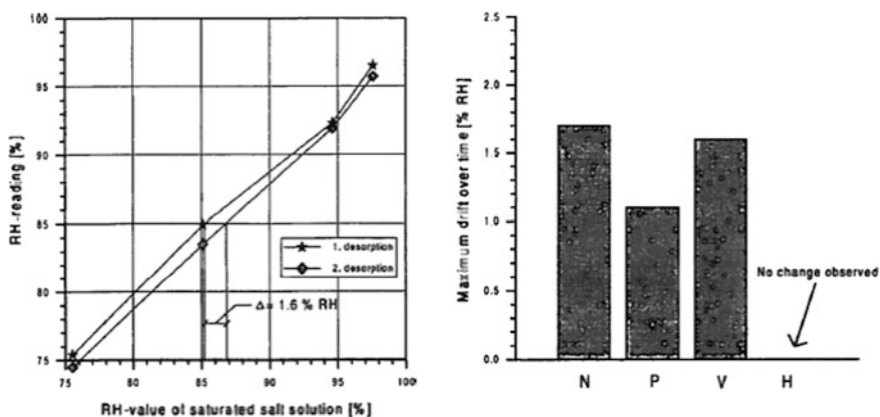


**Fig. 10.7** An example of drift over time for a period of 55 days (left). Maximum drift over time for a period of 55 days for four types of RH-instruments (right). From Hansen and Christensen (1998)

maximum drift is 1.6% RH at 85% RH. If a RH-instrument has high drift over time, the RH-instrument must be checked regularly by use of saturated salt solutions. In Fig. 10.7 maximum drift over time for four types of RH-instruments is compared.

It is relevant to mention that capacitive sensors in particular are susceptible to deviate from initial calibration upon subjection to high humidity environments (e.g. >90%) for relatively small periods. It is therefore recommendable to perform calibration checks after exposure to high humidity, Granja et al. (2014).

### 10.5.4 Hysteresis

A calibration curve performed under absorption (wetting) and a calibration curve performed under desorption (drying) might not be identical. The difference is called hysteresis. If the RH-measurement in the concrete is done over a short period the best result will be to correct the actual RH-reading with a calibration curve made under absorption. If the sensor is placed in the concrete for a longer period, where the sensor is drying together with the concrete, the best results will be to correct the actual RH-reading with the calibration curve made under desorption. In Fig. 10.8 an example of hysteresis for a RH-instrument is shown. It is seen that at 90% RH the difference between absorption and desorption values is 2.5% RH. In Fig. 10.8 the maximum hysteresis for four types of RH-instruments is compared.

### 10.5.5 Repeatability

Repeatability for a RH-instrument is a characteristic of goodness to obtain the same RH-reading when measurements are repeated after a short while. The repeatability is determined as the difference between two desorption curves performed immediately after each other. In Fig. 10.9 an example of repeatability for a RH-instrument is shown. It is seen that at 75% RH the difference between two readings is 0.9% RH. In Fig. 10.9 the repeatability for four types of RH-instruments is compared.

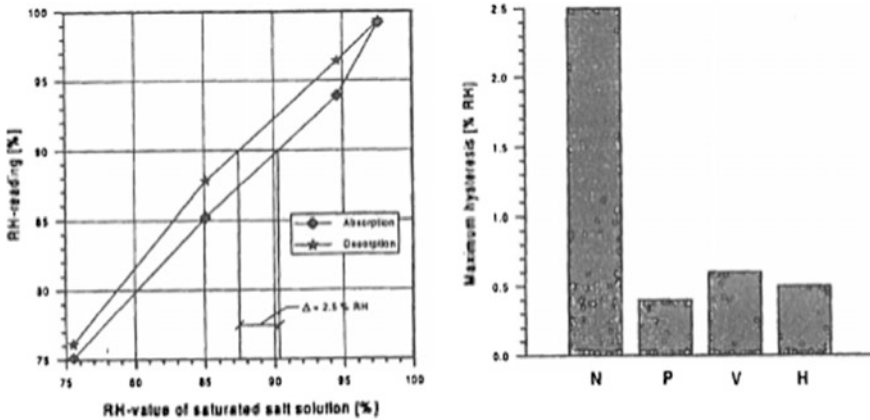


Fig. 10.8 An example of hysteresis and maximum hysteresis for four types of RH-instruments. From Hansen and Christensen (1998)

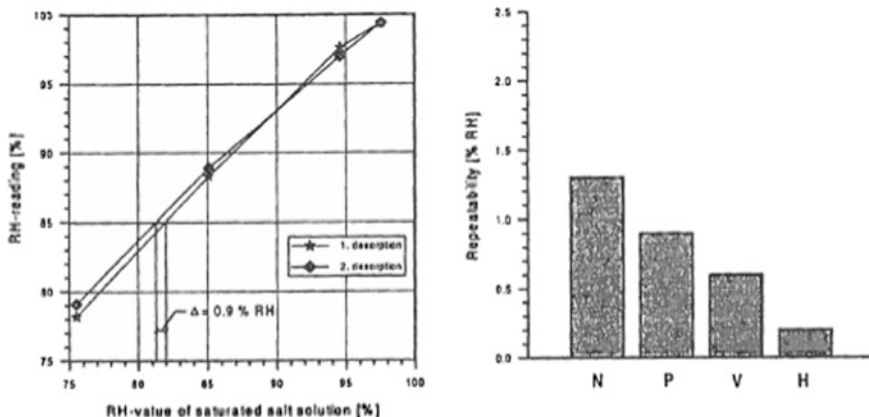


Fig. 10.9 An example of repeatability and repeatability for four types of RH-instruments. From Hansen and Christensen (1998)

## 10.6 Errors and Uncertainties

### 10.6.1 General

The errors can be divided in systematic errors and in accidental errors.

According to Hedenblad (1995) the systematic errors are:

- a. Systematic error for the saturated salt solution used at the calibration.
- b. Missing linearity for the RH-instrument.
- c. The measuring temperature is not equal to calibration temperature.
- d. Drift for the RH-instrument.
- e. Temperature difference between the RH-sensor and the concrete.
- f. The calibration is performed at another temperature than the temperature at the measuring site.

The accidental errors are:

- g. Hysteresis for the RH-instrument.
- h. Calibration error.
- i. Influence of temperature variation during measurement.

Hedenblad (1995) gives an example on calculation of the total uncertainty from the errors listed above.

### 10.6.2 Systematic Error Due to Moisture Capacities

The sample of a material, or the “contributing volume” of the material, gives off a small amount of moisture to humidify the enclosed air volume and the RH-probe.

This amount of moisture causes a drop in RH that will be a systematic error. The error is, Nilsson and Åhs (2012),

$$\Delta RH = \frac{m_w(RH_0, RH) + v_s(T) \cdot (RH - RH_0) \cdot V_{air}}{V_{sample} \cdot K(RH)} \tag{10.6.2}$$

where  $m_w(RH_0, RH)$  is the moisture capacity (kg) of the RH-probe between the initial humidity  $RH_0$  and the measured RH;  $v_s$  is the vapour content ( $\text{kg/m}^3$ ) at saturation at the current temperature  $T$ ;  $V_{air}$  is the volume ( $\text{m}^3$ ) of the enclosed air;  $V_{sample}$  is the volume ( $\text{m}^3$ ) of the sample;  $K$  is the moisture capacity ( $\text{kg/m}^3$ ) of the sample material at the humidity level RH.

This systematic error is shown in Fig. 10.10 for measuring on 20 g sample of a material with a density of  $2400 \text{ kg/m}^3$ . The error is directly proportional to the inverse of the density.

As seen in Fig. 10.10 the systematic error is small if the measurement is done on a material with a moisture capacity larger than some  $50 \text{ kg/m}^3$  but it is very dependent on the moisture capacity of the RH-probe.

This systematic error has been verified in an extreme case when measuring RH on small samples of high-performance concrete that has a very low moisture capacity, cf. Fig. 10.11. Hedenblad (1999) made a series of ten identical measurements on the same sample in a test tube and got a repeated difference of  $-0.6\%$  RH for each measurement.

The relevance of the size of the measuring pocket and the moisture capacity of the sensor itself have been found to be small to negligible in the cases of embedded probes for humidity measurement in concrete, Granja et al. (2014). Indeed, this embedding technique balances the measuring pocket and sensor with an inner surface of the measured concrete, which has enough moisture capacity to feed the measurement pocket/sensor without overall disturbance.

**Fig. 10.10** Systematic error when measuring RH on a small sample (20 g) of material with a density of  $2400 \text{ kg/m}^3$

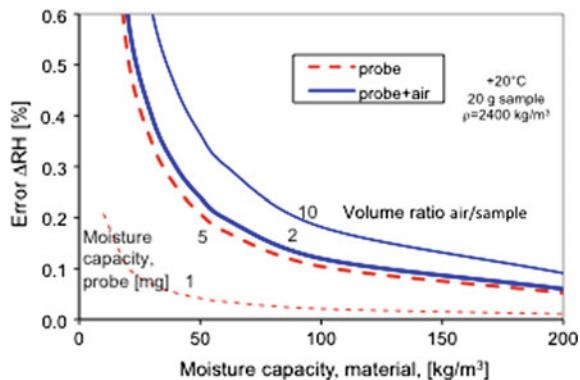
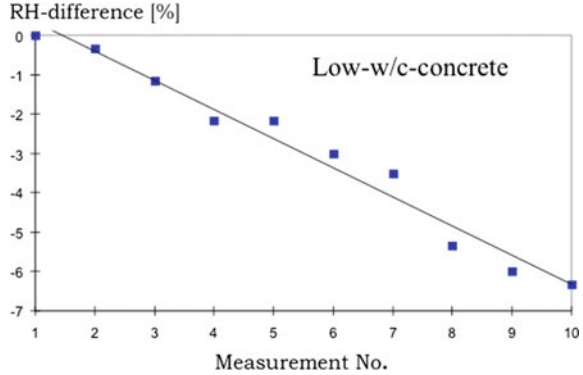


**Fig. 10.11** Systematic error of  $-0.6\%$  RH per measurement in ten repeated RH-measurements on a small sample of high-performance concrete, Hedenblad (1999)



In a recent study Johansson (2014) found large systematic errors, several % RH, when measuring RH on samples from low w/c concrete. The main reasons for these errors are the very low moisture capacity of the material and drying of the samples before being put into the measuring container. Parallel measurements in holes in the same concrete showed a very much-reduced systematic error mainly because no significant drying of the hole occurs. An example from Johansson (2014) is shown in Fig. 10.12.

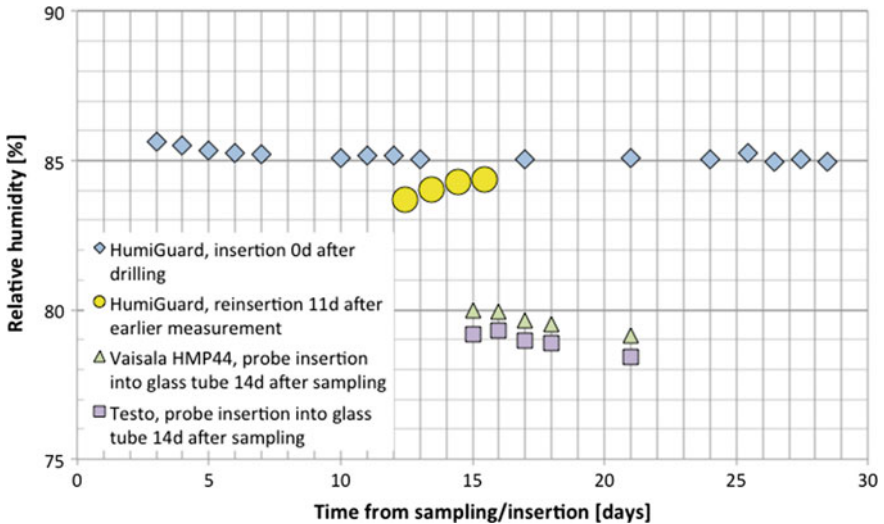


**Fig. 10.12** Comparison between RH-measurements on samples and in drilled holes in a concrete slab with low w/c. Data from Johansson (2014)

### ***10.6.3 Interface Between Measured Material and the Artificial Measurement Hole***

Grasley et al. (2014) have proposed the use of Gore-tex<sup>®</sup> membranes for protection of cast-in measurement sleeves in concrete. Gore-tex<sup>®</sup> is a densely knit fabric, known to be impermeable to liquid water, while allowing vapour transport.

Tests performed in cement paste by Granja et al. (2014) have compared the measurement performance of cast-in holes with and without Gore-tex<sup>®</sup> applied between the end of the hole and the measured material. Such comparison led to the conclusion that this type of membrane does not seem to affect the accuracy of measurements.

### ***10.6.4 Permanently Installed Probes or Intermittent Measurements?***

Most commercially available systems for humidity measurement in concrete through artificial holes (either drilled or cast-in) are based in the intermittent placement of humidity probe in the hole for taking measurements. In the periods when measurements are not being taken, the hole is sealed with a cap. In tests carried out to compare the performance of this strategy in regard to a potential permanent installation of the humidity probe (i.e. without disturbances associated to the opening/closing cycles of the cap), led to the observation of negligible differences in measurements along a two-month period, Granja et al. (2014).

# Chapter 11

## Pore Water Pressure



Lars-Olof Nilsson

The pressure of the pore water in a porous material is a measure of the state of the water. The pore water pressure  $P_w$  is related to the RH in the pores with the Kelvin equation

$$P_w = p_{sat} + \frac{RT\rho}{M} \ln\varphi \quad (11.1)$$

where  $p_{sat}$  is the vapour pressure at saturation,  $R$  is the gas constant,  $T$  is the absolute temperature,  $\rho$  is the density of water,  $M_w$  is the molar weight of water and  $\varphi$  is the relative humidity. For RH <100% the pore water is negative.

The pore water pressure is related to the capillary rise  $h$  (m) or capillary suction with the gravity  $g$  and density  $\rho$

$$P_w = \rho \cdot g \cdot h \quad (11.2)$$

The pore water pressure is related to the moisture content via a “suction curve” where the moisture content is given as functions of the pore water pressure or the capillary rise, similar to a sorption isotherm where RH is the independent variable. An example is given in Fig. 11.1. Note the scale on the horizontal axis with a capillary rise from 1 cm to 10 km.

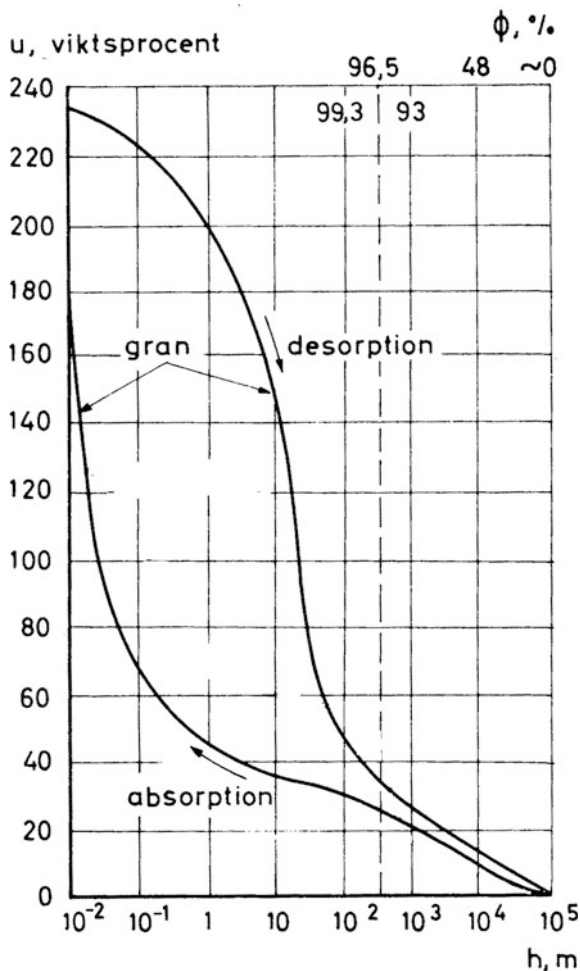
For RH close to 100% RH the RH is difficult to measure with good accuracy. One possibility is then to measure the pore water pressure directly, with a pressure transducer.

---

L.-O. Nilsson (✉)  
Lund University, Lund, Sweden  
e-mail: lars-olof.nilsson@byggtek.lth.se

L.-O. Nilsson  
Moistenginst AB, Trelleborg, Sweden

**Fig. 11.1** A suction curve for spruce, Penner et al. (1965), with the moisture content as a function of the capillary rise



An ISO standard (ISO 11276:1995) describes methods for the determination of pore water pressure in unsaturated and saturated soil using a tensiometer. The methods are applicable for in situ measurements in the field and soil cores.

For saturated soils traditional manometers of various types are used to measure the (positive) water pressure. Both for unsaturated soils and unsaturated building materials the pore water pressures are negative, however. That makes the pressure measurement somewhat more complicated. Traditional pressure transducers can still be used but the water next to the transducer must be de-aerated, Radocea (1992), which can be achieved by boiling the water.

Radocea (1992) used a simple pressure transducer connected to a small needle, cf. Figs. 11.2 and 11.3, to measure pore water pressures in fresh concrete.

An example of Radocea's results is shown in Fig. 11.4.

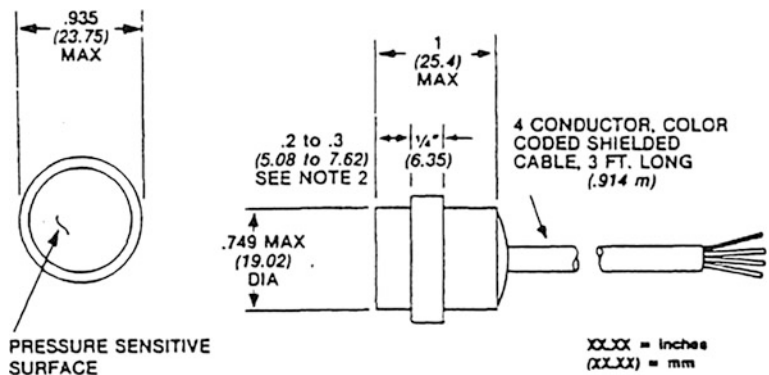


Fig. 11.2 A pressure transducer used by Radocea (1992) to determine pore water pressure in young concrete

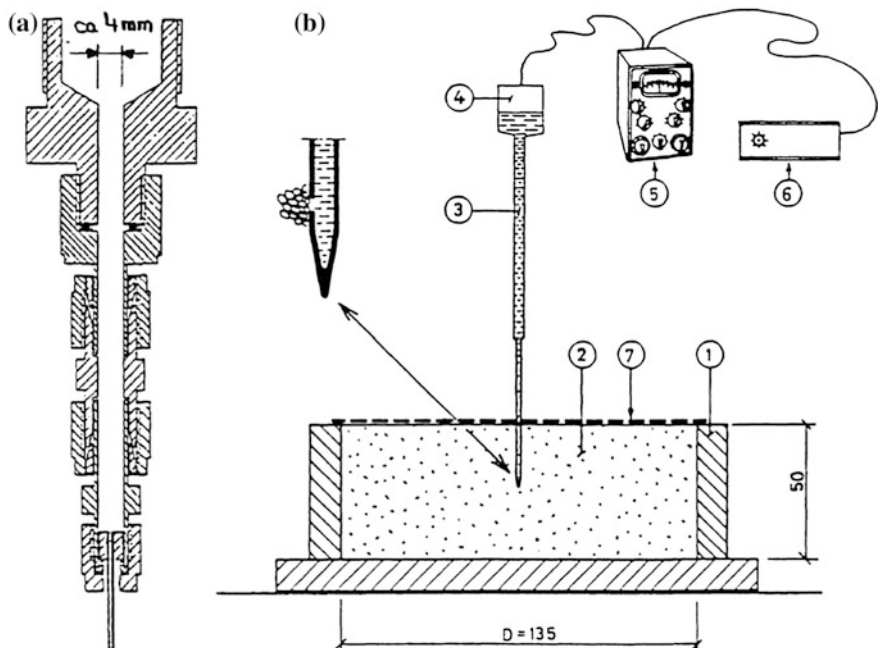
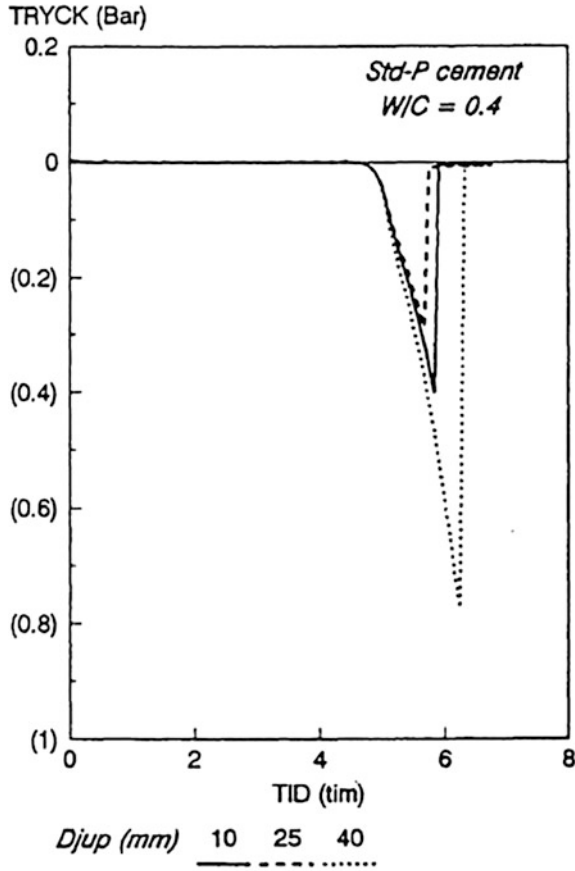


Fig. 11.3 A needle (a & b) used by Radocea (1992) to determine pore water pressure in young concrete

Pore water pressures down to close to  $-1$  bar could be determined. In many cases, however, the water inside the needle collapsed at higher pressures than that due to entrapped air voids expanding.

Fagerlund (1973) presented a modified suction plate apparatus for determining the pore water pressure of a sample, cf. Fig. 11.5.



a.  
Fig. 7.67 VAW = 0.5575

Fig. 11.4 Pore water pressures (“Tryck”) measured at three depths (“Djup”) in a fresh cement paste with a water-cement ratio of 0.45–6.5 h after mixing, Radocea (1992)

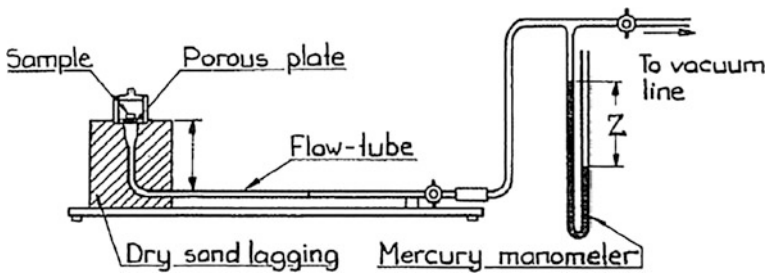


Fig. 11.5 A modified suction plate apparatus for determining the pore water pressure of a sample, Fagerlund (1973) after Cronney et al. (1952)

The sample is placed on the porous plate and covered with a protection against evaporation. The sample will suck water from the flow-tube. Decreasing the pressure with a vacuum pump prevents this. The pressure is adjusted so the meniscus in the flow-tube is kept fixed in position. The pore water pressure is read from a manometer or pressure transducer. Fagerlund (1973) claimed the technique is applicable for pressures down to  $-10^5$  Pa.

The limitations are of course the possibilities to achieve good contact between the sample and the porous plate.

# Chapter 12

## Introduction to Electromagnetic Radiation



Oliver Weichold

The following chapter focuses on the use of electromagnetic radiation to detect and determine the moisture content in civil engineering materials. This introduction intends to recapitulate the most important aspects of electromagnetic radiation and how it interacts with water.

### 12.1 Properties of Electromagnetic Radiation

Electromagnetic radiation (EMR) is the process by which energy propagates through space at the speed of light. Although the actual propagation speed of EMR depends on the refractive index of the transmission medium, the resulting speed is always the ultimate attainable one. Therefore, the energy of electromagnetic radiation does *not* depend on the propagation speed. This is in contrast to massive particles e.g. in  $\alpha$  or neutron radiation, which cannot reach the speed of light. Rather, the energy of EMR is directly proportional to the frequency and inversely proportional to the wavelength of the EMR. In the visible region, violet light at approx. 400 nm marks the high energy end and constitutes the border to even more energetic ultraviolet and gamma radiation. At the low energy end of the visible spectrum, red light of approx. 780 nm marks the border to the infrared and further down microwave and radio radiation.

Electromagnetic radiation spans more than 20 decades in terms of frequency, Fig. 12.1, and likewise in wavelength and energy. Calculating the energy at a given

---

O. Weichold (✉)  
IBAC, RWTH-Aachen, Aachen, Germany  
e-mail: weichold@ibac.rwth-aachen.de

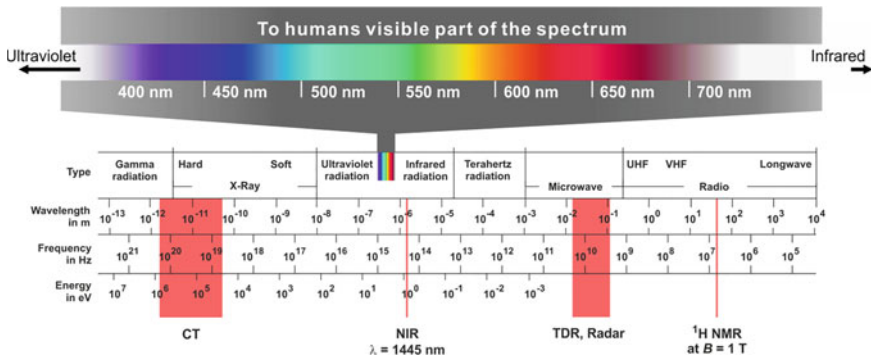


**Fig. 12.1** Selected part of the electromagnetic spectrum covering radiation used to detect moisture; very low frequent EMR  $<10^4$  Hz and cosmic radiation  $>10^{21}$  Hz not included

wavelength, e.g. the well-known yellow sodium-D line at 589 nm, results in a surprisingly low value of  $3.37 \times 10^{-19}$  J. The reason is that similar to all quantities in the subatomic region, the energy of EMR is quantized and resides in photons. The calculated value is, therefore, the energy of a single photon of  $\lambda = 589$  nm (it should be noted that a 100 W light bulb emits approx.  $10^{20}$  photons per second). Since the absolute energy of a single photo is rather low, it is usually not given in Joules, but a more manageable unit called electronvolt (eV). By definition, 1 eV is the amount of energy acquired by a single electron moved across an electric potential of one volt and is equal to  $1.6 \times 10^{-19}$  J. The photon of  $\lambda = 589$  nm in the example above, therefore, has an energy of 2.1 eV.

Unfortunately, the concept of photons turns out to be a bit tricky in explaining the properties of EMR. In a classical sense, photons are considered as particles and “photon radiation” can quickly become the attribute of “particle beam”. However, due to the enormous range of energies, it can be easily imagined that the behaviour of the EMR changes with changing frequency. Interestingly, this aspect even found its way into everyday language, since EMR in the radio band is usually referred to as wave rather than radiation and x-ray is called radiation rather than wave. However, physically it’s all photons and it turns out that photons can have both characteristics, namely those of particles and waves. This is called the wave–particle duality in quantum physics. As the everyday language indicates, the particle-like behaviour increases with increasing energy, so that photons propagating with low frequencies e.g. in the radio band behave mostly wave-like and show all classical indications of waves such as interference. In contrast, high-energy gamma radiation exhibit mostly particle-like behaviour and can undergo particle-particle collision. It should be noted that high-energy gamma radiation carries up to approx. 0.4% of the rest energy of a hydrogen atom. However, both radio waves and gamma radiation can undergo diffraction due to the wave–particle duality.

## 12.2 Physical Properties of Water that Allows It Detection by Electromagnetic Radiation

Since all types of electromagnetic radiation carry an oscillating electric and magnetic field, EMR naturally interacts with all molecular or atomic characteristics that have electric or magnetic properties. However, the type of interaction and the characteristic the EMR interacts with largely depends on the energy of the incoming radiation (wave-particle duality, *vide supra*). The most prominent electric and magnetic properties of the water molecule used for its detection are given in Fig. 12.2.

Hard, mostly particle-like X-ray and gamma radiation is scattered by the electron cloud surrounding atoms and molecules (Fig. 12.2a). The extent of scattering depends on the number of electrons in the cloud, so that atoms with high atomic weights such as iron or lead scatter the radiation more efficiently than e.g. hydrogen or oxygen. X-ray and gamma methods, therefore, detect differences in the scattering density of a sample and conclusions can be drawn from the low density areas about the location and concentration of water in the sample.

Infrared radiation stimulates oscillations in the OH bonds (Fig. 12.2b). The covalent bond between the oxygen and the hydrogen atom can be seen as harmonic oscillator with charged weights at the ends and is, therefore, able to interact with electromagnetic radiation. The resonant frequency of this particular oscillator is in the IR region of the electromagnetic spectrum. Of particular importance to the fast and non-destructive determination of water is the near-infrared (NIR) band at 1445 nm, at which a combination of symmetric and asymmetric stretching vibration of water is excited and which is used as calibration wavelength to determine the composition of beer (Fig. 12.3), Kington and Jones (2008). The interaction causes an attenuation of the incident beam, which is detected. In theory, monochromatic IR radiation of the appropriate frequency is capable of detecting nothing else than water. However, most solid materials are more or less opaque for IR radiation so that the beam does not penetrate too far into the material.

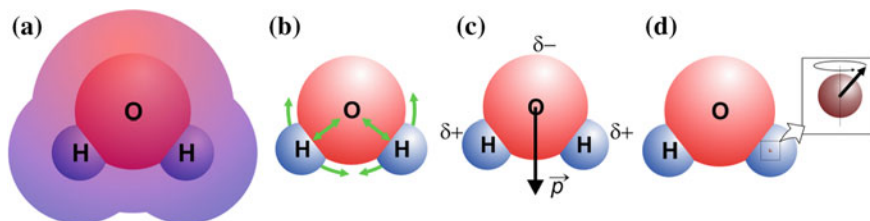
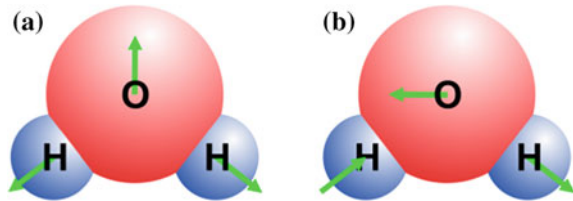


**Fig. 12.2** Molecular and atomic characteristics of the water molecule capable of interacting with electromagnetic radiation: **a** electron cloud surrounding the molecule; **b** OH bond-vibration; **c** permanent dipolar momentum; **d** spin of the hydrogen nucleus

**Fig. 12.3** Symmetric (a) and asymmetric (b) stretching vibration of water; a combination of these is excited with near-infrared radiation at  $\lambda = 1445$  nm



The electron cloud around the water molecule is not distributed isotropically. The oxygen atom has a greater pull on the electron cloud causing a deficit of electron density at the hydrogen atoms and the occurrence of permanent partial charges indicated as  $\delta^-$  and  $\delta^+$  (Fig. 12.2c). The latter give rise to a permanent dipolar momentum, which in turn causes the water molecules to align antiparallel to external electric field gradients e.g. in a capacitor. In an oscillating electromagnetic field the dipolar momentum constantly realigns with the periodic alterations of the EM field. However, the frequency of the microwave radiation used for radar and TDR measurements is approx. 4 orders of magnitude lower than IR radiation. As a consequence, microwave radiation acts on the dipolar momentum of the entire molecule and causes it to spin, while IR radiation “only” acts on the OH bond oscillator. The alignment of molecules with permanent dipolar momentum such as water in both constant and oscillating electromagnetic fields changes the permittivity of the medium. Thus, the border between zones with different moisture content presents a discontinuity in terms of permittivity causing the incident wave to be reflected. The transmission delay and the reflection characteristics can be used to detect water-containing areas in a sample.

Nuclear magnetic resonance (NMR) and the related magnetic resonance imaging (MRI) technique make use of a peculiar property of atomic nuclei in order to detect water. Similar to electrons, atomic nuclei possess a spin that gives rise to a magnetic moment. This can—in analogy to a spinning top—undergo Larmor precession (Fig. 12.2d). Excitation of this precession requires an external magnetic field and is then caused by radio waves, which are in the process attenuated. Information on the sample composition can be obtained in two ways, namely from the attenuated radio wave or from the so-called *echo*, a current induced in the receiver coil by the precessing spins. When applied in civil engineering, the latter is usually the method of choice due to the size of the structures and the resulting properties of the external magnetic fields. At a given magnetic field strength, each nucleus has a characteristic frequency which excites the Larmor precession and can, thus, be individually detected. The most important nucleus for magnetic resonance methods is the hydrogen isotope  $^1\text{H}$ , the most abundant form of hydrogen. Moisture in a sample can then be localised and quantified by focusing on the nucleic spin of the hydrogen atoms in the water molecule and the obtained echo is directly proportional to the amount of water.

### 12.3 Other

Although listed in this chapter, neutron radiation is in fact not electromagnetic radiation. Neutrons are one of the two particle types forming the atomic nuclei and are, therefore, called nucleons. In contrast to photons, neutrons are so-called massive particles meaning that their rest mass is greater than zero. As a consequence, neutron radiation cannot propagate at the speed of light and exhibits a pronounced particle-like behaviour.

Since neutrons propagate at a finite speed, neutron radiation is usually classified by means of the neutron temperature, which is a measure for the kinetic energy and, thus, the mean or better most probable velocity of the particles. The most prominent type is the so-called thermal neutrons, i.e. neutrons which are in thermal equilibrium with an ambient surrounding and having a mean kinetic energy of approx. 0.025 eV. For comparison, in the electromagnetic spectrum, this energy would correspond to a wavelength of 50  $\mu\text{m}$  (far infrared).

Although neutron radiation mirrors in terms of the transported energy large parts of the electromagnetic spectrum, its interaction with matter is totally different. Due to the pronounced particle-like behaviour, neutron radiation lacks the oscillating electric and magnetic field. Thus, while electromagnetic radiation usually interacts with an electromagnetic property of the material (*vide supra*), neutrons—being nucleons—interact with the atomic nucleus by particle-particle collision resulting in either scattering or absorption of the neutrons. The propensity of a nucleus to do so is called the neutron cross-section and varies widely from element to element and within the elements from isotope to isotope. Among all isotopes, hydrogen has the highest neutron cross-section. This property is used to detect moisture in concrete, since wet parts give rise to a more attenuated signal than dry parts.

# Chapter 13

## Nuclear Magnetic Resonance and Magnetic Resonance Imaging



Charlotte Thiel and Christoph Gehlen

### 13.1 Introduction

NMR (nuclear magnetic resonance) is a non-destructive technique that enables the depth-resolved determination of the water content inside a sample. It is versatile and can be adjusted to the particular demands of an experiment, Koptuyug (2012). In 1945, two working groups around Edward M. Purcell and Felix Bloch succeeded in finding the experimental proof of the nuclear magnetic effect simultaneously and independently, Blümich (2010). In 1952, the Nobel Prize in Physics was awarded to them. In the early 1950s, the first commercial NMR instruments were offered. Today we distinguish between NMR spectroscopy, NMR relaxometry (relaxation measurements) and MRI (Magnetic Resonance Imaging), see Fig. 13.1.

With NMR spectroscopy the electronic environment of individual atoms and interactions with neighbouring atoms can be analysed. This allows the elucidation of the structure and dynamics of molecules as well as the determination of the concentration. While NMR spectroscopy requires highly homogeneous magnetic fields, NMR relaxometry poses the least demands on magnetic field quality, Blümich (2009).

The oil industry's interest in reservoir rocks motivated the study of fluids in porous media by NMR relaxation, Blümich and Kremer (2006). Thus, new NMR instruments have been developed in recent decades, which are small and portable and can be placed on the object for detection. This enables measurements on samples unlimited in size. To image structural heterogeneity and mass transport in porous media the MRI method can be used.

---

C. Thiel (✉) · C. Gehlen  
Technical University of Munich, Munich, Germany  
e-mail: charlotte.thiel@tum.de

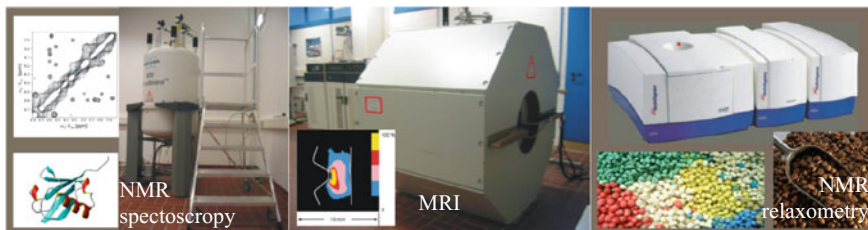


Fig. 13.1 NMR measurement types, Blümich (2016)

For the measurement of moisture in porous media  $^1\text{H}$  NMR relaxometry and MRI are of interest. Therefore this contribution is limited to these types of NMR.

## 13.2 Principle

NMR can be used to measure the hydrogen nuclei contained in porous media. NMR is based on the interaction of the magnetic dipole moment of a nuclei spin with an outer magnetic field. The orientation of the magnetic moments is manipulated by electromagnetic radio pulses at certain frequencies, compare Chap. 12. The resonance frequency depends on the type of nuclei and the outer magnetic field  $B_0$ , Abragam (1996) and Fukushima et al. (1991). For example, the frequency for protons  $^1\text{H}$  is 21.23 MHz in a magnetic field with  $B_0 = 0.5$  T, Blümich and Haber-Pohlmeier (2010). The electromagnetic energy is absorbed by the protons  $^1\text{H}$  who are put in phase-coherent oscillations and generate a signal. In case of NMR relaxation the phase coherence is broken due to energy transfer processes and the nuclei stop oscillating. The phase-coherent oscillations of the hydrogen nuclei are detected with the help of an antenna as AC-induced voltage. The computer can register two independent relaxation processes: The longitudinal or spin-lattice relaxation is described by the time  $T_1$ .  $T_1$  refers to the time it takes for the spins to recover after an excitation pulse along the main magnetic field  $B_0$  (z-axis). The transverse relaxation time  $T_2$  (or  $T_{2,eff}$  for measurements in inhomogeneous magnetic fields) corresponds to the loss of magnetization in the transverse plane (x-y plane), Casanova et al. (2011). Both relaxation times  $T_1$  and  $T_2$  are characteristic for the molecular mobility of the nuclei.

For measurements of the transverse relaxation, the detected NMR-signal can be described by following formula, Blümich and Haber-Pohlmeier (2010):

$$S(t) = S_0 \cdot \exp(-t/T_2) \quad (13.1)$$

where

$S_0$  signal amplitude (see Fig. 13.2)

$t$  time

$T_2$  transverse relaxation time

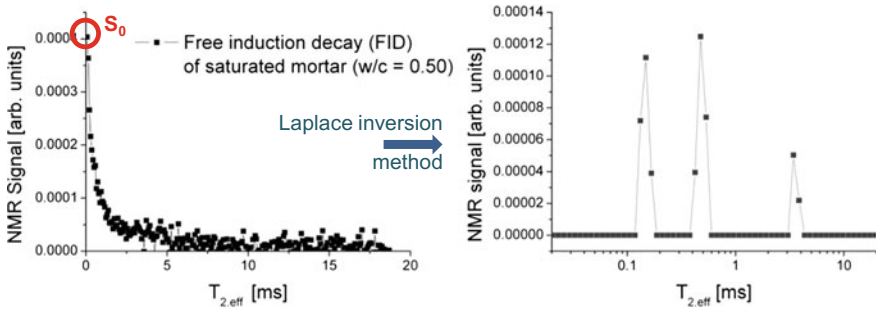


**Fig. 13.2** Left: Free induction decay (FID) of saturated mortar (Ordinary Portland Cement, w/c = 0.50). Right: Transformation of FID into a spectral distribution of the  $T_{2,eff}$  time by regularized inverse Laplace transformation with the UPEN program, Borgia et al. (1998)

The amplitude of the NMR signal  $S_0$  is an indicator for the number of hydrogen nuclei present in the screened volume and thus proportional to the total water content within a sample, see Fig. 13.2, left. Therefore, normalization of the signal amplitude of the sample with the signal amplitude of a water sample provides information on the total water content within the screened volume. The subsequent attenuation of the signals (free induction decay) is caused by relaxation mechanisms and characterizes the state of the hydrogen nuclei inside the sample.

Therefore,  $T_2$  measurements are commonly used to identify water in different pores. While pure liquid water at room temperature shows values for  $T_{2,eff}$  in the range of about 2000 ms, the relaxation time is severely reduced if a water molecule is chemically combined or adsorbed by a surface. As a consequence,  $T_{2,eff}$  of chemically bound  $^1\text{H}$  nuclei becomes so short that it cannot be observed within low-field NMR. Hydrogen of water in concrete covers a range of  $T_{2,eff}$  values from approx. 10 ms for capillary pores up to about 0.1 ms for gel pores, Wolter and Dobmann (1995). This is exemplarily shown in Fig. 13.2, right. The measurements were performed with a mobile NMR device operating at a frequency of 13.49 MHz. Here, data processing was carried out using inverse Laplace transformation. Inverse Laplace transformation is often multimodal where each peak represents a specific relaxation environment, Blümich (2009). Three peaks corresponding to physically bound water in gel pores (<30 nm) and in micro capillary pores (30–1000 nm) as well as loosely bound water in macro capillary pores (>1000 nm) and the capillary condensed bulk water are detected. By integrating the area of the peaks in combination with normalization to the total water content, it is possible to even determine the amount of water in the different pores, see for example Milachowski et al. (2012b).

Thus, it is not only possible to determine the total depth-resolved water content of a sample quantitatively, but also specify which pore sizes contain the water. Furthermore, MRI can be used to analyse the nature of transport and the characteristic features of moisture uptake or drying such as the front shape and its formation with time, Koptuyg (2012).

However NMR measurements depend not only on the water content of the investigated sample but also on the presence of magnetic or paramagnetic compounds in the sample or the environment, the temperature as well as the type and performance of the equipment and the settings used for one experiment.

For single-sided NMR also the surface texture as well as the size of the sample is important as rough or uneven surfaces affect the scanned volume. If the sample does not cover the whole sensitive volume, the NMR signal is affected by air and the scatter increases (moisture in form of vapour cannot be detected by low-field NMR).

The presence of magnetic or paramagnetic compounds leads to a shift in the magnetic field. By considering the presence of iron compounds in cement-based materials OPC, a  $T_1$  monitoring is less affected than a  $T_2$  monitoring, Nestle et al. (2002). However, calibration measurements enable the determination of the effect of paramagnetic compounds of a sample and therefore enable the performance of reliable results on materials with paramagnetic content, Orłowski (2012) and Antons (2013)

Changes in the temperature of the environment can affect the results. Hence, measurements should be carried out at constant environmental conditions.

The type and performance of the equipment is decisive for the outcome of the results. This issue is discussed in the next section.

### 13.3 Equipment

In practice, open or closed magnets are used for one and two dimensional moisture measurements, Fig. 13.3. The conventional tube arrangement (closed magnets) is applied to small samples in laboratory, Blümich and Kremer (2006). In contrast, single-sided NMR (open magnets) uses quite small devices and is therefore referred to as mobile NMR. The biggest advantage is that there are no restrictions on the sample size. This relatively new method is accomplished by using outer stray-fields instead of inner fields of magnet assembly and coil (Fig. 13.3 right). The external magnetic field shows a strong intrinsic gradient perpendicular to the sample surface. Hence, spatially resolved NMR signals can be measured without any additional gradient coils as they are needed for conventional NMR, Dobmann et al. (2013). In addition, total sampling depth up to 60 mm is currently under development. The restriction is not physical but practical due to the signal-to-noise-ratio, which gradually drops with increasing measuring depth, Dobmann et al. (2013). For the near surface concrete (0–4 mm) accuracies better than 1% have been achieved, Milachowski et al. (2012). In fact, the coefficient of variation for saturated concrete for one specific device increased from 0.4% for a total measurement depth of 4 mm to 10.1% for a total measurement depth of 24 mm.

With NMR relaxometry moisture profiles can be achieved by shifting the precision lift, which is moved automatically with a step motor. The sample is placed on a fixed plate plane parallel to the sensor, see Fig. 13.4 (left). The smallest move alignment is between 0.01 and 0.1 mm.

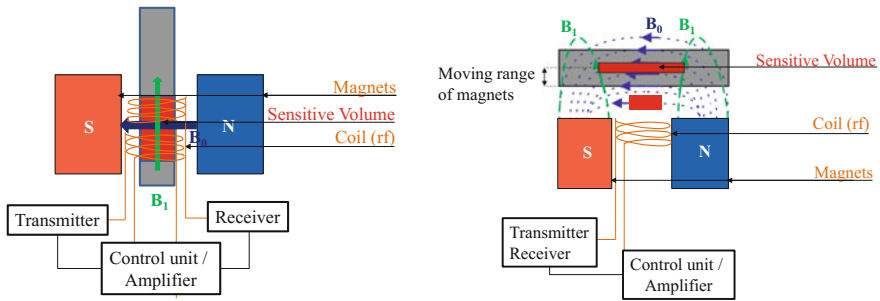


**Fig. 13.3** Left: Conventional NMR using closed magnets: Object is moved through the magnets. Right: Mobile or single-sided or inside-out NMR using open magnets, adapted from Blümich (2009)

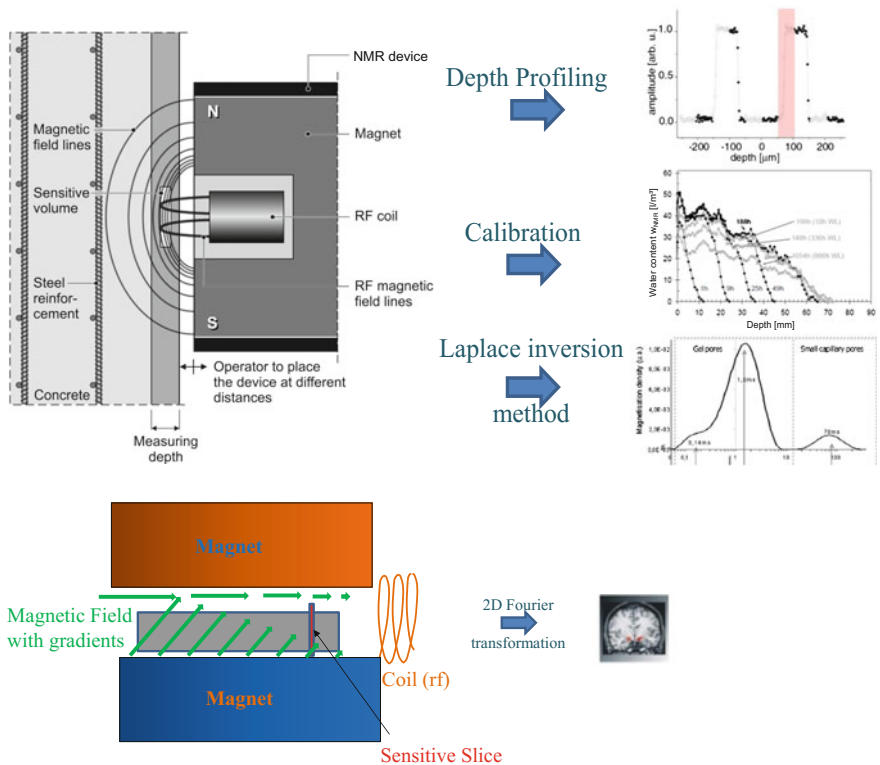


**Fig. 13.4** Top: Principle of NMR relaxometry adapted from Weiland (2016). Bottom: Principle of MRI based on Fieremans (2008)

To obtain two-dimensional images MRI is used, Fig. 13.4 right. Here, a gradient field is superimposed to the magnetic field  $B_0$ . The hydrogen nuclei appear according to their spatial location at different frequencies since there is different field strength at different locations of the sample. The direction of the field gradients is gradually moved  $n$ -times in  $x$ -direction and in  $y$ -direction by the angle  $180^\circ/n$ . The NMR Signal is registered and digitalized for  $n$  equidistant relaxation times in  $x$ - and  $y$ -direction. Then, computer-based programs calculate two-dimensional sections from the one-dimensional spectra using two-dimensional Fourier transformation. A detailed description on imaging is presented for example in Kimmich (1997).

### 13.4 Applications and Limitations

Conventional and mobile NMR are widely used to measure the water uptake and distribution as well as drying effects in cement-based materials, see Brameshuber et al. (2011), Dobmann et al. (2013), Faure and Rodts (2012), Fischer et al. (2015), Gorce and Milestone (2007), Milachowski et al. (2012) and Milachowski et al. (2012b) and in the field of cultural heritage monitoring, such as in the case of wall paintings, Proietti et al. (2014). Furthermore, the technique is applied to observe the hardening of concrete, Dobmann et al. (2013) or Philippot et al. (1998) and to control the effectiveness of water repellents, Keil, A. et al. (2011), Orlovsky (2011) and Zintel and Gehlen (2012). Antons (2017) developed a methodology to determine the penetration depth of hydrophobing agents after application on site. In addition, Faure and Rodts (2012) used MRI to follow drying processes. The MRI method was also used to study moisture dynamics in woods, Vaziri (2011), in limestone and mortar, Gummerson et al. (1979) and in bricks, Kopinga et al. (1998). Cano-Barrita et al. (2009) monitored the loss of evaporable water due to hydration/drying in cement based materials with small embedded NMR sensors. Blümich et al. (2014) used mobile NMR to determine the water content in the near-surface wall chapel in Chaalis quantitatively, Fig. 13.5. In all these studies, the results correlated very well with other techniques like traditional low field NMR or with gravimetric measurements.

The measurement time depends on the type of device and the settings used. Measurements from few seconds up to several hours or even days can be performed. Instructions on the setting of the experimental parameters can be found in Blümich and Haber-Pohlmeier (2010). For cement-based materials the size of aggregate influences the scatter. Bigger aggregates take up a large amount of the sensitive volume. Hence, the total water content might be over or underestimated due to an unfavourable distribution of large aggregates. The scatter can be reduced by increasing the amount of measured positions or even samples or by guaranteeing measurements of the exact same sensitive volume for continuous measurements.

While there are no limits on the sample size for Single-Sided NMR, the sample geometry must be adapted to the measuring instrument used. If possible, the dimensionality of an image should be reduced, Koptyug (2012).

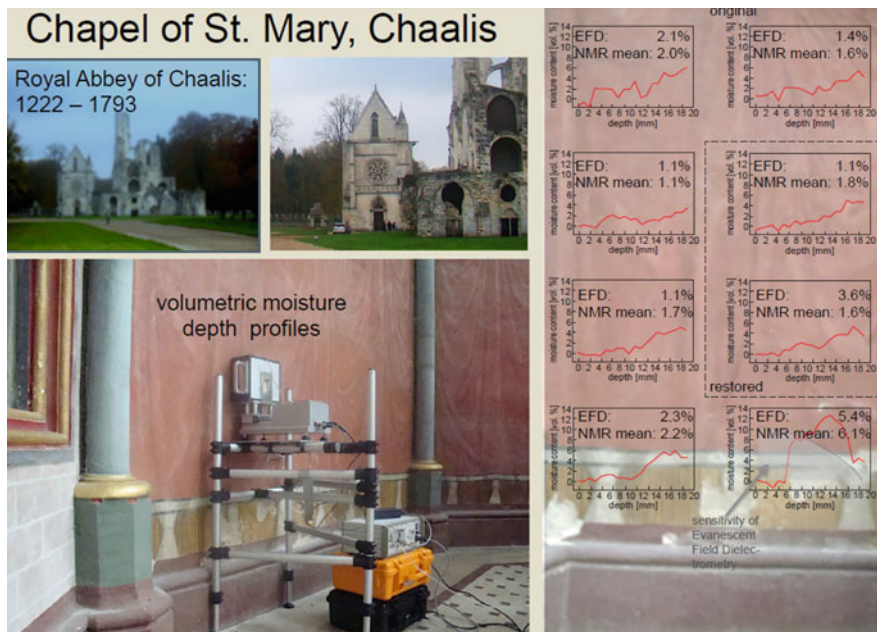


Fig. 13.5 Moisture measurement with mobile NMR in a chapel, Blümich et al. (2014)

Samples with low moisture content due to drying lead to a reduced Signal-to-Noise-ratio. With reduced moisture content the scatter increases and the signal intensity is reduced. However, this drawback can be partly compensated by optimizing the parameter settings. In addition, for single-sided NMR, increasing the measurement depth increases the Signal-to-Noise-ratio and therefore decreases the quality of the experiments.

For the analysis of dynamic moisture transport processes, a compromise between the shortest possible measuring time and the generation of reproducible results with the highest possible Signal-to-Noise-ratio must often be found. There are diverse options to reduce the influence of the noise and therefore to improve the quality of the results after a measurement. Sums or averages over a portion of the signal decay curve can be formed or the first points of the signal decay curve can be integrated, see Blümich and Haber-Pohlmeir (2010) or Koptuyug (2012) for more information.

To obtain a representative result, it should be ensured that the sample has constant water content during one measurement. It is therefore helpful to wrap samples in cling film.

As mentioned in Sect. 13.2, the method is also sensitive to temperature and magnetic compounds. For example, even small iron contents lead to a shift of the magnetic field and therefore to a change in the intended depth as well as to an increase in the Signal intensity. To take this into account, calibration measurements need to be performed. Figure 13.6 shows such a calibration for measurements of reinforcement. Calibration is also necessary when the moisture content should be

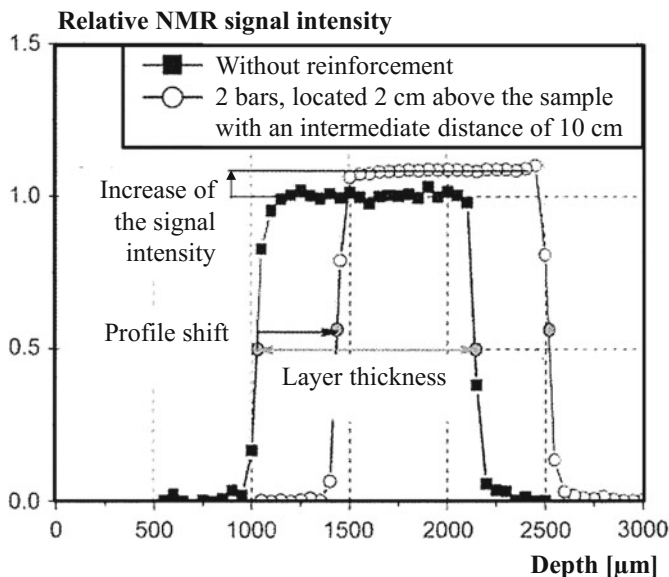


**Fig. 13.6** Depth profile of copper sulphate solution between glass (thickness 1 mm) with and without reinforcement in the environment, Orłowsky (2012)

quantified. One possibility is to use the NMR signal of copper sulfate solution with  $T_1$  of 100 ms or results of a non-NMR-technique to determine the moisture content quantitatively and to relate it to a corresponding NMR signal intensity.

In addition, the performance of the device used has to be taken into account. As shown in Fig. 13.3 the transmitter and the receiver can be served by one or two coils. If one coil serves as transmitter and receiver a certain dead time due to switching between sending and receiving occurs. Within this dead time no NMR signals are received. As a consequence, water in small pores that is bound by surface forces might relax within the dead time of the device.

Figure 13.7 shows that the water content for devices with a short dead time is directly proportional to the water content determined by gravimetry. Here, one calibration factor can be determined to calculate the total water content inside a sample.

Figure 13.7 bottom shows that for a device with a higher death time, water in smaller pores are not completely captured for the device used.

Both figures show the mean values of the NMR signal intensities after reaching the equilibrium moisture content in dependence of the corresponding average water content of concrete samples. Figure 13.7 illustrates also the corresponding pore radius of the pores in the appropriate storage humidity that are water filled according to the kelvin equation. Here, the measured signal intensity is only from storage at about 80–100% RH proportional to the water content. This means in

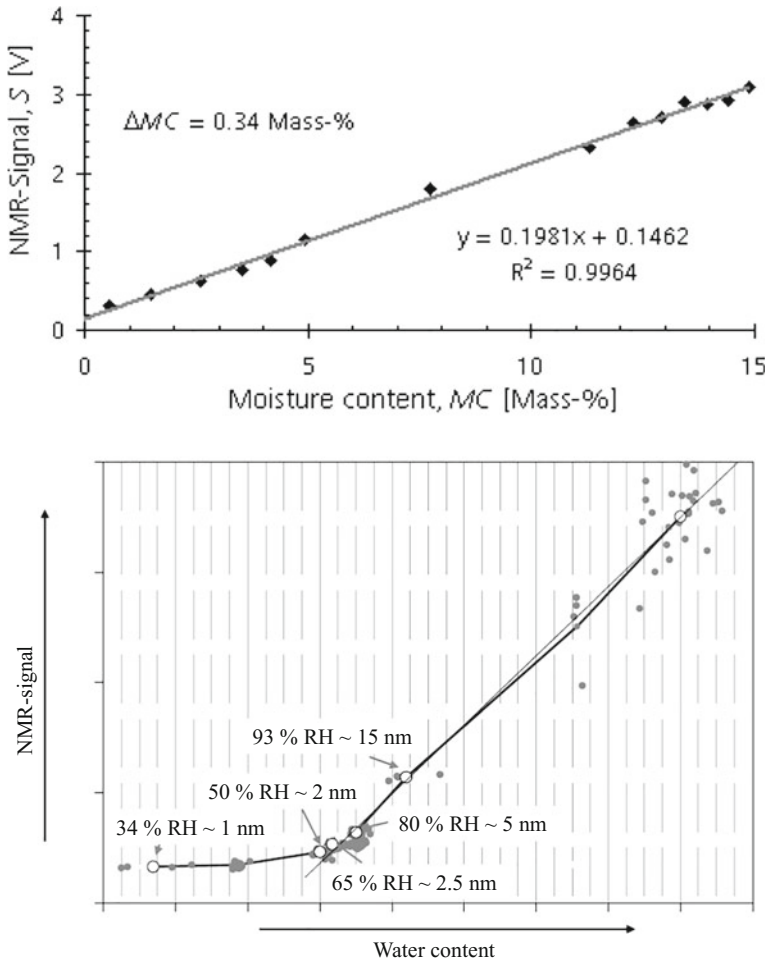


**Fig. 13.7** Calibration of the NMR Signal intensity  $S$  to gravimetric determined moisture content: Top: Calibration line for lightweight concrete using a device with a short dead time, Dobmann et al. (2002). Bottom: Calibration curve for ordinary concrete using a device with a longer dead time (RH: Relative Humidity), Rucker-Gramm (2008)

pores with a radii  $<5 \text{ nm}$ , the interactions between the water molecules and the pore walls are so strong that the relaxation time is within the dead time of the measuring coil. For this reason the water molecules are not fully captured by that specific NMR instrument.

NMR and MRI devices are commercially available either for standard or customized solutions. The prizes start by around 20000 €. Famous manufacturer are Bruker and Magritek.

## 13.5 Conclusions

This overview shows that NMR relaxometry and MRI yield satisfactory results to study different moisture phenomenon in building materials. The devices currently in use are mainly designed for indoor measurements on specimens. For routine applications, the influence of temperature and paramagnetic compounds on the NMR signals has to be determined. Current developments of mobile NMR will result in a powerful new test method for on-site measurements as first measurements on site showed promising results. Furthermore, NMR is the only technique that enables the determination of capillary and physically bound water inside a sample.

To conclude, NMR relaxometry and MRI enable the determination of the depth-resolved water content as well as the state of the water inside a sample non-destructively.

# Chapter 14

## Capacimetry



Jean-François Lataste, Walter Denzel and Hemming Paroll

### 14.1 Introduction

Capacimetry consists of the assessment of a material's electrical permittivity (or dielectric constant, noted  $\epsilon$ ). The relative permittivity is defined as normalized:  $\epsilon'_r = \epsilon/\epsilon_0$ , where  $\epsilon$  is the materials permittivity and  $\epsilon_0$  is the absolute permittivity of vacuum ( $8.854\dots \times 10^{-12}$  F.m<sup>-1</sup>). This value ( $\epsilon'_r$ ) is then always higher than 1.

The permittivity depends on the volumetric rate of the different phases of the material, the air, the solid dry phase and the water, whose relative permittivity is 1, lower than 15 (for building material) and higher than 78, respectively. Thus, the apparent permittivity for a material is mainly function of the water content in the investigated volume.

Practical assessment of permittivity is performed by measuring the electrical capacitance (C in farad), which is proportionally linked to  $\epsilon$ . The probe is made as a capacitor, where the insulating material between plates is the tested material, Fig. 14.1. The permittivity is deduced from the measurement and Eq. (14.1).

$$C = \epsilon_0 \epsilon'_r G \quad (14.1)$$

where G is the geometrical factor of the probe.

---

J.-F. Lataste (✉)  
Université de Bordeaux, Bordeaux, France  
e-mail: jean-francois.lataste@u-bordeaux.fr

W. Denzel  
DNS-Denzel, Börtlingen, Germany

H. Paroll  
Fuktcom AB, Espoo, Finland

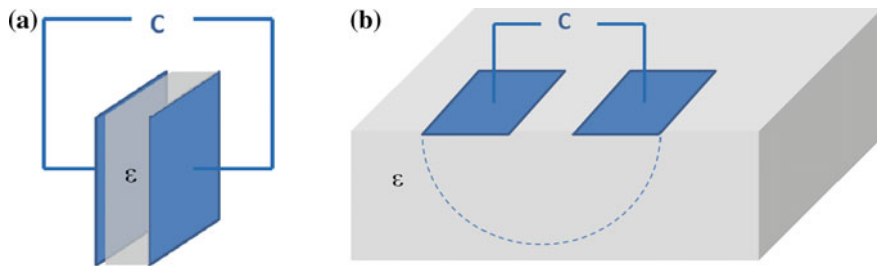


**Fig. 14.1** Capacitor (a), and schematic view of the capacity probe (b)

A number of humidity sensors use the capacitive properties. The principle is to put the insulating material (directly or indirectly) at equilibrium with the monitored material. Then, the capacitance is measured and the material moisture is deduced by a calibration curve. This way is relatively well mastered and leads to relevant results whatever the sensors-properties afford, Granja et al. (2014).

Beyond for monitoring along time by embedded sensors, this technology has been developed to allow moisture assessment through non-destructive investigation. The first works on civil engineering materials have been done for assessment of moisture on soils, Baron and Tran (1977) and granular materials, Tran and Ambrosino (1972). Some more recent applications are on moisture assessment in building materials, Dérobert et al. (2008), Siden et al. (2007), Khelidj et al. (2007), Aho et al. (2012), Tribius (2003a, b) and Strehle (2009).

## 14.2 Physical Principle and Measurement

The measurement consists of placing two (or more) electrodes on the outer surface of the samples and then applying an alternating electrical current between them. This capacitor, linked to a frequency analyser allows assessing the resonance frequency. The resonance frequency of the oscillating circuitry is a function of the capacitance, Eq. (14.2) and Fig. 14.2.

$$f = \frac{1}{2\pi\sqrt{LC}} \quad (14.2)$$

where  $f$  is the frequency,  $L$  the inductance and  $C$  the capacitance.

The response is function of the coupling between plates and materials, connections, and influence of ambient parameters (as temperature). Each part of the circuit is classically represented by a new capacitor in parallel, the global response of measurement is then the sum of each  $C$ , Baron and Tran (1977), Kuras et al. (2006).

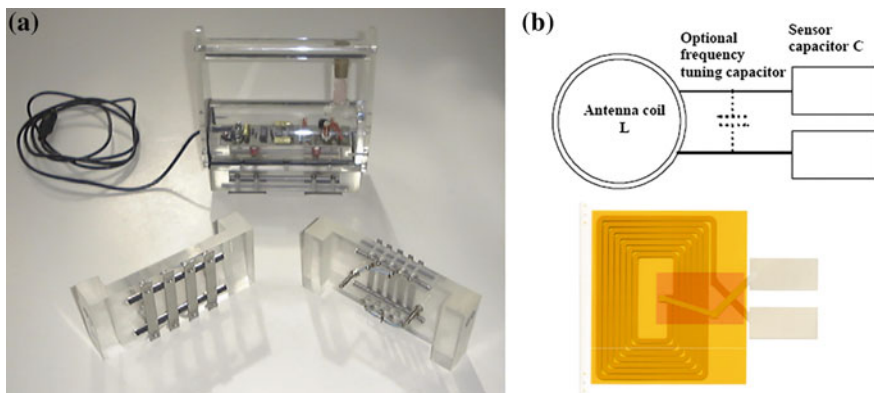


**Fig. 14.2** **a** View of a device (with several size for probes), Dérobert et al. (2008) for non destructive testing; **b** structure and photograph of a printed RFID-type moisture sensor, Aho et al. (2012)

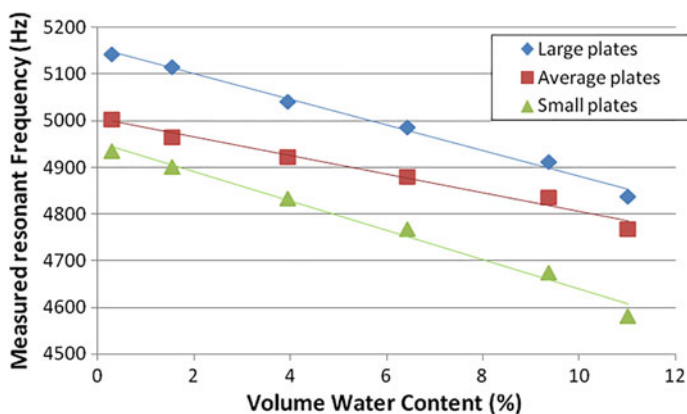


**Fig. 14.3** Resonance frequency measurement with capacity probes (three different sizes) on a concrete slab in the laboratory, versus volume water content, from Dérobert et al. (2008)

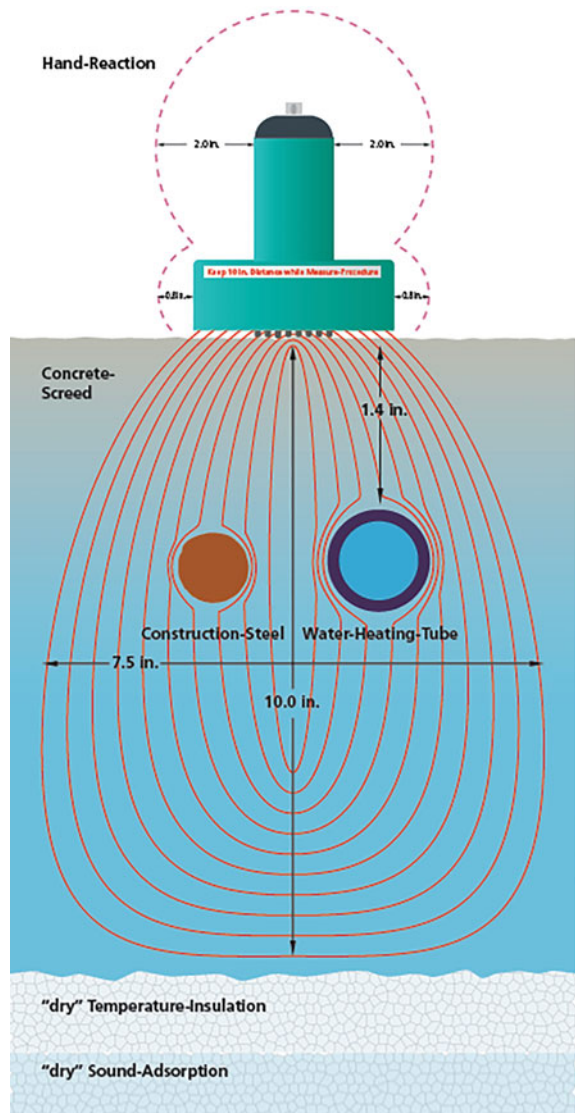
To decrease some biases (temperature for instance) the measurement is generally done in the range of 30–60 MHz. The relation between permittivity and moisture is approximated as linear, Fig. 14.3. The volumetric water content is used for express results, as long as the influence of water on measurement is function of its quantity in the investigated volume. The calibration curve between measurement and water content can be drawn from two or three calibration values, allowing then to generalize the NDT results to all of the investigated zone (making the hypothesis than all others parameters are fixed). For a known and constant water content, the technique can be used to asses porosity and its variation. Water salinity (due to

chloride for instance) does not influence the measurement when lower than 5 MHz are used.

From a practical point of view, the technique (as it is an electromagnetic method) is contactless. Nevertheless, the plates of the capacitor have to be placed on the surface. In case of excessively rough surface, the measurement may be too noisy to be considered, one of the capacitive-device-manufacturer uses spring-contacts instead of plates at the capacitor.

The probes are designed to characterize the cover concrete. The investigation depth depends mainly on the plates' sizes and design. A numerical approach leads

**Fig. 14.4** Measuring field of capacitance probes, Denzel (2015)



to estimate the penetration depth equals to 9, 20 and 80 mm for respectively plates wide of 5, 10 and 40 mm, Dérobert et al. (2008). Recently, works focus on the estimation of moisture gradient in depth. From investigation with several depths of investigations, an inversion process is proposed allow assessment the moisture distribution in depth from a surface, Fares et al. (2016). One manufacturer shows penetration-depths of more than 25 cm, Denzel (2015), cf. Fig. 14.4.

New developments are done for monitoring the moisture variations in concretes with RFID sensors (Radio Frequency identification), Aho et al. (2012). The principle of RFID sensors is to assess physical properties surrounding a sensor (a tag) emitting electromagnetic radio waves. An “active tag” need to be associated to a power source to generate their own magnetic field whom properties reflects surrounding material properties. A “passive tag” (embedded) is excited by a primary field created with a non-contact device called the inductor (operated from the surface). Thus the tag generates its own inducted electromagnetic field whom characteristics allow assessment of material properties. Their measurements could then be done with the inductor used now as a receiver. The passive way (as explained in Aho et al. (2012)) appears to be very promising regarding the low cost of these sensors, their very long service life. Developments are still needed but first results are encouraging for such a smart use.

### 14.3 Examples

An example of a real structure investigated with capacimetry is given in Sirieix et al. (2007). Where a series of investigations were carried out on a precast concrete duct in, which displayed damage patterns. The aim of the study was to rank 55 similar pipe segments in order to determine severity of the damage. Among the several techniques used, the capacitor method allows assess moisture variations along the entire pipe (Fig. 14.5).

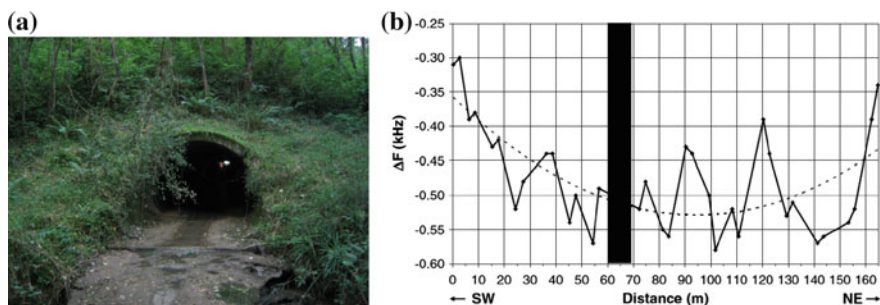


**Fig. 14.5** a SW entrance of the duct ( $x = 0$  m); b Difference in frequency as measured by the capacitor method, Sirieix et al. (2007)

Investigations lead to a qualitative assessment of the moisture distribution along the entire pipes, and are confirmed with other ND technique. More details on this example are found in Chap. [20](#).

# Chapter 15

## Time Domain Reflectometry



Alexander Michel, Henryk Sobczuk and Kurt Kielsgaard Hansen

### 15.1 Introduction

Originally, the TDR measurement technique was developed to detect defects in telecommunication cables and electrical wires, Moffitt (1964). Within recent decades, TDR was also applied to determine and monitor volumetric moisture contents in particulate and porous media, in particular soil but lately also building materials such as building bricks, concrete, sandstone, etc., see e.g. Dobson et al. (1985), Topp et al. (1980), and Phillipson et al. (2008). TDR is in general based on the measurement of the propagation time of an electromagnetic signal along a wave guide also referred to as probe, usually there and back. In the low frequency range, i.e.  $<10$  GHz, water possesses a considerably higher relative permittivity ( $\epsilon_w \approx 80$ ) than mineral compounds ( $\epsilon_s \approx 4$ ) or air ( $\epsilon_a \approx 1$ ). From the measurement of the propagation time of an electromagnetic signal along a wave-guide, the mean relative permittivity, which is among others moisture dependent, of the investigated dielectric material is derived from the reflection picture. Subsequently, the volumetric water content can be determined directly from the mean relative permittivity applying suitable material functions, which relate mean relative permittivity and volumetric moisture content.

Advantages of the TDR measurement technique include high spatial resolution, non-destructive nature, general applicability (in situ as well as laboratory), and high precision and stability. The high precision and stability of TDR allows for

---

A. Michel (✉) · K. Kielsgaard Hansen  
Technical University of Denmark, Kongens Lyngby, Denmark  
e-mail: [almic@byg.dtu.dk](mailto:almic@byg.dtu.dk)

H. Sobczuk  
Lublin University of Technology, Lublin, Poland

© RILEM 2018  
L.-O. Nilsson (ed.), *Methods of Measuring Moisture in Building Materials and Structures*, RILEM State-of-the-Art Reports 26,  
[https://doi.org/10.1007/978-3-319-74231-1\\_15](https://doi.org/10.1007/978-3-319-74231-1_15)

determination of relative changes in volumetric moisture contents up to  $0.001 \text{ cm}^3/\text{cm}^3$  (depending on calibration) and determination of volumetric moisture contents with an absolute standard error of  $0.01 \text{ cm}^3/\text{cm}^3$ , see e.g. Sobczuk and Plagge (2007) and Plagge et al. (1996).

## 15.2 Principle

The relative permittivity of a material can be calculated from the travel time of an electromagnetic signal in the investigated dielectric material. And the travel time can be measured by time domain reflectometry (TDR), i.e. measurement of a reflected signal delay with respect to the incident signal. The delay of the signal depends thereby on the square root of the relative permittivity,  $\epsilon_r$ , of the dielectric material, e.g. Sobczuk and Plagge (2007),

$$\sqrt{\epsilon_r \mu} = \frac{ct}{2L} \quad (15.1)$$

where  $\mu$  is the magnetic permeability, which can be set to 1 for non-magnetic materials,  $c$  the speed of light,  $t$  the travel time of the signal measured by TDR, and  $L$  the length of the signal travel within the investigated material. If the travel time of the signal for a given distance is known, the relative permittivity of the investigated material can be calculated according to Eq. 15.1. TDR allows for measurements of the signal travel time within the range of a few picoseconds accuracy by interpretation of the reflected signal visible on the trace of the probes in the material.

It has to be stressed that the relative permittivity is a complex function, Topp and Zegelin (2000), and in general cannot be treated as a real number. The complex part of the relative permittivity is frequency dependent and related to signal relaxation losses, which can be described using the Debye Relaxation model, Debye (1929). Within the application of volumetric moisture content measurements, TDR measurements are, therefore, commonly performed for a range of frequencies for which the complex component of the relative permittivity is small and can be neglected, Plagge (2003). Depending on the electrical conductivity of the dielectric medium, Plagge (2003) suggested signal frequencies between 80 MHz and 1.6 GHz for capillary porous media, for which the complex component of the relative permittivity can be disregarded.

A typical TDR probe signal with characteristic features for a capillary porous medium is shown in Fig. 15.1. At (a), a distinct minimum in the amplitude can be seen (caused by the resistor connected to one of the probe wires and coaxial cable) representing a time marker to ease measurement of the delay time of the further reflected signal. Afterwards, a maximum (b) in the amplitude can be observed, which represents the reflected signal at the beginning of the investigated dielectric material and a second maximum (c), which is the reflection from the end of the probe.

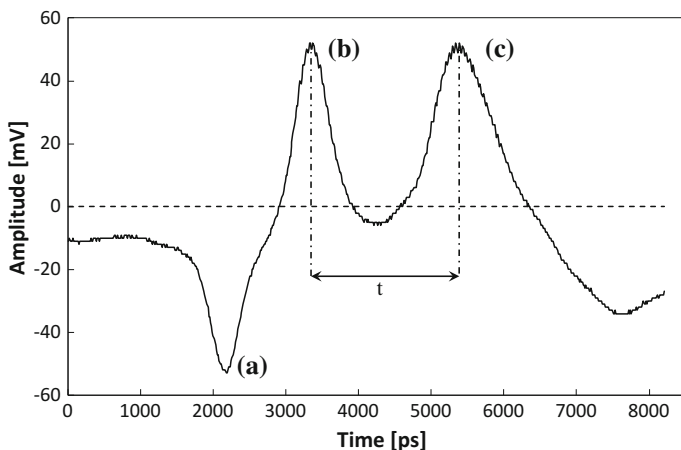


**Fig. 15.1** Typical TDR probe trace obtained from concrete specimen

The measurement time is equal to the delay of the second maximum with respect to the first maximum, which varies according to the relative permittivity of the investigated material. Among others, the volumetric moisture content of the dielectric material in which the probe is installed, has a considerable influence on the measured relative permittivity.

In capillary porous media not the entire water can be treated as free or liquid water. Water particles that are bound to solids due to Van der Waals forces cannot line up freely in the electromagnetic field. Bound water, therefore, exhibits a considerably lower value of relative permittivity than free water and may vary between that of ice,  $\epsilon_i = 3.2$ , and free water,  $\epsilon_w \approx 80$ . Phillips (1975), for example, suggested values for the relative permittivity of bound water that depend on the thickness of bound water molecule layers, i.e.  $\epsilon_b = 6$  for the first layer and  $\epsilon_b = 32$  for the second layer.

To determine the volumetric water content of a porous medium from TDR measurements, the relation between the measured mean relative permittivity and the volumetric moisture content must be known. A number of such relations have been proposed and can be found in the literature, see e.g. Dobson et al. (1985), Roth et al. (1990), Walley (1993), and Davis and Chudobiak (1975). In general, the proposed relations can be divided into models based on the mixture theory, see e.g. Tinga et al. (1973), Birchak et al. (1974), and de Loor (1968) and empirical models, see e.g. Topp and Zegelin (2000), Roth et al. (1992), and Malicki and Skierucha (1989).

Empirical models exhibit sufficient flexibility to fit experimentally determined relative permittivities including a varying number of adjustable parameters, however, without particular physical meaning. Often, empirical models are adjusted for a specific material enabling application without distinct knowledge of the particular material as it is often the case for field studies, e.g. in soil science.

Models derived from the mixture theory relate the relative permittivity of a dielectric medium to the volume fractions and relative permittivities of its constituents including implied geometrical assumptions and number of considered constituents. Such models, therefore, allow expressing the relation of the dielectric properties of a porous medium on a physical basis, while no additional adjustable parameters and thus no special reference data is required. Only the porous medium itself has to be known since not only the relative permittivity of its constituents but also the porosity and the fraction of bound water are required.

Models derived from the mixture theory are recommended when an analysis with a physical basis is required, the dielectric medium is well characterized, and no further reference data is available. If reference data is available, the application of empirical models is recommended due to the enlarged flexibility.

### 15.3 Equipment

A TDR system, suitable for relative permittivity measurements of dielectric media, consists in general of three essential components. The most important is a pulse generator also referred to as reflectometer, which realizes a fast rise time of the electromagnetic signal, a reflected signal analyzer, and a waveguide also referred to as probe, which is interconnected via a coaxial cable to the pulse generator and analyzer. In modern systems, application of multiple probes can be realized through multiplexers, which may be controlled via personal computers or data loggers. Collected reflection pictures can be automatically interpreted with the aid of computer programs and results presented in terms of e.g. travel time, mean relative permittivity of the dielectric medium, or volumetric moisture content.

Pulse generators or time domain reflectometers, produce and transmit a fast rise time electromagnetic signal, which is essential for the TDR measurement technique. Important measures for the performance of the TDR measurement system are stability and speed of the rise time of the pulse generator, influencing the systematic measurement accuracy and consistency. Rise time is thereby the measure of time required for the signal to change from a low state (signal off) to a high state (signal fully on), Phillipson et al. (2008).

Generally, TDR probes consist of a wave-guide (e.g. metal rod) installed in a body and connected to the measuring instruments via a coaxial cable connector, see Fig. 15.2 Typically, two, three, or multi parallel rods of defined length, fixed in the probe body are used as wave-guide. Varying probe lengths are used for field and laboratory tests, respectively, ranging from few centimeters to 50 cm. Recently, also surface probes have been developed that supersede placement of rod probes in dielectric media.



**Fig. 15.2** Two-rod TDR microprobe for laboratory volumetric moisture content measurements in building materials, from Scheffler (2009)

### 15.4 Applications and Limitations

In general, the TDR measurement technique can be applied in any capillary porous medium to determine and monitor the volumetric moisture content. Further applications include the determination of dielectric medium conductivity, salinity, and hydraulic conductivity, see e.g. Sobczuk and Plagge (2007).

Around 1980, the first applications of the TDR measurement technique to determine and monitor the volumetric moisture content have been reported in the field of soil science, see Fig. 15.3. For example, Topp et al. (1992) examined in situ the movement of a moisture front in soil utilizing TDR field probes. Drungil et al. (1989) and Kofalk and Plagge (1997) demonstrated the applicability of the TDR measurement technique in rocky soils. Plagge (1991) and Malicki et al. (1992) applied TDR lab probes in combination with tensiometers, to determine the hydraulic retention and unsaturated hydraulic conductivity under non-stationary conditions in soil. Plagge et al. (1991) and Sobczuk et al. (1992) were also able to

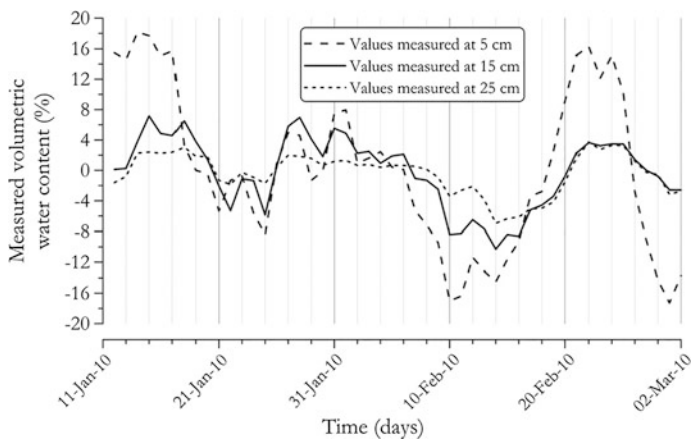


**Fig. 15.3** Relative variations (%) in volumetric moisture content of soil at various depths determined by TDR measurement technique, from Bechkit (2014)

measure the hysteresis of hydraulic properties under dynamic conditions applying TDR lab probes in soil.

More recently, the applicability of the TDR measurement technique for the determination and monitoring of volumetric moisture contents in other building materials, such as concrete, building bricks, sandstone, etc., has been reported. For example, Scheffler (2009) demonstrated the application of TDR measurement technique to determine the volumetric moisture content and monitoring of moving moisture fronts in various building materials, including building bricks, calcium silicate, aerated concrete, and lime-sand brick. An experimental set up to measure water uptake and monitor moisture profiles in a building brick with the TDR measurement technique is illustrated in Fig. 15.4 while results are presented in Fig. 15.5. Moisture uptake and volumetric moisture content within cellular concrete, applying TDR measurement technique, was also reported by Fiala et al. (2014). Similar results were presented by Phillipson et al. (2008) demonstrating the applicability of the TDR measurement technique in aerated concrete to monitor and measure the volumetric moisture content. Results of measured dielectric permittivity and determined volumetric moisture content during water uptake and subsequent drying with the TDR measurement technique and comparison to x-ray attenuation measurements are given in Figs. 15.6 and 15.7 for aerated concrete and sandstone, respectively.

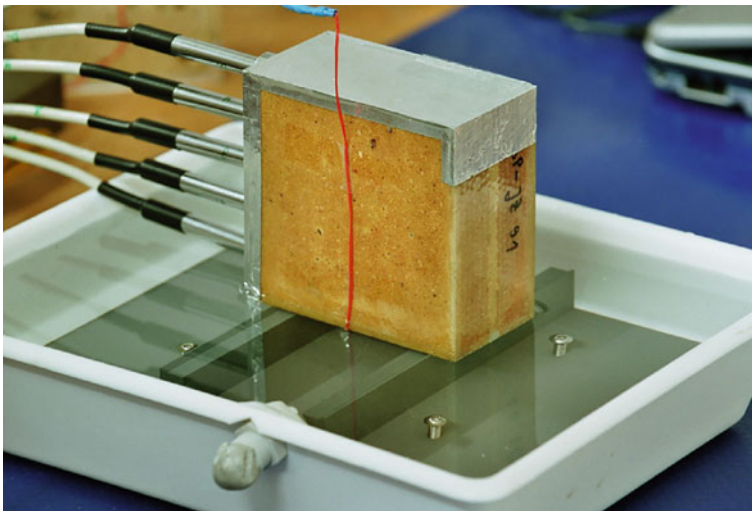


**Fig. 15.4** Experimental set up to measure water uptake and monitor moisture profiles in building brick with TDR measurement technique, from Scheffler (2009)

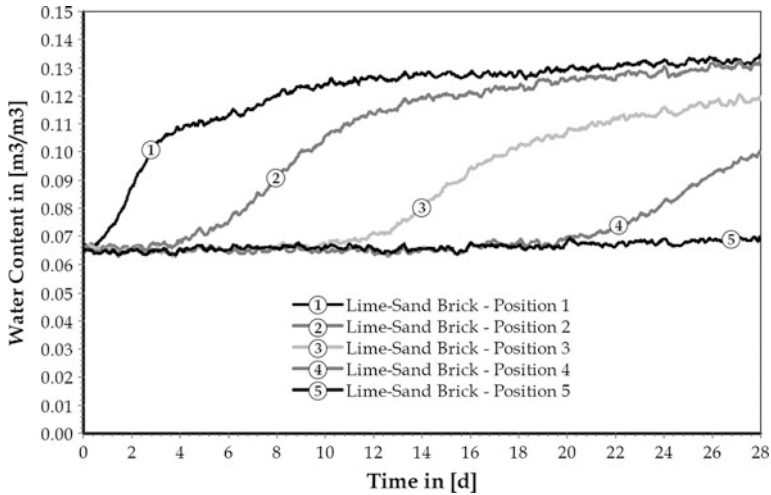


**Fig. 15.5** Determined volumetric moisture content profiles for lime-sand brick with TDR during adsorption process from 33 to 97% relative humidity, from Scheffler (2009)

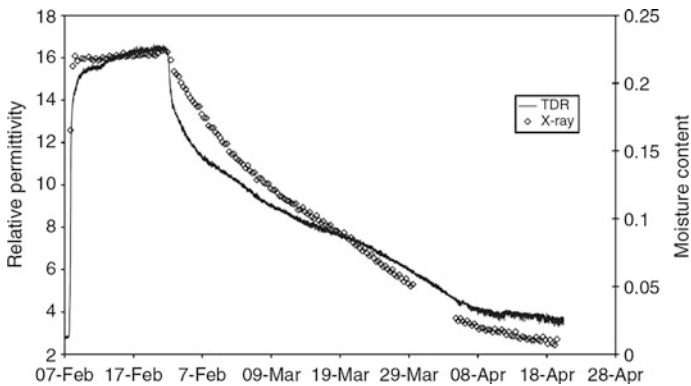


**Fig. 15.6** Measured dielectric permittivity and determined volumetric moisture content of aerated concrete during water uptake and subsequent drying experiment with TDR measurement technique and comparison to x-ray attenuation measurement results, from Phillipson et al. (2008)

Important sources of error that influence the accuracy of TDR measurements and thus determination of volumetric moisture contents of capillary porous media include among others jitter error, strobe amplitude influence, time scale stability, digitizing error, and external electromagnetic fields. For detailed information on the individual sources of error reference is made to e.g. Sobczuk and Plagge (2007).

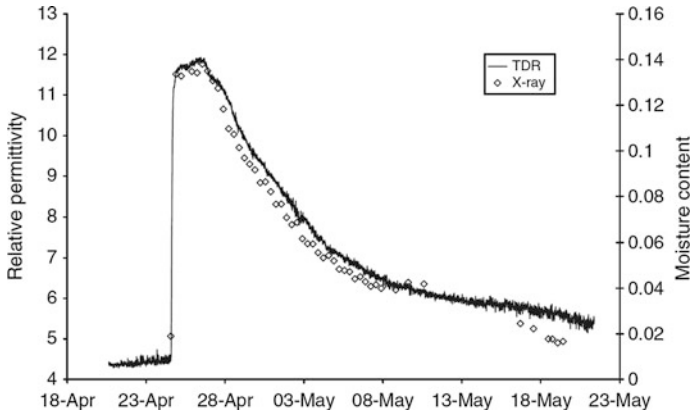


**Fig. 15.7** Measured dielectric permittivity and determined volumetric moisture content of sandstone during water uptake and subsequent drying experiment with TDR measurement technique and comparison to x-ray attenuation measurement results, from Phillipson et al. (2008)

Limitations of the TDR measurement technique include the local nature of measurements due to usage of TDR rod probes. It should be further mentioned that depth measurements of volumetric moisture contents along the probe are not possible. Finally, careful placement of TDR probes in specimens (e.g. contact between TDR probe and material) is imperative for reliable TDR measurement results.

# Chapter 16

## Microwave Reflection



Jean-François Lataste and Arndt Göller

### 16.1 Introduction

Electromagnetic methods in the range of microwaves have high sensitivity to moisture condition of building materials. Two methods are available for assessment of moisture according a non destructive way: the radar (Ground Penetrating Radar—GPR) which is a tool developed mainly for detection of internal structures in materials and which knows developments focusing on moisture assessment; and microwave technique specifically dedicated to moisture assessment. Both works with the same wavelength, but can be distinguished by the fact that for the first techniques (GPR) EM waves go through the material (transmission of the wave to material), for the second ( $\mu$ wave reflection) the waves are reflected by the material surface exposed to the EM stray field.

The investigation with Radar is done by moving an antenna on the surface to be tested. It allows high yield investigations. The antenna, linked to the processing unit, see Fig. 16.1, is composed of a transmitter and a receiver. The frequency (fixed for a given antenna) conditions the range for the investigation depth and resolution. For civil engineering use, frequencies are classically from some hundreds of megahertz to few gigahertz. Data records and representation of results are instantaneous.

An electromagnetic pulse is emitted via the transmitter antenna, reflected on the different boundaries on the surface and within the studied object, and then recorded via the receiver antenna. The characteristics of the received waves (its time of flight,

---

J.-F. Lataste (✉)  
Université de Bordeaux, Bordeaux, France  
e-mail: jean-francois.lataste@u-bordeaux.fr

A. Göller  
hf sensor GmbH, Leipzig, Germany

© RILEM 2018  
L.-O. Nilsson (ed.), *Methods of Measuring Moisture in Building Materials and Structures*, RILEM State-of-the-Art Reports 26,  
[https://doi.org/10.1007/978-3-319-74231-1\\_16](https://doi.org/10.1007/978-3-319-74231-1_16)

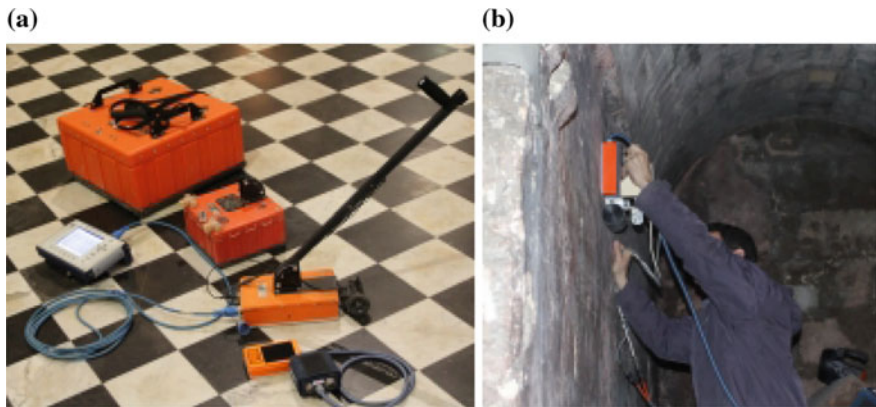


**Fig. 16.1** **a** View of GPR equipment: processing unit and 4 antennas, **b** GPR inspection on old masonry structure

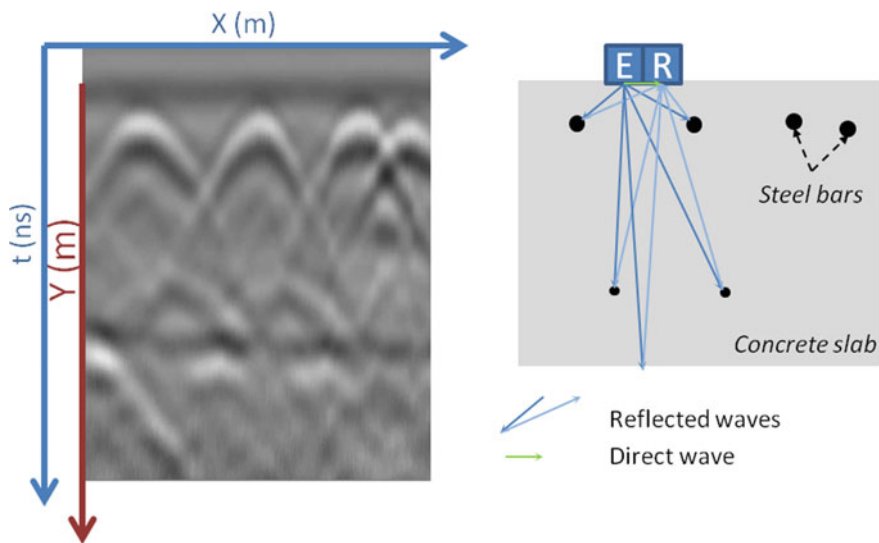


**Fig. 16.2** Radar section and corresponding physical layout

its amplitude) allow estimating the interfaces positions, and the crossed materials properties, cf. Fig. 16.2. The method is particularly well adapted for internal geometries detection, but some applications aim at assessment of moisture of concrete or salinity of interstitial fluids, cf. Soutsos et al. (2001), Laurens et al. (2005), Hughenschmidt et al. (2008) and Alani et al. (2012).

The core of microwave reflection moisture measurement is a fast and easy method by using several types of reflection microwave sensing heads. While conventional methods for moisture determination are affected by other mechanical, chemical and physical properties of the material, moisture measurements on microwave basis overcome most of these disadvantages. Microwave applicators can be made robust, and the interaction volume between electromagnetic wave and wet material can be made large enough to allow neglect of inhomogeneities in the material or small enough to get good spatial resolution.

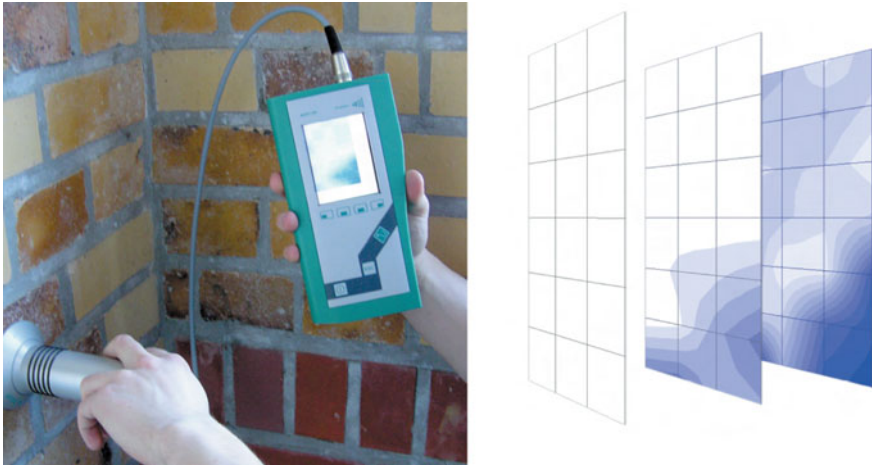
The principle of moisture investigation with microwave reflection sensors is to put the sensor at the position chosen on the material under test. The measurement is carried out by pressing the button at the handheld linked to the sensor and takes less than one second.

Portable microwave moisture meters using reflection type sensors became state-of-the-art through the past two decades and have a lot of advantages for moisture measurement in civil engineering. They are working non-destructively and very fast, are optimized for very simple acquisition of large numbers of moisture values, deliver real volume information of moisture content with high penetration depths up to dm-range, can be applied to different depth layers by choice of different microwave sensors and are independent from salinity. The menu-guided operation eases the acquisition of multi layer moisture maps. Up to 1 million readings can be stored in up to 1000 measuring arrays. Internal data processing enables visualisation of moisture maps directly in the handheld, i.e. at the place of measurement. Data transfer to PC software for graphical processing of multilayer moisture maps is carried out easily by USB interface.

Due to the statistical approach of moisture mapping this method delivers high statistical representativity of moisture distribution. Field operation and data analysis are supported by statistical functions that can be applied to each measuring array (Fig. 16.3).

Further graphical image processing of measured moisture distributions can be done using a special software for formatting moisture maps and their analysis (Fig. 16.4).

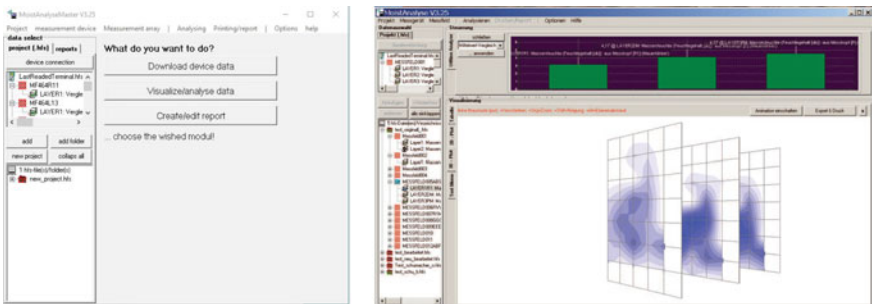
Like all dielectric methods microwave moisture meters are working indirectly and need calibration with reference to the absolute moisture content. Modern microwave moisture meters are material specific calibrated, containing a selection of calibration curves for most common building materials, that follow WTA standard for referencing. In the most advanced microwave meters the readings of different moisture sensors are directly comparable even for relative moisture index measurements in homogenous materials.



A/ Portable microwave moisture meter

B/ Multilayer moisture distribution

**Fig. 16.3** **a** View of portable microwave reflection moisture meter: volume sensor and handheld, **b** multilayer moisture distribution taken in different depth layers



A/ Main window

B/ View of multilayer plot

**Fig. 16.4** **a** Software for graphical image processing of moisture distributions, **b** view of multilayer plot and comparison of standard deviation for different layers

## 16.2 Physical Principles

Electromagnetic wave propagation is conditioned by electrical and magnetic properties of material: the electrical conductivity ( $\sigma$ ), the dielectric permittivity ( $\epsilon$ ), and the magnetic permeability ( $\mu$ ). The combination of these properties allows describing the various phenomena of wave transmission, and energy attenuation. Daniels explains largely these principles, and the place of influencing parameters on propagation.

The effective permittivity ( $\epsilon_e$ ) is described as a complex property:

$$\epsilon_e = \epsilon + \frac{\sigma}{j\omega} \tag{16.2.1}$$

where  $\sigma$  is the electrical conductivity,  $\epsilon$  the dielectric permittivity,  $\omega$  is the angular frequency,  $j^2 = -1$ . Generally the relative permittivity ( $\epsilon_r$ ) is more used. It is defined as:

$$\epsilon_r = \frac{\epsilon_e}{\epsilon_0} = \epsilon'_r - j\epsilon''_r \tag{16.2.2}$$

with  $\epsilon_0$  being the permittivity of air (real number) equal to  $8.854 \times 10^{-12}$  F/m.

The real part of  $\epsilon_r (= \epsilon'_r)$  is generally called the dielectric constant. It corresponds to the material ability to store energy. It primarily influences the wave velocity. The imaginary part of  $\epsilon_r (= \epsilon''_r)$  is called the loss factor, and corresponds to energy attenuation due to its partial absorption during propagation, Laurens et al. (2005). The ratio ( $\epsilon''_r / \epsilon'_r$ ) is named the loss tangent, written ( $\tan \delta$ ).

Some relative permittivity value are given in Table 16.1 for civil engineering materials.

One can see the very high value for water compared to others materials. The presence of free water in porosity, influence the material’s conductivity (allowing more mobility for ionic species –see electrical resistance chapter), thus increasing attenuation of EM-waves. According to Laurens et al. (2005) the existence of dispersion in concrete results only from the presence of free water in the pores and the volume water content governs its significance.

For wood, typically orthotropic material, the electromagnetic properties are influence also by the fibre direction. Generally one distinct EM-property depending on the direction, and the use of a tensor, is adapted to described wood’s complete

**Table 16.1** Typical range of dielectric characteristics of various materials measured at 100 MHz, from Daniels (2004)

Material	Conductivity (S/m)	Relative permittivity range
Air	0	1
Concrete dry	$10^{-3}$ – $10^{-2}$	4–10
Concrete wet	$10^{-2}$ – $10^{-1}$	10–20
Granite dry	$10^{-8}$ – $10^{-6}$	5
Granite wet	$10^{-3}$ – $10^{-2}$	7
Limestone dry	$10^{-8}$ – $10^{-6}$	7
Limestone wet	$10^{-2}$ – $10^{-1}$	8
Water (fresh)	$10^{-6}$ – $10^{-2}$	81
Ice (fresh water)	$10^{-4}$ – $10^{-3}$	4
Sea water	$10^2$	81
Ice (sea water)	$10^{-2}$ – $10^{-1}$	4

behaviour, RILEM TC-215 AST (2010). Actually, the transverse and radial direction show relatively similar values, different from longitudinal direction (along fibre length). Generally, dielectric constant and loss tangent are higher in the L direction than according R and T, RILEM TC-215 AST (2010).

The maximum of dielectric losses for free water is to be found around 20 GHz. This corresponds to a wavelength in air of about 15 mm and in many materials of about 5–10 mm. So a good measuring effect could be seen at this frequency, but only slight penetration of the material would be possible. That is why moisture measurement at very high frequencies is not useful for many applications.

A lot of experiments have shown that the well-known ISM frequency band around 2.45 GHz is a good choice for non-destructive moisture measurement in civil engineering applications. At this frequency, the wavelength is in the order of 122 mm (in air), allowing penetration depth into building materials in the decimeter range. The real part  $\varepsilon_r'$  of the permittivity is in the order of 80, while  $\varepsilon_r'$  for many building materials ranges between 3 and 6. This large difference of permittivities causes a well-pronounced measuring effect. Additionally and only at microwave frequencies dielectric losses of water molecules are very high, causing strong attenuation of irradiated microwaves in presence of water. Therefore at microwave frequencies two measuring effects, irrespective of microwave power, can be used, being a great advantage of microwave moisture measuring methods compared to other methods.

In building materials two types of electrical losses can be found: conductivity losses caused by moisture and salt ions and dielectric losses only caused by water. The sum of these losses can be described by the loss tangent

$$\tan \delta = \tan \delta_\varepsilon + \tan \delta_k = \frac{\varepsilon_r''}{\varepsilon_r'} + \frac{\sigma_{\text{ion}}}{\varepsilon_0 \varepsilon_r' 2\pi f} \quad (16.2.3)$$

As can be seen from Eq. (16.2.3), the denominator of the second summand contains the measuring frequency. The higher the frequency, the smaller the contribution of ion conductivity is. At microwave frequencies the sum of electrical losses is dominated by permittivity losses, whereas conductivity losses become small enough to be negligible.

In many cases microwave reflective arrangements are best choice for solving a moisture measurement problem because one-side access is possible to the sample to be measured. The principle construction of microwave reflection sensing heads is simple. They contain a microwave source, a circulator or a reflectometer separating forward and backward wave and some microwave detectors (Fig. 16.3).

Using reflection methods electromagnetic energy is transmitted by a microwave applicator to the material. Both transmitted wave and reflected wave are separated and measured. The reflection coefficient is the ratio of reflected and transmitted wave:

$$\Gamma = \frac{u_{\text{backward}}}{u_{\text{forward}}} \quad (16.2.4)$$

Reflection sensors only need access to one side of the material. They are put onto the material or mounted in a small distance with fixed size. Since Eq. (16.2.4) is a ratio, the measurement is independent of power level and can be carried out with very low power (0.1 mW). They allow integral measurement of permittivity across the depth of the material but also measurements with some depth resolution (Fig. 16.5).

The instantaneous output signal of microwave sensors is not an absolute material moisture per definition, but an equivalent to the microwave reflection coefficient in (16.2.4). The so called Moisture Index MI as the basic output signal of the microwave sensors results from multiplying the reflection coefficient with a fixed factor:

$$MI = 4000 * \Gamma \quad (16.2.5)$$

At 2.45 GHz it is possible to construct microwave antennas, which are small enough to be handled easily and which still are good focussing microwave radiation. The focussing allows to raise the penetration depth into a material up to several times the penetration depth of a omnidirectional radiator at the same frequency and effective wavelength (Fig. 16.6).

The use of radiating antenna structures like patch antennas gives larger recording depth up to 30 cm. This permits measurement of the interior moisture content of thicker samples. In addition to the near field interaction an antenna emits electromagnetic waves into the sample medium. For a patch antenna placed above the sample surface with a definite air gap the resulting feed point impedance and so the input reflection coefficient  $\Gamma$  measurably depends on the samples dielectric constant.

Open Stripline resonators are suitable as moisture sensing devices due to their inherent planar geometry. The extension of their middle range stray field is comparable to the distance between oppositely oscillating charge centers (maximum distance  $\lambda/2$ ).

If the microwave applicator is no antenna, but a stray field applicator like an open resonator, interaction volumes of about  $20 \text{ cm}^3$  and penetration depths of about 3 cm can be reached.

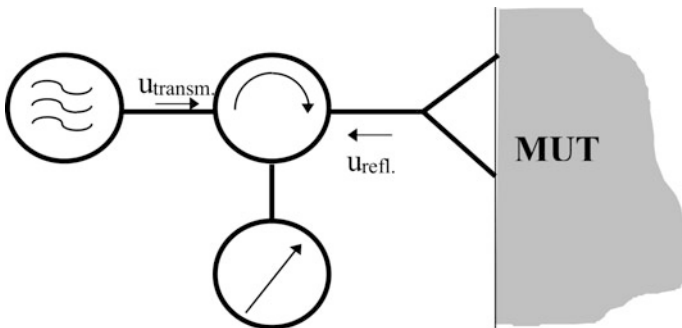


**Fig. 16.5** Microwave reflection measurement



*Microwave antenna sensing head*

*Microwave stray field sensing head*

**Fig. 16.6** Microwave sensing heads for volume and surface measurement

Using these basic microwave principles and comparing the results of surface and volume measurement one can get information about moisture distribution at the surface of material sample and in its core (Table 16.2).

**Table 16.2** Comparison of radar and microwave reflection measurement for moisture measurement

Feature	Radar	Microwave reflection
Measuring principle/device type	Pulse radar FMCW radar	Reflection coefficient (scalar or vectorial)
Electromagnetic principle	Wave propagation	Stray field Wave propagation Stray field + wave propagation
Signal processing	Time domain	Frequency domain
Temporal sequence of signal processing	Pulse sequence signals Execution sequentially, never simultaneously (transmitted wave -> object/reflected wave -> receiver)	Continuous wave (CW) Execution simultaneously (transmitted and reflected wave are existing parallel)
Measuring frequencies	Different frequencies for different penetration depths (different antennas)	Fixed frequency band (ISM band, 2.45 GHz)
Applicators	Different antennas	Different stray field applicators (like open resonators) Different antennas
Measuring method	Complex (radar signal processing)	Simple (calculation of reflection coefficient)

(continued)

**Table 16.2** (continued)

Feature	Radar	Microwave reflection
Variation in penetration depth	Different frequencies necessary (different antennas)	Same frequency, but different microwave applicators
Data evaluation/storage	Complex (specialists needed)	Simple just: measurement pointwise + data storage for each measuring position + map = one process
Maturity of method/experiences	Relatively young for moisture measurement application (few experience in practice)	Basic methods: 50–60 years practical technology: 20 years many practical experiences + applications

### 16.3 Moisture Mapping with Microwave Reflection Sensors

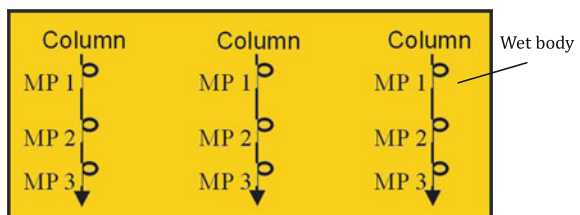
Single point measurements at buildings are not representative for the moisture status of the whole object. For this reason the method of moisture mapping was developed, where moisture values are taken systematically point-by-point in columns. It ensures the statistical relevance of the result by the always given large number of moisture readings. Moisture maps are more representative than single destructive measurements. Otherwise moisture maps deliver very descriptive moisture distributions that help to evaluate the moisture status of the building object quite well.

Figure 16.7 shows the principle of moisture mapping in the x–y–plane with the volume of microwave field interaction of the surface sensing head (Fig. 16.8).

To get a rough information concerning moisture distribution in the z–direction different sensing heads with different penetration depths can be used, as the combination of surface sensor and volume sensor. The principle is shown in Fig. 16.9.

Microwave sensors can be designed with different field geometries. Different field geometries are corresponding to different microwave applicators. These microwave applicators can be used in microwave sensors for different penetration depths. This leads to an expansion of the moisture mapping principle towards tomographic investigations. With their help a rough depth resolution becomes possible. Currently microwave sensors for layer depths up to 3, 6, 10, 25 and 80 cm

**Fig. 16.7** Principle of moisture mapping



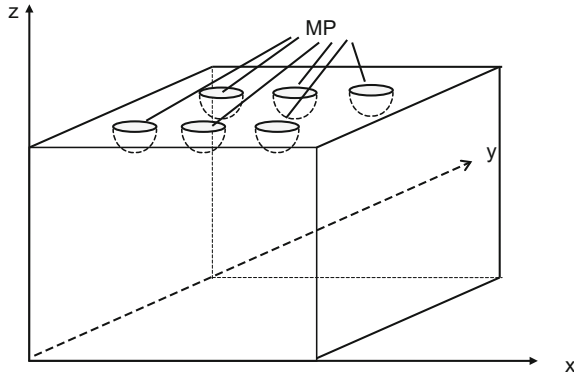


**Fig. 16.8** Lateral distribution of measuring volumes—surface sensing head

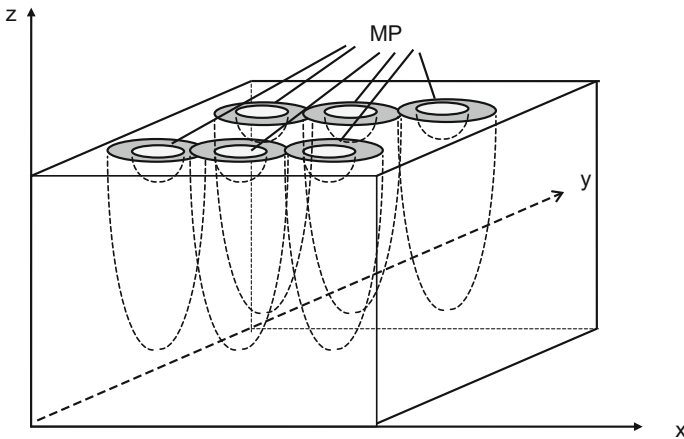


**Fig. 16.9** Lateral distribution of measuring volumes—surface + volume sensing head

are available. With these sensors a depth gradation in totally 5 steps can be carried out, whereas 4 depth steps are in the order of penetration depths that are typical for civil engineering applications.

The depth resolution principle is based on the following effects: Different microwave applicator types have different field geometries with different field depths, causing different interaction of microwaves in one layer. Each type of sensor “sees” one layer with a weighting factor different from the other sensors. From measurements with different applicators a rough depth distribution can be derived.

The most open line structures are TEM or quasi-TEM lines. In many cases they are not symmetrical, but the decrease of the electrical field is similar to

$$E, H \sim \frac{1}{r^2} \quad (16.3.1)$$

with  $r$  being the distance to the line. Sometimes the exponent of  $r$  is even higher than 2. Other structures like open resonators show exponential decrease of electric and magnetic field.

The radiation field applicators interact with the surface layer too but most part of the microwave radiation passes through this layer and therefore it causes only small interaction. This can be demonstrated easily using a simple Hertzian dipole as example: For its transversal component of the electric field (4) is derived from Maxwell's equations:

$$E_{\vartheta} = jZ_0 \frac{\vec{I} \Delta l \sin \vartheta}{2\lambda} \frac{e^{-j\frac{2\pi r}{\lambda}}}{r} \left( 1 + \frac{1}{j\frac{2\pi r}{\lambda}} + \frac{1}{(j\frac{2\pi r}{\lambda})^2} \right) \quad (16.3.2)$$

The brackets on the right side contain three terms. The first one stands for the far field of the Hertzian dipole. The other two terms describe the near field.

From (16.3.2) can be seen, that the electrical far field is decreased with  $1/r$

$$E_{J, farfield} \sim \frac{1}{r} \quad (16.3.3)$$

while the near field follows  $1/r^2$  and very close to the radiator  $1/r^3$ . Similar equations can be given for the other components of electrical and magnetic fields.

For other types of antennas the variation of the components of electrical and magnetic fields are described by radiation patterns. In case the radiation is concentrated into one direction—like for a directional antenna—this leads to a total decrease of the E-field which is different from (16.3.2).

On the other hand applicators can be designed which are somewhat mixed from strayfield applicators and radiation field applicators. Therefore a more general description of the decrease of the electromagnetic fields is

$$E, H \sim \frac{1}{r^{\alpha}}, \quad (16.3.4)$$

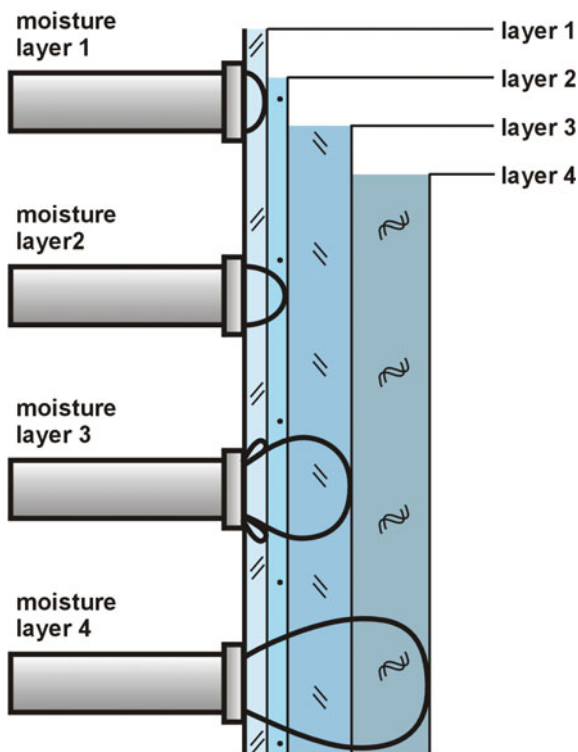
where the exponent  $\alpha$  theoretically can range between zero and infinity. In practical applications this range will be much lower, but in principle it allows the design of various applicators with different penetration depths and their combination (Table 16.3).

As shown in Fig. 16.10 this principle can be used for moisture detection in more than two layers. It allows to realize arrangements with minimum depth resolution in steps of some mm for the commonly used ISM band and maximum step sizes in  $z$ -direction in the decimeter range.

Microwave moisture measurement is an indirect measuring method. A calibration is necessary to get quantitative readings of moisture content in

**Table 16.3** Microwave applicator types and orders of their interaction geometry

Applicator type	Spat. resolution	Field range	Measuring vol.
Strayfield linear (lines)	mm	mm	Some mm <sup>3</sup>
Strayfield linear (resonators)	mm	cm	Up to some cm <sup>3</sup>
Strayfield round, symmetrical	cm	cm	Up to 100 cm <sup>3</sup>
Radiation field, planar, not directed	cm	dm	Up to 10 l
Radiation field, planar, directed	cm	dm to m	Up to 200 l

**Fig. 16.10** Depth gradation of different microwave moisture sensors, Göller (2010)

building materials. The state-of-the-art portable microwave moisture meters contain a selection of calibration curves for building materials. To get valid absolute moisture readings with these calibration curves, the physical properties of the building materials under test, especially their dry density, have to conform with those of the reference materials the calibration curves were derived from.

Exclusion criterions for microwave moisture measurement methods are the presence of large metallic conducting areas like metal foils and of air gaps in layered media with more than 1.5 cm thickness. When using a microwave reflection methods those air gaps cause additional reflections superimposing the measuring signal and impairing the clarity of measuring results.

Another problem arises from the inhomogeneity of real building materials, especially in terms of density and porosity variations. This problem can be solved partially with statistical methods that are already implemented in today microwave moisture meters.

A large part of practical moisture measurements has to be carried in layered media. The combination of different building materials with various layer thicknesses causes superimposing of reflections from the different boundary layers making ambiguities possible. Therefore an absolute microwave moisture measurement in certain layers of layered media is not possible with the technology available today. Using the available technology of moisture mapping relative moisture distributions can be won, that in most cases are sufficient for these applications.

## 16.4 Examples of Development of the GPR Technique—Concrete

Soutsos et al. (2001) have studied the link between the relative permittivity or the conductivity, and water content. Materials characterization on samples conditioned in the range of 0–18% for volume water content have been done with a network analyser, for various concretes, Fig. 16.11. This technique cannot be used on site but authors have constituted a database allowing calibrations. The link between these properties and moisture has been studied by Laurens et al. (2005), who propose an approach that is more adapted to onsite investigations. A part of the works considers the wave velocity during its reflection on the first interface (here the bottom of the slab). This approach, developed on slabs in lab, highlights the potential of the technique. Direct modelling completes these experimental results, to suggest that inversion process should be possible for an assessment of moisture content from radar investigation Fig. 16.12. The limit stays mainly in the knowledge of parameters influencing measurement (thickness for instance) and the presence of a gradient in depth.

Estimation of wave velocity in concrete is possible according to another way, working on the direct wave: those who go directly from transmitter to receiver. The measurements are done according to WARR methodology (Wide Angle Reflection and Refraction) that is to say by measuring time of flight for different distances between transmitter and receiver. One picks up the first time of arrival corresponding to the waves going along the surface. The estimation of wave's velocity (and then of dielectric constant), is then improved and is not influenced by internal damage of concrete. Some results, Dérobert et al. (2008) show that this manner underestimates the dielectric constant relatively to estimation with a lower frequency technique (capacimetry). The main interest of works with wave velocity is that dielectric constant is influenced only by moisture volumetric content.

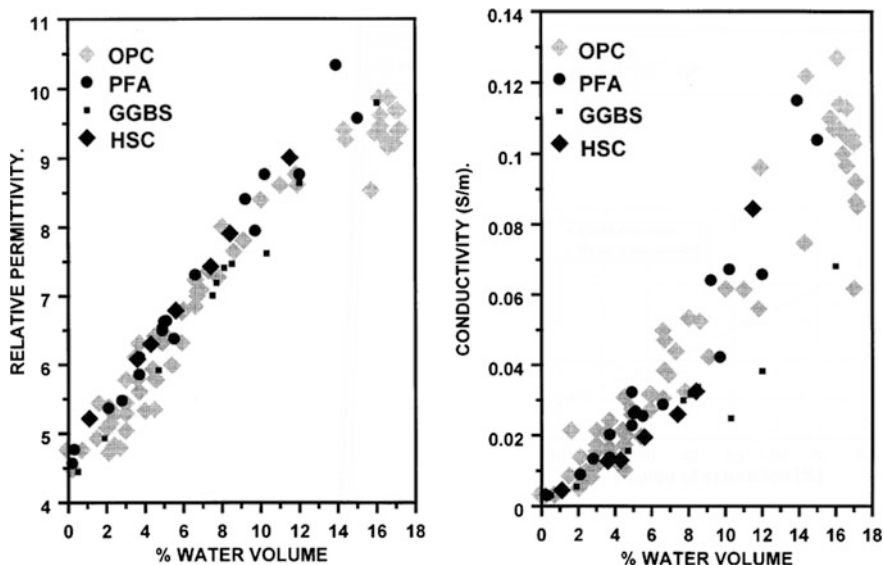
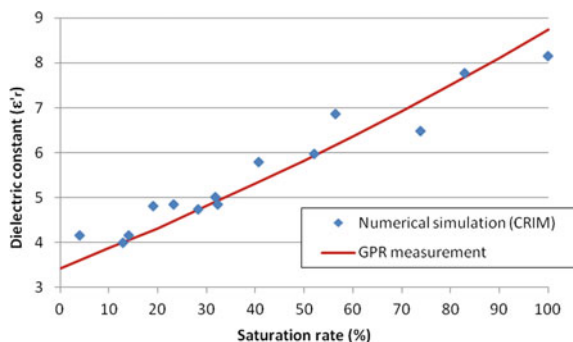


**Fig. 16.11** Relative permittivities and conductivities for Ordinary Portland cement (OPC), pulverized fuel ash (PFA), ground granulated blast furnace (GGBF), high-strength concrete (HSC), Soutsos et al. (2001)

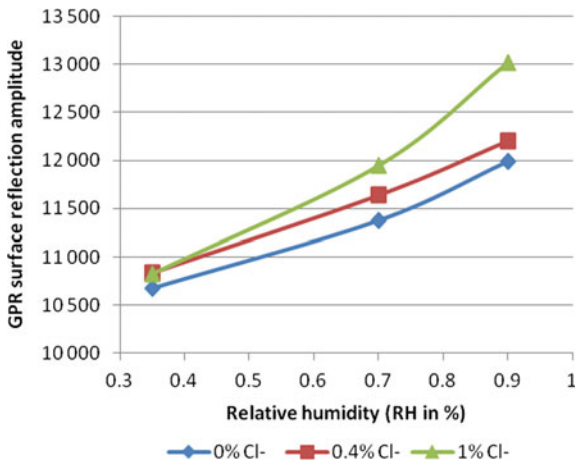
**Fig. 16.12** Dielectric constant versus saturation rate, from GPR measurement and modeling data, Laurens et al. (2005)



The difficulties stay nevertheless in the way to accurately assess the velocity, and the gradient in depth effect.

The amplitude or the attenuation of radar waves linked to moisture is also used for NDT. Indeed, moisture influences the electrical conductivity (increase of moisture generates increase in conductivity). The analysis of radar waves amplitude, easier than to record their velocity, leads to identify the effect of moisture. Sbartai et al. (2007) work on the direct wave to show how moisture effect is preponderant on concrete composition. For various concretes (W/C ranging between 0.5 and 0.8), attenuation is about 5 dB ( $\pm 0.5$ ) for dry materials and higher than 11 dB ( $\pm 1$ ) when these concretes are saturated. A similar approach was

**Fig. 16.13** Amplitude of surface reflection versus relative humidity of concrete and for various chloride content, Hugenschmidt and Loser (2008)



developed by Hugenschmidt and Loser (2008) with air-coupled antennas. The authors worked on the reflection on the surface, for various saturation degrees of concretes. Working with attenuation leads to interesting results on the influence of conductivity on EM-properties. In fact, these measures are then influenced by moisture, but also but ionic composition of the interstitial fluids. The link between attenuation and moisture is then not so trivial, Fig. 16.13.

### 16.5 Examples of Development of GPR the Technique—Wood

Several tests have been performed on various wood species. The sensitivities of radar waves to moisture content in wood is clearly show, on both the parameters dielectric constant, and loss factor (which could also be expressed in term of loss tangent). Tests show that if the both parameters are significantly sensitive to moisture content, the loss factor sensitivity is higher. Concerning the behaviour observed among wood species, the more the density is high, the more the GPR wave is influenced by moisture, Fig. 16.14. Concerning the orientation of investigation relatively to wood fibres: the propagation times are higher for transverse measurements compare to longitudinal, Fig. 16.15. Nevertheless the evolution rate between the three moisture conditions is similar whatever the orientation: if saturated degree is the reference, one observes for the both orientation a 4% decrease for middle moisture, and between 7 and 9% decrease for low moisture.

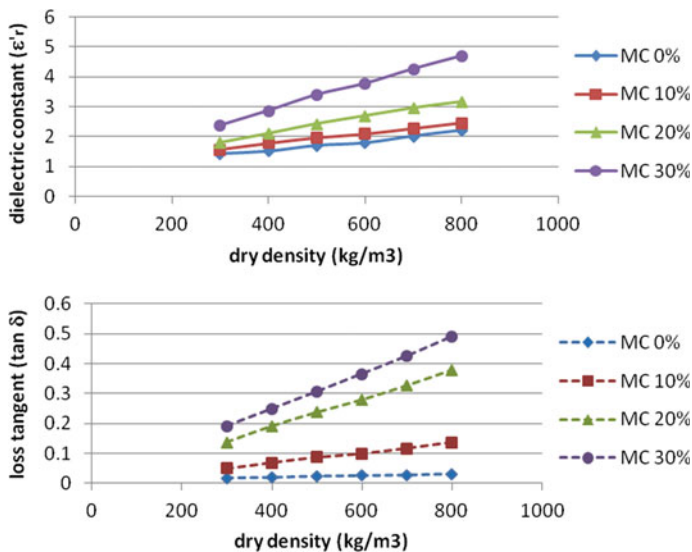
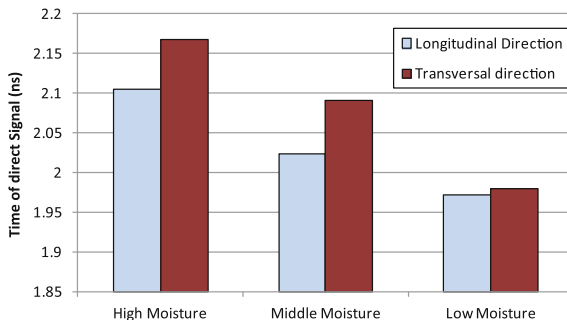


**Fig. 16.14** Effect of moisture content (MC) and density on dielectric properties on wood, Stalnaker and Harris (2002)

**Fig. 16.15** Effect of moisture and fibers direction (on epicea sample) on the propagation time of GPR Wave, Sbartai and Lataste (2008)



## 16.6 Examples of Development of the GPR Technique—Masonry

The advantages of GPR for investigation on masonry have been clearly shown, and the possibility to doing high-speed investigations, totally non-destructively, is an important parameter when one considers historical structures. Binda et al. (1994) have shown how the GPR is able to detect moisture in the three phases of saturated, partially saturated and unsaturated zone. Either the attenuation or the velocity analysis can be done. Nevertheless if the first parameter allows detecting the moistened sectors (appearing as shadowing zone on radar section), the second seems to be more interesting for accurate analysis. A RILEM Technical Committee

(TC177 Masonry durability and on-site testing) has, besides elaborate a recommendation relatively to the determination of the moisture distribution and level using radar in masonry, to formalise the good use of GPR for moisture diagnosis.

Good results have been obtained with radar velocity related to moisture content, ONSITE FOR MASONRY (2006) and Maierhofer et al. (2008). By proposing a calibration on drilling powder, Cardani et al. (2013) have showed the good reliability of GPR investigation (velocity of radar waves) to moisture content.

## 16.7 Investigation on a Real Structure in a Church Masonry Wall

A study was done with GPR, Lataste (2016), in an old church in the area close to Bordeaux (France). The question was to identify the moisture distribution in a masonry wall, in the crypt under the church's ground level.

Four different antennas were used with respective central frequency in the range of 2.6 GHz, 900, 400 and 200 MHz, to assess properties at several depths and with accurate resolution. The investigation was performed from the church soil, and from the crypt on the masonry wall.

Results presented in Fig. 16.16 are four horizontal profiles distributed on a same wall of the crypt, at different levels from the crypt's soil. They allow identification of the moisture distribution along this wall and in function of the height. The

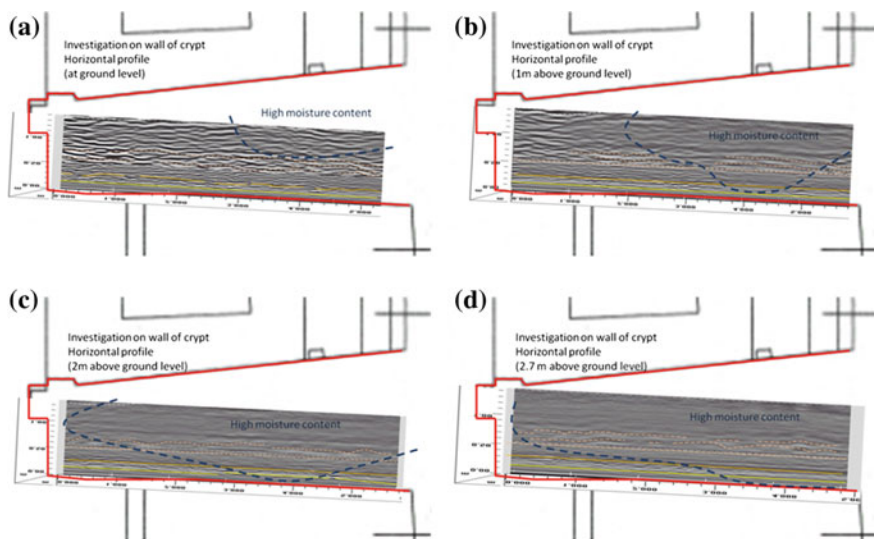


**Fig. 16.16** Horizontal combined radar Sects. (2.6 GHz, 900 and 400 MHz), respectively at ground level (a), at 1 m, (b) 2 m, (c) and 2.7 m (d) above

profiles show clearly the increase of attenuation of the radar signal, in function of the elevation of the sections. The distribution of the attenuated part of each profiles forms roughly a cone where the base is up and pointing downward. These results are very coherent with others investigations in the church. Surprisingly, they indicate that the moisture is coming from the crypt roof (in other word, the structure above the crypt) and not from the soil, as classically observed with capillary rises.

GPR investigations on this structure, by a qualitative analysis of radar wave attenuation, have identified the origin of moisture flow, allowing to orient conservation of this remarkable built heritage.

# Chapter 17

## Neutron Radiography



Zhang Peng and Zhao Tiejun

### 17.1 Introduction

Neutron radiography is in general based on the universal law of attenuation of radiation transmitted through the tested matter. Since the transmission differs for different compositions and thickness, the information on the structure and composition of the tested materials can be obtained by radiographic measurement.

For thermal neutrons (25 meV) the cross section of water is 112 b/molecule, while for the main elements (Ca, Mg, O) of many building materials, it is normally between 3.2 and 5.5 b/atom ( $1 \text{ b} = 10^{-24} \text{ cm}^2$ ). Compared to X-ray attenuation, for a better comparison, it can be seen from Fig. 17.1 that the thermal neutron mass attenuation coefficient shows no correlation with the atomic number; whereas for X-ray it is a relatively smooth curve over most of the region of the atomic number. This unique feature makes neutron capable of detecting elements or even isotopes that cannot be seen by X-ray. Besides, in contrast to X-ray, thermal neutrons are particularly attenuated by certain light substances such as hydrogen, and lithium; whereas they can penetrate easily through aluminum, lead, calcium, etc. Therefore, even for a small amount of water its movement can be detected by neutron imaging with a good contrast between water and the materials. Neutron radiography makes it possible to measure moisture in building materials, such as concrete, stone, mortar, etc. in a qualitative and quantitative way with high sensitivity.

---

Z. Peng (✉) · Z. Tiejun  
Qingdao University of Technology, Qingdao, China  
e-mail: peng.zhang@qut.edu.cn; zhp0221@gmail.com

Z. Peng  
Karlsruhe Institute of Technology, Karlsruhe, Germany

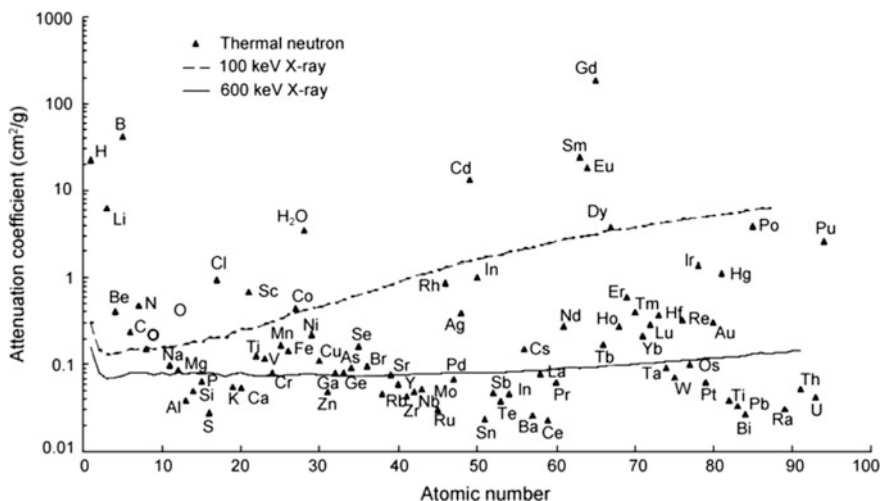


Fig. 17.1 Comparison of thermal neutron and 100, 600 keV X-ray mass attenuation coefficients versus the atomic number, ASTM (2002)

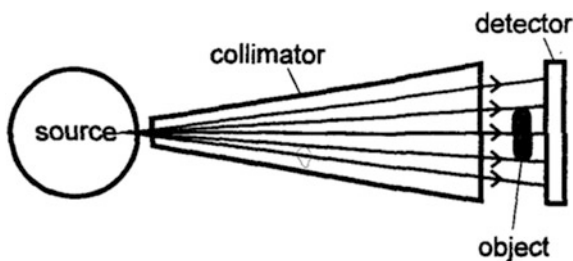
## 17.2 Facility and Principle

### 17.2.1 Facility

A neutron radiography system consists basically of a neutron beam through the collimator and a detector system, as shown in Fig. 17.2, Pleinert (1998). The source can be an isotopic neutron source, an accelerator, a nuclear reactor or a subcritical assembly. The collimator is a beam-forming assembly, which defines the geometric properties of the neutron beam and generally also contains filters to influence the energy spectrum of the beam and to reduce beam pollution by  $\gamma$ -rays. Several detector types for neutron radiography are available, consisting either of a scintillator screen and a CCD-camera or of neutron sensitive imaging plates read out by a laser scanner.

Since the mid-1980s neutron radiography is being performed by scientists and engineers in more than 30 countries. The main facilities updated until Feb. 2008 in

Fig. 17.2 Basic experimental neutron radiography set-up



these countries are listed in [http://info.casaccia.enea.it/triga/NR\\_Sites/](http://info.casaccia.enea.it/triga/NR_Sites/). With the increased interest in neutron radiography, it becomes obvious that additional neutron sources will be needed in the future to meet our needs. Unfortunately, with the increasing animosity towards nuclear power and nuclear science, and the lack of governmental support, the research reactors are being closed at an alarming rate. It therefore becomes absolutely necessary to develop alternative neutron sources that the public can be convinced are safe.

### 17.2.2 Principle

As shown in Fig. 17.2 the investigated sample is placed in the beam between the collimator exit and the detector. When the neutrons pass through the samples, the radiography detector will record an image which is a projection of the object on the detector plane and which contains spatial information on the intensity of the radiation reaching the detector. As known the attenuation of the neutron beam is due to the interaction of neutrons with the nuclei of the atoms in the object material, which can occur either by scattering or absorption. The degree of the attenuation of the object depends on the thickness and density of the tested sample. It is normally described on the macroscopic level by the macroscopic neutron cross section  $\Sigma(E)$ , which is the sum of its macroscopic absorption and scattering cross-sections. The total cross section of a material containing several chemical elements is the sum of the partial cross-sections of the  $N$  elements contained in it weighted by their mass fractions  $m_i$ :

$$\Sigma(E) = \sum_i^N m_i \Sigma_i(E) \quad (17.2.1)$$

It follows that the total cross-section of a porous material containing an unknown quantity of moisture is a linear function of the moisture content. The macroscopic cross-section of water and typical macroscopic cross-section for a dry brick and concrete are shown in Fig. 17.3, Pleinert et al. (1998). The total cross-sections of brick and concrete containing moisture as functions of the moisture content are shown in Fig. 17.4, Pleinert et al. (1998). It can be seen that the cross-section of water is much larger than those of the building materials and therefore the presence and movement of water can be detected with high sensitivity by neutron radiography.

The output of the detector is an image representing the macroscopic structure of the sample interior, as the neutron beam is attenuated depending on the sample material and geometry according to the law of radiation attenuation. It is described in Eq. (17.2.2) in first order approximation, Harms and Wymann (1986).

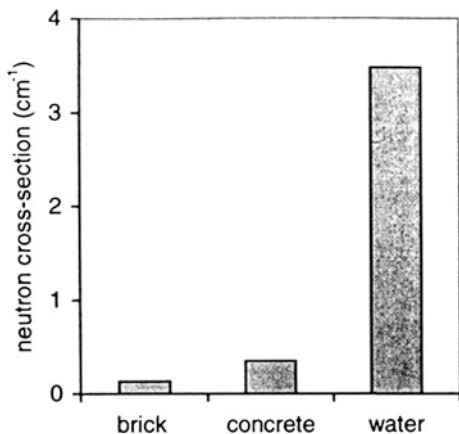


**Fig. 17.3** Comparison of the macroscopic neutron cross-section of water and of dry brick and concrete

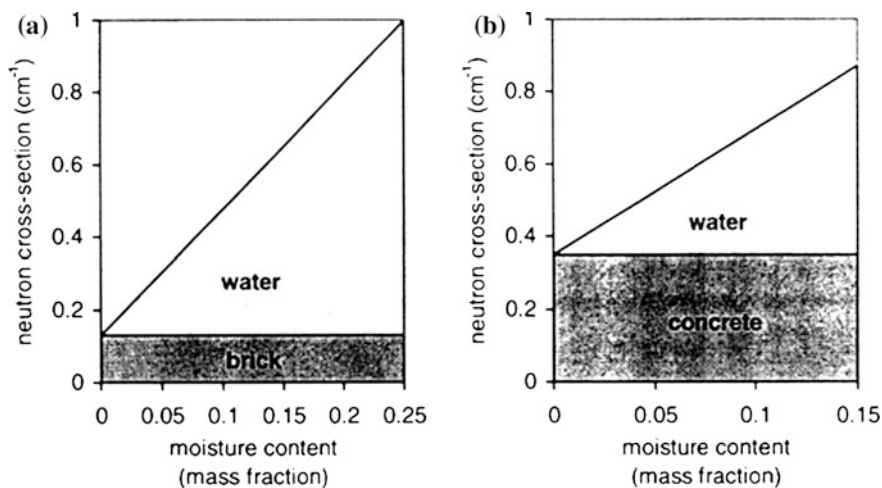


**Fig. 17.4** The total macroscopic neutron cross-sections of **a** brick and **b** concrete as functions of different moisture content

$$T(s, E) = \frac{I(x, y, z)}{I_0(x, y, E)} = e^{-\sum_{\text{tot}}(x, y, E)s} \tag{17.2.2}$$

where  $I_0(x, y, E)$  is the flux density leaving the collimator and penetrating into the object [ $\text{cm}^{-2} \text{s}^{-1}$ ];  $I(x, y, z)$  is the flux density transmitted through the object and reaching the detector [ $\text{cm}^{-2} \text{s}^{-1}$ ];  $s$  is the thickness of the sample [cm], and  $\sum_{\text{tot}}$  is

the total macroscopic neutron cross-section of the sample material [ $\text{cm}^{-1}$ ],  $T(s, E)$  is the transmission value.

However, when neutrons react in the sample, most of them are scattered by the atomic nuclei, only a few neutrons are absorbed. Scattered neutrons are not necessarily removed but can reach the scintillator and appear in the radiographs. Therefore, the transmission value of the neutron beam through the sample is overestimated somehow by the measurement. The attenuation and the sample density are underestimated, unless the scattering contribution is taken into account. For the quantitative evaluation of the radiographs, scattering correction based on Point Scattered Functions is applied by Hassanein (2006). In this approach the scattering distribution of neutrons from a directed point source through a layer of the sample material is simulated by the MCNPX Monte Carlo code. The energy spectrum of the neutrons, the sample material and thickness, detector type and distance are parameters for this simulation. More details about the neutron transmission analysis can be referred to Hassanein (2006), Hassanein et al. (2005) and (2006).

In order to further quantify the moisture content and the spatial distribution in the tested materials, the neutron images of the reference dry and wet concrete are evaluated for the mass thickness of water. They represent the mass thickness that a bar of water would have to cause the same transmission as measured. The transmission values of dry and humid building materials, such as concrete, stones, can be computed as Eqs. (17.2.3) and (17.2.4), respectively.

$$T^{\text{dry}} = e^{-\Sigma^{\text{dry}} \cdot \tau^{\text{dry}}(x,y)}. \quad (17.2.3)$$

$$T^{\text{humid}} = e^{-\Sigma^{\text{humid}} \cdot \tau^{\text{humid}}(x,y)} = e^{-\Sigma^{\text{dry}} \cdot \tau^{\text{dry}}(x,y) + \Sigma^{\text{H}_2\text{O}} \cdot \tau^{\text{H}_2\text{O}}(x,y)}. \quad (17.2.4)$$

Then the ratio between Eqs. (17.2.3) and (17.2.4) can be calculated:

$$R = \frac{T^{\text{humid}}}{T^{\text{dry}}} = \frac{e^{-\Sigma^{\text{dry}} \cdot \tau^{\text{dry}} + \Sigma^{\text{H}_2\text{O}} \cdot \tau^{\text{H}_2\text{O}}}}{e^{-\Sigma^{\text{dry}} \cdot \tau^{\text{dry}}}} e^{\Sigma^{\text{H}_2\text{O}} \cdot \tau^{\text{H}_2\text{O}}} \quad (17.2.5)$$

Therefore, the mass thickness of water  $\tau^{\text{H}_2\text{O}}$  can be obtained. Since the thickness of the tested sample is known, the mean water content in the wet samples along the transmission can be further calculated.

### 17.3 Applications of Neutron Radiography

Neutron radiography was first widely used in industrial applications in the mid-1950s and real time neutron radiography was first demonstrated by Berger (1966). After that, a commercially X-ray fluoroscopy system was modified for neutron radiography and used by Haskins (1973), Bracher and Garrett (1983),

at Harwell, U. K. Lindsay (1978) assembled and demonstrated the first successful neutron radiography facility at University of Missouri. At about the same time, Richards developed a neutron radiography facility at the McClellan Air Force Base for the purpose of detecting corrosion in aircraft assemblies. That was the first facility, which could take a full size, fully assembled jet aircraft. It is still one of the largest facilities worldwide capable of radiographing extremely large objects.

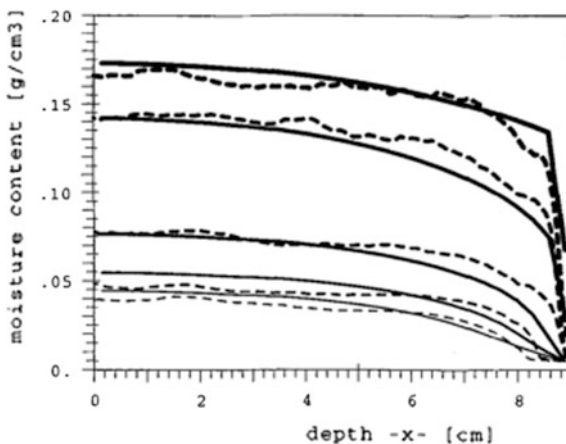
In today's world, there are a wide range of subjects and items that can be studied with neutron radiography, such as corrosion of components in aerospace industry, water flow in plants, study of nuclear fuels, and combustion of engine, etc. Measuring the moisture movement and their distributions in building materials such as concrete, mortar, stone, wood, etc., in a qualitative and quantitative way is one of these important applications.

Pleinert et al. (1998) studied the moisture distribution in mortar under drying condition by means of neutron radiography with high resolution. The time and space dependent moisture distributions in a brick sample had been determined, and the subsequent of the moisture transfer coefficient was also calculated based on the experimental results from neutron radiography, see Fig. 17.5.

Hassanein et al. (2006) also presented the possibility and successfully studied the water imbibitions into three different porous stones using neutron radiography. The process of water penetration into the stones had been recorded by neutron imaging. For instance, the neutron images one hour after the beginning of water penetration are shown in Fig. 17.6. The distributions of the intruding water in the stones had been determined quantitatively, as shown in Fig. 17.7. In addition, Masschaele et al. (2004) also performed neutron radiography to study the fluid motion into porous sandstone and limestone in three dimensions visibly.

De Beer et al. (2005) investigated the water sorptivity of concrete based on the results of neutron radiography. The neutron images of three types of concrete at two hours of water absorption are shown in Fig. 17.8. The effect of water cement ratio

**Fig. 17.5** Moisture profiles in the drying brick sample after 1, 2, 7, 14 and 21 days. Comparison between experiments (dashed curves) and numerical simulation (solid curves)



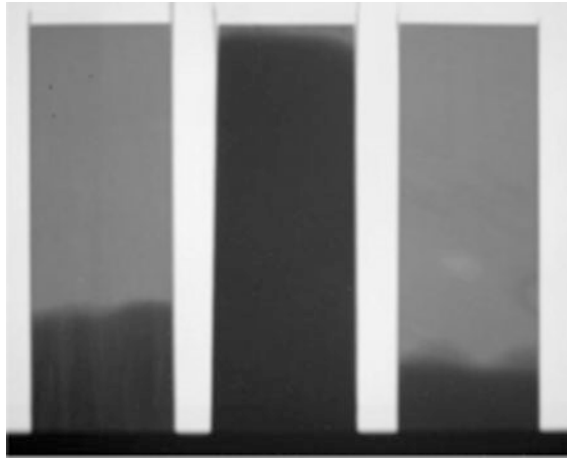


**Fig. 17.6** Neutron images one hour after the water imbibitions (upwards). The samples are, from left to right: Salem, Mansfield, and Hindustan

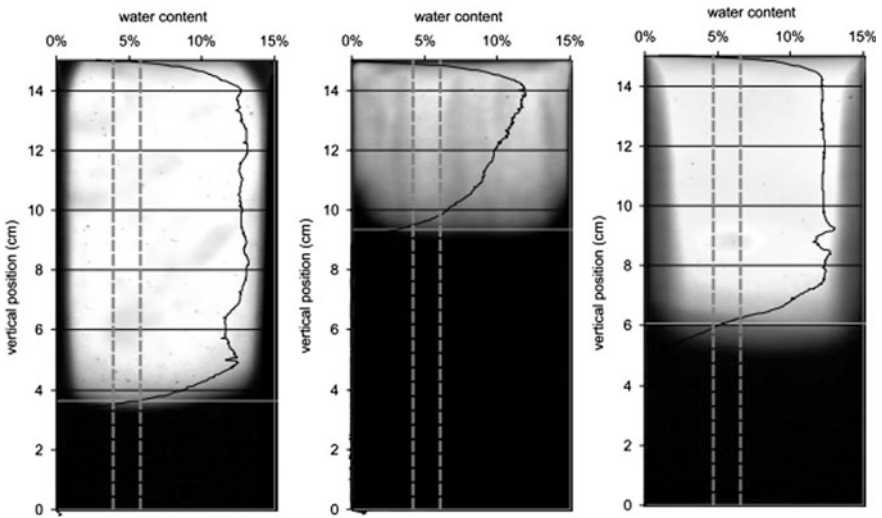


**Fig. 17.7** Images of the water content in the downwards experiments. The white line marks the front position of the water intrusion. The black curve shows the vertical profile of the water content between the two dashed lines

on water sorptivity can be clearly demonstrated. But the moisture distributions within the concrete samples were not analyzed in the contribution.

Zhang and Wittmann et al. (2011) also applied neutron radiography to follow the process of water absorption of two types of concrete with different water-cement ratio, namely 0.4 and 0.6. The typical results are shown in Fig. 17.9. In addition,

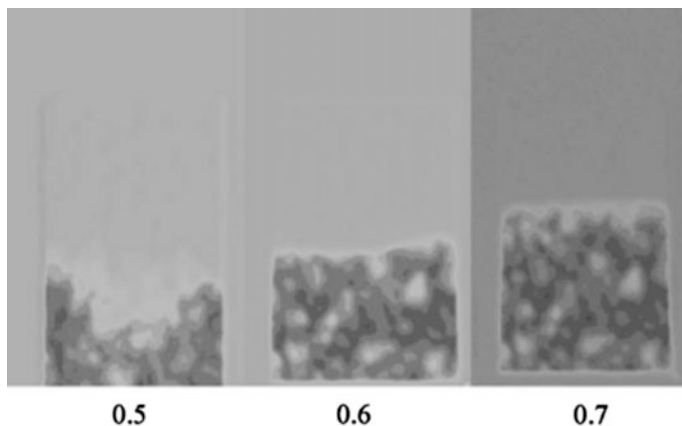


**Fig. 17.8** Neutron images of water absorption after two hours in three types of concrete with W/C ratio of 0.5, 0.6 and 0.7

the time-dependent moisture distributions in the concrete at different time had been analyzed and presented, as shown in Fig. 17.10.

Brew et al. (2009) also used neutron radiography and tomography to examine differences in water transport through cement pastes and mortars. Bulk residual water contents and sorptivity curves determined using neutron radiography are compared with data obtained gravimetrically. In addition, macro-pore volume distributions of each sample were measured. Furthermore, it was possible to use neutron radiography to monitor the change in the mass of water when samples were dried or when water moved into the samples. The trends and absolute values of weight loss and gain obtained using both approaches are very consistent for mortars, especially when a neutron scattering correction is applied.

Derluyt et al. (2013) visualized the capillary uptake of water, sodium sulphate and sodium chloride solution in limestone with neutron radiography. Both the moisture distribution and salt distribution during the capillary uptake had been measured. The typical results on moisture distribution in limestone are shown in Fig. 17.11. Dewanckele et al. (2014) also performed similar tests on water uptake processes inside porous limestone with both neutron radiography and X-ray computed tomography.

Hanzic et al. (2003, 2002) studied the liquid transport processes in concrete with neutron radiography. With this method, the height of the liquid front inside specimens had been measured. The experiment was performed with water and fuel oil for three different types of concrete. The results were compared with the sorptivity measured by the gravimetric method.

Kanematsu et al. (2009) and Zhang et al. (2010a) had studied the process of water penetration into concrete through cracks with different widths by means of neutron radiography. The neutron images had been taken serially at different time; and the moisture contents in concrete samples had been measured quantitatively. The typical results from these studies are shown in Figs. 17.12, 17.13 and 17.14.

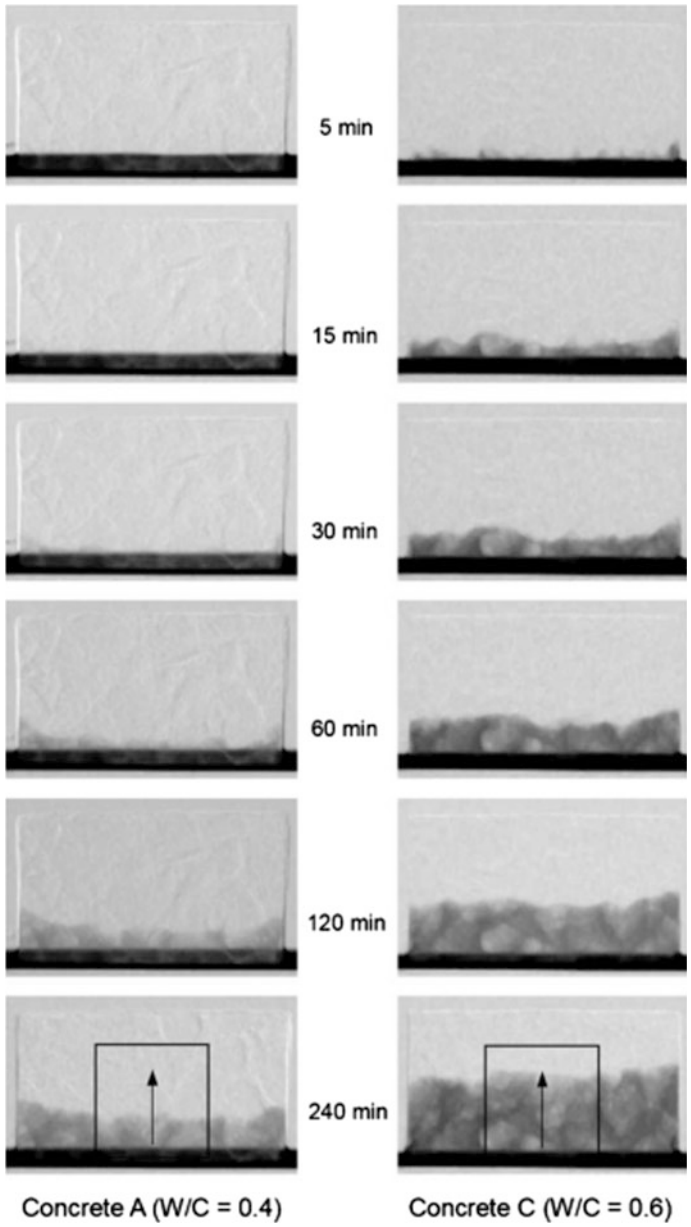


**Fig. 17.9** Neutron images of water absorption in types of concrete (left: W/C = 0.4; right: W/C = 0.6) up to 240 min

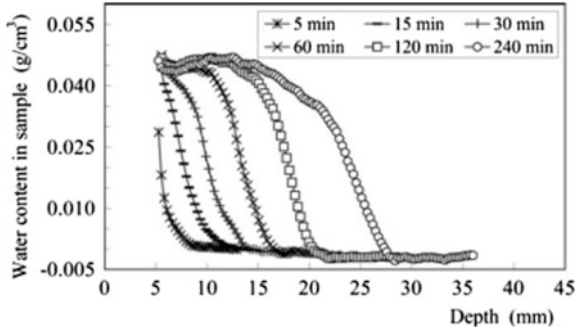


**Fig. 17.10** Moisture distribution in concrete (W/C = 0.6) as measured after different durations of contact with water

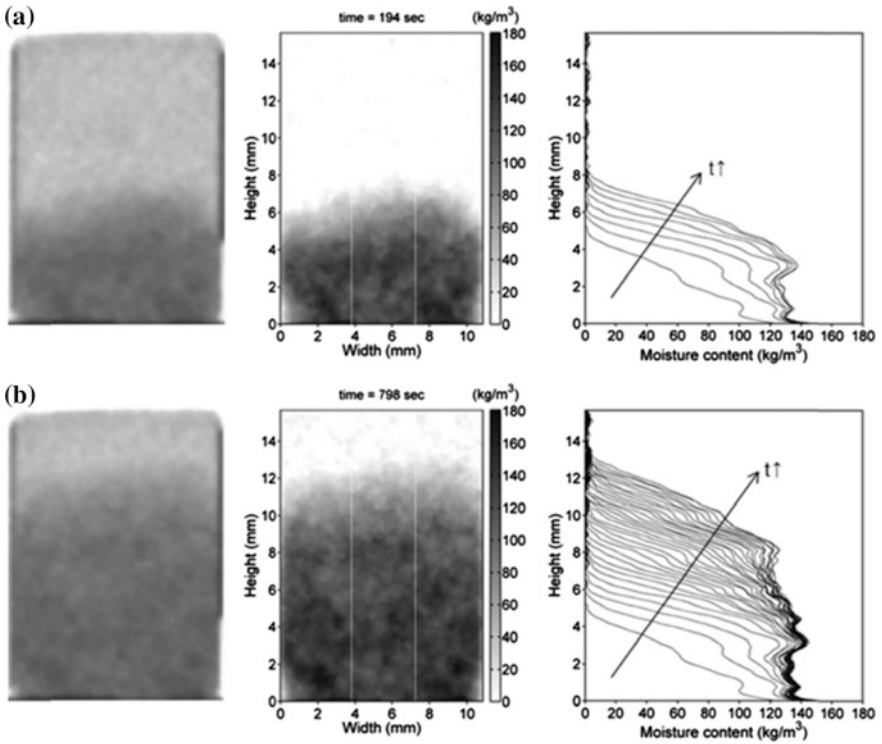


**Fig. 17.11** Neutron images, moisture distribution and moisture profiles at **a** 194 and **b** 798 s. The white lines marked the central area over which the average value of water content was measured

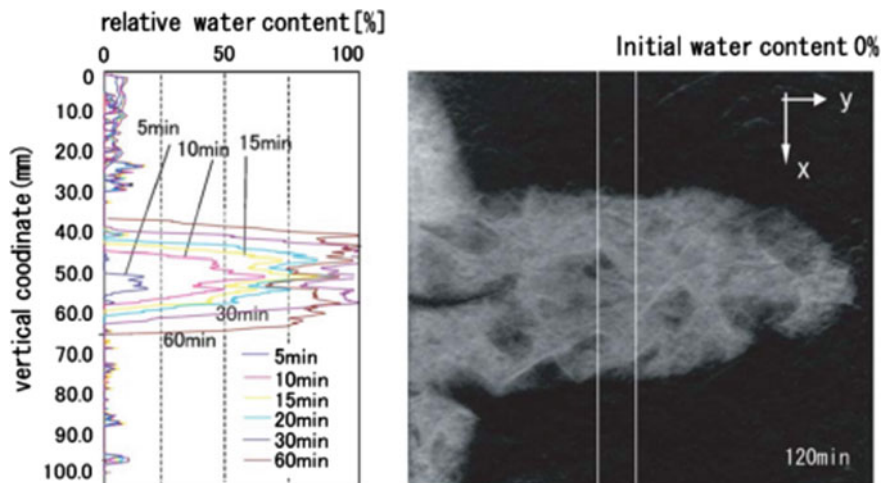


**Fig. 17.12** Quantitative measurement of water penetration into concrete through a crack with width of 0.05 mm

Both Trtik et al. (2011) and Maruyama et al. (2009) had studied the behaviour of water transfer from saturated lightweight aggregates to cement paste matrix by means of neutron radiography. The release of water from aggregates had been recorded in particular visually. The time-dependent spatial water distributions around the aggregates had been also measured carefully with this method.

Snoeck et al. (2012) and Van Tittelboom et al. (2013) had studied the effect of self healing on water penetration into cracked cementitious materials with neutron radiography.

In addition, Lieboldt and Mechtcherine (2013) and Zhang et al. (2010b) had performed neutron radiography to study the water capillary transport through textile-reinforced concrete and strain hardening cementitious composites with PVA fibres, respectively. The process of water penetration into the materials had been followed serially; and the moisture distribution and moisture profiles in the materials had also been measured. Recently, Schroeffl et al. (2015) studied the process of water penetration into composites specimens of steel reinforced concrete strengthened with SHCC by neutron imaging. Qualitative and quantitative image evaluation revealed that water capillary suction was very intense; within 1.2 min the cracks in both SHCC and RC filled with water completely, deep into the interior, as shown in Fig. 17.14.

More recently, Lucero et al. (2015) had performed very similar tests on water penetration into cement mortar by means of neutron radiography. The interesting part of this work is to quantify the degree of water saturation in air-entrained mortar based on the Beer's Law and the mixture proportions calculation without the reference image in the dry state. The results shown in Figs. 17.15 and 17.16 indicate well the feasibility of this method to quantify water movement and moisture

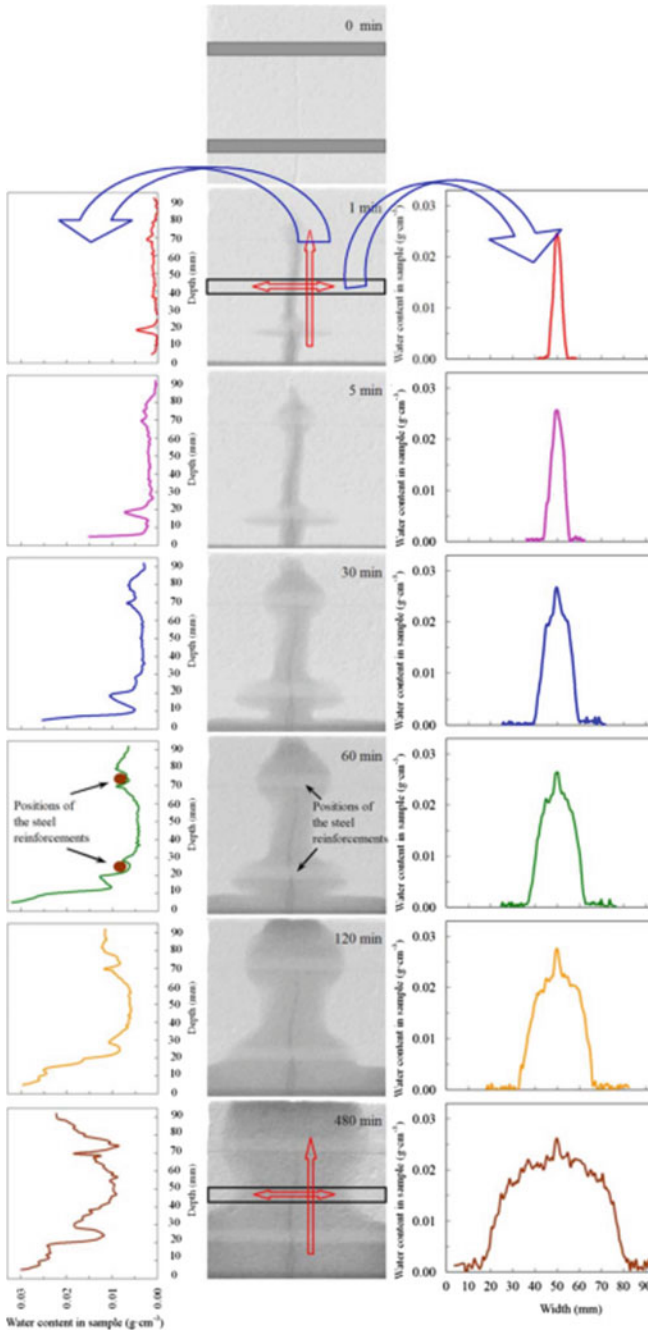


**Fig. 17.13** Neutron images of water penetration into cracked (crack width of 0.35 mm) steel reinforced mortar during contact with water for up to 480 min and the corresponding quantitative water profiles along a vertical and horizontal axis

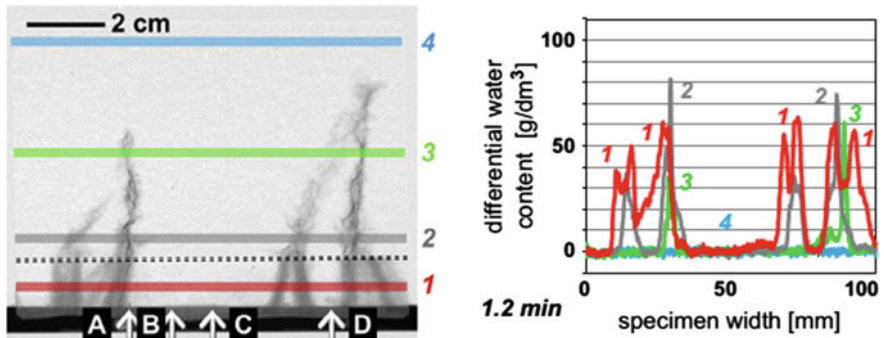


Fig. 17.14 Neutron image at time of 1.2 min contact with water and the water content at the four heights; the black dash double line marks the boundary between SHCC and RC

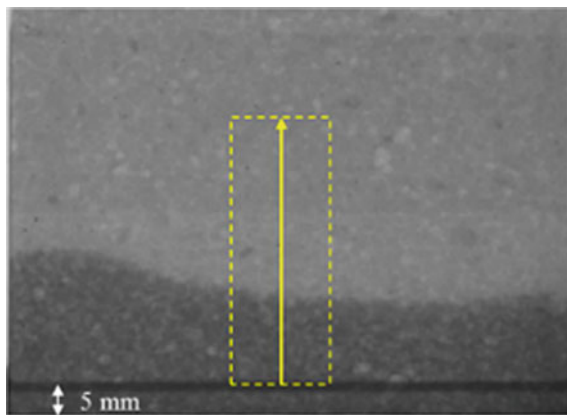


Fig. 17.15 Area of analysis of a typical mortar sample exposed to water on the bottom surface

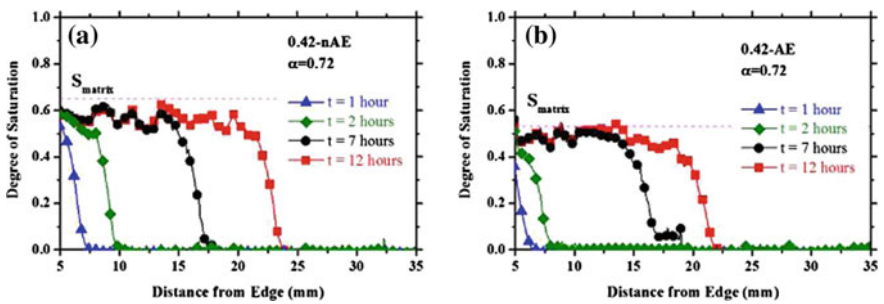
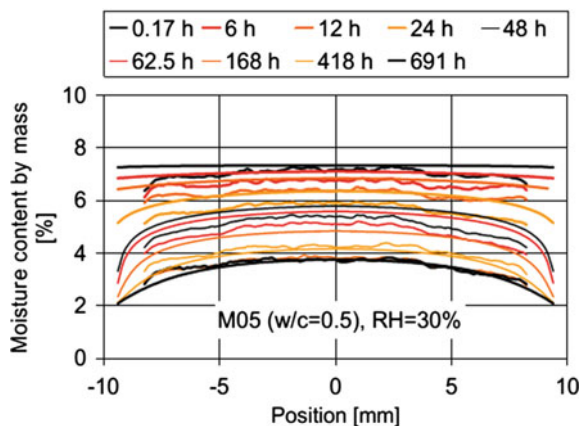


Fig. 17.16 Moisture profiles in mortar **a** without air entrainment and **b** with air entrainment

**Fig. 17.17** Comparison of moisture profiles obtained by inverse analysis (smoother curves) and measured by neutron radiography



distribution in the cement-based mortar. However, this model cannot be applied to concrete with large aggregates because of its influence on cross section of the material.

By means of neutron radiography, water transportation and the time-dependent moisture distributions in the building materials can be studied in detail visually and quantitatively. Taking this advantage of the technique, Tremsin et al. (2015) had studied the cement hydration by measuring the water mass in the cement-based materials.

There was also a study from Villmann and Slowik et al. (2014) using neutron radiography to measure the time-dependent moisture distributions in cement mortar during drying process instead of penetration into the material. Based on the obtained results from neutron radiography the drying models considering both vapour and liquid water transport had been studied in detail with inverse analysis. One selected result from the experiment and inverse analysis is shown in Fig. 17.17.

## 17.4 Neutron Tomography

Neutron radiography is based on measuring the transmitted intensity of neutrons through an object in two dimensions, while neutron tomography is in three dimensions). A single neutron image is a 2D shadow image of the object under investigation. All object layers in the beam direction are superimposed and cannot be readily distinguished. Neutron tomography overcomes this limitation and provides a full 3D sample structure. In this case, the projections are acquired with equiangular steps over either  $180^\circ$  or  $360^\circ$  to cover the whole sample. The transform of the projection data into a three-dimensional image is a computationally task handled by reconstruction software.

During the reconstruction process, the images are generally assumed to be parallel projection. After normalization of the 2D radiographs, the Radon transform is applied to the data, producing sinograms. The calculation is implemented in the filtered back projection algorithm, which is commonly used, Lehmann et al. (2014).

Tools for the reconstruction steps are available on a commercial basis, Masschaele et al. (2004), and as developed by Kaestner (2011). The resulting stacks of horizontal slices can be then taken as input data for a 3D volume visualization. Finally, it gives complementary information about the bulk material in three dimensions, especially on water distribution and migration in concrete. Qualitative and quantitative data analyses are then often undertaken on transverse, sagittal or coronal slices obtained from the volume rendering.

## 17.5 Conclusions

This short overview shows that Neutron Radiography is a powerful method to measure the time-dependent moisture movement and the spatial moisture distributions in typical building materials both in a qualitative and quantitative way with high sensitivity. The water movement in two directions, water penetration into the materials and vaporizing out of the materials, can be studied in detail with this technique. The results obtained from neutron radiography provide direct information about the water movement and distributions in the materials. This will help us a lot to better understand the deterioration processes related to the presence and movement of moisture in building materials.

## References

- Kaestner AP (2011) MuhRec-A new tomography reconstructor, *Nucl. Instrum. Meth. A* 651:156–160
- Lehmann EH, Kaestner A, Grunzweig C, Mannes D, Vontobel P, Peetermans S (2014) Materials research and non-destructive testing using neutron tomography methods. *Int. J. Mater. Res.* 105:664–670
- Masschaele B, Dierick M, van Hoorebeke L, Cnudde V, Jacobs P (2004) The use of neutrons and monochromatic X-rays for non-destructive testing in geological materials, *Environmental Geology* 46:486–492

# Chapter 18

## X-Ray and Gamma-Ray



Owe Lindgren and Lars-Olof Nilsson

### 18.1 Measurement Principles

X-ray (and gamma-ray<sup>1</sup>) techniques have been used for many years to determine moisture distribution in laboratory specimens, cf. Shang and Pere (1997) and Hansen and Bentz (1999). The attenuation (loss of intensity) is a measure of the density and the thickness of the object between a source and a sensor. By performing a second measurement on the same, dried, object the moisture content of the object exposed to the beam can be quantified.

X-ray beams are sent and detectors measure the X-ray radiation that is transmitted through the object (Fig. 18.1).

The transmitted X-ray radiation can be related to the attenuation<sup>2</sup> coefficient of the X-ray by the object by the Lambert–Beer exponential law under the assumption of a monochromatic ray and a linear propagation of the beam in the object, Davis and Wells (1992), Lindgren (1992) and Bucur (2003):

$$I = I_0 \cdot e^{-\mu X} \quad (18.1.1)$$

where  $I$  is the intensity of the transmitted X-ray beam passing through the object,  $I_0$  is the intensity of the incident X-ray beam,  $e$  is Euler's constant = 2.718,  $X$  is the

---

<sup>1</sup>Gamma-ray sources are very little used today due to the radioactivity of the source.

<sup>2</sup>Attenuation = loss of intensity

O. Lindgren  
Luleå University of Technology, Skellefteå, Sweden

L.-O. Nilsson (✉)  
Lund University, Lund, Sweden  
e-mail: lars-olof.nilsson@byggtek.lth.se

L.-O. Nilsson  
Moistenginst AB, Trelleborg, Sweden

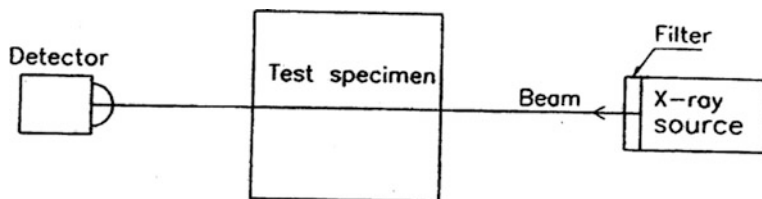


**Fig. 18.1** The transmission beam from the X-ray source through the object to the detector, Hansen and Bentz (1999).

thickness of the object (length unit), and  $\mu$  is the linear attenuation coefficient of the material along the transmission path (length unit<sup>-1</sup>).

## 18.2 The X-Ray Attenuation Coefficient

In order to quantify the distribution of moisture in the object from the difference in attenuation between the wet and dried object the attenuation coefficients for the dry material and for water must be known. These attenuation coefficients are not constants but depend on the type of material, how the water in the pore system is bound, on the energy level of the X-rays and even the thickness of the object, see Fig. 18.2.

An example of how the attenuation coefficient can be measured is shown in Fig. 18.4a.

## 18.3 Geometrical Arrangements

The alternative arrangements of the source and the detector(s) are several. The simplest one is a single beam from the source, through the object, to a single detector. The beam has a certain size, which decides what material volume is

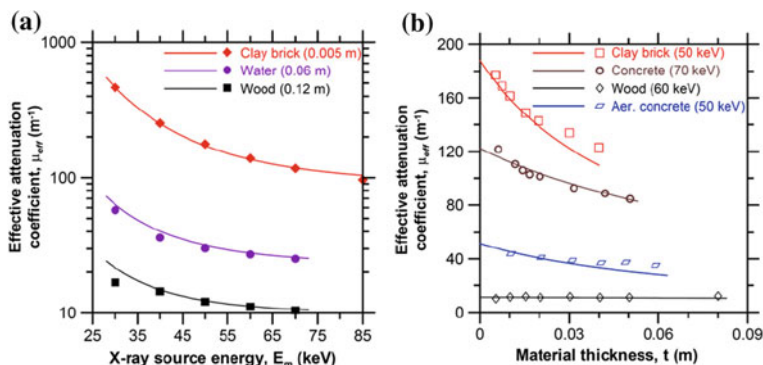


**Fig. 18.2** Influence of the energy level of the X-ray source (a) and material thickness (b) on the effective attenuation coefficient for water and some building materials, Pease et al. (2012)

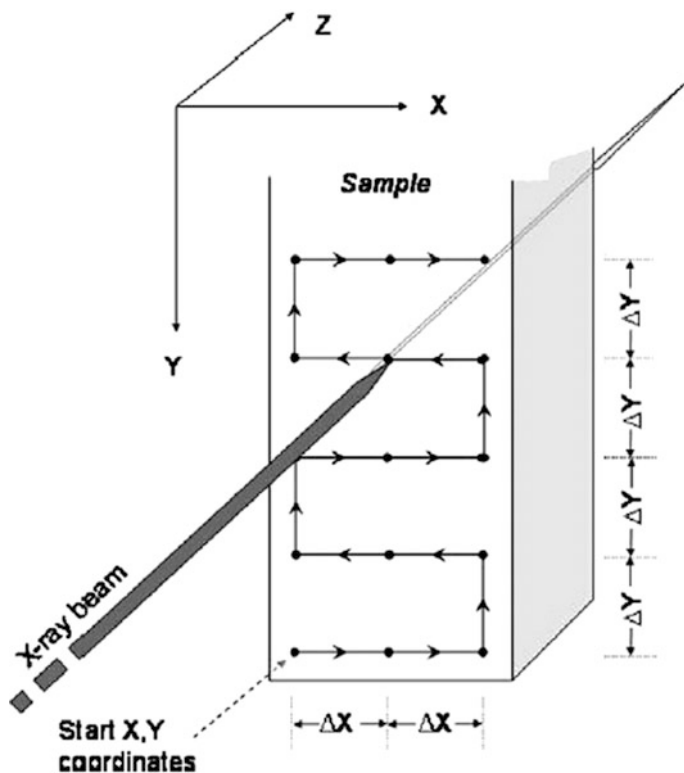


Fig. 18.3 An example of scanning pattern of an object, Baker et al. (2007)

included in each measurement. The source and the detector, or the object, are moved vertically and horizontally to make measurements in several material volumes. In heterogeneous materials it is extremely important that the position at each measurement can be reproduced in a later measurement of the dry object. An example of a scanning pattern with a single beam is shown in Fig. 18.3, Baker et al. (2007).

A more advanced geometrical arrangement is a single source and a 2D “X-ray camera” where a large number of detectors are combined into a 2D array. In this case the X-ray beam is spread in a conical way through the object and the intensity of the transmitted X-ray beam is detected in 2D. The setup is shown, in principle, in Fig. 18.4.

The “X-ray camera” used by Pease et al. (2012) had a size of 25 mm  $\times$  25 mm. With the object in the center between the source and the 2D-detector the material volume in each measurement corresponds to some 12 mm  $\times$  12 mm of the object. To cover larger objects the source and the “camera” are moved to a series of vertical and horizontal positions, with some overlap.

A really advanced geometrical arrangement is using computer tomography, CT-scans, where the source and the detector are rotated around a large object. From

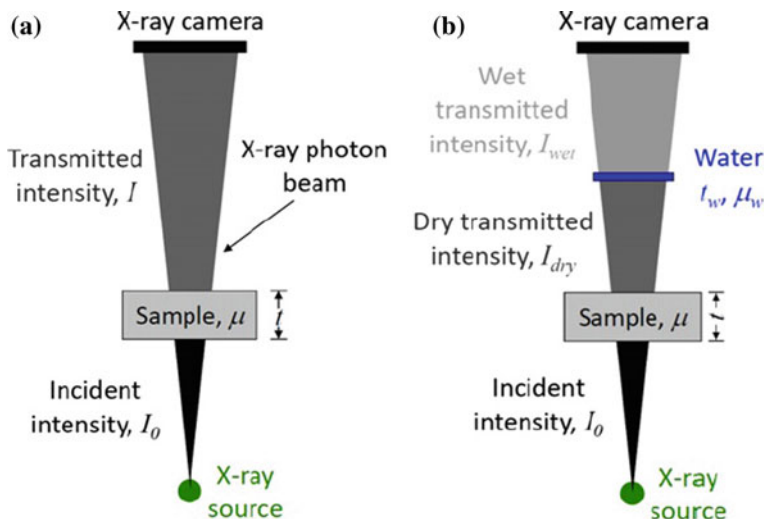


**Fig. 18.4** The setup with an X-ray point source and a 2D X-ray camera with a sample in-between (a) and a sample plus a container with water (b) for calibration, Pease et al. (2012)

this arrangement a 2D-distribution of density can be determined; a second measurement of the dried object can give the 2D moisture distribution. CT-scanning for moisture distribution measurements are described in detail in the next section.

#### Examples of measurements

Using X-ray to measure moisture distributions in 2D is excellent, cf. Pease (2010) and Weiss et al. (2015). An example is shown in Fig. 18.5.

Hansen and Bentz (2000) followed the exchange of water between two freshly made cement paste specimens attached to each other, see Fig. 18.6.

Moisture profiles determined by x-ray and gamma-ray techniques are numerous. One example is shown in Fig. 18.7.

## 18.4 Computed Tomography (CT)-Scanning

Computed tomography (CT)-scanning offers many advantages compared to other measurement methods of moisture content. It is a non-contact, non-destructive and three-dimensional measurement. Using medical scanners the measurements are also fast, in the order of 1 s.

CT-scanning has mostly been used for wood. However, measurements on wood are not straightforward. A CT-image is a map of X-ray attenuation coefficients,

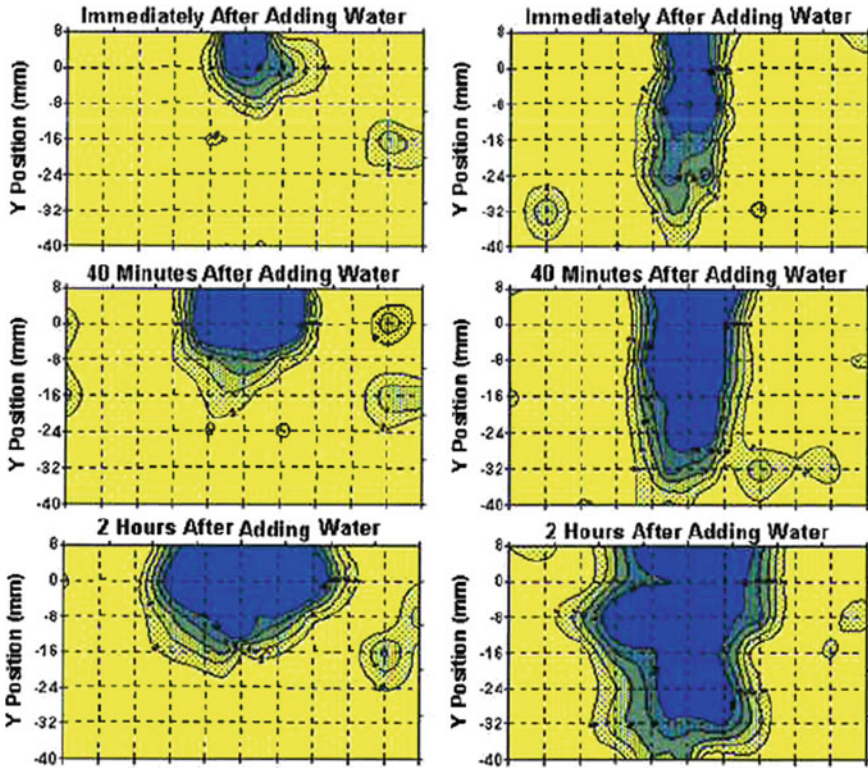


Fig. 18.5 Normalized plots of X-ray attenuation around the tip of a sawcut for uncracked (left) and cracked (right) concrete various times after being exposed to water, Weiss et al. (2015)

which are strongly dependent on density. However, the coefficients are also depending on chemical composition. For example a wooden sample showing a density of  $500 \text{ kg/m}^3$  not containing any water shows a higher coefficient than a sample containing  $450 \text{ kg/m}^3$  of wood and  $50 \text{ kg/m}^3$  of water. Therefore two measurements are necessary; a first image of the unknown distribution and a second image taken as a reference at a known moisture content level.

Furthermore, wood itself absorbs water into the wood material, which causes swelling and distortions. This has been handled by using image processing. During the last year tests have been performed using dual energy CT-scanning showing promising results. Here instead of comparing before and after images above, images achieved at two different X-ray energies are compared. This is a much faster method, as conditioning to a known moisture content level is not necessary.

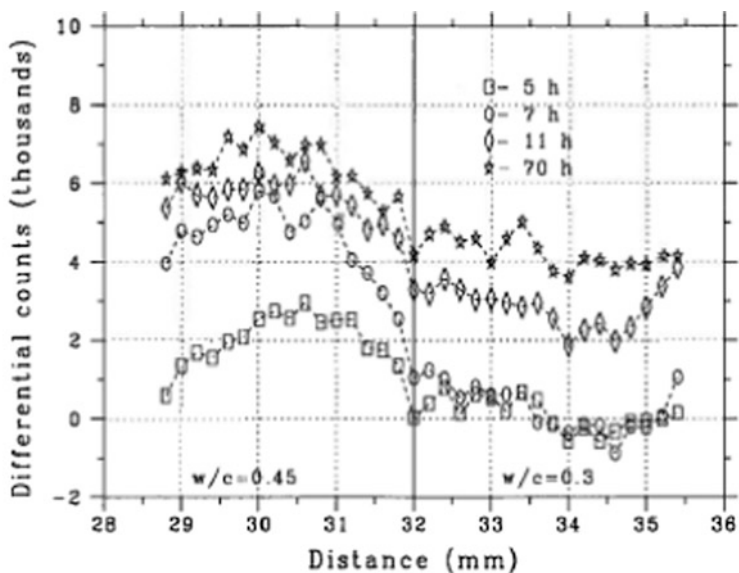


Fig. 14. Differential density profiles (relative to 3 h) for layered cement paste (0.3 over 0.45) open to the chamber environment.

Fig. 18.6 The exchange of water between two cement pastes measured with x-ray beams, Hansen and Bentz (2000)

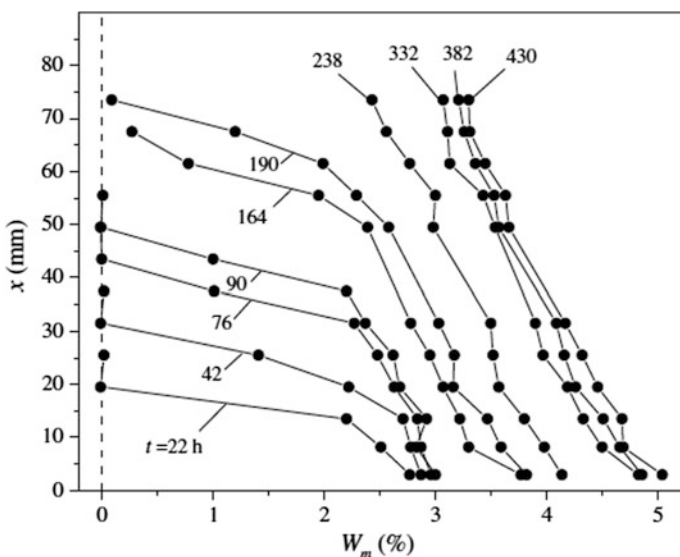


Fig. 18.7 Moisture content profiles during a sorption test with the bottom surface of cellular concrete exposed to humid air, measured with gamma-ray, Nizovtsev et al. (2008)

### ***18.4.1 Image Reconstruction in CT-Scanning***

X-ray scanners follow the theorem of Radon (1917) who theoretically demonstrated that the internal structures of an object can be reconstructed from single or multiple projections of the object, depending on the number of directions considered.

X-rays are emitted during rotation around the object. Detectors are at the same time measuring how many photons that have passed through the object. After complete rotation the cross-section is reconstructed showing a map of the attenuation coefficients. In medical CT-scanners these values are normalized and compared to the coefficient of water nowadays called the CT-number. See Fig. 18.8.

### ***18.4.2 Wood Density***

In the model of Tsai and Cho (1976), the linear attenuation coefficient  $\mu$  is the sum of two absorption coefficients, each of them being directly proportional to the material density  $\rho$ . Several other authors suggested that the linear attenuation coefficient  $\mu$  can be directly related to the material density as follows (Davis and Wells 1992; Lindgren 1992; Wang 1997; Macedo et al. 2002; Bucur 2003).

The other factors involved are the chemical composition of the material (Tsai and Cho 1976; Lindgren 1992; Rojas et al. 2005; Freyburger et al. 2009) and the incident beam energy that is related to the type of scanner used (Macedo et al. 2002; Bucur 2003; Freyburger et al. 2009). All of these factors are not independent. Material density  $\rho$  has the main influence for high-energy X-ray beams, whereas chemical composition has the main effect at low energy (Macedo et al. 2002; Freyburger et al. 2009).

The attenuation coefficient for green (wet) wood can be seen in Fig. 18.9. As expected it is a very linear relationship. The accuracy is in the order of  $\pm 6 \text{ kg/m}^3$ .

### ***18.4.3 Wood Moisture Content***

Wood moisture is an important property to be measured and is highly related to wood density that can be monitored using CT. One of the most important industrial applications of CT images is monitoring of wood moisture during the drying process. Figure 18.3 shows how wood density increases with moisture content for a sample of wood showing a dry density of  $500 \text{ kg/m}^3$ .

Wood swells from 0–30% moisture content until the so-called Fiber Saturation Point (FSP) is reached. Above FSP the wood cell wall cannot absorb more water and wood stops swelling.

As shown above the correlation between density and attenuation coefficient is very high. Therefore this relationship can be applied to evaluate “before and after”

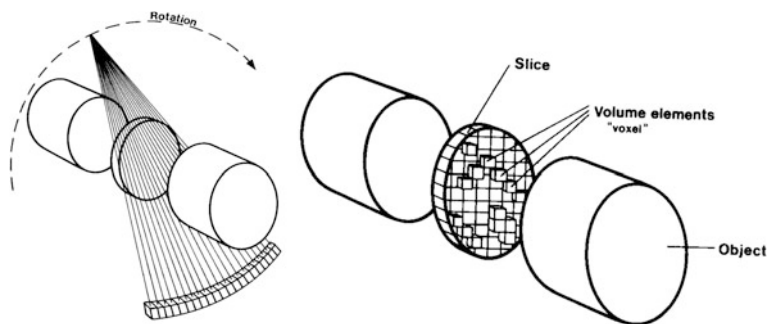


**Fig. 18.8** X-rays emitted during rotation being detected and then calculated to a map of attenuation coefficients

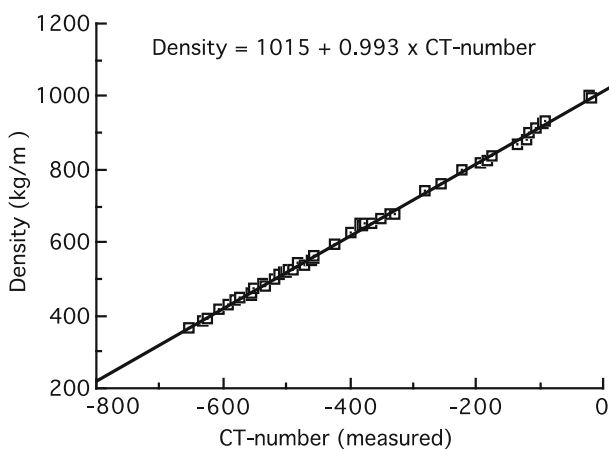


**Fig. 18.9** Relationship between green wood density and attenuation coefficient (CT-number)

images. This is done using image processing. The simplest software to obtain is a free software called ImageJ developed at National Institute of Health (NIH).

An example is shown below. Top left you find a CT-image where the moisture content is unknown. Top right shows corresponding cross-section when the sample has been dried to 0% moisture content. Bottom left you find the resulting image after geometrical correction (warping), image subtraction to achieve the density difference depending on moisture content and finally using the relationship shown in Fig. 18.10 calculating the moisture content (Fig. 18.11).

The accuracy of this process of CT-scanning, image processing and moisture content calculation is in the order of  $\pm 1\%$  below FSP and  $\pm 3\%$  above FSP with a 95% confidence interval in a randomly chosen  $2\text{ mm} \times 2\text{ mm} \times 2\text{ mm}$  volume element inside i.e. in a log.

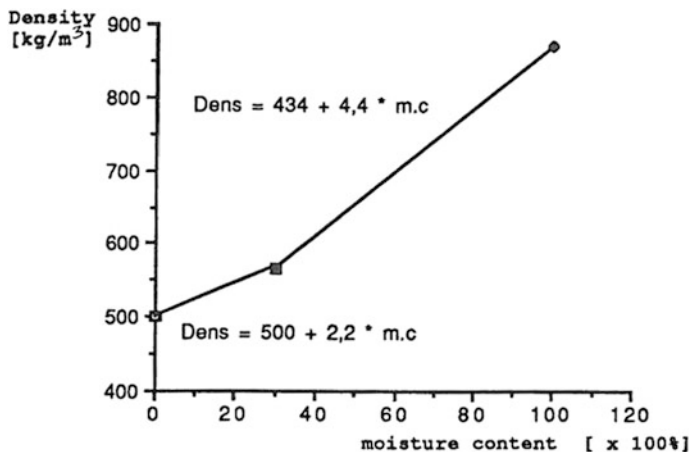


Fig. 18.10 Wood density increase with increasing moisture content for a sample of wood showing a dry density of 500 kg/m<sup>3</sup>

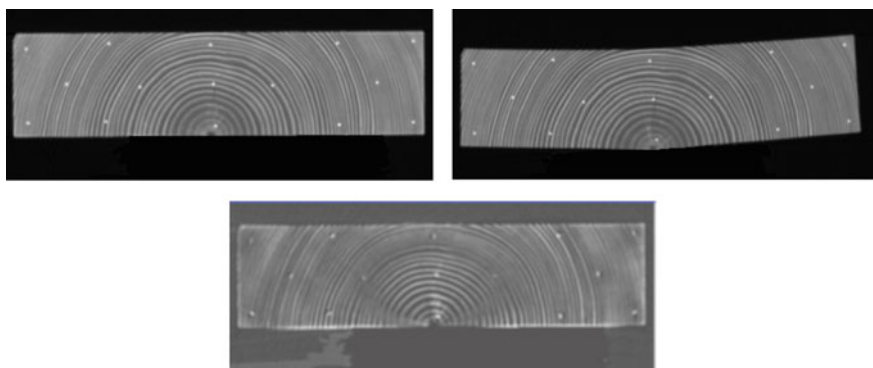
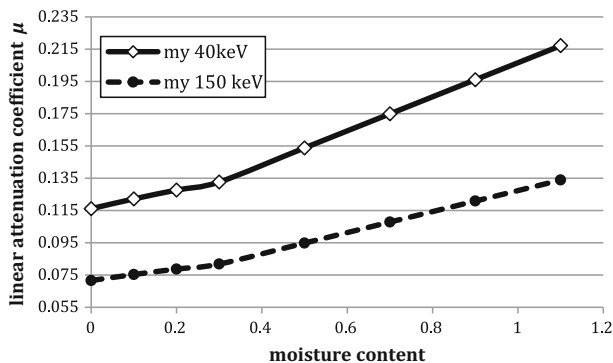


Fig. 18.11 Wet wood cross-section (top left). Same cross section after drying (right). Moisture content distribution (below left) White dots in the image are reference points to measure warping accuracy

### 18.4.4 Dual Energy CT-Scanning

As stipulated before the attenuation coefficient changes depending on difference not only density, but also effective atomic number and X-ray energies. Figure 18.12 shows how the relationship changes depending on only change in X-ray energy. In this case 40 and 150 keV were used in the calculations and a wood density of 500 kg/m<sup>3</sup> at different moisture content levels.



**Fig. 18.12** Linear attenuation changes with moisture content for a sample showing a dry density of  $500 \text{ kg/m}^3$

These differences in slopes raises the expectation that a change in X-ray energy could result in being able to separate moisture content in wood from the total wood density.

Kullenberg et al. (2010) have investigated this and tests showed promising results. According to X-ray physics the process using CT-scanning instead of using the radiography method they used would require to divide the pixel values in two CT-images taken at two different X-ray energy levels. This is naturally under the assumption that the two CT-images are matrices showing the attenuation coefficient in each pixel.

The relationships stipulated in Eqs. (18.4.1) and (18.4.2) are valid as representations of Eq. 18.1 as also stipulated by Kullenberg et al. (2010):

$$N_1 = N_{0,1}e^{-\mu_1 X} \quad (18.4.1)$$

$$N_2 = N_{0,2}e^{-\mu_2 X} \quad (18.4.2)$$

where

$N_i$  is the observed transmitted count rate for energy  $i$ ,  
 $N_{0,i}$  is the count rate for energy  $i$  with no attenuator  
 $\mu_1, \mu_2$  are the linear attenuation coefficients for energy  $i$  and  
 $X$  is the thickness of the sample.

Equations (18.4.1) and (18.4.2) can also be rewritten into Eqs. (18.4.3) and (18.4.4)

$$\ln(N_{0,1}/N_1) = \mu_1 X \quad (18.4.3)$$

$$\ln(N_{0,2}/N_2) = \mu_2 X \quad (18.4.4)$$

The count rates without attenuator could be determined besides the object or attenuator. From Eqs. (18.4.3) and (18.4.4) an expression called  $k$  can be derived by dividing the two equations, cf. Eq. (18.4.5)

$$k = (\ln(N_{0,1}/ N_1)) / (\ln(N_{0,2}/N_2)) = \mu_1 X / \mu_2 X = \mu_1 / \mu_2 \quad (18.4.5)$$

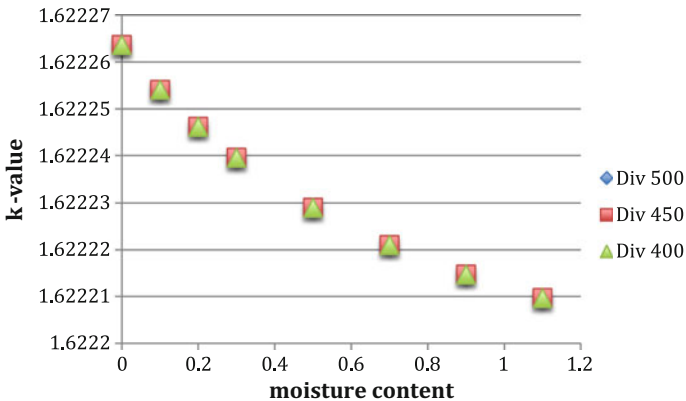
The expression in Eq. (18.4.5) is only dependent of the linear attenuation coefficient, which in its turn is only dependent on the change of moisture content.

Figure 18.13 shows the results of the calculated  $k$  values, and it can be found that the constant is the same independent of wood density and decreases with increasing moisture content level. Here the X-ray energies of 40 and 150 keV were used as an example.

Therefore a straightforward solution might be to CT-scan the sample first at one low X-ray energy and secondly to CT-scan the sample at a high X-ray energy. If then the images are exported into an image-processing program the two images can be divided with each other, which should result in a representation of  $k$ . The  $k$ -value in its turn is a function of moisture content. This is a much simpler procedure than the one used by Lindgren (1992). Figure 18.14 shows the results of a first test, Lindgren et al. (2016).

The image furthest to the right should be a representation of a 2-D moisture content distribution according to Eqs. (18.4.1)–(18.4.5). However, a full calibration has not yet been performed.

By stacking images in the image-processing program, a 3-D representation of moisture content is possible (Fig. 18.15) to achieve.



**Fig. 18.13** The  $k$ -value stays constant at different wood densities, ranging from 400 to 500 kg/m<sup>3</sup>, but decreases with increasing moisture content levels

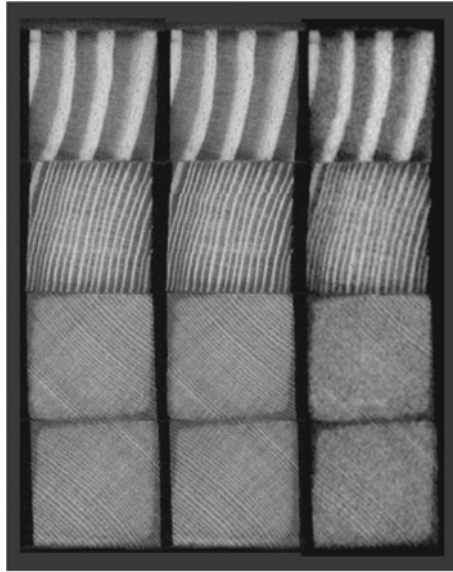


**Fig. 18.14** To the left CT-image at 200 kV, in the middle CT-image at 60 kV and to the right the result after dividing image at 200 kV with image at 60 kV



**Fig. 18.15** Three-dimensional visualisation of the moisture distribution

### 18.4.5 Examples

For modeling the kiln drying process of boards, CT images have been used to determine moisture flux and diffusion coefficients, e.g., Danvind and Morén (2004), to validate mathematical models in the case of radiata pine (*Pinus radiata* D. Don), Pang and Wiberg (1998) or of Norway spruce (*Picea abies* (L.) Karst.), Eriksson et al. (2007), to assess wet-wood distributions in heartwood in the case of subalpine fir (*Abies lasiocarpa* (Hook.) Nutt.), Alkan et al. (2007), and to assess moisture content distribution, two-dimensional (2D) displacements, and related strains in the case of Scots pine, Danvind (2002) and Danvind and Morén (2004).

Outside of monitoring drying processes, CT images were also tested to assess moisture content distribution during microwave heating of Scots pine boards (Hansson and Antti 2008) and to describe water sorption in specimens made of Norway spruce wood Sandberg (2006) or of European aspen (*Populus tremula* L.), English oak (*Quercus robur* L.), and Scots pine wood, Johansson and Kifetew (2010).

An example of measuring moisture content changes during sorption is Fredriksson and Lindgren (2012) where water present at the butt-end of a sample moves further into wood when wood is surrounded by a water-saturated climate.

## Part II

# Applications

In the previous chapters a large number of moisture measuring principles are described. All these measuring principles are available when moisture in a material is going to be measured in a certain application, but for various reasons some of them are more suitable and are more frequently used than others.

In the next chapters, methods to measure moisture in a number of applications are described. The applications are grouped into five main types:

- a. Lateral distributions, where surfaces or structures are “scanned” for moisture differences
- b. Moisture depth distribution in a structure/specimen
  - (1) ND-methods
  - (2) Coring/drilling/sampling techniques
  - (3) Installation of probes
  - (4) Specimen or core; in the laboratory (sides available)
- c. Assessment of moisture in a substrate before applying a surface cover
- d. Monitoring, on-site measurements, remote measurements
- e. Heterogeneous materials.

# Chapter 19

## Spatial Distributions



**Jean-François Lataste, Kurt Kielsgaard Hansen, Lars-Olof Nilsson,  
Charlotte Thiel, Angelika Schießl-Pecka, Arndt Göller  
and Christoph Gehlen**

In many applications moisture measurements are made to estimate the moisture differences between different points in a structure. Here, it is often more important to use a “simple” method that is easy and rapid to use in many points instead of necessarily obtain the exact moisture level in each point. The objective with “moisture indications” like that could very well be to select points where more accurate moisture measurements are to be made. The measuring principle to apply is of course a trade-off between accuracy and simplicity.

---

J.-F. Lataste (✉)  
Université de Bordeaux, Bordeaux, France  
e-mail: jean-francois.lataste@u-bordeaux.fr

K. K. Hansen  
Technical University of Denmark, Kongens Lyngby, Denmark  
e-mail: kkh@byg.dtu.dk

L.-O. Nilsson · C. Thiel · C. Gehlen  
Technical University of Munich, Munich, Germany  
e-mail: lars-olof.nilsson@bygtek.lth.se

C. Thiel  
e-mail: charlotte.thiel@tum.de

A. Göller  
HF Sensor GmbH, Leipzig, Germany

A. Schießl-Pecka  
Ingenieurbüro Schiessl Gehlen Sodeikat, Munich, Germany

## 19.1 Suitable Moisture Measuring Principles; Advantages and Limitations

Lateral distributions (near-surface distributions) could be quantified with most of the measuring principles described in Chap. 3. Here the most relevant ones are described, with respect to advantages and limitations.

The general manner is to perform measurements with a technique, on various locations. The depth of investigation, and other characteristics are fixed (by the technology, or the sensor): with capacitometry or with electrical resistivity, the depth of investigation is fixed by the array size; for radar, the central frequency of the antennas imply the investigation depth; for infrared thermography the investigation consist of a very shallow evaluation. This result could be issued from continuous survey (as for instance with radar, or infrared thermography which is a shot of an entire surface), or from the gathering of discontinuous and local measurements (in case of NMR, capacitometry and electrical resistivity). Then, the final results are represented either in term of profile or section (1D), or in term of map (2D) for the measured parameter: dielectric permittivity, electrical resistivity, attenuation or celerity of the signal, etc.

The analysis of the relative variations of the physical parameter supports mainly the interpretation for relative zoning of moisture. When the link between the measured parameter is known, or if it is possible to simply link the both parameters (according some hypothesis, or calibration in case of capacitometry for instance), the map (or profile) could be translated in term of moisture. In others cases the map (or profile) of the physical property is the final results with indications for “more wet” and “more dry” zones.

Moisture measuring principles that could be used for this application are summarized in Table 19.1, with their advantages and limitations.

## 19.2 Application Example: Moisture Profiling Along a Concrete Precast Duct

[Resistivity + capacitometry + infrared thermography; from Sirieix et al. (2007)].

The structure is 165 m long and consists of 55 pipe segments each 3 m long. Each pipe section is roughly ovoid in shape with a height of 1.7 m and a width of 1.8 m and the concrete thickness is about 20 cm. Only the internal surface of the duct could be inspected and showed some damage, such as cracks, which sometimes contained calcite and which were mainly to the upper part of the duct.

Measurements have been carried on the upper part of 17 pipe segments (which corresponds to one segment out of three) only a part of the duct which has been previously repaired by sprayed concrete (between abscissa 60–70 m) was not evaluated due to surface condition avoiding measures. Results from three NDT methods are presented, for the resistivity, Fig. 19.1, for the infrared thermography, Fig. 19.2,

**Table 19.1** Moisture measuring principles suitable for detecting spatial moisture distributions; their advantages and limitations

Principle	Advantages	Limitations
Capacitance microwave	<p>Directly linked to the volumetric moisture content, quantitative assessment possible if a calibration is available</p> <p>Sensor technology well mastered</p> <p>Can detect moisture through a (thin) surface cover</p> <p>Quick and cheap. Microwave: large penetration depths are possible</p>	<p>Capacitance: very influenced by surface roughness. Limited penetration depth, i.e. thickness and type of surface cover</p>
Radar	<p>Very quick to use (contactless method)</p> <p>Can detect moisture through a (thin) resistive, surface cover</p>	<p>Depth of investigation function of the antenna used</p>
Resistivity resistance	<p>Depth of investigation could be adapted to the study, from some centimetres to meters</p> <p>Cheap and easy to use</p> <p>Two-pin technique especially suitable for wooden-based materials</p>	<p>The measurements are largely influenced by the quality of electrical contact between electrodes and material</p> <p>The resistivity is a function of numerous parameters, which are hardly identified separately (interpretation is difficult)</p>
IR thermography	<p>Can be used from a distance</p> <p>Very fast investigation is possible. Very adapted for rapid zoning of a structure</p>	<p>No quantitative assessment of moisture available</p> <p>Needs a thermal dynamics to operate (no way for instance in a tunnel or an thermally insulated cave)</p>
NMR relaxometry (single-sided) Example of equipment, see Sect. 21.3	<p>High accuracy and high resolution (depth profiles with a resolution up to 5 <math>\mu\text{m}</math> can be achieved);</p> <p>Not influenced by salts;</p> <p>Different states of water depending on their physical state can be determined <math>\rightarrow</math> for fully saturated specimens information on the pore structure can be derived. Can detect moisture through a (thin) surface cover</p>	<p>The detection depth is limited, differently for different type of equipment; some 65 mm</p> <p>Calibration curves need to be generated for quantification</p>
Neutron (single-sided)	<p>Linear count rate and moisture content in weight-%</p> <p>Not influenced by salt</p> <p>Average moisture content measured up to 250 mm depth</p> <p>Easy scanning of large areas</p>	<p>Needed:</p> <p>(1) Standardization check on a reference standard at beginning of measurement</p> <p>(2) Determination of a calibration curve for the actual material</p> <p>Handling, storage and transport of the radiation source unit need permission from national authorities</p>

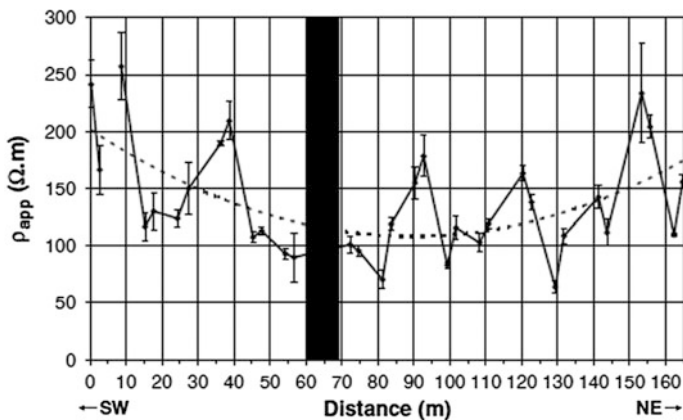


**Fig. 19.1** Average values and error bars of electrical resistivity measured in three points, along the keystone of the duct

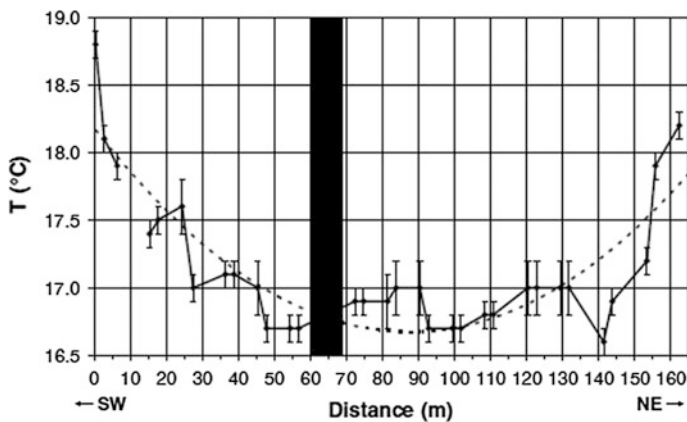


**Fig. 19.2** Average values and error bars of the surface temperature of the keystone as measured by thermal imaging. Each image was  $38 \times 46 \text{ cm}^2$

and for the capacity, Fig. 19.3. The arrays, and methodology for capacitance and resistivity are chosen to integrate some centimetres in depth, infrared thermography investigate a limited zone (few decimetres square) on each studied element.

The results are very coherent between each technique and allow insuring the diagnosis. No attempt to quantify exactly the moisture content of concrete is done.

On the three graphs the dotted curved line simply comes from a second-order polynomial regression on the experimental data. Its only merit is to highlight the gross trend but it does not provide any explanation. On all the cases, it could be observed the dryer condition on the extreme parts of the duct, relatively to the central part (more moistened), qualitatively describing the moisture condition of the duct.

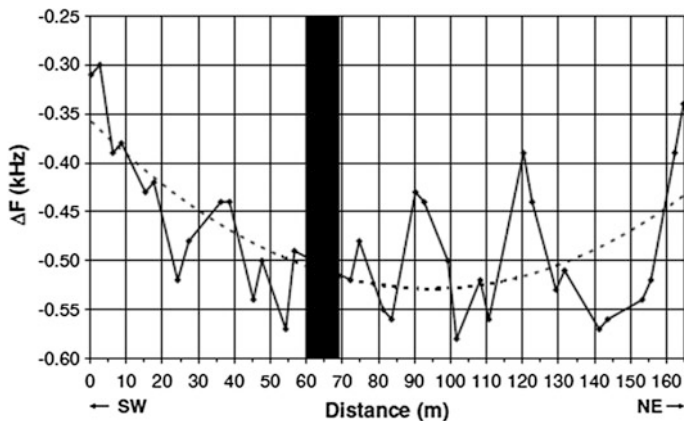


Fig. 19.3 Difference in frequency as measured by the capacitor method

### 19.3 Application Example: Moisture Mapping in a Car-Park

[Radar + electrical resistivity; from Sbartai et al. (2007)].

On-site investigations were carried out on the reinforced concrete slab of a car park located in the city of Sherbrooke (Quebec, Canada). The goal of the inspection was to rapidly locate the zone favourable to rebar corrosion, that is to say zone with high moisture content, and high chloride content. The study focuses on moisture. This paper does not deal with the quantitative evaluation of the physical condition of concrete, since this is currently impossible on-site due to the great variety of concretes that may be encountered. The focus is on the aptitude of radar technology to detect physical contrasts in concrete structures. The reliability of this information was notably deduced from a comparison study on-site between radar and electrical resistivity techniques, Fig. 19.4.

Resistivity measurement was done with a 4-electrodes on line device (Wenner probe). The resistivity (evolving between 100 and 1000  $\Omega$ ) was translated in term of conductivity, and normalised relatively to the higher value.

GPR investigation was done with a 1.5 GHz dipolar bow tie antenna. Data are treated to extract the direct wave attenuation. This attenuation lays between 9 and 13 dB, and is also normalised relatively to the higher value. The drawing of the two maps shows the high level of coherence of the two techniques (supported also by laboratory tests, and complementary statistical analysis). The higher conductivity zones correspond to the higher attenuation zones and are interpreted as the more moistened sectors.

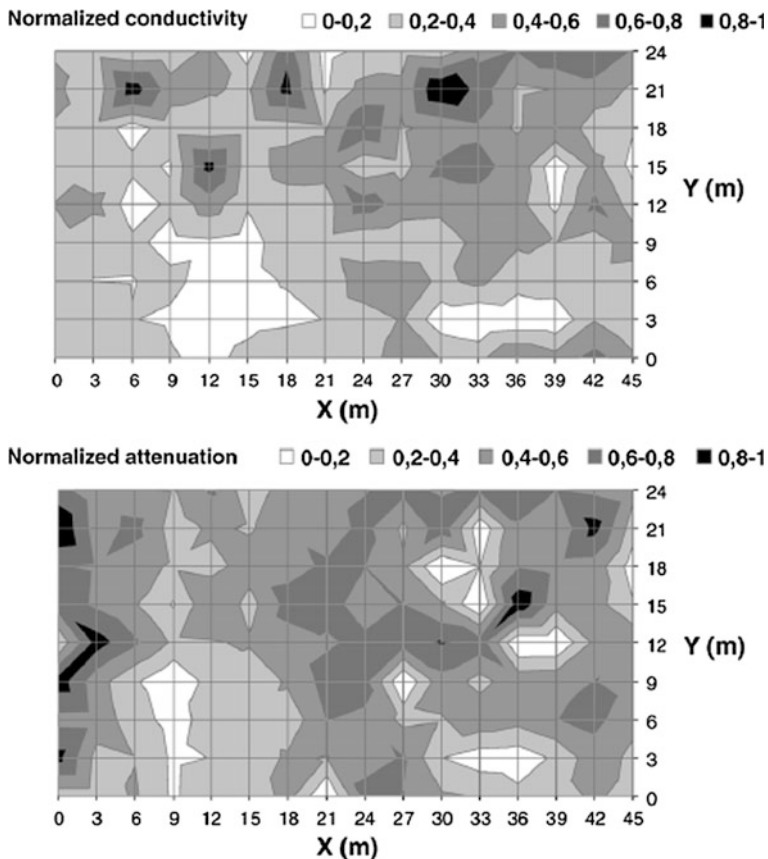


Fig. 19.4 Comparison between apparent conductivity map and direct wave attenuation map, on the concrete slab

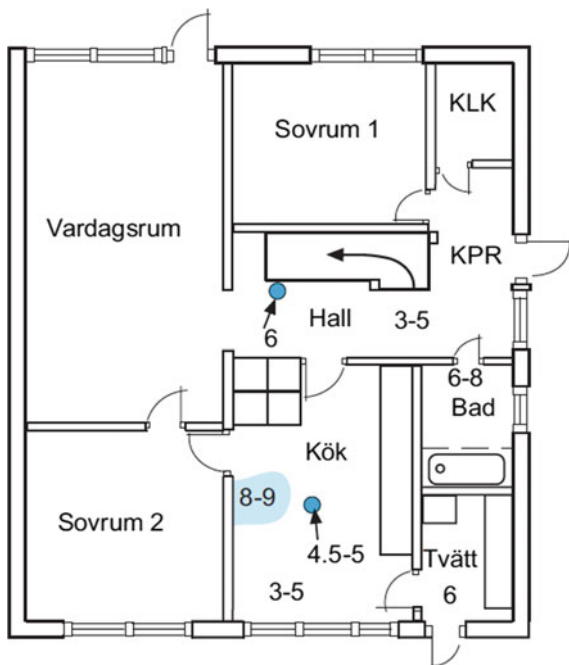
### 19.4 Application Example: Moisture Distribution in a Concrete Floor Slab

[Electrical capacimetry; from Nilsson et al. (2006)].

Moisture indicators based on electrical capacity are frequently used to “scan” large areas for moisture variations. The depth of sensitivity for that kind of equipment is limited, a few centimetres only, but can be used in cases where the substrate has high moisture content all the way up to the surface. Excellent applications are structures that are covered with something having a large resistance to moisture flow. Equipment based on electrical capacity can still “reach” the substrate and can indicate the moisture variations non-destructively.

An example is shown in Fig. 19.5 for a one-family house with a concrete floor slab and different floor coverings.

**Fig. 19.5** Moisture variations in a concrete floor slab in a one-family house indicated with an equipment based on electrical capacity, Nilsson et al. (2006). (Courtesy: Formas)



The equipment gave no signal in the rooms with parquet or textile flooring. The parquet boards are too thick for the detection depth of the equipment. The textile flooring allowed drying of the concrete slab so its surface was too dry to give a signal. A signal could, however, be found in the rooms with a PVC-flooring and the variations in the moisture content beneath the flooring could be indicated.

The readings from different rooms, with different PVC-flooring, cannot be compared since the flooring had different thicknesses. Within each room, however, excellent indications of moisture variations were achieved. In the “hall” a small spot could be found with larger (“6”) signal. A wooden stick down into the soil was found when a core was taken from the concrete slab.

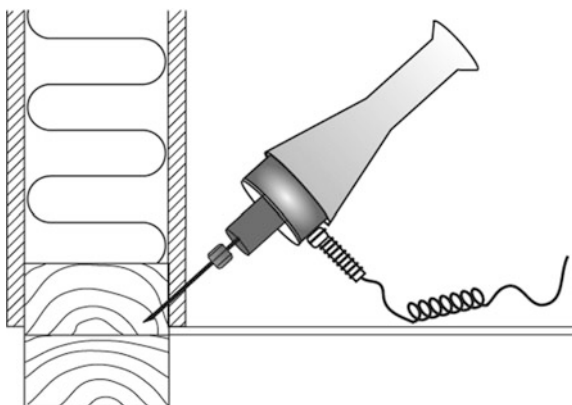
In the kitchen (“kök”) one area with a size of some  $1 \times 1 \text{ m}^2$  gave an indication of much wetter conditions (“8–9”). A check into the structure revealed a local defect in the capillary breaking system.

## 19.5 Application Example: Moisture Distribution in Wooden Sills

[Electrical resistivity; from Nilsson et al. (2006)].

A wooden resistance meter is an excellent moisture indicator in wooden materials. With that kind of equipment moisture variations in wooden floors and along

**Fig. 19.6** An example of using a wood resistance meter as a moisture indicator in a wooden wall, Nilsson et al. (2006). (Courtesy: Formas)



wooden walls can easily be detected to find locations where more accurate measurements should be done, in situ or by sampling.

One technique being used is indicating moisture variations along walls by inserting insulated pins into the same position in several locations. The pins are inserted in the same vertical position in each spot and with the same angle. In this way the position will be almost identical in each spot, cf. Fig. 19.6.

The example shown in Fig. 19.6 is a way to find moisture variations in a wooden, outer wall with two sills on top of each other. The wooden wall has a façade of brickwork, which makes the accessibility from outside very limited. From the inside only the inner part of the top sill was reachable. This is not expected to be the most wet part of the two sills. By checking this exact position in a series of locations, however, the moisture variation indicated should also be an indication of moisture variations in the more wet part of the sills, the outer, bottom part. An example is shown in Fig. 19.7.

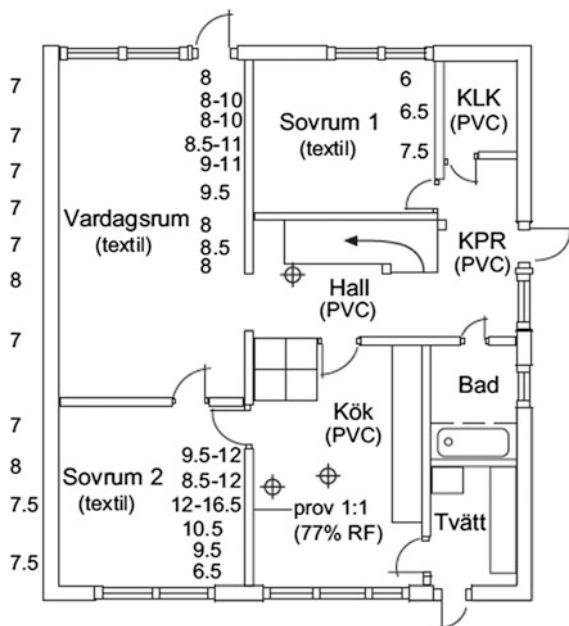
The numbers in the figure are moisture contents in wood, in per cent by weight. The numbers are mostly very low since the location of the tips of the two pins is in a part of the two sills that is expected to be fairly dry. In the (left) outer wall no variation was found; the numbers are almost the same along the wall.

In the (left) inner wall the variations are much larger. From the top numbers around 8–11 were found but in the kitchen (“kök”) wall much higher numbers (up to 16.5) were found locally. The location of this part of the sills happened to be the same as the location of the most wet part of the floor in Fig. 19.5. The reason for this was the same; moisture was sucked up from the ground locally.

## 19.6 Application Example: Moisture Variations in a Large, Flat, Warm Roof

[Neutron method; from Nordtest (1989)].

**Fig. 19.7** A case where the technique shown in Fig. 19.6 was used moisture indication for outer and inner, wooden walls; the same one-family house as in Fig. 19.5. (Courtesy: Formas)



The neutron method used covers determination of the moisture content of building materials or building structures by moderation or slowing of fast neutrons where the neutron source and the thermal neutron detector both remain at the surface, cf. Fig. 19.8.

The method is preferably used for flat warm roofs where areas, damaged by leaks and water infiltration to the insulating material, give high neutron count in relation to dry areas. The method can also be used in building structures, e.g. concrete, brickwork, etc.

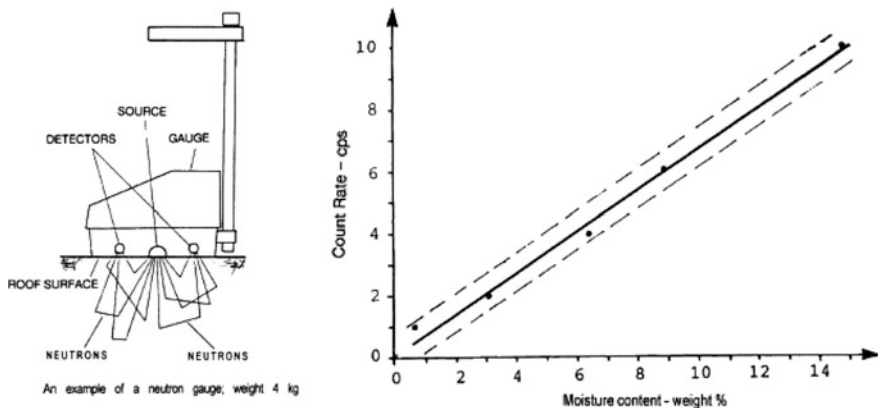
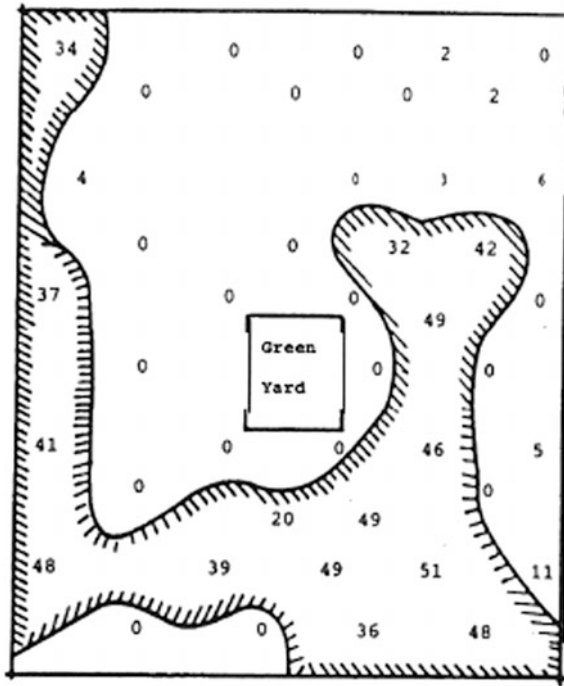


**Fig. 19.8** An example of a neutron gauge (left) with a weight of 4 kg and a calibration curve (right) for brickwork with a thickness of 108 mm, from Nordtest (1989)

**Fig. 19.9** Variations in moisture contents [ $\text{kg}/\text{m}^3$ ] in a  $3600 \text{ m}^2$  large, flat, warm roof measured with the neutron method in Fig. 19.8



In measuring any structure it should be taken into account that:

- Material closest to the detector gives the highest response,
- Any material containing hydrogen will provide a response,
- Materials containing chlorine or boron will disturb the measurement.

The method was used on a  $3600 \text{ m}^2$  flat, warm roof. Figure 19.9 shows the variation in the moisture content [ $\text{kg}/\text{m}^3$ ].

The area bounded by the hatched curve in Fig. 19.9 has a moisture content that exceeds  $20 \text{ kg}/\text{m}^3$ .

## 19.7 Highway Tunnel

[gravimetric method + “moisture balance” + carbide method, microwave; A. Schießl-Pecka, A. Göller and C. Gehlen].

In a 20 year-old highway tunnel high chloride contents were determined in the tunnel walls. Active reinforcement corrosion was only detected in isolated areas.

For those parts of the highway tunnel with very low probability of reinforcement corrosion, it was decided to apply a surface protection system to prevent further water and chloride ingress and to assure a uniform desiccating process. To be able

to detect the time when the durability of the surface protection system is exceeded and as a consequence chlorides may penetrate into the concrete structure a monitoring system was foreseen.

The chosen surface protection system was a hydrophobic impregnation (water repellent agent). In comparison to traditional hydrophobic impregnations, which do not penetrate much into the concrete, modern water repellent agents on a silane- or siloxane-basis have elevated penetration depths. After the material application on the concrete surface, the material is transported by capillary suction into the concrete. Polymerisation starts inside the concrete when the silanes come in contact with the alkaline pore solution forming a thin network of polymer siloxan or silicon resin. As a consequence the capillary action of the pores is suppressed and liquid water cannot longer be transported through the treated concrete, cf. Johansson et al. (2008) and Gerdes (2001).

Water repellent agents on a silane- or siloxane-basis are commercially available in the pure state or diluted, as aqueous emulsion or as a suspension of a fine mineral. Depending on the producer, these products are sold as pastes, creams, gels or liquids in different concentrations.

The advantage of creams or gels is a longer contact time between the concrete surface and the liquid and volatile silane, cf. Meier and Wittmann (2001), especially when repellent agents are applied on inclined and vertical surfaces.

Earlier projects had shown that the success of hydrophobic treatment depends on the combination of specific project conditions, e.g. w/c-ratio (permeability), moisture content of concrete, kind of application and specific product.

For that reason moisture measurements have been performed to check the (absolute) moisture content in the concrete before applying the hydrophobic treatment and subsequently to monitor the moisture state of cover concrete to get some information about the effectiveness of the treatment.

During first inspections, in 6 different tunnel blocks moisture content was checked by the carbide method (CM). CM-values have been determined by two different inspectors at two different times.

1,4 CM-%, (04/2015)

1,5 CM-%, (04/2015)

1,4 CM-%, (04/2015)

1,8 CM-%, (06/2016)

2,5 CM-%, (06/2016)

1,9 CM-%, (06/2016)

From those measurements it was concluded, that tunnel surfaces are potentially dry enough for trial treatments with different hydrophobic agents (liquids, gels, cremes).

Best performing material was identified by a combination of tests (water absorption according to DIN EN 1062-3 determined at different depths of extracted cores which were grinded mm-wise, FTIR-spectroscopy, determination of the contact angle between a liquid and a solid surface at different depths, determined

active agent contents in the pre-determined depth), c.f. Schießl-Pecka and Gehlen (2016).

To design the final treatment procedure, in July 2016 further moisture measurement methods were performed (microwave method, gravimetric measurements, “moisture balance”, CM-value). The first two methods do provide, as the carbide method, absolute moisture contents; the third method was used for estimation of the moisture state on site. In the following, the results are presented and compared.

To determine the two-dimensional depth-dependent distribution of moisture on the tunnel walls, microwave measurements were performed with a microwave moisture meter MOIST 350B. For the microwave moisture meter MOIST 350B calibration curves for the concrete strength classes C20/25 and C30/37 are available. By use of these calibration curves for moisture mapping absolute moisture measurements with high accuracy are possible.

In the tunnel three measuring fields were determined on three blocks, each field with a size of  $5 \times 2 \text{ m}^2$  and a grid dimension of 20 cm. In one measuring field, the moisture map consists of 26 columns and 11 rows in each layer, cp. Figs. 19.10 and 19.11.

Absolute moisture measurements were performed with four different microwave sensors in different penetration depths:

- Sensor MOIST R1 up to a depth of maximum 2 cm
- Sensor MOIST R2 up to a depth of maximum 5 cm
- Sensor MOIST D up to a depth of maximum 10 cm
- Sensor MOIST P up to a depth of maximum 25 cm

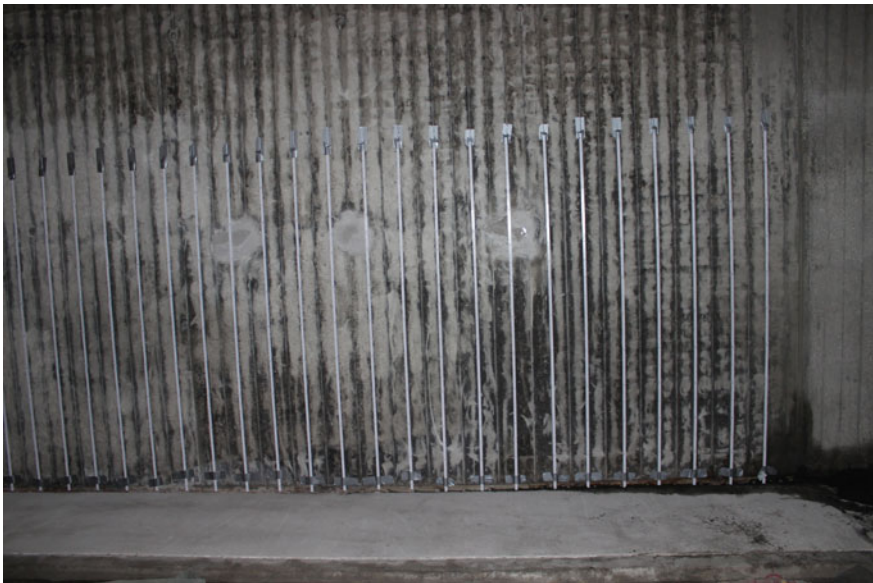


**Fig. 19.10** Tunnel wall element selected for microwave moisture measurement



Fig. 19.11 Measuring marks

Figures 19.12, 19.13, 19.14 and 19.15 show moisture maps in the four different depths taken in one of the blocks. The x-axis and y-axis show the dimensions of the measuring field and the colour scale on the right side gives the absolute moisture values. As can be seen from these images, the inhomogeneity in moisture distribution is higher at the surface and decreases towards the inner layers. The moisture map of the volume sensor MOIST P in Fig. 19.15 gives a very homogenous moisture distribution

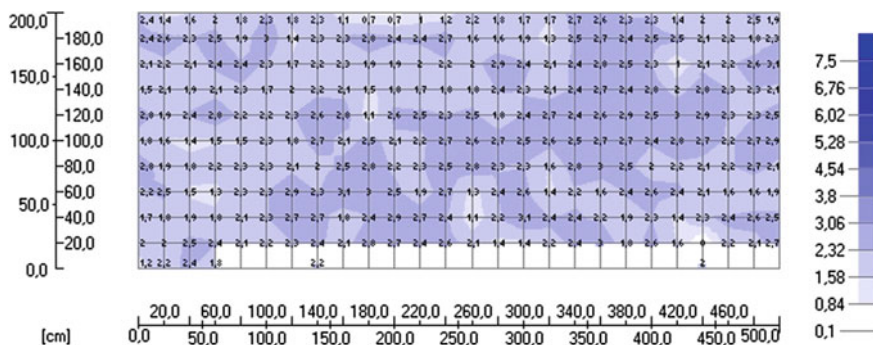


Fig. 19.12 Moisture map taken on block 17/18 using microwave sensor MOIST R1 (penetration depth max. 2 cm)



To make a comparison between microwave moisture mapping results and gravimetric measurements, the following data were generated out of one measuring field:

- Statistical evaluation of one field’s microwave measurements in each layer (mean value, standard evaluation)
- Single measurements only from the locations corresponding to the points, where cores were taken for gravimetric measurements (in the middle of column 1, 14 and 25 in each block).

The results are presented in Table 19.2. The mean values of the different depth layers show an increase of absolute moisture values from the concrete surface into the depth. Besides, the standard deviation decreases with increasing concrete depth, being a consequence of a possible drying process at the surface.

To be able to determine absolute reference moisture values, sampling cores for gravimetric measurements were taken at three points of each measurement array (column 01, 14, 25), cp. Fig. 19.16. The coring area was located about halfway up the total height of the measuring field. To achieve a minimum sample weight of 500 g several sample cores were taken at each point.

Table 19.3 shows the results of the gravimetric measurements. With regard to the average microwave readings from Table 19.2, the comparison of both methods shows a very good correspondence of gravimetric moisture values, representing mainly the moisture content in deeper layers up to 15 cm, with the data collected by the volume measurements MOIST D and MOIST P. The difference is only in the order of 0.2–0.3%.

To get a quick on site information about absolute moisture values, additional moisture reference values were determined using a “moisture balance”, cf. Fig. 19.17, that contains a halogen heater to dry at e.g. +105 °C. For this purpose a special field method was developed. Parts of the concrete wall were chiseled out above the centric core holes, cf. Fig. 19.18.

The samples were crushed and analyzed with the moisture balance. The results are given in Table 19.4. The results mainly represent surface moisture values. Additional determined CM-values are presented in Table 19.4, too.

**Table 19.2** Mean moisture content/standard deviation for each layer of the moisture map (left side) and from three readings in the middle of single columns

Field 02 (block 17/18)	(a) Moisture content of one measuring array		(b) Moisture content of three readings (measured in the middle of a column)		
	Mean value	Standard dev.	Column 1	Column 14	Column 25
	[% mc drybase]	[% mc drybase]	[% mc drybase]	[% mc drybase]	[% mc drybase]
R1 (2 cm)	2.20	0.48	2.46	2.27	2.50
R2 (5 cm)	3.06	0.37	3.17	3.33	3.13
D (10 cm)	3.77	0.34	4.07	3.77	3.53
P (25 cm)	3.52	0.32	3.60	3.73	3.60



**Fig. 19.16** Coring area for gravimetric measurements

**Table 19.3** Sampling and moisture analysis (oven drying) in array 02, block 17/18

Name	Sample position	Surface temp. (°C)	Total weight (g)	Moisture content (% of dry mass) (%)
Sample 04	Column 01, centre	10.8	656	3.69
Sample 05	Column 14, centre	10.6	658	3.67
Sample 06	Column 25, centre	10.8	630	3.81



**Fig. 19.17** Determination of reference values using a “moisture balance”



**Fig. 19.18** Sampling points for moisture balance measurements

**Table 19.4** Reference moisture determination, array 02, block 17/18 by moisture balance and CM method

Name	Sampling point	Sample weight (g)	Moisture content (moisture balance and CM method)
Sample MB <sup>a</sup> 04	Column 01, centre	32.40	3.19%
Sample CM <sup>b</sup> 04			1.0 CM-%
Sample MB 05	Column 14, centre	40.69	3.15%
Sample CM 05			0.8 CM-%
Sample MB 06	Column 25, centre	27.07	2.92%
Sample CM 06			0.9 CM-%

<sup>a</sup>Sample MB xx = reference sample moisture balance

<sup>b</sup>Sample CM xx = reference sample CM method

Due to harsh conditions at the construction site (strong wind, construction traffic) measurement deviations cannot be ruled out. So far the moisture balance values deliver only an estimation of the moisture content and not the absolute moisture content.

The discrepancy between the reference values using the gravimetric method and those determined by the moisture balance is in the range of approximately 0.6%. When comparing these values one should keep in mind that the absolute moisture acquired by the moisture balance only represents a surface moisture, whereas the values derived from sample cores depict volume moisture.

## Expectation

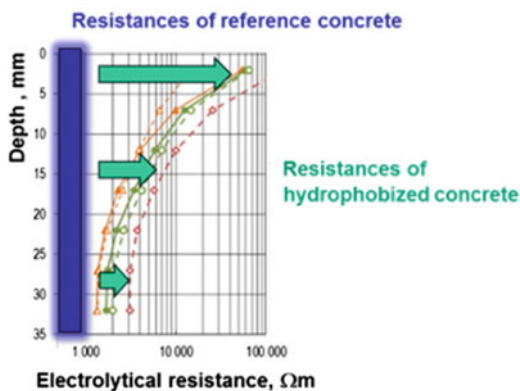


**Fig. 19.19** The inserted multi-ring-electrode equipment (left) and the profiles of resistances

The CM measurements are significantly lower when compared to gravimetric reference moisture values. A deviation of up to a maximum of 1.5% between gravimetric moisture values and CM moisture values is already mentioned in literature, but does not explain the observed difference of 2.8%.

In addition to the previously utilized methods, multi-ring-electrodes (MRE) have permanently been installed in the tunnel walls to monitor the depth dependent moisture content. This resistivity-based method only provides information about relative moisture contents. This method was considered in order to get information if hydrophobic treatment was effective and will be effective in the future. So far, no results are available yet. However, Fig. 19.19 exemplarily shows the results being obtained by MRE for concretes with and without hydrophobic treatment in another tunnel project. The electrolytical resistance of concretes without hydrophobic treatment is usually in the range of 1.000  $\Omega\text{m}$  (blue area). With hydrophobic treatment, the resistance of the concrete significantly increases (green arrows), especially near the surface (here: 0–25 mm). When the resistance decreases again, the effectiveness of the hydrophobic treatment decreases and a new surface protection has to be applied.

# Chapter 20

## Moisture Distribution in a Structure/ Specimen—General



Lars-Olof Nilsson

In a lot of applications there is a need to measure the distribution of moisture in a material, i.e. the moisture content or the state of moisture, at a certain, defined position or a series of positions.

Moisture distributions could be quantified with most of the measuring principles described in Chaps. 5–18 but not all of them are useful or suitable for all types of applications where moisture distributions are to be determined. It depends very much on the conditions in each application.

In the next chapters four different types of applications are presented:

1. Non-destructive methods, from the surface and inwards,
2. Methods that utilize sampling from defined positions,
3. Methods where probes or sensors are inserted,
4. Methods when also the sides of a specimen or core are available.

The differences between these applications are shown in Fig. 20.1.

In the first three applications only one surface of the structure (or specimen) is available. This is the common case for most in situ measurements. A typical case is measurements in a floor slab. From the available surface moisture measurements are to be done at one or a series of depths from this surface. In most cases this could be looked upon as a one-dimensional problem where the moisture content and/or the state of moisture varies with the depth. This depth dependency is what usually is called a “moisture profile”.

For such cases we have three alternatives, cf. Fig. 20.1. If possible, we would like to make the measurements non-destructively but the possibilities for this kind

---

L.-O. Nilsson (✉)  
Lund University, Lund, Sweden  
e-mail: lars-olof.nilsson@byggtek.lth.se

L.-O. Nilsson  
Moistenginst AB, Trelleborg, Sweden

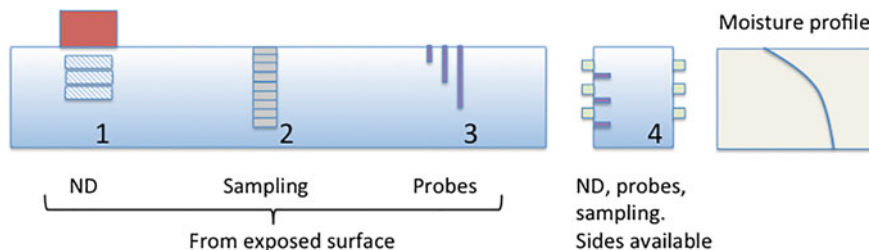


**Fig. 20.1** Four different types of applications where a moisture distribution with depth, a “moisture profile”, is to be measured

of measurements are limited. Instead, the most common ways to determine moisture profiles from one surface are the other two: take samples from different depths or insert probes to different depths.

The fourth type of application is mostly a laboratory application where measurements are done on a specimen or a drilled core where also the sides are available, not only the “exposed surface”. In a pure one-dimensional case, where the moisture content and the state of moisture only varies with depth, a number of measuring principle are suitable. An equipment could be applied at one of the sides, a series of probes could be inserted from the sides or a sender and receiver could be applied on opposite sides for a series of depths.

These various applications are described in the next few chapters and the advantages and limitations of alternative techniques are discussed.

# Chapter 21

## ND-Methods—From a Surface



Kurt Kielsgaard Hansen, Jean-François Lataste and Charlotte Thiel

A complicated application is to measure a moisture distribution with depth from a surface non-destructively. Only a few methods are suitable for such a case.

### 21.1 Suitable Moisture Measuring Principles; Advantages and Limitations

Moisture measuring principles that could be used for this application are summarized in Table 21.1 with their advantages and limitations.

The general strategy to assess moisture profiles should be to interpret the measured physical parameter for a known and mastered depth. There is more or less only one method allowing to focus on a single depth, NMR. This approach is not possible with other classical and totally non-destructive techniques. Indeed, the main problem is that other ND-techniques are used from the surface and their volumes of investigation integrate the depth from the surface.

For some techniques, some methodologies allow to consider successively deeper and deeper volumes using the knowledge of surface properties to deduct (in an

---

K. K. Hansen (✉)

Technical University of Denmark, Kongens Lyngby, Denmark  
e-mail: kkh@byg.dtu.dk

J.-F. Lataste

Université de Bordeaux, Bordeaux, France  
e-mail: jean-francois.lataste@u-bordeaux.fr

C. Thiel

Technical University of Munich, Munich, Germany  
e-mail: charlotte.thiel@tum.de

© RILEM 2018

L.-O. Nilsson (ed.), *Methods of Measuring Moisture in Building Materials and Structures*, RILEM State-of-the-Art Reports 26,  
[https://doi.org/10.1007/978-3-319-74231-1\\_21](https://doi.org/10.1007/978-3-319-74231-1_21)

**Table 21.1** Moisture measuring principles suitable for measuring a moisture distribution from a surface non-destructively; their advantages and limitations

Principle	Advantages	Limitations
NMR, cf. Chap. 13	High accuracy and high resolution (depth profiles with a resolution up to 5 $\mu\text{m}$ can be achieved). Different types of water according to their state can be distinguished	The total detection depth is limited, differently for different type of equipment; typically less than 5 cm. Calibration curves need to be generated (see Chap. 13). Steel reinforcement will interfere; separate calibration is required
Electrical resistivity tomography, ERT, cf. Chap. 8	Depth of investigation can be adapted to the study, from some centimetres to meters. Cheap equipment	Under development. Steel reinforcement will interfere
Microwave reflection, cf. Chap. 16	Comparably inexpensive. Easy to handle	Calibration is necessary
Neutron, cf. Chap. 17	Linear Count Rate and Moisture Content in weight-%. Not influenced by salt. Average moisture content measured up to 250 mm depth. Easy scanning of large areas, cf. Chap. 19	Needs a standardization check on a reference standard at the beginning of measurement. Requires determination of a calibration curve for the actual material. Handling, storage and transport of the radiation source unit need permission from national authorities

iterative process) the properties deeper and deeper. This way is not always possible. For instance, for infrared thermography and radar, two very performing techniques for mapping, the volumes of investigation are fixed and there is no data treatment today allowing assessment of gradients in depth. Infrared thermography is limited to properties along the surface. For radar, even if the frequency of the antenna determines the depth of investigation, the results integrate all depths of investigation with no possibilities for sharper discretisation.

However, for some others techniques the analysis of measurements for various volumes are possible. For capacitometry and for electrical resistivity the depth of investigation is a function of the array size. Consequently, repeated measurements with various arrays make it possible to obtain data for retro analysis of information, as functions of depth. This approach should be theoretically possible for capacitometry; nevertheless, no code for data inversion is today available. It may be a very promising tool to assess moisture profiles.

For electrical resistivity, the arrays called Electrical Resistivity Tomography (ERT) have been developed for some years, which will probably proceed to industrial applications in the next few years.

The principle of ERT is to place several electrodes on the surface and perform measurements according to a planned sequence. Several combinations of four probes are used and by varying the positions and distances between probes the depth of investigation can be varied. This technique is largely used in geophysics. Some results are known for onsite masonry, for concrete, see Sbartai and Lataste (2008), and wood, Lin et al. (2012), but not for moisture assessment in the last case. The main technical limitation of this tool is that reducing the distance between probes, for increasing the resolution, put a question on the diameter of the electrodes relative to their spacing. So, if the technique is suitable for applications on masonry with decimetre spacing between electrodes, it is more difficult to adapt the device for concrete where centimetre spacing is needed to assess the cover depth sharply.

When data are acquired, some inversion code exists to transform apparent resistivity measured from the surface to various depths into true resistivity at a given depth, Loke and Barker (1996). The principle is to compare the apparent resistivity tomography (pseudo-section) measured to the pseudo-section deduced from direct computation of a model resistivity distribution in depth. An iterative process modifying the model at each step stops when the two pseudo-sections (measured and computed) are similar. The final model is then considered as the better model. A limitation of this approach (without consideration to classical numerical approximations and hypothesis supporting the computation) is that the results are given as a slice, in depth, for resistivity distribution, although the electrical resistivity measurement integrates in fact the half space.

Results are generally given in terms of resistivity distribution (as a map or a profile in depth). The translation in terms of moisture could only be done if calibration is done on a sample, du Plooy et al. (2013), or on-site by monitoring, Schiebl and Breit (1995).

## 21.2 Application Example—ERT on Concrete

In the frame of the French research project EVADEOS (granted by the French national agency for research, 2012–2015) the assessment moisture gradient in depth was notably addressed, Villain et al., 2016. The use of electrical resistivity tomography (ERT) was tested and developed in this aim, by I2M from the University of Bordeaux as well as by IFSTTAR. Tests were notably done on a dry concrete slab to identify the sensitivity of the ERT to the re-humidification process. Concrete slabs with the same composition have been studied. They have been preliminary stored to be dry, then put in water from one face. The measurements have been performed regularly during the wetting process. The moisture ingress was monitored by a THR-sensor inserted in the slabs, Fig. 21.1.

The devices are composed of 16 or 14 probes (depending on institutions) on line devices. The probe spacing is 2 cm, as found in previous works, Sbartai and Lataste (2008) and du Plooy et al. (2013). The length of the device, which classically

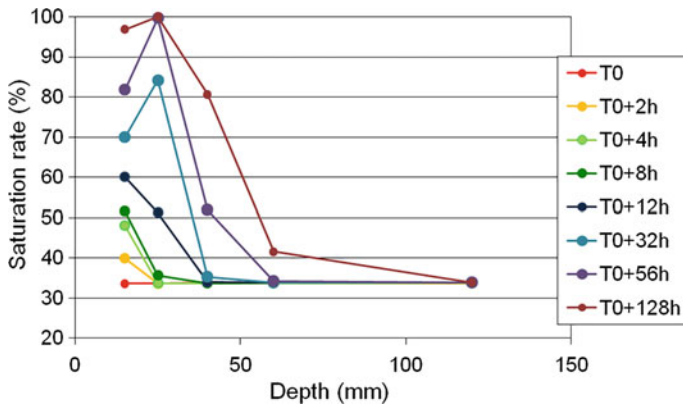


Fig. 21.1 Moisture profiles, from THR-sensors inserted in slabs

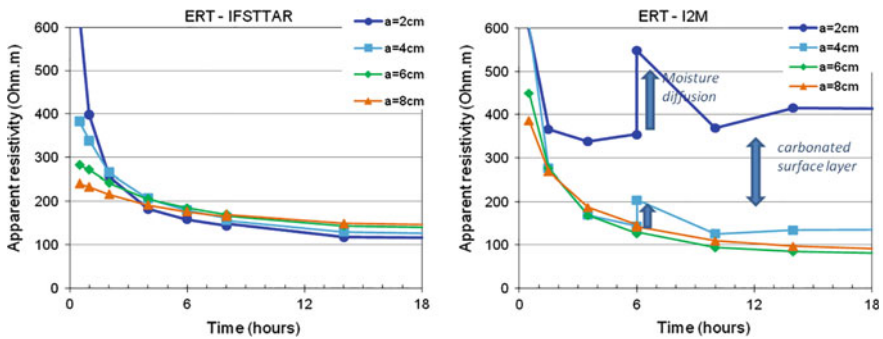


Fig. 21.2 Resistivity profiles as function of moistening time for ERT-measurements at the exposed surface by IFSTAR and I2M, Villain et al. (2016)

allows detecting the distribution of resistivity in the material, was not used in this aim. An example is the investigation of the cathedral of Lucca in Italy presented in the framework of the ONSITEFOR MASONRY (2006) and where the ERT has allowed the characterisation of moisture distribution in a masonry wall.

In this study we can consider the moisture gradient laterally regular and the investigation length is justified here (1) to be able to integrate various investigation depths; (2) to assess the variability of measurement. Measurements have been done with a low frequency signal leading to results similar to that of direct current.

The results are presented in function of the probe spacing: 2, 4, 6 or 8 cm, which corresponds to the increase of the investigation depth. One can consider that an order for the investigation depth is about half the spacing. Results show, Fig. 21.2, that the resistivity is quite similar for the two institutions except for the smallest spacing between probes (2 cm) which is very influenced by surface properties. It is associated to a carbonation layer on the sample from I2M, not observed on the

IFSTAR sample. The resistivity decreases during the moistening, to a steady state. This behaviour is associated to the penetration of moisture in depth with time. This is also supported by the resistivity shift at 6 h observed for the I2M sample, which corresponds to the diffusion of moisture during the first night (the sample was then stored out of water). Inverse analysis of these results is studied and still in progress to propose a representation of the saturation rate directly from the assessed resistivity.

### 21.3 Application Example—NMR on Lightweight Concrete

Hydrogen Nuclear Magnetic Resonance Relaxometry ( $^1\text{H-NMR}$ ) enables the determination of the depth-resolved water content non-destructively, see Chap. 13.  $^1\text{H-NMR}$  can be applied from one side to the sample (e.g. a building wall) so that there are no restrictions on the sample size. In addition, small NMR sensors can be embedded into the structure for process integrated monitoring.

Wolter et al. (2003) used Single-Sided NMR to measure moisture depth-profiles in lightweight concrete pillars on-site, Fig. 21.3.

The red line shows the water profile measured on-site up to a depth of 26 mm. The whole measurement took only about 30 min. The inaccuracy was better than 0.5%, Wolter et al. (2003). The water content clearly increases with depth. However, the measured water content could be distorted by reinforcement. To analyse the effect of reinforcement on the measurement, a drilling core 150 mm in length was drawn without the steel reinforcement and investigated in the laboratory. In order to determine the water content of the whole specimen, it was sawn into 3 samples of about 50 mm in length. By measuring from the upside and from the

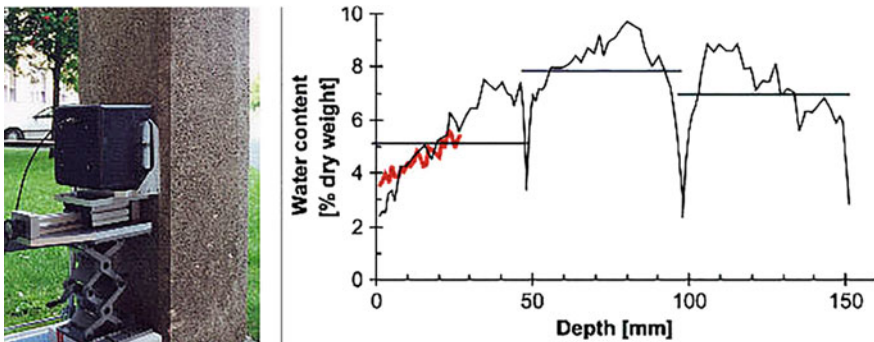


**Fig. 21.3** Moisture profile measurement on a lightweight concrete pillar. The diagram on the right shows the on-site measuring result (red line) as well as the moisture profiles (black line) and the integral moisture values (grey straight lines) from laboratory measurements, Wolter et al. (2003)

bottom side of each piece, it was possible to determine the water content over the total depth of 150 mm. The black line in Fig. 21.3 shows the resulting water profile. Besides minor differences at the beginning, probably as a result of the one-day delay between on-site measurement and sampling, a good accordance between the “on-site” profile and the “laboratory” profile is obvious. Therefore, the steel reinforcement only had minor influence on the measurement. The strongly decreased water contents at the first 100 mm from the surface of the samples are due to sawing. The integral moisture contents of the cut samples were also determined by weighing, drying and re-weighing (grey straight lines in Fig. 21.3). The water content determined with NMR is in good agreement to the water content determined with gravimetry.

# Chapter 22

## Coring, Drilling and Sampling Techniques



Lars-Olof Nilsson and Elisa Franzoni

### 22.1 Sampling Techniques, in Principle

An obvious method to determine the distribution of moisture in a material or structure is to take a sample from the intended position and then determine the moisture content or state of moisture on that sample.

Most of the measuring principles described in Part I are useful for measuring moisture on a sample but the result depends very much on the sampling technique that was used. Here the possibilities, limitations, errors and uncertainties with different sampling techniques are described.

The techniques used to take a number of samples from a series of depths in a structure or a specimen are several. The key issues are three:

- (a) taking the samples from the intended depths and documenting the actual depths,
- (b) taking representative samples, if required,
- (c) avoiding disturbing (drying) the samples as much as possible until the measurement.

The main principles of taking a series of samples are

- 1. drilling a (cylindrical) core, taking a larger piece of the material or taking a whole specimen and split it into smaller samples from different depths,
- 2. drilling holes and take the drill dust as samples,
- 3. using hammer and chisel to take samples from a specific depth.

---

L.-O. Nilsson (✉)  
Lund University, Lund, Sweden  
e-mail: lars-olof.nilsson@byggttek.lth.se

L.-O. Nilsson  
Moistenginst AB, Trelleborg, Sweden

E. Franzoni  
University of Bologna, Bologna, Italy

## 22.2 Drill Dust as Samples

In a drilling procedure, which allows to obtain powdered samples and which is one of the most used method, the issue of moisture loss is particularly challenging. According to some recommendations the time for powder extraction must be limited for preventing water evaporation. In masonry, the rate of penetration of the drill bit should 2 mm/s or faster, obtained by means of drills with rotation speed  $1200 \pm 100$  rpm, RILEM TC 127-MS.

According to other recommendations and authors, low speed drills are recommended to avoid water evaporation connected to the temperature increase in the bit. In masonry materials, rotation speed  $<50$  rpm is recommended by NORMAL 41/93 (1993) for sampling in painted surfaces and  $<150$  rpm for masonry materials in general, Massari and Massari (1993), while rotation speeds higher than 1200 rpm or even 2000 were shown to cause a moisture loss up to 4 wt%, especially in hard materials (e.g. hard stones), Binda et al. (1996), Fabozzi et al. (1999).

## 22.3 Dry and Wet Coring

To be able to take samples from larger depths more easily, and to limit the moisture loss during sampling, a core is first taken by drilling with or without water-cooling. The core is then split into smaller samples using different techniques.

Dry coring will of course cause some drying of the core surfaces of the cylinder taken out. If the samples are taken fairly quickly and at some distance from the surfaces, significant moisture loss should be possible to avoid. One technique is shown in Example 1, see Sect. 22.6.1, where a large “core” was taken by drilling a series of narrow holes in a circle. Samples were then taken from the centre of that large core.

Wet coring will of course cause water absorption of the more or less dry surfaces of the core and the two ends. To avoid taking samples that are wetted by the cooling water, the samples must be taken immediately after coring and the samples must be taken from the centre of the core. A technique for this is shown in the next section.

Sampling after wet coring is of course only relevant for materials that do not absorb water very quickly. The experience is good from wet coring in concrete structures such as floors, bridges, nuclear reactor containments etc. Cores taken by divers from submerged parts of concrete bridges after wet coring are fully suitable for taking samples for moisture measurements, Andersen (1996).

## 22.4 Splitting a Core or a Specimen into Samples

The main method used for taking samples from a core or a larger specimen is a hammer and chisel. This method does of course include a lot of work and take some time. The challenges are to limit drying of the samples during sampling and to document the exact position of each individual sample.



**Fig. 22.1** Splitting a concrete specimen by using rulers and a compressive strength test machine, Johansson (2012)

Johansson (2005) tried a “giljotine” to split mortar bar specimens into several smaller pieces at one time. The technique did not work very well.

A better technique to take samples from a specimen or a core is to put a ruler at the top and bottom of the specimen/core in a compressive strength-testing machine and split the specimen into slices, see Fig. 22.1.

A core can be divided along the axis with the same technique, cf. Fig. 22.2. Nilsson (1997) used this technique to split concrete cores into four “wedges”. Each wedge could then be easily split perpendicular to the axis to obtain samples at specific depths from the exposed surface, cf. Fig. 22.2. To avoid the errors due to absorption of water during drilling, the samples were taken from the inner parts of the wedges.

This technique is applicable on stones, bricks, concrete etc. but the size of the “slices” is limited and depends on the thickness of the specimen/core, the size of the aggregate, presence of cracks.

For splitting slices into thinner thicknesses and smaller samples a hammer and chisel is preferred., cf. Fig. 22.3.

To obtain a suitable size of the samples, larger particles are crushed with a hammer and the larger pieces are selected.

## 22.5 Moisture Loss During Sampling

Johansson (2012) studied the drying when splitting a large concrete specimen into samples by first using rulers and a compressive strength test machine and then hammer and chisel to split the pieces into smaller samples.

The weight loss depends on the size of the particles in the sample, the surrounding climate and the time it takes to handle the sample. Johansson used 56 g samples, meant for RH measurements, from a concrete with w/c 0.38 having an RH of around 85%. The surrounding climate was 20 °C and 55% RH. The samples were placed on a balance and the weight loss was registered. An example is shown in Fig. 22.4.

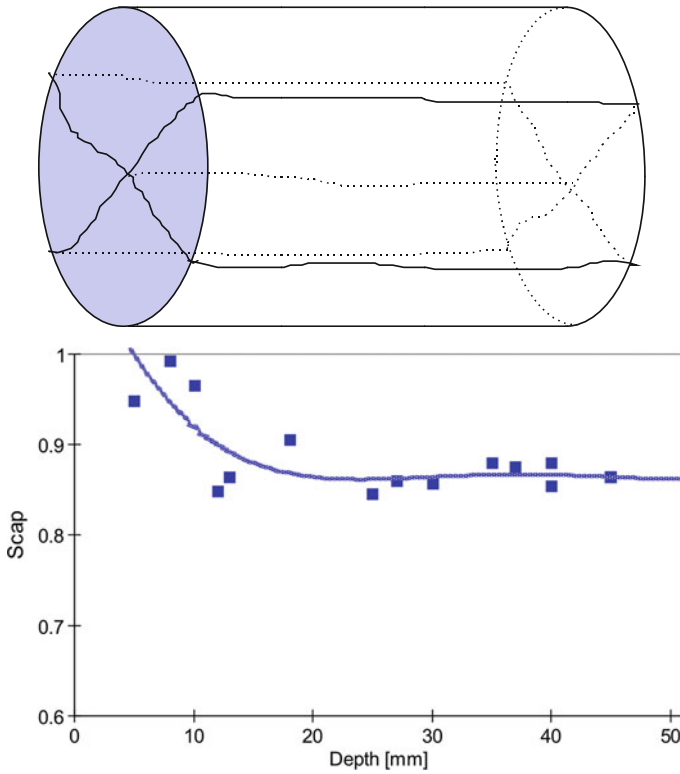
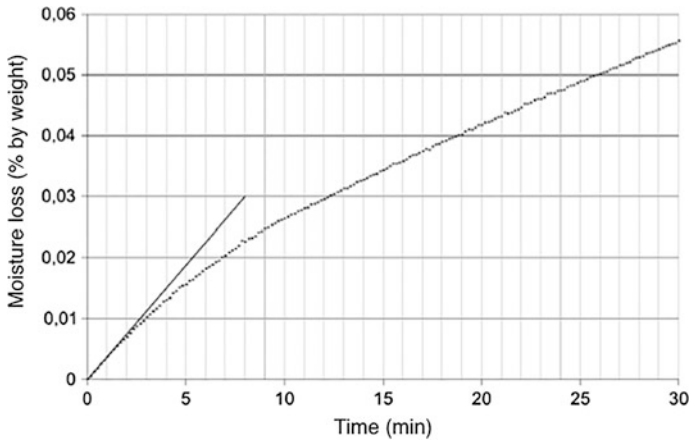


Fig. 22.2 Splitting a concrete core by using rulers and a compressive strength test machine (top) and examples of results (bottom), Nilsson (1997)



Fig. 22.3 Splitting a large concrete slice into smaller slices and samples with hammer and chisel, Johansson (2012)

The actual sampling took only a few minutes. The weight loss due to drying was then less than 0.01% by weight, corresponding to a systematic error of less than 0.1% RH.



**Fig. 22.4** Moisture loss during sampling from 15 mm concrete particles from a concrete with  $w/c = 0.38$  and 85% RH in  $+20\text{ }^{\circ}\text{C}$  and 55% RH, Johansson (2012)

In a later, larger study Johansson (2014) showed that the loss of water was significant if the samples are taken by drilling a core to a certain depth and then using hammer and chisel to sample small pieces. Depending on the heating during drilling, the size and shape of the samples taken and the type of concrete a systematic error of several % RH could be obtained for low- $w/c$  concretes.

## 22.6 Examples

A few examples are shown here where one of the techniques to take samples from different depths is used. Sometimes two techniques are combined.

### 22.6.1 Example 1: Dry Drilling and Hammer and Chisel in Concrete Floor Slabs on Grade

In Example 1 samples were taken from a series of depths in a 0.1 m thick concrete floor slab on grade. First, a series of holes were drilled through the slab, in a circle. A hammer and chisel were then used between the holes to be able to remove the large “core”, some 0.15–0.20 m in diameter.

The core was then split into smaller pieces and samples were taken from different depths, avoiding the volume near the surfaces with the drill-holes where some drying occurred. The moisture content and the RH of various samples were then determined. Results from three floors are shown in Fig. 22.5.

Samples were also taken from the expanded clay particles underneath the concrete floor slabs; at depths larger than 110 mm. These samples were taken by

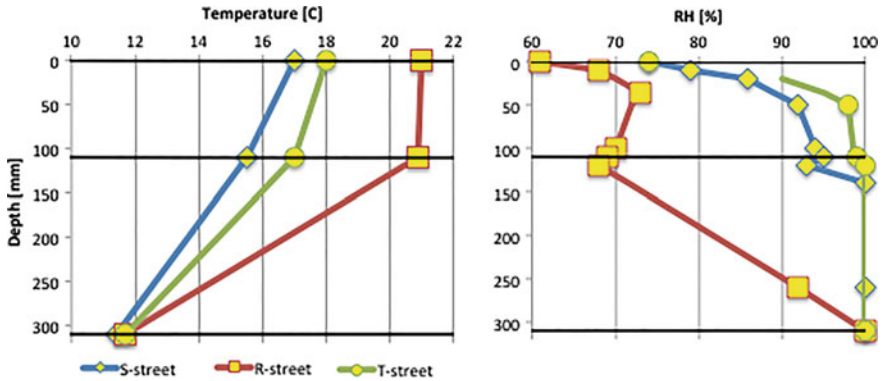


**Fig. 22.5** RH-profiles (right) from three 0.11 m thick concrete floor slabs on grade with a 0.2 m layer of heat insulation of expanded clay particles. Samples taken by drilling small holes in a circle and then sampling by hammer and chisel, Nilsson (1976). Temperatures (left) measured with thermo-couples a few days after the sampling

simply picking out samples from the particle layer, avoiding mixing particles from different depths, Nilsson (1976). Samples with some content of cement-paste stabilization were preferred since the cement paste has a much larger moisture capacity that will reduce the measurement error when determining the RH of a small sample.

**22.6.2 Example 2: Wet Coring, Splitting and Hammer and Chisel in a Field Exposed, Submerged Concrete Slab**

For measuring the moisture distribution in 0.1 m thick concrete slabs that have been exposed to sea-water, partly submerged, for five years cores were taken by wet

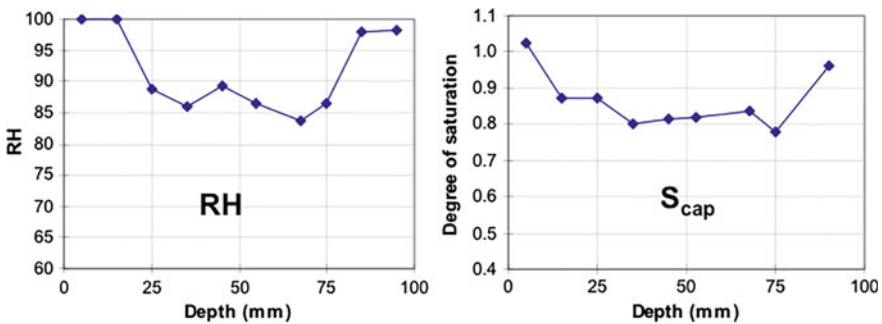


**Fig. 22.6** Profiles of RH (left) and DCS (right) from samples from the centre of one core drilled with water-cooling from a water depth of 0.5 m in a partly submerged 0.1 m thick concrete slab continuously exposed to sea-water from both sides for five years. Concrete with SRPC, fly ash and silica fume with a w/b of 0.35. Data from Tang (2003)

coring. The cores were then split as described in Sect. 22.4, Fig. 22.2, and samples were taken from the inner parts of the core, at different depths from the exposed surfaces. Example of results are shown in Fig. 22.6.

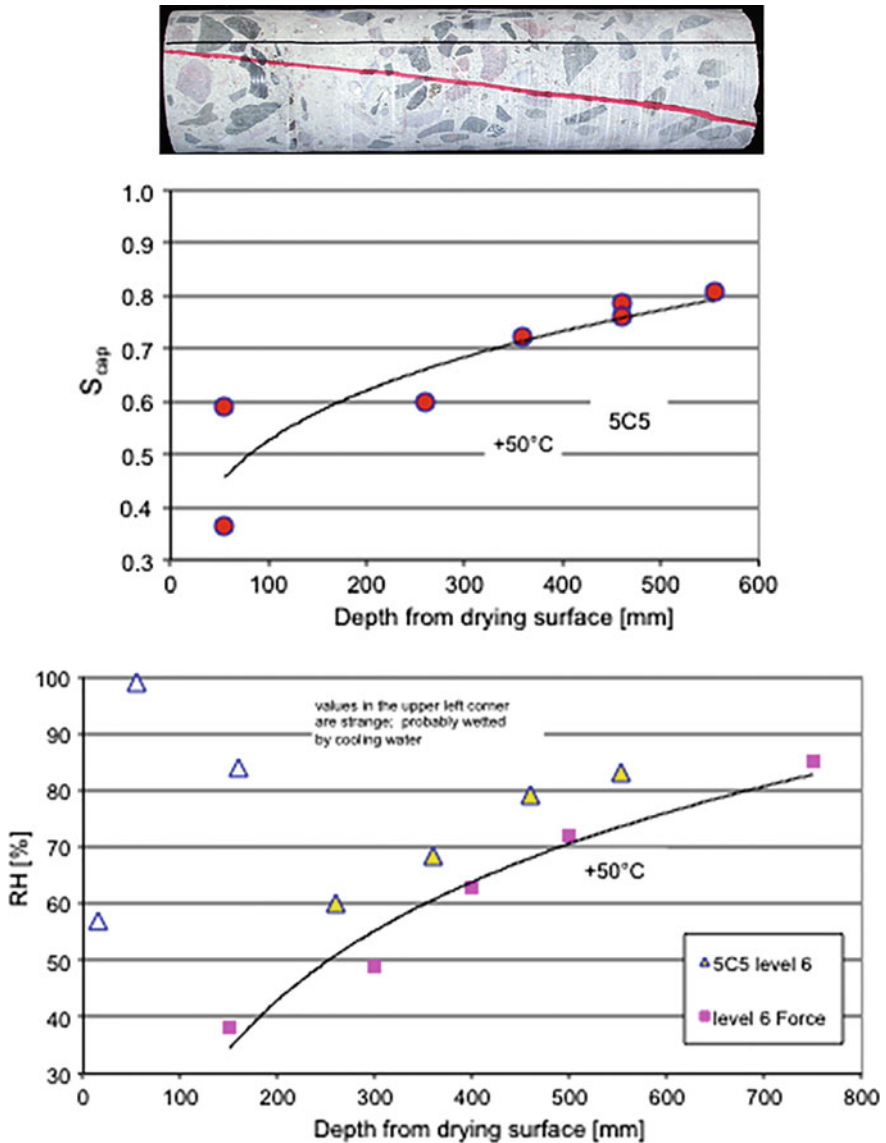


Fig. 22.7 Profiles of DCS ( $S_{cap}$ ) (top) and RH (bottom) determined on samples taken by hammer and chisel from a 600 mm long concrete core (far top) drilled from a 800 mm thick reactor containment wall using water cooling. Comparison with a RH-profile from probes inserted in small, drilled holes (“level 6 Force”) at a location nearby. Data from Nilsson (2004)

Several smaller pieces were taken from a series of depths into glass test tubes for determining RH. One large piece at a series of depths was taken into plastic bags for determining the moisture content and the degree of capillary saturation DCS ( $S_{\text{cap}}$ ).

### ***22.6.3 Example 3: Wet Coring, Splitting and Hammer and Chisel in a Nuclear Reactor Containment Wall***

A few large cores, 800 mm long, were drilled from a reactor containment wall using water-cooling. The cores cracked, especially close to the dry surface. These parts were avoided when sampling by splitting the cores and using hammer and chisel (Fig. [22.7](#)).

# Chapter 23

## Installation of Probes



Lars-Olof Nilsson, Franck Agostini and Charlotte Thiel

### 23.1 Introduction

The principles of installation of probes to measure moisture in a certain position in a structure or specimen are shown in Fig. 23.1.

The probe is meant to come into equilibrium with a certain portion of the surrounding material. To achieve a more precise measuring depth a tube is often inserted in a hole or cast-in to define the depth, cf. Fig. 23.1. Without a tube the measuring depth will easily become more undefined, cf. the right part of Fig. 23.1.

Some examples of the use of various probes are given below together with examples of results obtained.

### 23.2 RH-Probes in a Drilled Hole

An RH-probe is usually put into a drilled hole as shown in Fig. 23.2. After drilling the drill dust is removed and using a vacuum cleaner cools down the hole. Then the hole is sealed with a plastic tube and a rubber cork.

---

L.-O. Nilsson (✉)  
Lund University, Lund, Sweden  
e-mail: lars-olof.nilsson@byggtek.lth.se

L.-O. Nilsson  
Moistenginst AB, Trelleborg, Sweden

F. Agostini  
École Centrale de Lille, Villeneuve-d'Ascq, France  
e-mail: franck.agostini@centralelille.fr

C. Thiel  
Technical University of Munich, Munich, Germany  
e-mail: charlotte.thiel@tum.de

© RILEM 2018

L.-O. Nilsson (ed.), *Methods of Measuring Moisture in Building Materials and Structures*, RILEM State-of-the-Art Reports 26,  
[https://doi.org/10.1007/978-3-319-74231-1\\_23](https://doi.org/10.1007/978-3-319-74231-1_23)

207

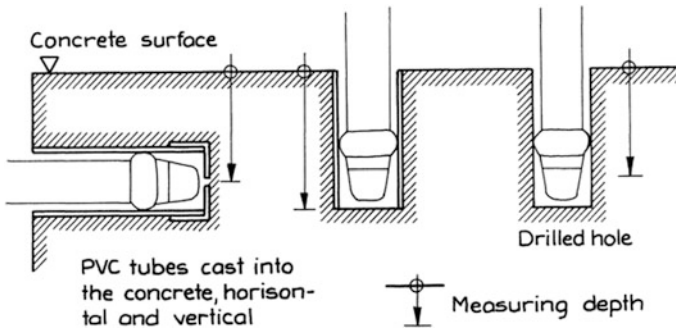


**Fig. 23.1** Three principles for installing a probe at a certain position: cast-in tubes (left), tubes inserted into a drilled hole (middle) or probes inserted into a drilled hole without any tube, Nilsson (1980)

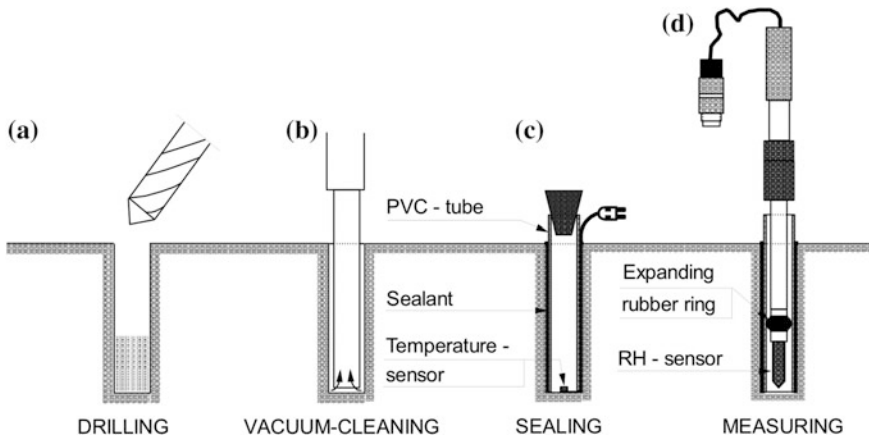


**Fig. 23.2** Placing an RH-probe into a drilled hole: **a** drilling, **b** vacuum-cleaning, **c** sealing the hole with a tube, **d** placing the RH-probe

The RH-probe cannot be placed into the hole until the temperature effects after drilling are small. This takes several days, cf. Fig. 23.3. Pastrav (1990) saw a very large error if the probe is placed too early, more than 10% RH!

This temperature effect was first seen by Pihlajavaara and Parroll (1974), which explained it by carbonation of the fresh surfaces in the drilled hole. He later saw a similar effect in bricks where there is no carbonation. This temperature effect is still not fully understood or explained.

It is important to seal the hole during the measurements, cf. Fig. 23.4. With a tube along the surfaces in the hole, except at the bottom, the final value will be more correct. Without the tube, the measurements will give faster results but a much lower RH.

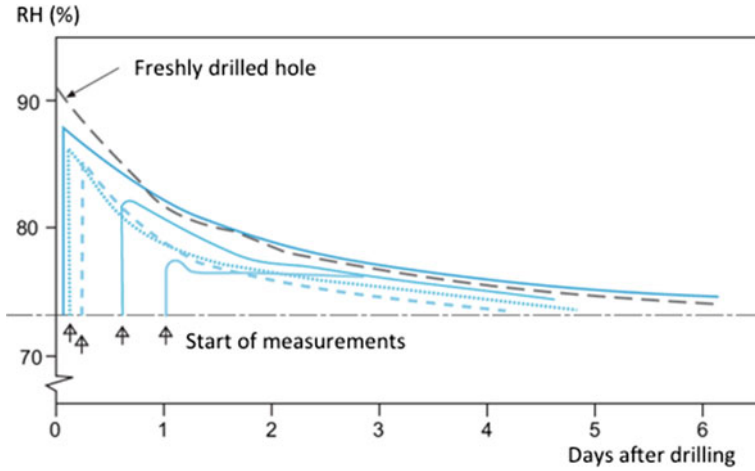


Fig. 23.3 Systematic error by placing an RH-probe into a drilled hole at different times after drilling, after Pastrav (1989) (Courtesy Formas)

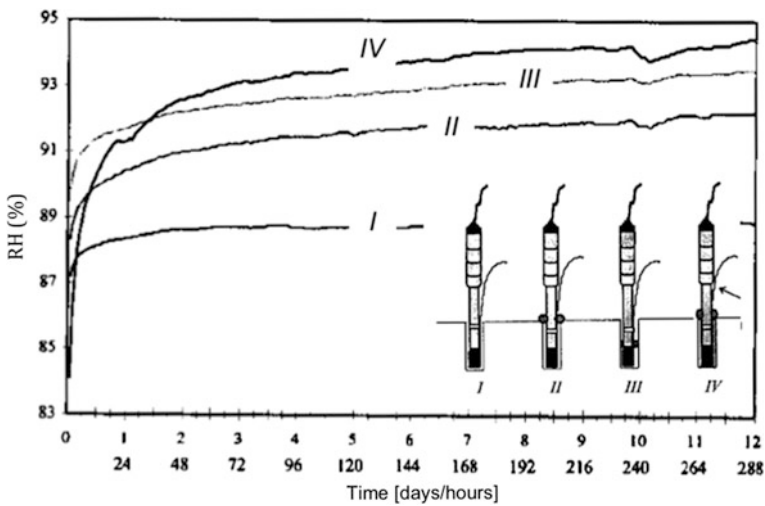
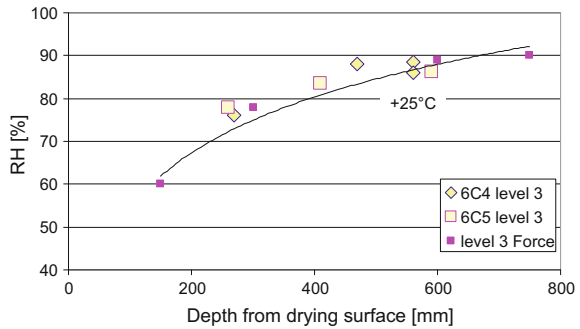


Fig. 23.4 Systematic errors depending on how the hole is sealed; no seal (I), top seal (II), bottom seal (III) and a tube (IV)

An example of using RH-probes in very deep drilled holes are shown in Fig. 23.5. Here the holes were up to almost 0.8 m deep and had no tubes or seal.

**Fig. 23.5** RH-profiles from very deep installation of probes (small, filled squares) compared to profiles by coring by water-cooled drilling and sampling (diamonds and large squares). From a 0.8 m thick nuclear reactor containment wall after 30 years of one-sided drying, Nilsson (2007)



### 23.3 Tubes for Probes for Accurate RH-Measurements in Drilled Holes

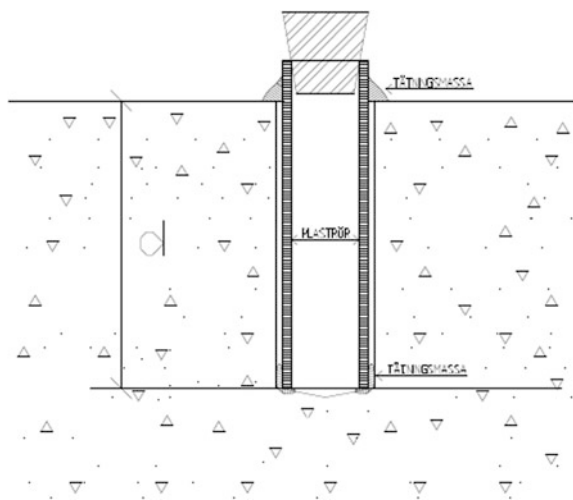
To measure RH in a drilled hole at a well defined depth only the bottom of the hole should be open and in humidity contact with the air in the hole. To ensure a thorough sealing of a hole a tube can be inserted and sealed against the material.

A standardized way of doing this is developed by RBK (the Council for Building Control, in Swedish), cf. Fig. 23.6.

The tube used could be different for different RH-probes. Figure 23.6 shows the principle that could be used for most probes. The tube is sealed at the top and the bottom with a sealant. The seal is tested so there is no air leakage with a rubber ball.

Some types of probes have a system of their own for inserting the probes. Two examples are shown in Fig. 23.7.

**Fig. 23.6** The insertion of a tube inside a drilled hole for measuring RH with a probe, RBK (2010:6), sealed at the top and bottom (Courtesy RBK)



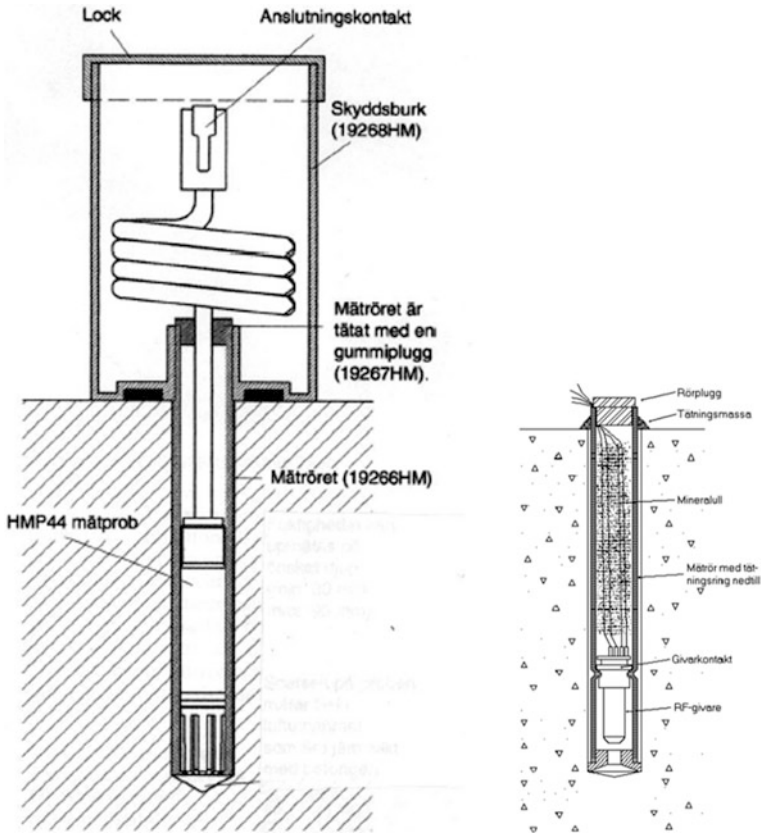


**Fig. 23.7** Two examples of tubes for insertion of an RH-probe to a certain measuring depth into concrete: Vaisala HMP44 (left) and HumiGuard (right), RBK (2010:8) and RBK (2010:9) (Courtesy RBK)

### 23.4 RH-Probes in a Cast-In Tube

In a similar way, tubes can be cast-in into a concrete specimen or a concrete structure on site in such a way that the ends of the tubes will have an open concrete surface at an intended distance from the exposed surface of the specimen/structure. This technique was used by e.g. Nilsson (1997), see Fig. 23.8, and Nilsson (1979).

An example of results is shown in Fig. 23.9.

When using this technique in situ the temperature differences between the RH-sensor and the concrete surface in the hole may give large scatter and systematic errors. The scatter in Fig. 23.9 for the largest depth is about 5% RH, which corresponds to a temperature difference of only 1 °C.

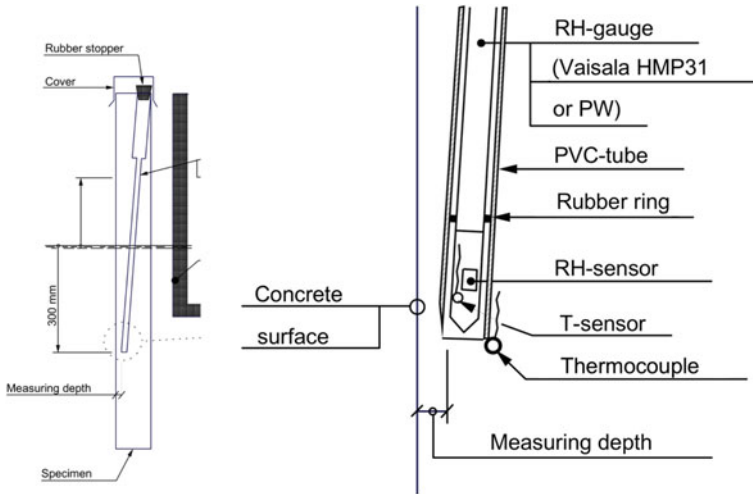


**Fig. 23.8** A cast-in PVC-tube with an inserted RH-probe in a concrete slab partly submerged in sea water for years, Nilsson (1997)

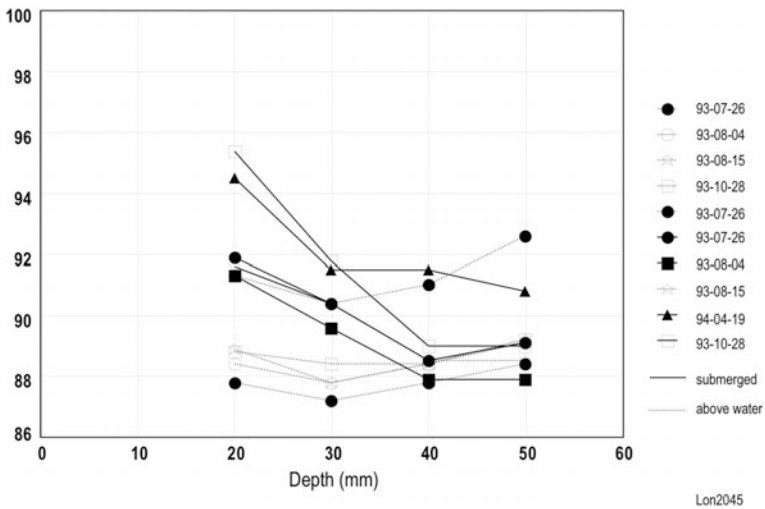


**Fig. 23.9** Examples of measurement results from four depths with the technique shown in Fig. 23.4, Nilsson (1997)

### 23.5 The OE-Probe for T- and RH-Profiles

A gravimetric method to determine the RH-profile in a structure is the so-called OE-probe; OE after the inventor Oskar Esping. The probe is a series of wooden rings separated by rubber sheets, cf. Fig. 23.10, cf. Sjöberg (2004).

If the temperature profile is to be determined simultaneously, a series of steel rings are put in-between the wooden rings, all separated by rubber sheets as in Fig. 23.10.

The probe is placed in a drilled hole in the structure and left there for some time, for the wooden rings to come into moisture equilibrium with the surroundings at each depth in the hole. The rubber sheets will ensure that no moisture flow occurs parallel to the probe. Each ring will then, eventually, achieve a moisture content corresponding to the RH at the depth of that ring.

When equilibrium has been reached the probe is taken out and the temperatures of the steel rings are read immediately by an IR-pistol. If this is done in a few minutes the temperatures of the surfaces of the rings are not changed.

Then the RH or the weight of the wooden rings is measured, by placing each ring in a glass test tube or on a balance. In the test tube the RH can be determined directly with the method described in Chap. 10. Determining the weight of each wooden ring requires a thorough calibration of the relationship between the weight and RH for each ring.

An example of measurements with OE-probes is shown in Fig. 23.11.

The profiles from the different techniques are very similar. One week of exposure of the OE-probe in the hole seems to be enough in this particular case.

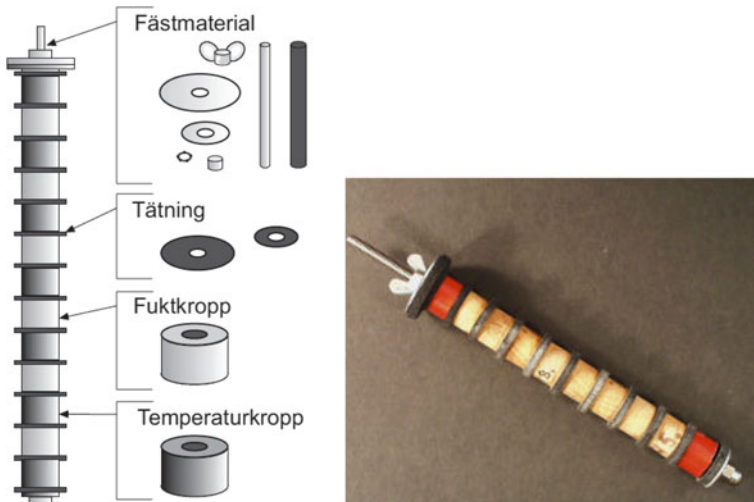
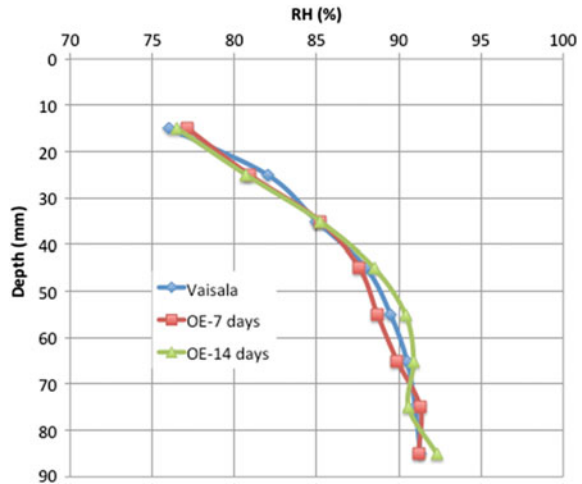


**Fig. 23.10** An OE-probe for determining the RH-profile and temperature profile in a structure (“Fuktkropp” = wooden ring, “Temperaturkropp” = steel ring, “Tätning” = rubber sheet), Sjöberg (2004)

**Fig. 23.11** RH-profiles in a 130 mm thick concrete slab drying upwards. Profiles from samples (Vaisala) compared to profiles from the OE-method with two exposure times in the hole, Ohlsson and Mikolajewski (2003)



The main advantage with the OE-probe is that profiles of RH (and T) can be determined simultaneously with one probe. The alternative methods require samples to be taken from a series of depths or a series of probes inserted into a series of tubes in holes.

The limitations, however, are several:

- The technique is not commercially available.
- The probe has to very well conditioned in a known climate for a significant time period before each new measurement.
- A systematic error depending on the moisture capacity of the material; the probe needs some moisture from the material. This should be quantified in each case.
- The effect of hysteresis when the wooden rings absorbed moisture from a material should be quantified in each case.

### 23.6 Permeability Probes Casted into Concrete: “Pulse Sensor”

Permeability probes can be used to measure moisture in concrete structures. The probes are placed in the concrete before casting. If the structure is not made of reinforced concrete, a steel cage can be used to maintain the probe during casting, see Fig. 23.12, Liu et al (2013). Otherwise, existing reinforcement rebar can be used to measure the moisture in a given position of the structure, in order to obtain a spatial moisture repartition or a moisture profile in a concrete wall for example, see Fig. 23.13.

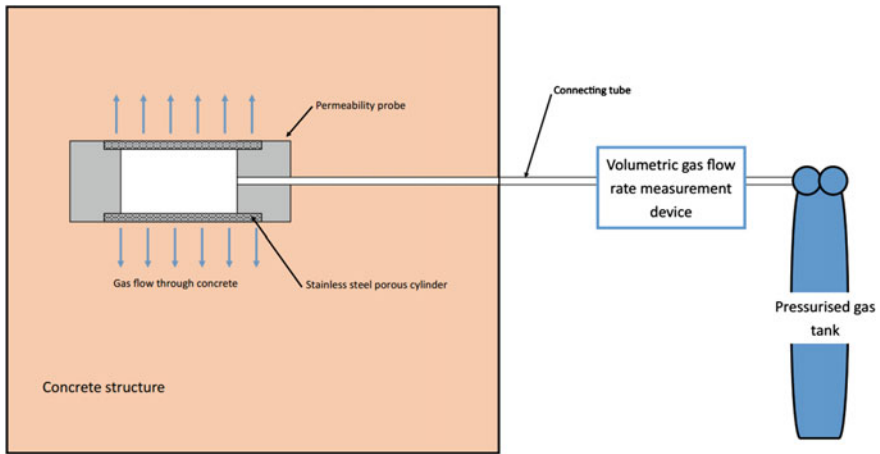
The measurement principle consists in measuring the volumetric gas flow rate injected in the concrete. Therefore, the sensor has to be connected to a measurement device able to generate a gas pressure and to measure the gas flow rate. The



Fig. 23.12 Picture of a “permeability probe” inside a cage



Fig. 23.13 Picture of “permeability probe” disposed in a reinforced concrete wall for moisture profile determination



**Fig. 23.14** schematic view of “pulse” permeability probe cast in concrete connected to measurement device

connection between the sensor and the measurement device can be a plastic tube, cf. Fig. 23.12, or a stainless steel tube, cf. Fig. 23.13.

Figure 23.14 present a schematic view of the measurement system composed of the probe (a hollow stainless steel cylinder cast in concrete), the measurement device and the connection tube.

## 23.7 Multi-ring Electrode (MRE)

The multi-ring electrode (MRE) measures the electrolyte resistivity between each two adjacent ring electrodes made of stainless steel, which are installed at different depths, see Chap. 8. By default, the MRE consists of nine rings having a thickness of 2.5 mm which are kept isolated from each other by plastic rings. By applying an AC voltage between each two adjacent rings (ring 1—ring 2, 2–3, 3–4 ...), a resistivity profile in eight 7 mm thick steps can be obtained. The required cell constant (geometric factor) was determined experimentally and by numerical simulations to 0.1 m (Orlowsky 2015). The MRE can also be assembled according to specific requirements like a certain depth profile.

While MREs are directly set in the concrete of newly built structures, the installation in existing buildings is conventionally carried out using a thin (appr. 2 mm thick) layer of coupling mortar, see Fig. 23.15 right. Calibration with respect to the “water content—resistance” relationship of the building materials is required to determine the moisture content quantitatively when retrofitting. In addition, here knowledge about the moisture balance of the materials involved is necessary. This can be easily and sufficiently accurately determined by a simple measurement of the sorption isotherms of the mortar and the surrounding concrete

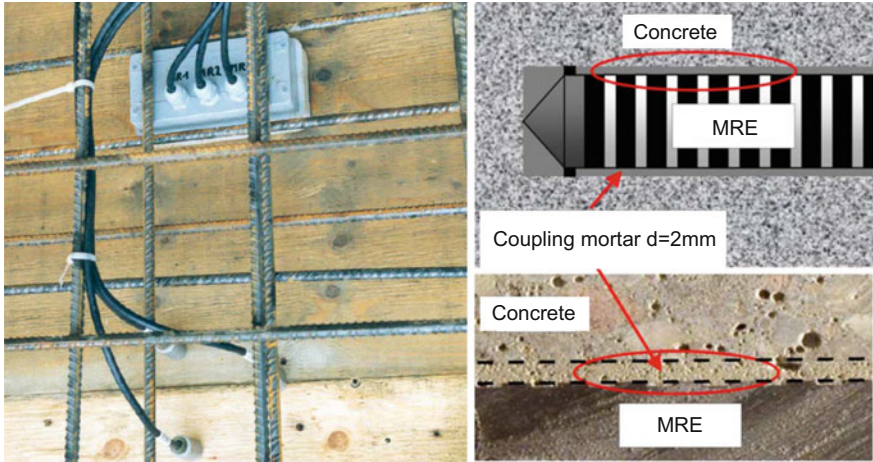


Fig. 23.15 Direct installation of MREs by mounting on the inside formwork (left) and subsequent installation in boreholes in hardened concrete (right), Dauberschmidt (2008)

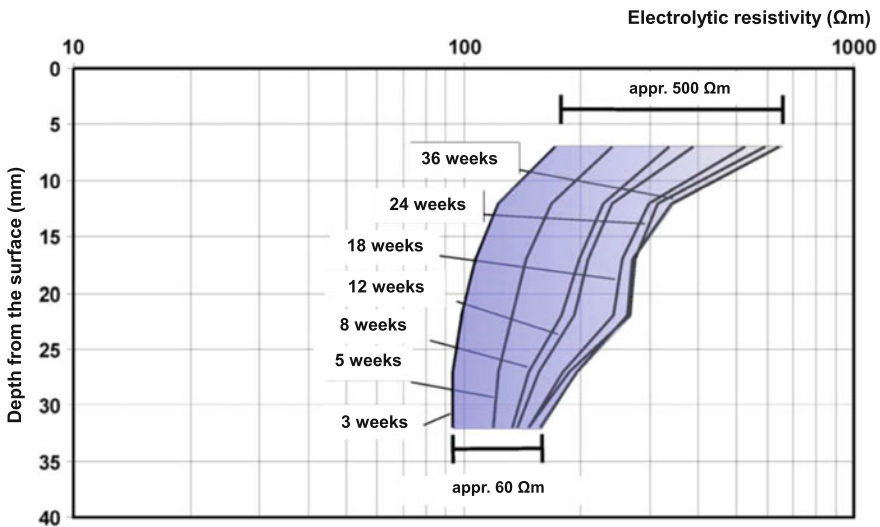
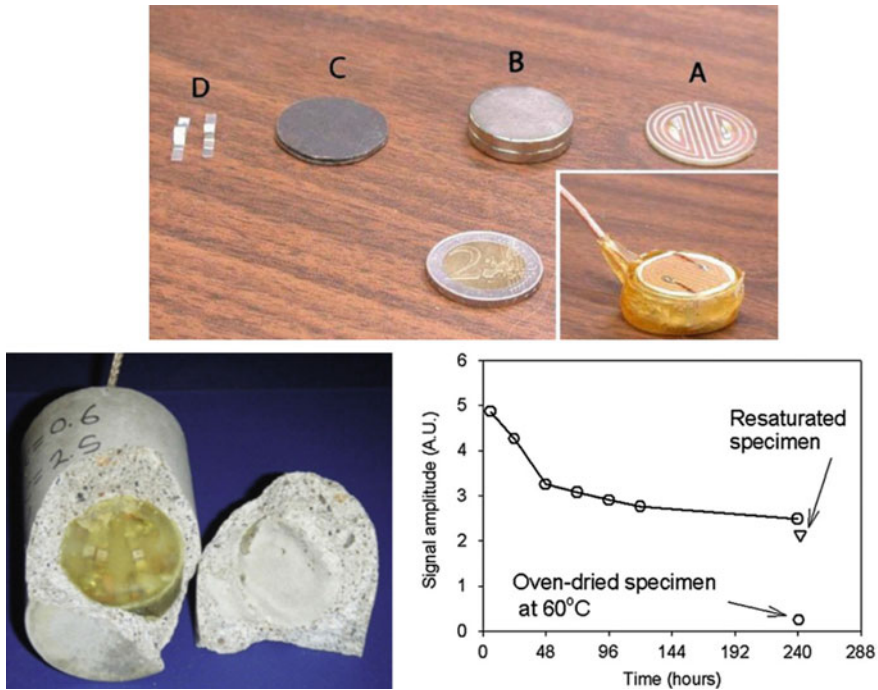


Fig. 23.16 Electrolyte resistivity profiles of a retrofitted multi-ring electrode (MRE) under an OS 11 system with zinc coating with a pronounced increase in values within the first 36 weeks after application of the coating, (Dauberschmidt 2008)

Figure 23.16 shows the exemplarily the electrolyte resistivity profile of an MRE under an OS system with zinc coating for the first 36 weeks after applying the coating on a parking roof, Dauber Schmidt (2008). The measured values clearly increase over the entire measurement depth. The increase of appr. 60 Ωm within the deeper measuring points is mainly due to two phenomena: the relative strong

increase in the first eight weeks is due to the adjustment in moisture state of the initially wet coupling mortar and the dryer surrounding concrete. Afterwards, the coating leads to further drying of the coupling and the surrounding mortar which is shown by the relatively slow increase in measured resistivity between week 8 and week 36.

The near-surface measurement points show an increase in resistivity of appr.  $500 \Omega\text{m}$  during the investigated period. Again, for the first 8 weeks the adjustment of the moisture states of the coupling mortar and the old concrete is the main driving force. The rapid increase in resistivity values as compared to the deeper measurement points indicates a larger moisture gradient between the wet coupling mortar and the surrounding concrete. As a result thereof, the water content in the coupling mortar decreases faster and deeper than in larger depths. Again, the resistivity increase in the later measurements can be related to the gradual drying of the concrete through the coating. This shows that the drying of the coated concrete can be determined with retrofitted MREs.



**Fig. 23.17** Top: Miniature NMR sensor construction (Marble et al. 2007); A RF coil (A) etched on a printed circuit board sits atop a stack of disk magnets (B). Iron disks (C) below the magnets are used to adjust the field strength above ( $\approx 0.24$  T). The RF coil is tuned to the Larmor frequency ( $\approx 10.2$  MHz) with small capacitors (D) mounted to a PC board below the magnets, and fed through a thin coaxial cable. The 2 Euro coin is shown for scale. Left: NMR sensor (30 mm in diameter and 12 mm in height) embedded in a Portland cement mortar specimen (diameter = 40 mm). Right: NMR signal during hydration of a sealed Portland cement mortar specimen (diameter = 40 mm), (Cano-Barrita et al. 2009)

## 23.8 NMR Sensors

As described in Chap. 13, NMR is a versatile tool that can measure the moisture content non-destructively and can be used for all kind of applications. For example, Cano-Barrita et al. used miniature single-sided NMR sensors to measure hydration processes in cement (Cano-Barrita et al. 2009). They applied an NMR disk of 30 mm in diameter and 12 mm in height, see Fig. 23.17 left. The measurement frequency was 10.2 MHz and the used echo times were in the range of 160  $\mu$ s.

The shown signal amplitude is directly proportional to the evaporable water content. Therefore, the evaporable water content decreases with increasing hydration. The water content is further decreased by oven drying at 60 °C (drying at 105 °C or higher is not possible since this would damage the magnets). As expected, most of the water content recovered after re-saturation. It should be noted that temperature affects the signal amplitude. This influence has to be considered in field experiments. However, the main advantages of such small sensors are the low costs and the possibility to permanently monitor moisture transport processes in building materials (Cano-Barrita et al. 2009).

# Chapter 24

## Specimen or Core; In the Laboratory (Sides Available)



Kurt Kielsgaard Hansen, Jean-Francois Lataste, Lars-Olof Nilsson,  
Charlotte Thiel and Alexander Michel

### 24.1 Introduction

When also the sides, of a specimen or a core from a structure, are available during the moisture measurement procedure numerous techniques are applicable compared with when only the exposed surface is available.

A number of non-destructive methods can be used from the sides, see the next sections. A sender and receiver could be placed on opposite sides of the specimen, cf. the top part of Fig. 24.1, and moved up and down to cover the depth dependency. The whole width of the specimen would then influence the results. Various equipments could be placed on one side of the specimen, as in the bottom part of Fig. 24.1, and be moved up and down. Then only a portion of the width of the specimen participates in the measurement.

The moisture distribution can of course also be determined by inserting probes from the available sides, cf. bottom left part of Fig. 24.1, or by taking samples from different positions in the specimen/core. This is to some extent already described in

---

K. K. Hansen · A. Michel  
Technical University of Denmark, Kongens Lyngby, Denmark

J.-F. Lataste  
Université de Bordeaux, Bordeaux, France

L.-O. Nilsson (✉)  
Lund University, Lund, Sweden  
e-mail: lars-olof.nilsson@byggttek.lth.se

L.-O. Nilsson  
Moistenginst AB, Trelleborg, Sweden

C. Thiel  
Technical University of Munich, Munich, Germany

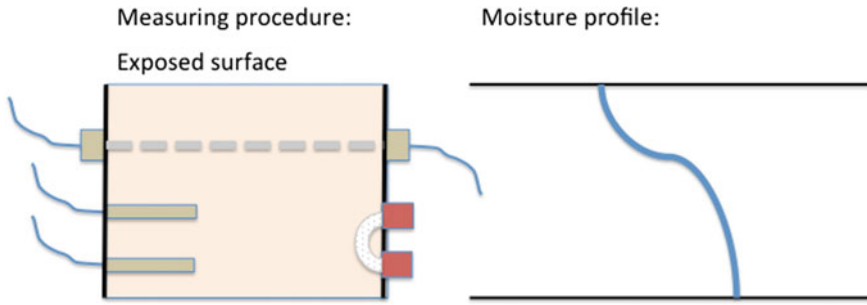


Fig. 24.1 Measuring principles when the sides of a specimen or core are available

Chaps. 22 and 23. Inserting probes from the sides, however, compared to inserting them from the (top) exposed surface will reduce the risk of introducing “leakage paths” for the moisture flow in a specimen with moisture flow perpendicular to the probes.

## 24.2 Suitable ND Measuring Principles

Moisture measuring principles that could be used for this application are summarized in Table 24.1, with their advantages and limitations.

**Table 24.1** Moisture measuring principles suitable for measuring a moisture distribution in a specimen or core non-destructively, their advantages and limitations

Principle	Advantages	Limitations (materials, size, resolution, etc.)
Surface-NMR Constant field-NMR	High resolution and accuracy. Different types of water according to their state can be distinguished	Calibration curves need to be generated, see Chap. 13. A flat surface is preferred
Electrical resistivity	Very simple device and easy to adapt	The two opposite faces of test body have to be strictly parallel, and well surfaced. Calibration required for each material
X-ray	Fast and accurate. Useful for transient moisture flow. 2D possible. High resolution	Large, expensive and sensitive equipment. Dry reference required; identically positioned. Limited thickness. Settings need to be determined
CT-scan with X-ray (for wood) Dual energy	2D & 3D possible. Dry reference not required. Possible resolution: 1 μm	Expensive equipment. The diameter of the specimen must be <0.5 m

(continued)

**Table 24.1** (continued)

Principle	Advantages	Limitations (materials, size, resolution, etc.)
$\gamma$ -ray		No longer frequently used since the source is radioactive
TDR-rods		Careful drilling to avoid air and non-parallel holes
TDR-surface	Results in volume-%. Average of measuring area $70 \times 200$ mm. Shape of TDR drying profile as gravimetric profile. Not influenced by salt	Pulse generator, reflected signal analyser and computer program needed. Standard error $\sim -25$ wt% in range 0–335 wt%, i.e. TDR measures less than the gravimetric method
Ultra-sound	Emitter and receiver on opposite sides of the specimen. Results in m/s. Easy method	Contact gel needed. Determination of a calibration curve for the actual material needed. Without that only the shape of the moisture profile is indicated

### 24.3 Application Example—Six ND-Methods Compared

Roels et al. (2004) compared several ND-techniques on specimens from calcium silicate blocks and bricks during capillary suction experiments. An example from their study is shown in Fig. 24.2.

In the example in Fig. 24.2 all measurements are done on the same specimen during a capillary suction experiment. Since the experiment is fairly rapid the individual profiles are measured at different stages of the capillary suction. To make a comparison the profiles are shown as function of  $x/\sqrt{t}$ , a so-called Boltzmann transformation.

The comparison shows that the results from most of the techniques coincided very well. Since the capillary uptake is pretty fast the gamma-ray-technique gave a profile that deviates from the profiles from the other techniques.

### 24.4 Application Example—Resistivity

For using resistivity the principle consists of the injection of an electrical intensity through the entire height of a sample or a core. Then by measurements of the potential drop between different positions one can assess the resistivity of various layers on the test body. If the measurement is done successively on layers along the test body, the distribution with depth can be assessed. This methodology needs to use the same device as the one used for calibration in laboratory. It can be easily adapted to various sizes and dimensions of the specimen. du Plooy et al.

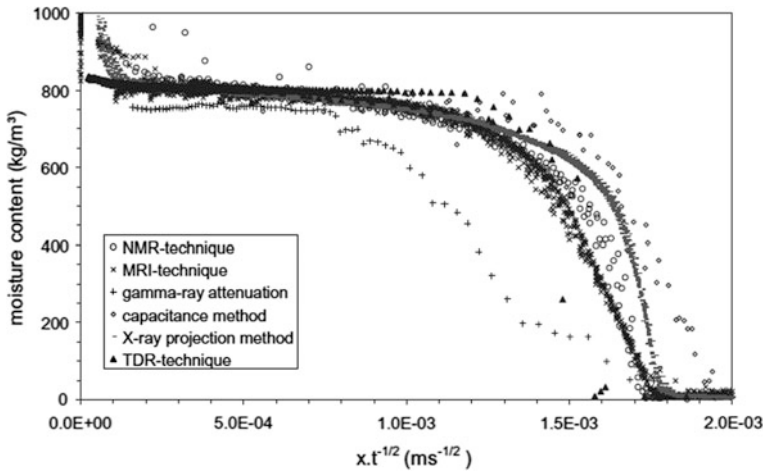


**Fig. 24.2** Moisture content profiles determined with six different ND-methods on the same specimen of calcium silicate during a capillary suction experiment, Roels et al. (2004)

(2013) have developed a device for calibration of resistivity measurement for assessment of gradient in concrete on samples with 75 mm diameter and 70 mm height. In spite that the cell is profiled to be able to directly assess distribution of resistivity along the core, the authors prefer to make calibration on measurement on homogenised samples (in term of moisture), at various dates. The measurements obtained from the various rings (for a saturation level homogenised on the entire sample) are then only used to assess uncertainties in resistivity measurement.

The evaluation of the resistivity of each slice is done by Eq. (24.1) (Fig. 24.3).

$$\rho_{\Omega_i} = \frac{S}{l_i} \cdot \frac{\Delta U_i}{I} \quad (24.1)$$

where  $\rho_{\Omega_i}$  is the resistivity of slice  $i$  [Ohm m],  $S$  the cross section of the core or sample [m<sup>2</sup>],  $l_i$  the thickness of the slice  $i$  [m],  $\Delta U_i$  the potential drop over slice  $i$  [V] and  $I$  the injected current intensity [A]

## 24.5 Application Example—X-Ray for Cracked Concrete

Pease et al. (2012) used a GNI X-ray attenuation measurement system located at the Technical University of Denmark was used to monitor water sorption in 50 mm thick steel fibre reinforced concrete (SFRC) wedge split test (WST) specimens, shown in Fig. 24.4. A polychromatic X-ray source and a 25 mm × 25 mm X-ray camera are housed in a programmable, moveable frame. X-ray source energy settings of 110 keV and 15  $\mu$ A were used for all measurements. The 25 mm × 25 mm

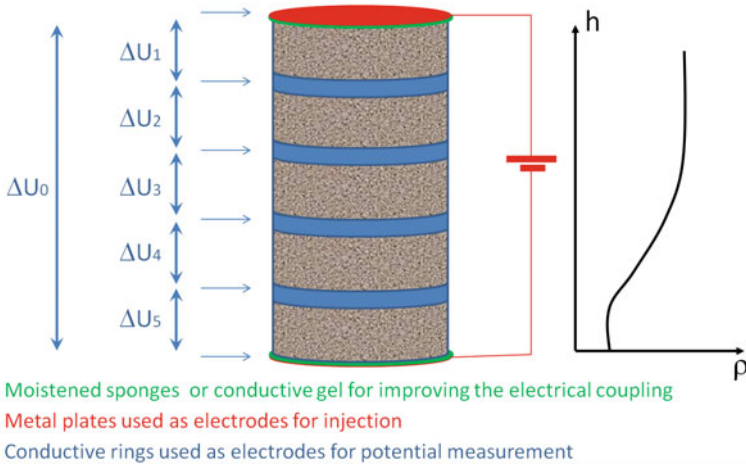


**Fig. 24.3** The setup of using resistivity to determine the moisture profile in a core

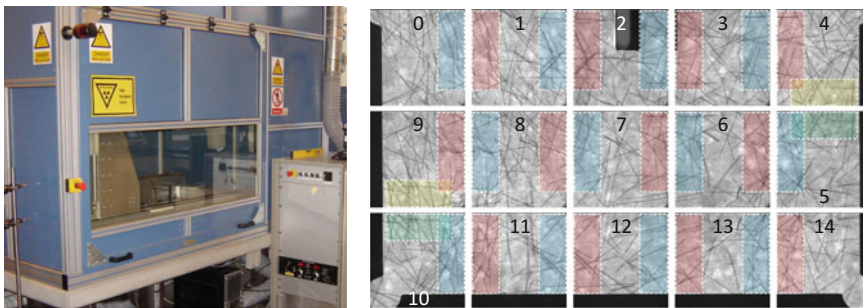


**Fig. 24.4** X-ray attenuation equipment (left) and an example (right) of 15 summed images making up a single measurement, with overlapping regions used for local normalization indicated, Pease et al. (2012)

X-ray camera captured images of 15 locations, providing data from an 80 mm × 55 mm region from the WST specimens. The measured region was centred horizontally with the notch and vertically the measurement area began approximately 5 mm above the specimen bottom. At each measurement location a total integration time of 60 s (60 images with 1 s exposure time) were captured and summed. Figure 24.4 shows typical X-ray attenuation images from the 15 measurement locations. Steel fibres can be clearly seen. The black areas on the perimeter of the measurement area and at the notch are caused by a 6 mm thick steel shield.

By means of an example, contour plots illustrating the moisture content distribution in the 50 mm thick WST specimens are shown in Figs. 24.5. The contour plots are determined from X-ray attenuation measurements calculated after various

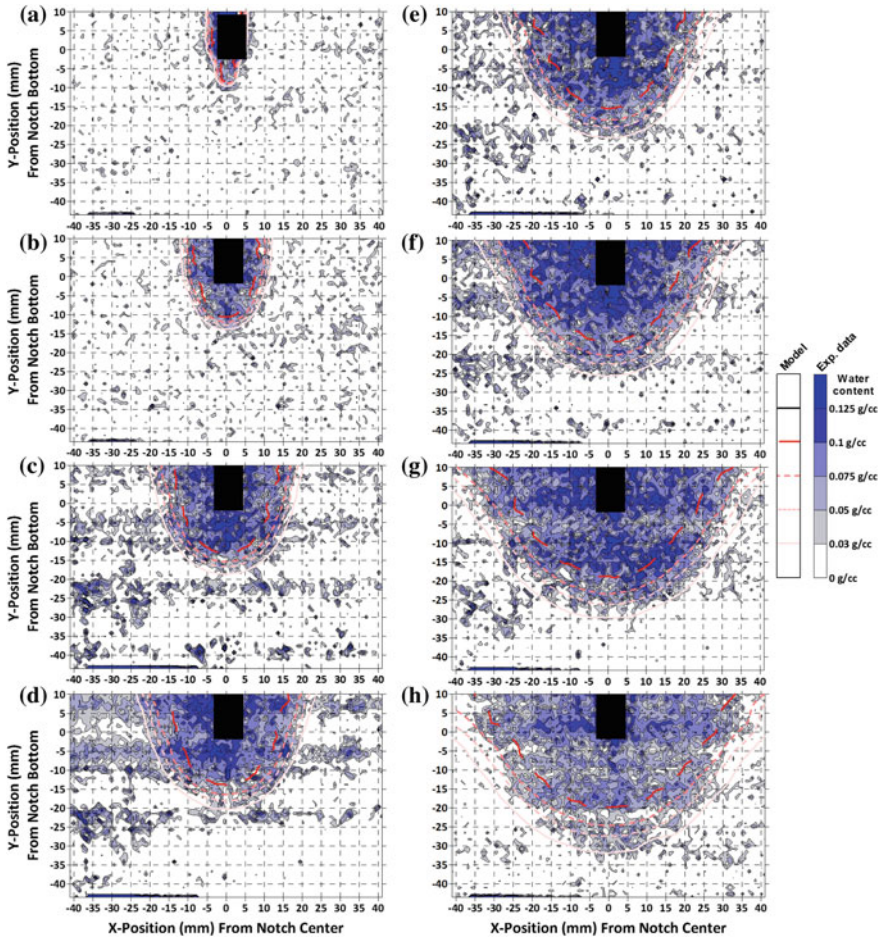


**Fig. 24.5** Experimental (blue) and modelled (red) ingress results for peak load WST specimen after **a** 3, **b** 30 min, **c** 1.5, **d** 2, **e** 3, **f** 4, **g** 6, and **h** 7 h of exposure to liquid water in the 6 × 12 mm notch (black), Pease et al. (2012)

times of exposure to liquid water to the loaded/cracked SFRC WST specimens. The black boxes on the contour plots identify the location of the notch and a steel shield that was used to cover the notch. The steel shield causes a small area near the notch to be incalculable due to the intense attenuation provided by 6 mm of steel plus 50 mm of concrete. An additional artefact in the contour plots is the false indication of water. In nearly all contour plots, there are at least small areas where moisture is indicated, but likely not actually present.

### 24.6 Application Example—Cast-in Tubes for RH-Probes from the Sides

Hedenblad (1993) determined RH-profiles in concrete specimens during five years by measuring RH in a series of cast-in plastic tubes perpendicular to the moisture flow direction, see Fig. 24.6. Only the end of the tubes was opened to the concrete.

Because of the fairly large diameter of the tubes the distribution close the top and bottom surfaces could not be determined.

### 24.7 Application Example—Ultrasound Transmission in ASR-Cracked Concrete

An ultrasound transmitter (T) and a receiver (R) was placed on each side of an ASR-cracked concrete beam, see Fig. 24.7, during an experiment where the beam was in contact with water at one end.

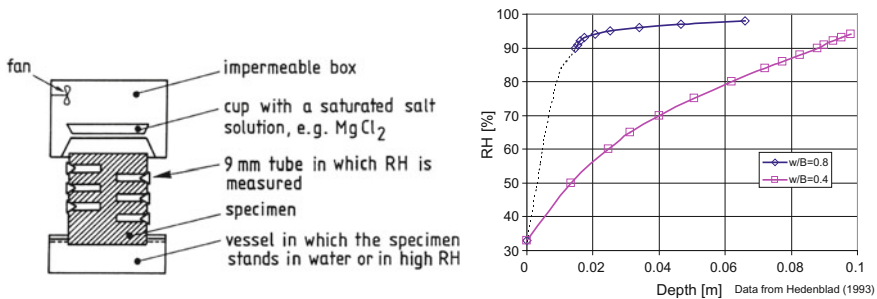


Fig. 24.6 The experimental arrangement (left) by Hedenblad (1993) with six horizontal tubes for determining the vertical RH-profile. RH-profiles for two concretes (right)



Fig. 24.7 Measurement setup using direct transmission of ultrasound (left) in several positions of an 80 × 20 × 10 cm large, ASR-cracked concrete beam (right) in contact with water at the left end surface, McNair (2015)

After 2 weeks											
Water	534	186	0	-89	92	181	116	-114	0	104	101
	477	285	178	78	85	0	195	405	103	109	0
	785	537	534	244	89	381	204	103	246	82	0

After 7 weeks											
Water	748	391	372	92	92	89	0	-114*	-103*	0*	101*
	477	285	273	333	266	107	0	405*	103*	109*	0*
	785	628	639	523	279	381	100	103*	160*	167*	0*

After 13 weeks											
Water	748	390	372	190	190	281	116	-114	-103*	0*	101*
	477	285	273	425	364	220	195	296	103*	109*	0*
	785	822	748	523	381	601	204	103	160*	167*	0*

**Fig. 24.8** Ultrasound velocity changes after 2, 7 and 13 weeks of exposure to water at the left end of an ASR-cracked concrete beam, McNair (2015). (\*) marks a number based on a previous measurement

The water penetration in the horizontally oriented crack system could be followed in time with the ultrasound measurements, see Fig. 24.8.

# Chapter 25

## Moisture in a Substrate Before Surface Covering



Lars-Olof Nilsson

### 25.1 Background

A very common application of moisture measurements is to quantify the moisture conditions of a substrate before applying a surface cover. One example is when flooring materials are to be attached to a concrete floor. Another example is when ceramic tiles are to be put at a floor or a wall. A third example is when wooden windows are to be painted.

The moisture measurement is done before the surface cover is applied. That means that the moisture distribution in the substrate will change after applying the surface cover. The requirements for accepting a certain level of moisture at the occasion of the measurement are very different for different applications and very different in different countries for the same application. The requirements are usually set to what will happen after the redistribution of the remaining moisture in the substrate.

The principle of the measuring situation before applying a surface cover and the following moisture redistribution is shown in Fig. 25.1.

The substrate is usually dried to some extent before the cover is to be done. Consequently, the surface of the substrate is drier than the rest of the substrate, cf. the left picture in Fig. 25.1. The substrate may have had some drying as well from the other surface. In some cases there is a moisture flux to the other surface and this is wetter than the rest of the substrate.

After the moisture measurement is done, and the surface cover is applied, the remaining moisture will redistribute to a moisture distribution that us shown in

---

L.-O. Nilsson (✉)  
Lund University, Lund, Sweden  
e-mail: lars-olof.nilsson@byggtek.lth.se

L.-O. Nilsson  
Moistenginst AB, Trelleborg, Sweden

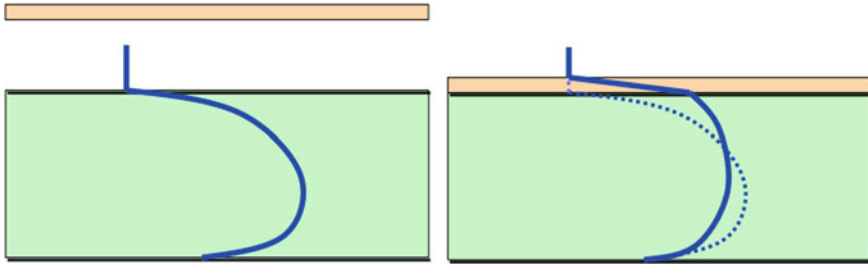


**Fig. 25.1** The moisture distribution, in principle, when a moisture measurement is done (left) before a surface cover is to be applied at a substrate and the redistribution (right) after the cover is applied

principle in the right part of Fig. 25.1. The surface of the substrate has become wetter and the moisture level has been somewhat reduced at larger depths in the substrate. This redistribution will depend on the type of materials in the substrate and the surface cover, the moisture level and distribution, the thicknesses of the two materials and the surrounding climatic conditions. Different approaches to this measuring situation are described here and commented upon.

## 25.2 Measuring the Whole Moisture Profile

The obviously correct approach is to determine the complete moisture distribution in the substrate and then analyse the redistribution that will occur after the surface cover is applied. This involves a number of moisture measurements at a series of depths in the substrate. The analysis of the redistribution is somewhat complicated since a correct analysis must consider that the moisture changes at some depths will follow scanning curves. That means that the analysis requires the sorption and scanning curves to be known.

If the substrate and/or the surface cover consist of more than one material there is no option today; the full moisture distribution has to be determined. The analysis must be done by considering the scanning-curves.

Such an approach was presented by Åhs (2011) when applying a surface cover and a self-levelling compound at a partly dried concrete floor slab. This approach could be used for any similar measuring situation before a surface cover is to be applied.

The moisture profiles before and after applying two surface covers are shown in principle in Fig. 25.2.

To be able to estimate what the final RH will be in the three-material combination, Åhs (2011) proposed a simple model to evaluate measurements at a series of depths in the substrate. The measurement situation is shown in Fig. 25.3.

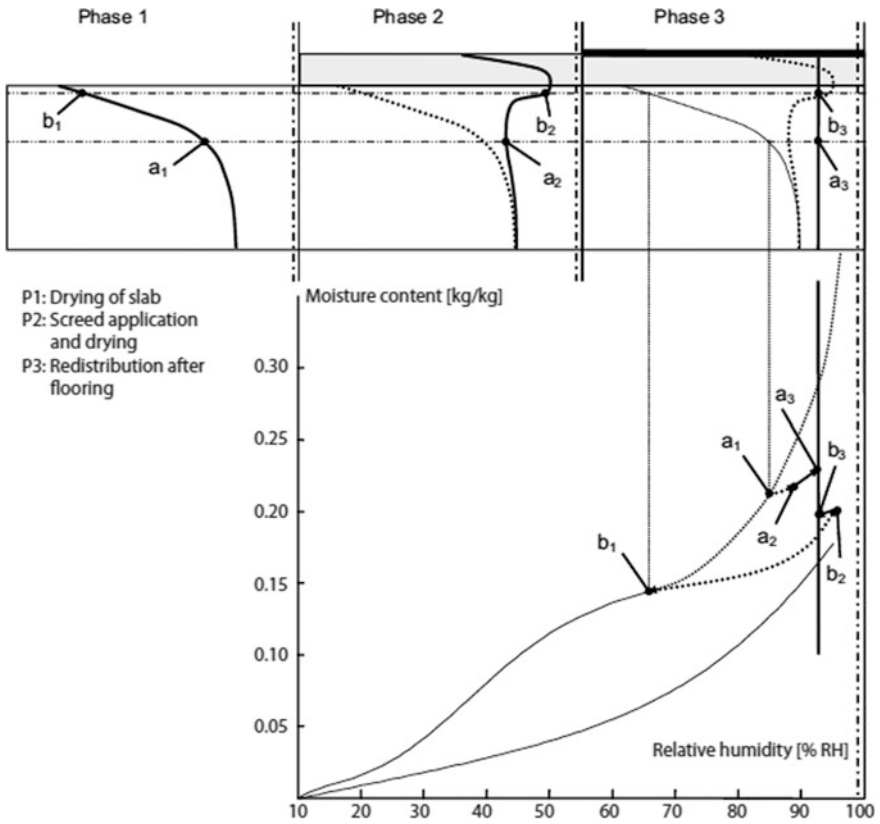


Fig. 25.2 RH-profiles before and after applying two surface covers at a substrate, Åhs (2011)

The measurements in Fig. 25.3, the slope of the sorption and scanning curves and a guessed final RH are used, Åhs (2011), to calculate a final RH from an equation

$$\varphi_{\infty} = \frac{\sum_{\Delta x_i} \overline{\varphi}_i \cdot d_i \cdot \left(\frac{dW_e}{d\varphi}\right)_i}{\sum_{\Delta x_i} d_i \cdot \left(\frac{dW_e}{d\varphi}\right)_i}$$

where  $\varphi_i$  is the measured RH at depth  $i$  in a sample with thickness  $d_i$ .

If the guessed RH differs too much from the calculated a new guess is done.

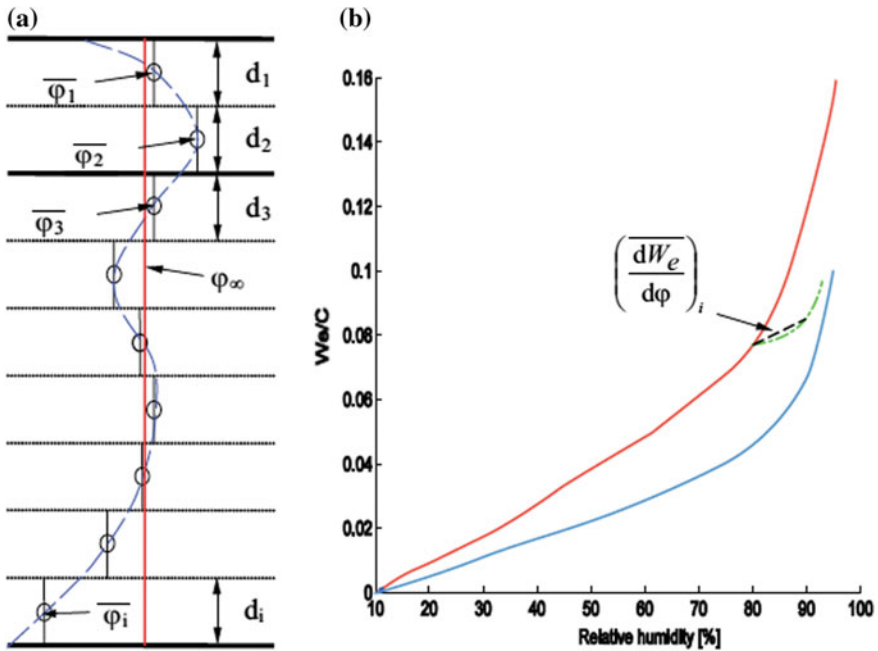


**Fig. 25.3** Examples of measured RH at several depths (left). The red vertical line is the expected final RH. The left figure shows the scanning curves in principle. Åhs (2011)

## 25.3 Measuring at a Characteristic Depth

A more simple way to perform an assessment of the moisture conditions after redistribution of the remaining moisture when the surface cover is applied is to measure moisture at only one depth, a “characteristic depth”. This depth is chosen in such a way that the moisture conditions at that depth when it is measured is equal to the moisture conditions in the surface of the substrate beneath an impermeable surface cover, cf. Fig. 25.4.

Nilsson (1979) showed that this characteristic depth  $x_1$  is approximately 40% of the thickness  $L$  of the substrate if the substrate has dried one-way and the surface cover is impermeable. This assessment was underestimating the characteristic depth since the effect of scanning curves in the surface region at depths smaller than  $x_1$  was not considered.

If the surface cover is more or less permeable, the drying requirements are changed so a larger RH is accepted at the characteristic depth.

This approach is of course simpler than the one where the full moisture profile is measured and evaluated. The drawback, however, is a much larger uncertainty in the evaluation. For permeable surface covers the resistance to moisture flow of both the cover and the substrate must be known to make a proper choice of the required dryness.

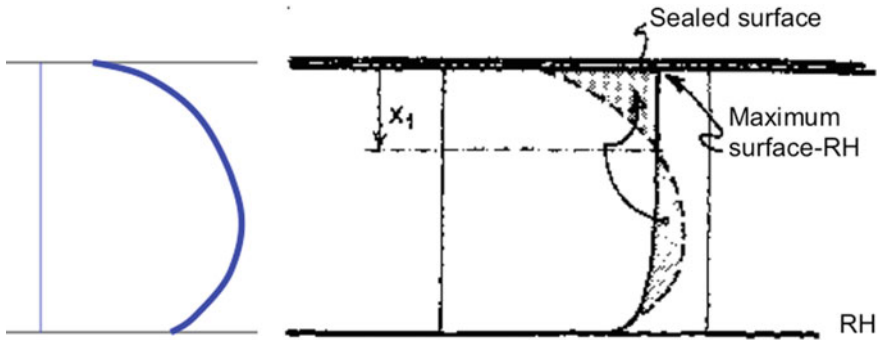


**Fig. 25.4** The moisture profile before and after redistribution beneath an impermeable surface cover with a characteristic depth  $x_1$  defined, Nilsson (1979)

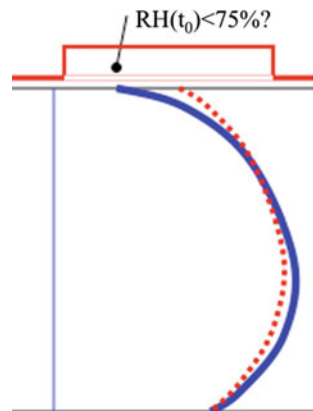
### 25.4 Measuring the Surface-RH Beneath an Applied Membrane

An alternative approach to assess whether a substrate is dry enough for surface covering is to seal the surface with a membrane and measure the RH beneath the membrane. Eventually, in theory the RH will reach the final, maximum level that can be expected but the complete redistribution will take such a long time, perhaps months or years that an evaluation must be done after a short time, before the redistribution has been completed.

An extrapolation of the redistribution could be done from the measured RH with time beneath the membrane but this never demonstrated to work and the uncertainty of such an approach could be large.

A British standard, BS 8203, gives a method to use this approach by measuring during 72 h, cf. Fig. 25.5. If the RH beneath the membrane is below 75% after 72 h of redistribution the substrate is regarded as dry enough.

**Fig. 25.5** The principle of the approach in British standard BS 8203 for assessing the dryness of a substrate



### 25.5 Measuring the Moisture Flux from the Surface

An American standard, ASTM F1869, gives a completely different approach to assess the dryness of a substrate before applying a surface cover. The flux of moisture from the dried surface is determined by placing a “cup” on top of the surface. Inside the cup there is a small container with a hygroscopic salt controlling the RH inside the cup. The salt absorb the moisture from the moisture flux and by determining the increase in weight of the salt during a certain time interval the flux of moisture can be evaluated. The principle is shown in Fig. 25.6.

ASTM F1869 gives acceptance limits for the flux of moisture from a damp substrate.

This approach is dubious since the flux of moisture from a substrate has very little do with the moisture conditions of the substrate. The temperature, the previous

**Fig. 25.6** The principle of ASTM F1869 for measuring the flux of moisture from a damp substrate

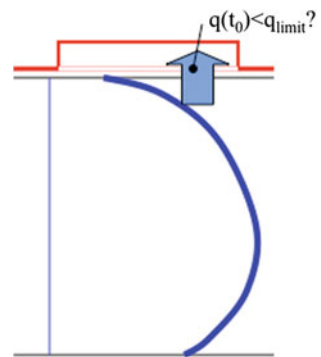
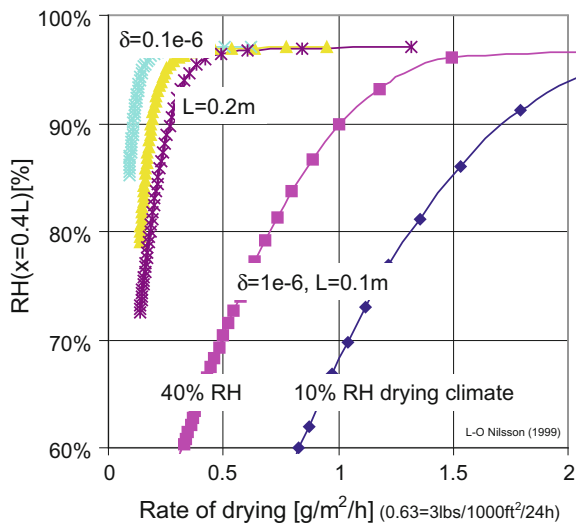


**Fig. 25.7** A comparison between the moisture level, characterized by the RH at a characteristic depth (vertical axis) and the moisture flux from the dried surface (horizontal axis), Nilsson (1999)



drying conditions and the resistance to moisture flow of the substrate are more important than the moisture level.

A comparison is made in Fig. 25.7 between the approach by using the characteristic depth and the approach by determining the flux of moisture from the surface of substrates with different moisture levels, cf. Fig. 25.7.

From Fig. 25.7 it is obvious that, for the same moisture level, the flux of moisture from a partly dried substrate can be very different depending on the previous drying climate (40 or 10% RH), the thickness of the substrate (0.1 or 0.2 m) or the moisture transport properties of the substrate ( $\delta = 0.1$  or  $1 \times 10^{-6} \text{ m}^2/\text{s}$ ).

# Chapter 26

## Monitoring, Remote Measurements



**Franck Agostini, Elisa Franzoni, Kurt Kielsgaard Hansen,  
Hemming Paroll and Lars-Olof Nilsson**

### 26.1 Introduction

A special group of applications is “monitoring” where a series of moisture measurements are to be done in the same position at a number of occasions. This kind of application requires certain measures to overcome some special challenges when measurements are done during a longer period of time. Examples of such challenges are

- robustness of equipment for in situ measurements (against weather exposure, construction work, etc.),
- climatic variations during measurements,
- long-term usage of a delicate measurement setup,
- less possibilities for repeated calibration,
- time lag between moisture variations and measurements,
- equipment/probes disturbing the moisture distribution to be measured,

---

F. Agostini  
École Centrale de Lille, Villeneuve-d’Ascq, France

E. Franzoni  
University of Bologna, Bologna, Italy

K. K. Hansen  
Technical University of Denmark, Kongens Lyngby, Denmark

H. Paroll  
Fuktcom AB, Espoo, Finland

L.-O. Nilsson (✉)  
Lund University, Lund, Sweden  
e-mail: lars-olof.nilsson@byggtek.lth.se

L.-O. Nilsson  
Moistenginst AB, Trelleborg, Sweden

- remote collection of data from the measurements,
- etc.

In the next sections a number of application examples are described where one or more of these challenges are handled in various ways.

## 26.2 Monitoring RH in Concrete Structures Under Temperature Variations

In concrete bridges the durability is influenced by concrete moisture conditions, excessive water and relative humidity in pores. An appropriate dryness of the substrate is needed when the waterproofing is laid on a new bridge or an existing bridge during repair work, Lunabba and Paroll (2011a). Monitoring is needed to follow the influence of the variation of relative humidity (RH) and temperature on bridge deck coating. Monitoring gives also a possibility for quality control of performed work in building new and repairing old bridges.

Monitoring of relative humidity and temperature has frequently been carried out in new and old concrete bridges to find out moisture behaviour and the influence of the variation of relative humidity (RH) and temperature in outdoor conditions in Finland, Paroll (1997), Paroll et al. (1998), Lunabba and Paroll (2011a). Previous manually made moisture and temperature measurements have given too little data to follow the moisture behaviour during daily and seasonal temperature variations and have therefore been replaced by continuous and periodic monitoring.

The results of monitoring during four months shown in Fig. 26.1 represent a typical bridge at the time of water proofing works. The water proofing installation starts when the surface is dry enough. After the waterproofing is laid, the relative humidity will rise again close to 100% RH particularly when the temperature is above +20 °C. This is due to the moisture transport from the deeper wet layer. At Kasarminkatu Bridge, Oulu, blistering of the sheet membrane started soon after the membrane was laid. The rise of temperature caused vapour pressure simultaneously as the bitumen glue of the membrane lost the bond. The temperature under the membrane is supposed to reach a level of +50 °C or more when the asphalt is laid or due to strong sun radiation. This will cause vapour pressure high enough to generate blisters.

Nowadays the concrete top surface will always be sealed by epoxy before the membrane is laid. Epoxy shall, according to the Finnish quality requirements, have bond strength of at least 1.5 N/mm<sup>2</sup>, which is strong enough to prevent blistering.

Temperature changes influence the relative humidity RH in material pores where the relative humidity change follows the temperature change. This is contrary to the room and outdoor air relative humidity where the change of the relative humidity is influenced by a temperature change in the opposite way, in other words, when the temperature is increasing the RH is decreasing and when the temperature is decreasing the RH is increasing. In a material this occurs due to the temperature

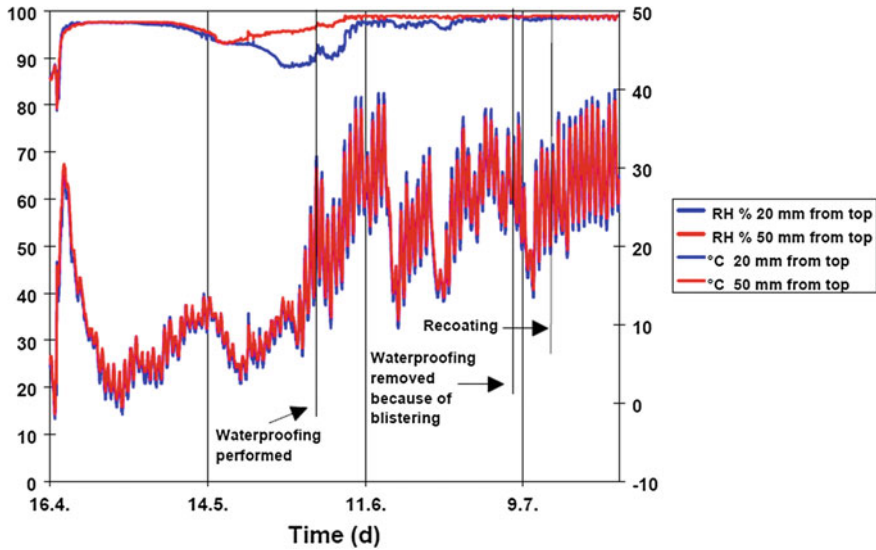


**Fig. 26.1** Relative humidity—temperature measurements on Kasarminkatu Bridge in Oulu 16.4.1997–27.7 1997 cast 17.4.1997. Monitoring started at casting of concrete using a resistive cast-in MS-sensor. The first temperature rise was caused by the hydration reaction between cement and water, Paroll (1997)

influenced vaporisation of the capillary water bound in the pores and the resulting water vapour transfer in capillary passages between the pores.

An example of how temperature changes influence the relative humidity RH, and causes the RH change to follow the temperature change, is presented in Fig. 26.2.

The criteria presented above, that the relative humidity change follows temperature change for correct relative humidity measurements in concrete, must be fulfilled by the used sensors. This can be checked from the received monitoring measurement data where the graph curvature trends must be like the curves presented in Fig. 26.1, where RH follows the temperature.

In carried out measurements this criteria is not always fulfilled. It has been observed that the relative humidity does not follow temperature changes due to insufficient temperature insulation of the sensor, Paroll (1997). This causes a standard error in relative humidity measurements.

An effective insulation has been achieved in carried out measurements by using cast-in resistive sensors in concrete, Paroll (1997), Paroll and Nykänen (1998) and Lunabba and Paroll (2011a). The cast-in sensor method using resistive sensors has given reliable measurement results during temperature variation.

This is due to the fact that temperature changes can cause temperature differences between the RH sensor and the concrete causing RH measurement errors, if the RH sensor is put in a drilled hole in concrete. There is no temperature difference between cast-in sensors and concrete.

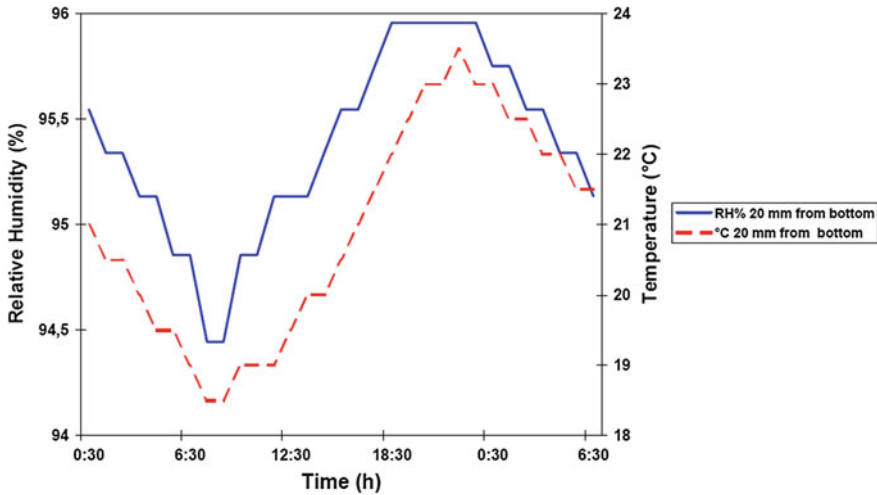


**Fig. 26.2** An example of the temperature change influence on the relative humidity RH that causes the RH to follow the temperature change. Direct measurement data from concrete bridge measurements using a resistive cast-in FuktCom MS-sensor. The graph is used as a proof that the measurement results fulfil the criteria demanding that the measured RH changes must follow the temperature changes. Thus the measurement data can be accepted, Paroll (1997)

An example of wrong RH measurement is presented in Fig. 26.3. Two capacitive AHEAD Hygrotemp II sensors were installed in two 50 mm deep, drilled holes in a concrete bridge. In the figure it is seen that that the RH curves do not follow the temperature curves due to insufficient heat insulation causing temperature differences between the sensor and the material, Paroll (1997). Instead the concrete RH curves behave like the ambient air RH curve also presented in the figure.

Another example of RH measurements in concrete using cast-in resistive RH-sensors and capacitive RH-sensors installed in drilled holes in a concrete bridge is presented in Fig. 26.4, Paroll (1997), Paroll et al. (1998).

Near the two cast-in resistive MS sensors (nowadays FuktCom's "Sahlén-sensor") at the depths of 20 and 50 mm two capacitive HMP 44 sensors were installed in two 50 mm deep-drilled holes. One of the capacitive sensors was installed according to the using the sensor manufacturer's 'sleeve and cover' insulation and the second sensor was insulated using insulating material wrapped around the sensor, cf. Fig. 26.5.

The measurements were made manually for 24 h to check the reliability of the sensor measurement curves. The measurement interval was 3 h. The results presented in Fig. 26.4 show that the RH curves for the capacitive sensors did not follow the temperature curves due to insufficient insulation. In this figure the RH curves from the cast-in resistive MS sensors follow the temperature but the RH curves from the capacitive Vaisala HMP 44 sensors in holes do not.

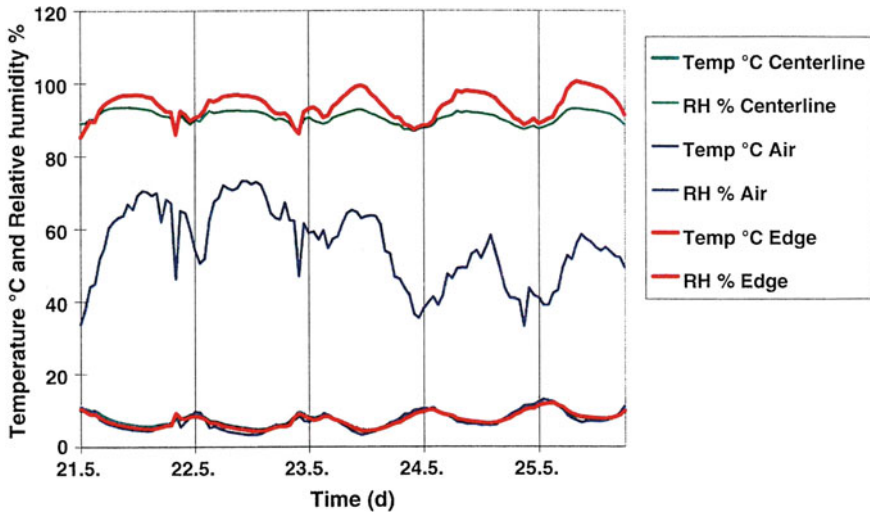


Fig. 26.3 Diurnal RH and temperature measurement curves from a concrete bridge using two capacitive AHEAD Hygrotemp II sensors in holes. The gridlines of the time-axis represent measurement at 4 p.m. Data from Paroll (1997)

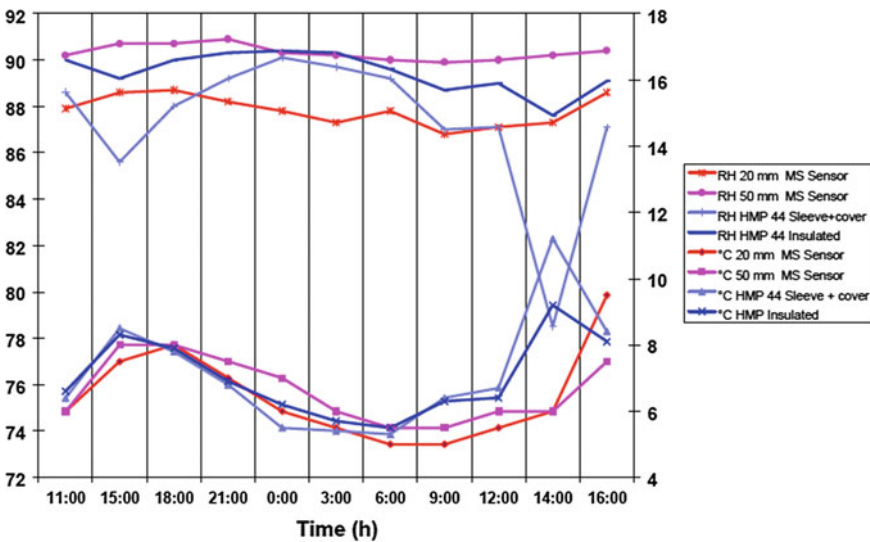


Fig. 26.4 Diurnal RH (left axis) and temperature (right axis) measurement curves for two capacitive HMP 44 sensors, in drilled holes, with different heat insulation and the corresponding cast-in resistive MS sensor curves on a concrete bridge. Only the cast-in sensors gave measurement results that filled the criteria that the RH must follow the temperature, Paroll (1997)



**Fig. 26.5** Heat insulation wrapped around the capacitive RH and temperature probe AHEAD Hygrotemp II. The orange box contains the 'sleeve and cover' insulation where the HMP 44 probe had been put in the drilled whole, Paroll (1997)

The two sensors types were cast-in or installed in a drilled hole at the depth of 50 mm from the surface. An additional MS-sensor was cast-in at 20 mm depth. At this 20 mm depth the RH was lower than at 50 mm depth indicating a dryer bridge deck surface region.

At about 14 o'clock (2 p.m.) the temperature curves for the capacitive sensors show a temperature increase due to a temporary occasional sunshine on the bridge surface on an otherwise cloudy day. This temperature increase from 7 to 11 °C causes a relative humidity decrease from 87 to 78% RH for the capacitive HMP 44 sensor with the 'sleeve and cover' insulation. RH from the resistive MS sensor did not react to this sudden temperature increase and gave the reliable measurement result 92% RH at the reliable temperature 6 °C. The RH difference (= error) was 14% between the MS and HMP 44 sensors and the temperature difference (= error) was 5 °C between these sensors (at about 14 o'clock or 2 p.m.).

The temperature curves from the capacitive sensors did not coincide with the ones from the cast-in sensors at 50 mm depth. The difference between the curves, indicating the magnitude of the error, varied during the whole measurement. This is due to the improper insulation of the capacitive sensors installed in drilled holes.

The results presented in Figs. 26.3 and 26.4 show that insufficient heat insulation can cause significant errors at temperature changes:

1. in relative humidity RH measurements, when the RH curves do not follow the temperature curves and
2. in temperature measurement, when the sensor and the concrete have different temperatures.

In Fig. 26.5 sensor measurement preparations are shown. The heat insulation is wrapped around the AHEAD Hygrotemp II sensor.

This insulation proved to be insufficient for the two types of capacitive sensors AHEAD Hygrotemp II and HMP 44. However, the insulation proved to be better than the ‘sleeve and cover’ isolation shown by the orange box on the photo.

Monitoring relative humidity using a cast-in sensor is recommended because the cast-in sensor is the only one where RH measurement results truly follow the concrete temperature, which is critical in order to obtain a correct RH-measurement. The criterion is that the relative humidity must follow the temperature. There have been problems using capacitive sensors due to difficulties in temperature insulation, Paroll (1997).

The installation of resistive cast-in Sahlén-sensors is easy to do and the sensors are connected to a logger with a wireless connection to a computer. Logger measurement interval can be adjusted from a few minutes to several hours. Monitoring can continue for years without much additional costs, because of wireless connection and no need for calibration of cast-in resistive sensors Lunabba and Paroll (2011b). Monitoring the relative humidity using cast-in resistive Sahlén-sensors is cheap and less time consuming than any other method, Aho (2012).

### 26.3 Embedded Probes—Disturbance of the Moisture Field

Certain types of large embedded probes for moisture measurements have a small sensor at one side of the probe. This is especially relevant for wire-less probes where the probe has a battery. In such a case it is important to consider the orientation of the probe so the sensor will be in contact with a representative part of the material. The problem is shown in principle in Fig. 26.6.

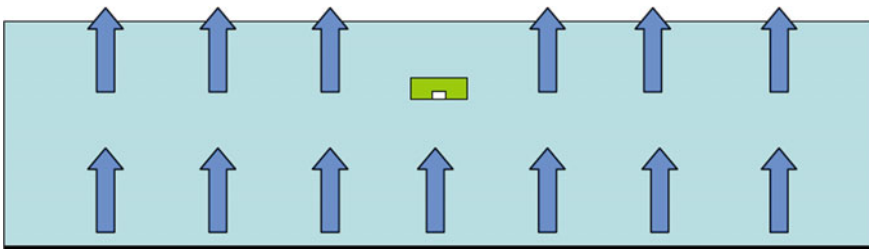


**Fig. 26.6** The problem, in principle, when an embedded probe has a sensor at one side (here at the bottom) and is disturbing the moisture flow in the structure

The embedded probe will disturb the moisture flow around itself. That could cause the moisture conditions to be different close to the sensor compared with the same location without the probe. The orientation of the sensor in the probe could give large systematic errors.

Nilsson and Fredlund (2009) quantified this systematic error for two types of probes and orientations, cf. Fig. 26.7. One of the probes is larger but has the sensor at the side. The other is smaller but has the sensor underneath.

Nilsson and Fredlund (2009) simulated the 3D moisture distribution in a 1 m<sup>2</sup> large slab without and with a probe in the centre and the sensor at a depth of 40 mm. The vertical RH-distributions through the sensor is shown in Fig. 26.8 and compared with the distribution in the same section without the sensor.

The RH at the location of the sensor differs some 10–11% RH for the larger width and some 6–7% RH for the smaller.

For the larger probe in Fig. 26.7, with the sensor at the centre of one of the vertical sides, the same quantification gave a systematic error of only some 0.4% RH.

The simulations also show that the position of the sensor in the vertical direction is extremely important where the moisture gradient is large. The systematic error due to a 1 mm too deep position gives a larger error than the effect of the embedded probe.

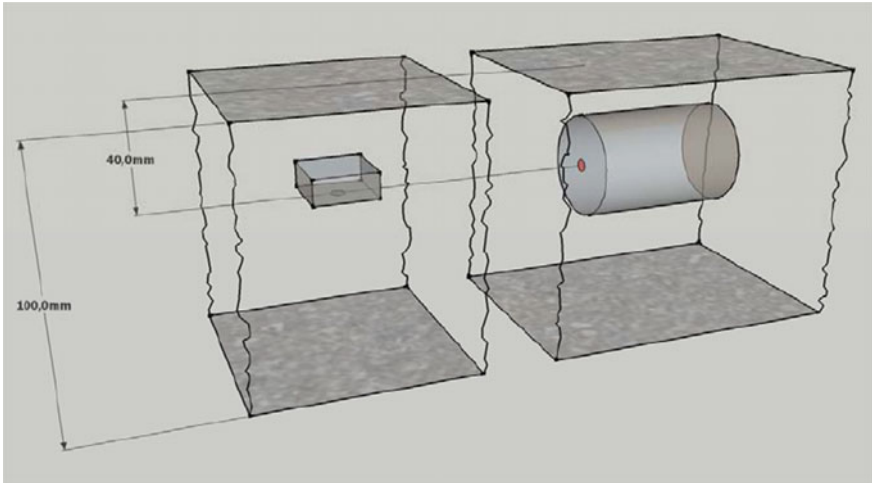


**Fig. 26.7** The two types of probes with their sensor locations (red spots) at a depth of 40 mm in a 100 mm thick concrete slab drying upwards, Nilsson and Fredlund (2009)

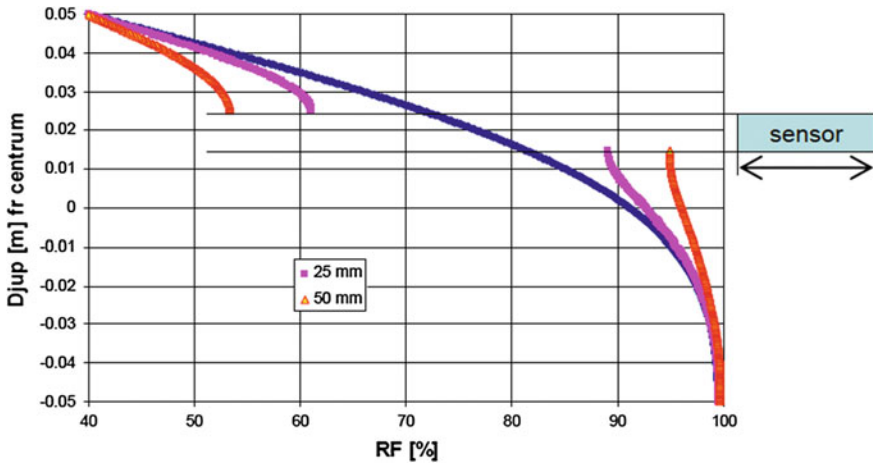


Fig. 26.8 The RH-distributions through the centre of the slab without and with the small probes with a sensor at the bottom. Two different probe widths

## 26.4 Monitoring Rising Damp in Historic Masonries

The application of systems for the removal, or at least mitigation, of rising damp in old brick and stone masonries is very frequent, but often encounters problems, giving unsatisfactory outcome Franzoni (2014). For this reason, an accurate assessment of the actual drying occurrence after the treatment is necessary and suitable techniques for monitoring moisture during several months are strongly needed. However, such measurement is extremely challenging, as any monitoring technique should meet many requirements Franzoni (2014):

- being quantitative and unambiguous;
- being accurate in a huge moisture amount range (from almost dry up to saturated materials);
- giving comparable results when measurement is repeated some months apart (especially in masonries built with highly heterogeneous materials);
- not altering the moisture amount and/or salt distribution in the zones under testing;
- giving results that are not influenced by climatic fluctuations (T, RH, wind, etc.); this can be achieved by measuring moisture deep in the wall and not on the surface only;
- being scarcely destructive (for heritage buildings);
- being cheap.

Several not destructive techniques have been proposed for this purpose, but some of them exhibited limits in accuracy and reliability in comparison with direct measurement by gravimetry, mainly due to calibration issues in heterogeneous materials. On the other hand, traditional oven drying technique performed on drilled

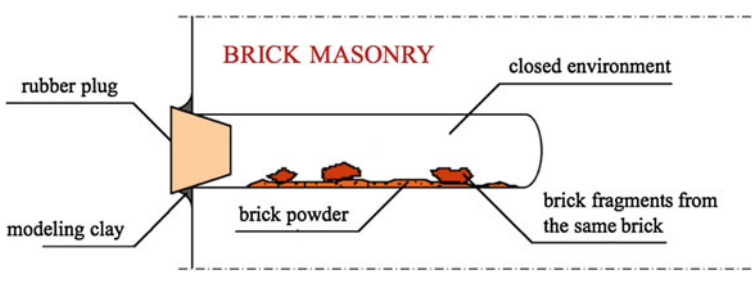


**Fig. 26.9** Cross-section of a permanent sampling point Sandrolini and Franzoni (2006)

powders exhibits some limitations, due to the fact that sampling points change every time and again the heterogeneity of materials raises some issues.

To overcome this problem, a procedure based on the gravimetric method, employing ‘permanent sampling points’, has been proposed Sandrolini and Franzoni (2006) and successfully applied to lab masonry models and historic buildings Franzoni et al. (2011); Franzoni et al. (2014a). The procedure consists in drilling holes in some selected bricks in the masonry, for about  $\frac{3}{4}$  of the length of the brick (holes are approximately 1.5 cm in diameter and 18 cm in depth), and inserting in each hole some small fragments taken from exactly the same brick where the hole was drilled (Fig. 26.9). The holes are henceforth sealed and the thermo-hygrometric equilibrium between the fragments and the surrounding brick is reached Sandrolini and Franzoni (2006), so the fragments can be extracted every 1–2 months for the moisture determination by oven drying and then re-inserted in the hole and re-used for additional measurements. This procedure assures an accurate and fully reliable moisture measurement whatever the single brick microstructure.

The same fragments can be also used (destructively, in this case) for soluble salts determination Franzoni et al. (2014b).

## 26.5 Embedded Wooden Rondella for Monitoring in Structures

One way to monitor moisture variations in structures is to embed a hygroscopic material and monitor the moisture content variations in that material. Commercialized equipment that uses this method is the “wooden rondella”, see Fig. 26.10, BMTinstruments (2016). The principle is hygrometric—the material of the rondella, a piece of Douglas fir plywood, is changing its moisture content when the RH of its surroundings changes.

The hygrometric principle makes it of course possible to follow the RH of the surroundings of the rondella. Consequently, the method could be used for all sorts



**Fig. 26.10** The wooden rondella for monitoring the moisture variations of its immediate surroundings, BMTInstruments (2016), by monitoring the resistance between the electrodes and the temperature. The electrodes are covered by epoxy coating

of structures, not only wooden structures. The translation of the resistance between the electrodes requires a temperature measurement to get the moisture content of the wooden piece in the rondella. The rondella is pretty large which means that it cannot follow very rapid changing moisture variations. The translation of the moisture contents of the rondella to the surrounding RH must also consider the hysteresis of the wooden piece; a moisture content corresponds to somewhat different RH depending on the moisture history.

## 26.6 Wireless in Situ Monitoring of Moisture Content in Timber

Monitoring moisture contents in timber is an example where fully commercialized systems for remote monitoring of moisture measurements is available, see e.g. Sandberg et al. (2011) and BMTInstruments (2016). The two-pin sensors and the gateways being used by Sandberg et al. (2011) are shown in Fig. 26.11.

The wireless “sensor” includes two screws or nails for measuring resistivity. These screws or nails can be directly used as a two-pin resistance sensor or just for attaching the “sensor” to the structure. An RH-sensor and a temperature sensor are also included, together with a battery and electronics. The “sensor” is connected to the gateway with an antenna, seen in Fig. 26.11.



**Fig. 26.11** The wireless sensors (left), Safety express (2016), and the gateway (right) (photo: L-O Nilsson) used by Sandberg et al. (2011)

The “sensor” can instead be connected with wires to another two-pin sensor in the neighbourhood as shown in Fig. 26.12.

The system for distribution of data is shown in Fig. 26.13. BMTinstruments (2016) uses a similar system.

After two years experience with this system Sandberg et al. (2011) concluded that relative humidity could be measured between 10 and 90%  $\pm$  2.5% and temperature could be measured with an accuracy of  $\pm$ 0.5 °C at 25 °C. The moisture content at different depths in timber structures could be measured between 8% and fibre saturation point (FSP) with an accuracy of  $\pm$ 1%. The sensors were “easy to set up and build in, some problems with the operation of the devices and the need for restarts after power failures; the effective range from the gateway to the sensors depends on the individual building structure”.



**Fig. 26.12** Five wireless sensors, protected against rain and direct sunlight, each connected to a two-pin sensor or a surface sensor (top right) (photo: L-O Nilsson)

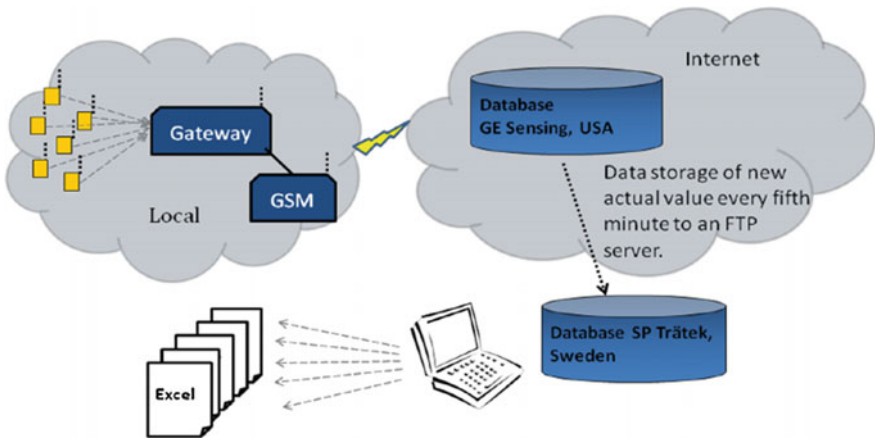


**Fig. 26.13** The system for distribution of data from the wireless sensors and the gateway by GSM connected to Internet, Sandberg et al. (2011)

# Chapter 27

## Heterogeneous Materials



Lars-Olof Nilsson and Elisa Franzoni

Measuring moisture in heterogeneous materials in a specimen or in a structure is a delicate task for several reasons. Examples of materials where this is relevant are e.g. bricks, concrete, (historic) masonry, etc.

The moisture content of a small sample of a material that is heterogeneous at a large scale has a very large scatter. Reducing this scatter requires special techniques.

Many materials are heterogeneous in such a way that the composition varies randomly from point to point at every scale. The moisture content of such a material, in one point, is not relevant for all other points. Historic masonry, brick masonry and ceramic bricks are good examples of such materials.

Some materials are heterogeneous in a systematic and continuous way, like concrete in a slab where separation has occurred. Here the moisture contents in different locations within a structure are not comparable.

A very good alternative in cases like this is to use hygrometric methods or pressure methods, i.e. to determine the relative humidity RH or pore water pressure on site or RH on samples. RH and pore water pressure are comparable also in heterogeneous materials. These techniques, for various applications are described in previous sections.

To measure moisture contents of heterogeneous materials, however, requires special considerations. Some possibilities are described in the following sections.

---

L.-O. Nilsson (✉)  
Lund University, Lund, Sweden  
e-mail: lars-olof.nilsson@byggttek.lth.se

L.-O. Nilsson  
Moistenginst AB, Trelleborg, Sweden

E. Franzoni  
University of Bologna, Bologna, Italy

© RILEM 2018

L.-O. Nilsson (ed.), *Methods of Measuring Moisture in Building Materials and Structures*, RILEM State-of-the-Art Reports 26,  
[https://doi.org/10.1007/978-3-319-74231-1\\_27](https://doi.org/10.1007/978-3-319-74231-1_27)

251

### 27.1 Historic Masonry

Moisture measurement in old masonries raises additional problems connected to the heterogeneity of historical building materials (fired clay bricks, stones, etc.). Even adjacent bricks or stone ashlar may exhibit extremely different mass transport properties due to their far different porosity and pore size distribution. In Fig. 27.1, the pore size distributions of nine brick samples from a single masonry in the SS. Crocefisso Church in the Monumental Cemetery of Ravenna (1817) are reported as an example (Sandrolini et al. 2006). Their impressive difference is due to the pre-industrial bricks technology, involving variable firing temperatures. Significant microstructural heterogeneity may be found also in stone ashlar, due to their different location in the quarries, different sedimentary members, etc.

Due to this heterogeneity, calibration should be theoretically performed for each single brick element or stone ashlar, which of course would cancel the advantages of non-destructive survey. In any case, a significant number of samples should be considered for a suitable calibration.

When monitoring of historic masonry is carried out, the measurement of moisture always in the same points is highly recommendable.

The degree of capillary saturation could be a useful tool for measuring moisture in masonry, see the next section.

### 27.2 Degree of Capillary Saturation

The degree of capillary saturation is an excellent tool when measuring moisture content profiles of structures or specimens of heterogeneous materials like concrete with large aggregate and masonry.

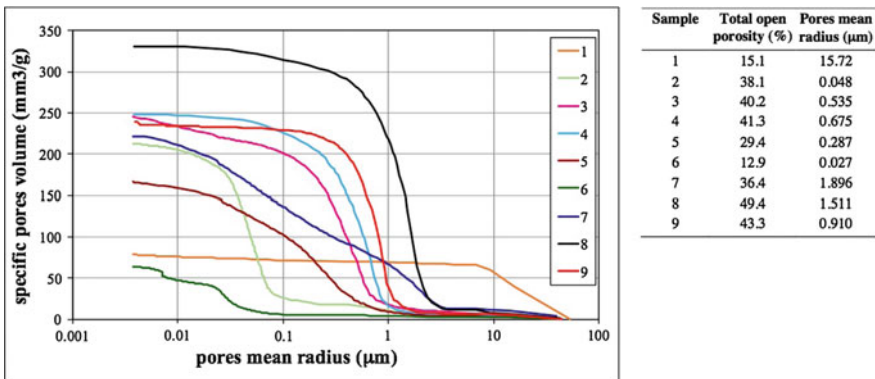


Fig. 27.1 Pore size distribution of some brick samples from the SS. Crocefisso church in Ravenna, 1817 (Sandrolini et al. 2006)

### 27.2.1 *Uncertainty Due to Sample Inhomogeneity*

If a composite material consists of a mix of a porous part that can contain moisture and a non-porous part that has no moisture content, the determination of the moisture ratio of such a material depends on the representativity of the sample taken. With small samples from a material with large non-porous parts the representativity might be extremely bad. An obvious example is a small sample from a concrete with large aggregate particles.

The error  $E$  of the representativity can be expressed by

$$E = \Delta m_{\text{dry}} / m_{\text{dry}} (-) \quad (27.2.1)$$

where  $m_{\text{dry}}$  is the dry weight of a perfectly representative sample and  $\Delta m_{\text{dry}}$  is the weight of the “additional” amount of non-porous parts making the sample non-representative.

The moisture ratio  $u$  of such a sample would be

$$(m_{\text{wet}} - m_{\text{dry}}) / (m_{\text{dry}} + \Delta m_{\text{dry}}) \quad (27.2.2)$$

which is equal to

$$u \cdot (m_{\text{wet}} - m_{\text{dry}}) / (m_{\text{dry}}(1 + E)) = u_0 / (1 + E) \quad (27.2.3)$$

where  $u_0$  is the moisture ratio of a perfectly representative sample. The error in the moisture ratio is a factor of  $1/(1 + E)$ .

The error is of course smaller the larger sample (larger  $m_{\text{dry}}$ ) that is taken. To overcome the drawback when it is essential to take small samples from a heterogeneous material the degree of capillary saturation can be determined.

### 27.2.2 *The Principles of the Degree of Capillary Saturation*

The principle of determining the degree of capillary saturation DCS is to measure the moisture ratio of the same (small) sample twice, before and after the sample has been capillary saturated. Since the capillary saturation is only saturating the porous parts of the sample the effect of the error in the representativity can be significantly reduced.

The moisture ratio  $u_{\text{sat}}$  of the capillary saturated sample will be

$$\begin{aligned} u_{\text{sat}} &= (m_{\text{sat}} - m_{\text{dry}}) / (m_{\text{dry}} + \Delta m_{\text{dry}}) = (m_{\text{sat}} - m_{\text{dry}}) / (m_{\text{dry}}(1 + E)) \\ &= u_{\text{sat},0} / (1 + E) \end{aligned} \quad (27.2.4)$$

where  $m_{\text{sat}}$  is the weight of the capillary saturated sample.

By dividing the two moisture ratios with each other one gets the degree of capillary saturation

$$DCS = u/u_{\text{sat}} = u_0/u_{\text{sat},0} \quad (27.2.5)$$

and the error is gone!

The two measurements of  $u$  and  $u_{\text{sat}}$  are ordinary gravimetric measurements. The capillary saturation process, however, is what is new. The process used by Hedenblad and Nilsson (1985) was this:

1. After determining the initial wet weight, the sample is put in contact with a water table in a container in such a way that air can escape from the sample when it is sucking water.
2. Evaporation is prevented by a putting a lid on top of the container, preferably a transparent glass lid so the samples can be observed.
3. Capillary saturation is assumed to have been reached when the top surface of the samples visibly turned dark. Alternatively, the weight of the samples can be monitored till weight gain is slow.
4. When the samples are capillary saturated, “loose” water at the surfaces of the sample has to be removed, e.g. with a wet cloth.
5. The weight of the capillary saturated sample is determined.
6. The weight after drying is determined.
7. DCS is calculated, from Eq. (27.2.5).

The definition of the point of capillary saturation is of course somewhat uncertain. The colour change and weight monitoring should ensure that the knick-point has been reached. A longer capillary suction time than that will add only little systematic error to the measurement.

In the capillary absorption test, also after the water fringe has reached the top face of the specimen, the attainment of capillary saturation may require much longer time, as in the example below. According to EN 15801:2010 (Conservation of cultural property—Test methods—Determination of water absorption by capillarity), capillary saturation is attained when the difference between two successive weighings (24 h) is not greater than 1% of the mass of water absorbed by the specimen (Fig. 27.2).

Some application examples are shown in the next section.

### 27.2.3 Examples of Using DCS

DCS was used by Sandin (1973) for moisture profiles in a historic masonry wall in a church. The applications of DCS to concrete samples are described in detail by Hedenblad and Nilsson (1985). Examples of their measurements are shown in the next sections.

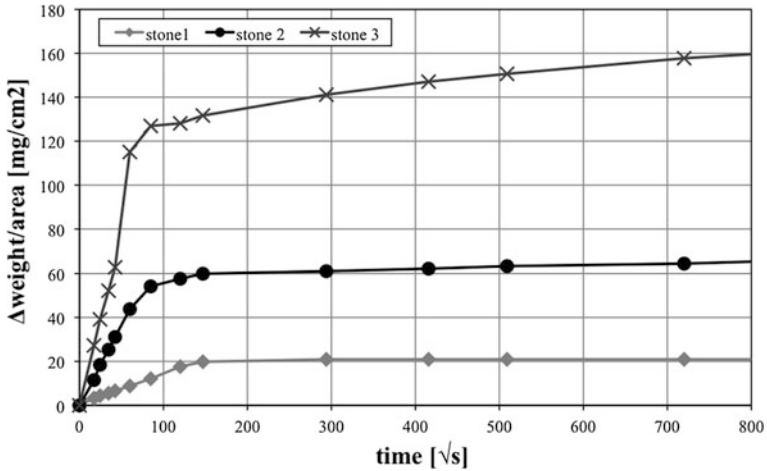


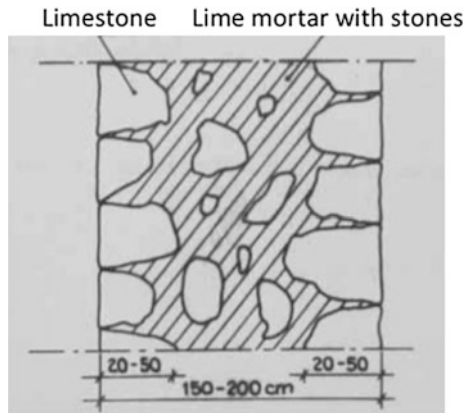
Fig. 27.2 Capillary absorption curves for three different kinds of stone (sandstone and pietra serena). Depending on the porosity of the material, capillary saturation is reached more or less gradually, Franzoni and Sassoni (2011)

27.2.3.1 DCS in a Historic Masonry

Sandin (1974) took moisture samples of lime mortar in a church wall, see Fig. 27.3. The samples contained different amount of smaller and larger limestone stones that were mixed with the mortar. The samples were taken from the left surface and up to 80 cm depth. The results are shown in Fig. 27.4.

The moisture ratio profile is not systematic and gives an impression of lower moisture content to the right. The degree of capillary saturation, however, shows that the wall is almost fully saturated;  $S_{cap}$  is close to 1.0.

Fig. 27.3 Vadstena church wall where Sandin (1974) took moisture samples



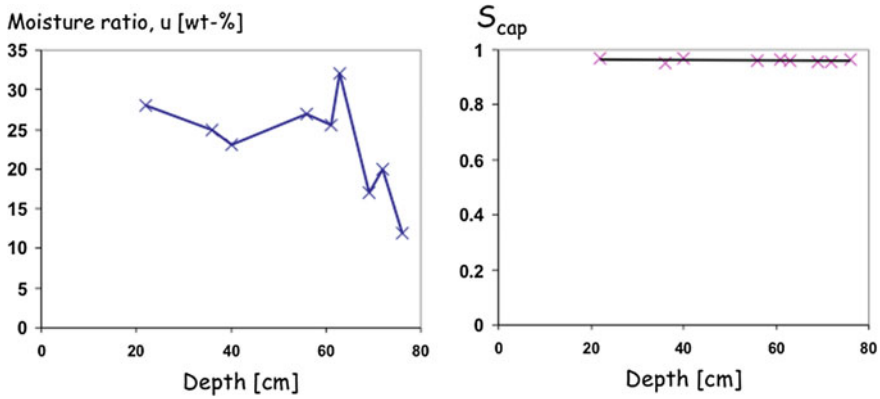


Fig. 27.4 Moisture profiles through a church masonry wall with lime binder: Moisture ratio (left) and degree of capillary saturation (right). Data from Sandin (1974)

**27.2.3.2 DCS in a Concrete Slab with Separation**

Hedenblad and Nilsson (1985) took samples from different heights in concrete cylinders that were cast and vibrated vertically, see Fig. 27.5, and cured under sealed conditions. The moisture contents and the DCS from different levels are shown in the figure.

As seen from Fig. 27.5 separation of the aggregate in the concrete gave a systematic moisture profile, from top to bottom. The DCS, however, is more or less uniform through the concrete cylinder, in spite of the separation with height.

Fig. 27.5 Moisture contents (u) and DCS from different levels in a concrete cylinder that was cast and vibrated vertically, Hedenblad and Nilsson (1985). Numbers are errors (%) from the mean value

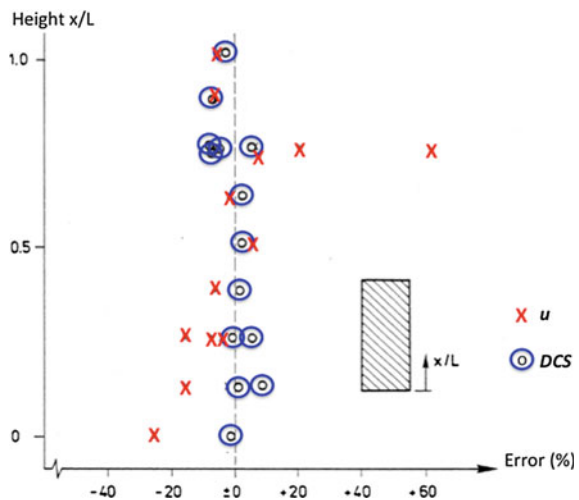
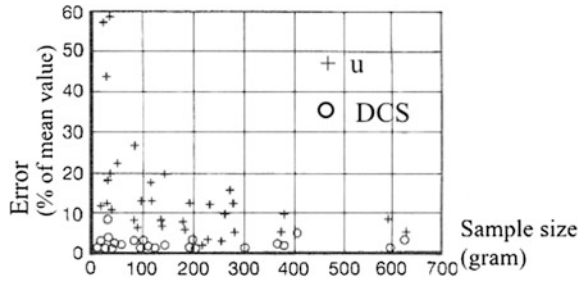


**Fig. 27.6** Deviations from the mean value of  $u$  and  $DCS$  values on samples from one concrete cylinder, Hedenblad and Nilsson (1985)



**27.2.3.3 DCS in Small Concrete Samples**

Hedenblad and Nilsson (1985) measured the moisture content  $u$  and the degree of capillary saturation  $DCS$  on small and larger samples of concretes with different aggregate size. All samples were from the same concrete cylinder that had been cured under sealed conditions. The sample size varied from below 20 grams up to some 600 grams. An example of results is shown in Fig. 27.6. The “error” is the deviation from the mean value of the moisture content of the large cylinder.

The errors in the moisture content measurements could be up to 60%., for the small samples. Even for the very small samples the error in the  $DCS$  measurements was less than 10%.

**27.3 Moisture Content of a Heterogeneous Sample Versus a Relevant Parameter**

When using the degree of saturation of a sample of heterogeneous materials the moisture content is related to the moisture content at capillary saturation. In the same way the moisture content of such a sample could be related to another relevant parameter that varies in the same way as the moisture content in the heterogeneous material.

In cementitious materials like concrete or mortar the moisture content of a small sample has a very large scatter, larger the smaller the sample and larger the aggregate. When the aggregate is non-porous and do not contain any moisture, the moisture content varies in the same way as the binder content at least if the degree of reaction of the binder is constant. A component of the binder could be a relevant parameter to relate the moisture content to.

In many cases  $CaO$  has been used as such a parameter for Portland cement-based materials, e.g. Åhs (2011). This works only if the aggregate does not contain any limestone.

# **Part III**

## **Conclusions**

# Chapter 28

## Conclusions



Lars-Olof Nilsson

From the description in the previous chapters of the state-of-art of methods for measuring moisture in building materials these conclusions can be drawn:

- There are many techniques to determine moisture conditions in materials and structures, suitable for various applications.
- There are no methods that are better than others in absolute terms, but for any application the best method/methods must be selected on the basis of the material, the purpose of the analysis and the resolution required. Such a selection requires deep understanding of moisture in materials and structures and of the advantages and limitations of each individual technique to measure the moisture content MC or the relative humidity RH.
- There is no non-destructive method to measure the absolute moisture content in a series of points in a material, from the surface, without extensive calibration.
- Surface-NMR can, with extensive calibration, but to a very limited depth.
- Microwave reflection can, to larger depths but with lower resolution in depth.
- All other methods require drilling, coring, sampling, inserting probes or the sides being available.
- All methods are “indirect”, except the gravimetric and chemical methods; they require calibration.
- All indirect methods to determine absolute moisture content require calibration for each new material!
- Measuring relative moisture contents, i.e. “moisture mapping”, can be done with several techniques in an excellent way without the need for calibration.

---

L.-O. Nilsson (✉)  
Lund University, Lund, Sweden  
e-mail: lars-olof.nilsson@byggtek.lth.se

L.-O. Nilsson  
Moistenginst AB, Trelleborg, Sweden

- Hygroscopic methods to determine the state of moisture do not require calibration for each material but the equipment requires calibration before and after measurements.

# References

- Abbas A, Carcasses M, Ollivier J-P (1999) Gas permeability of concrete in relation to its degree of saturation, *Materials and Structures/Matériaux et Constructions*, vol. 32, Jan–Feb 1999, pp 3–8. 1359-5997/99, © RILEM SCIENTIFIC REPORTS
- Abragam A (1996) *Principles of nuclear magnetism*. Oxford Science Publications University Press, Oxford
- AFREM (1996) *Durabilité des bétons, Essai de perméabilité aux gaz du béton durci: mode opératoire recommandé* (in French), 1996
- Ahlgren (1972) *Moisture fixation in porous building materials* (in Swedish). Ph.D. thesis report 36, Building Technology, Lund Institute of Technology, Sweden
- Aho T (ed) (2012) *Sustainable rehabilitation of existing civil engineering and building structures. Evaluation report. Inspection and monitoring. Report nr 131*. Department of mechanical engineering, University of Oulu, Oulu, p 103
- Aho T, Lunabba T, Wuorenjuuri J, Häkkinen J (2012) *Sustainable rehabilitation of existing civil engineering and building structure, evaluation report nr131*. University of Oulu, Oulu, 103p
- Åhs M (2011) *Redistribution of moisture and ions in cement based materials*. Ph.D.-thesis TVBM-1028, Division of Building Materials, Lund University, Lund
- Alani AM, Aboutalebi M, Kilic G (2012) Applications of ground penetrating radar (GPR) in bridge deck monitoring and assessment. *J Appl Geophys* 97:45–54
- Alfasensor (2016) <http://www.alfasensor.com/default.asp?Language=en>
- Alkan S, Zhang YL, Lam F (2007) Moisture distribution changes and wet-wood behavior in subalpine fir wood during drying using high X-ray energy industrial CT scanner. *Drying Technol* 25(3):483–488
- Andersen A (1996) *Moisture and chloride profiles in a column in the Vejle fjord bridge after 18 years of exposure to marine environment, work report May 1996*. Department of Building materials, Chalmers University of technology, Gothenburg
- Andrade C, Martinez I (2009) Embedded sensors for the monitoring of corrosion parameters in concrete structures. In: *NDTCE'09, Non-destructive testing in civil engineering*, Nantes, France, June 30th–July 3rd, 2009, p 8
- Antón C, Climent MA, de Vera G, Sánchez I, Andrade C (2013) An improved procedure for obtaining and maintaining well characterized partial water saturation states on concrete samples to be used for mass transport tests. *Mater Struct* 46:1389–1400
- Antons, U (2017) *Untersuchungen zur Dauerhaftigkeit hydrophober Schichten im Beton mittels NMR*, doctoralthesis. RWTH Aachen, Germany
- Antons U, Raupach M, Weichold O (2014) Einsatzmöglichkeiten der NMR-MOUSE® in der Bauforschung- aktueller Stand der Arbeiten am ibac. In: Wittmann F (ed) *Restoration of buildings and monuments*, vol. 20, No. 5. Freiburg 2014, S 299–310
- Archie G (1942) The electrical resistivity log as an aid in determining some reservoir characteristics. *Trans Am Inst Min Metall Eng* 146(1942):54–62
- ASTM E 748-02 (2002) *Standard practices for thermal neutron radiography of materials* [S]

- ASTM D2216–10 (2010) Standard test methods for laboratory determination of water (Moisture) content of soil and rock by mass
- ASTM E104-02 (2012) Standard practice for maintaining constant relative humidity by means of aqueous solutions, ASTM International, 100 Barr Harbor Drive, PO Box C700, West Conshohocken, PA 19428-2959. United States
- ASTM F1869 - 16a. Standard test method for measuring moisture vapor emission rate of concrete subfloor using anhydrous calcium chloride. ASTM International
- Baker PH, Bailly D, Campbell M, Galbraith GH, McLean RC, Poffa N, Sanders CH (2007) The application of X-ray absorption to building moisture transport studies. *Measurement* 40: 951–959
- Baron JP, Tran NL (1977) Méthodes de mesure et de contrôle des teneurs en eau des matériaux dans les LPC. *Bulletin de Liaison des laboratoires des Ponts et Chaussées* 87:85–96
- Basheer PAM, Nolan U (2001) Near-surface moisture gradients and in situ permeation tests. *Constr Build Mater* 15(2001):105–114
- Basset J, Denney RC, Jeffery GH, Mendham J (1978) *Vogel's textbook of quantitative inorganic analysis*. Longman, London
- Bechkit MA, Flageul S, Guerin R, Tabbagh A (2014) Monitoring soil water content by vertical temperature variations. *Groundwater* 52(4):566–572
- Bentz D, Hansen KK (2000) Preliminary observations of water movement in cement pastes during curing using X-ray absorption. *Cem Concr Res* 30:1157–1168
- Berger H (1966) Characteristics of a thermal neutron television imaging system. *Mater Eval* 24(9):475–481
- Beziat A (1987) Etude expérimentale de la conductivité thermique de matériaux argileux hautement compacts. Contribution à l'étude du stockage de déchets radioactifs. Thèse de doctorat de l'université d'Orléans
- Binda L, Colla C, Forde MC (1994) Identification of moisture capillarity in masonry using digital impulse radar. *Constr Build Mater* 8(2):101–107
- Binda L, Squarcina T, Van Hees R (1996) Determination of moisture content in masonry materials: calibration of some direct methods. In: *Proceedings of the international congress on deterioration and conservation of stone*, Berlin, 30 Sept–4 Oct 1996, pp 587–599
- Birchak JR, Gardner CG, Hipp JE, Victor JM (1974) High dielectric constant microwave probes for sensing soil moisture. *Proc IEEE* 62(1):93–98
- Blümich B (2009) NMR at low magnetic fields. *Chem Phys Letters* 4777:231–240
- Blümich B (2016) Mobile NMR: concepts and application. Available at <http://www.nmr-mouse.de/download/MobileNMRconcepts.pdf>. Accessed 18 Sept 2016
- Blümich B, Haber-Pohlmeier S (2010) “Handbook of mobile NMR”. Institute of technical and macromolecular chemistry, RWTH Aachen University, Aachen
- Blümich B, Kremer K (2006) “Mobile NMR zur Feuchtemessung”; Aedificatio Verlag; Berichtsband zum Workshop 2003, Innovative Feuchtemessung in Forschung und Praxis 1, pp 391–394
- Blümich B, Haber-Pohlmeier S, Zia W (2014) Compact NMR, de Gruyter, Berlin, Chapter 7: Porous Media and Section 8.1: Painted Walls and Stone
- BMT instruments (2016) [www.bmtinstruments.dk](http://www.bmtinstruments.dk)
- Borgia GC, Brown RJS, Fantazzini O (1998) Uniform-penalty inversion of multiexponential decay data. *J Magn Reson* 132:65–77
- Bower JH (1934) Comparative efficiencies of various dehydrating agents used for drying gases (a survey of commercial drying agents). *Bureau of Standards Journal of Research* 1934 (12):241–248
- Bracher DA, Garrett DA (1975) Abstract only. *Materials Evaluation*, 33: 47
- Bramshuber W, Rahimi A, Weise F (2011) Tiefenabhängige Feuchtemessung in Betonbauwerken - Vergleichende Untersuchungen mit der Multiring-Elektrode und dem Kernspinresonanz-Verfahren: Depth-Dependent Measurement of the moisture content in concrete structures—comparative investigations with the multiring electrode and the nuclear

- magnetic resonance spectroscopy. Aachen: Institut für Bauforschung, RWTH Aachen University, 2011. - Forschungsbericht Nr. F 974; Berlin: Bundesanstalt für Materialforschung und -prüfung, BAM, 2011, in German
- Brew DRM, De Beer FC, Radebe MJ, Nshimirimana R, McGlenn PJ, Aldridge LP, Payne TE (2009) Water transport through cement-based barriers—a preliminary study using neutron radiography and tomography. *Nucl Instrum Methods Phys Res A* 605(1/2):163–166
- Breyse D, Sirieux C, Lataste JF (2012) Quality of concrete condition assessment using several non destructive techniques. *Struct Infrastruct Eng* 8(6). <https://doi.org/10.1080/15732479.2010.505375>
- Bruker <http://www.bruker.com/products/mr/nmr/avance-iii-hd/overview.html>. Accessed 09 Oct 2013
- Brunauer S (1957) Some Aspects of the physics and chemistry of cement, Bulletin 80, of the Research Department of the Portland Cement Association, New York
- Brunauer S, Odler L, Yudenfreud M (1970) The new model of hardened Portland cement paste. *Highway Res Rec* 328:89–107
- Bruttel P, Schlink R (2006) Monograph on water determination by Karl Fischer Titration, Metrohm Ltd., CH-9101 Herisau, Switzerland
- BS 8203:2001 Code of practice for installation of resilient floor coverings. British Standard Institute
- Bucur V (2003) Nondestructive characterization and imaging of wood. Springer, Berlin, Springer Series in Wood Science, p 354
- Buettner M, Ramirez A, Daily W (1995a) Electrical resistance tomography for imaging concrete structures. In: Structural materials technology and NDT conference, San Diego (CA), 20–23 Feb, p 7
- Buettner M, Ramirez A, Daily W (1995b) Electrical resistance tomography for imaging the spatial distribution of moisture in pavement sections. In: Structural materials technology and NDT conference, San Diego (CA), 20–23 Feb, p 7
- Burlion N, Skoczylas F, Dubois T (2003) Induced anisotropic permeability due to drying of concrete. *Cem Concr Res* 33(5):679–687, May 2003, ISSN 0008-8846
- Campbell-Allen D, Thorne CP (1963) The thermal conductivity of concrete. *Mag Concr Res Cem Concr Assoc* 15:39–48
- Cano-Barrita PF, Marble AE, Balcom BJ, García JC, Masthikin IV, Thomas MDA, Bremner TW (2009) Embedded NMR sensors to monitor evaporable water loss caused by hydration and drying in Portland cement mortar. *Cem Concr Res* 39:324–328
- Carcassès M, Abbas A, Ollivier J-P, Verdier J (2002) An optimised preconditioning procedure for gas permeability measurement. *Mater Struct* 35:22–27
- Cardani G, Cantini L, Munda S, Zanzi L, Bonda L (2013) Non invasive measurements of moisture in full-scale stone and brick masonry models after simulated flooding: effectiveness of GPR. In: Büyükoztürk et al. (eds.) Non destructiv testing of material and structures, proceedings of NDTMS-2011, Istanbul (Turkey), Springer, Berlin, pp 1143–1150
- Carr HY, Purcell EM (1954) Effects of diffusion on the precession in nuclear magnetic resonance experiments. *Phy Rev* 94:630–638
- Casanova F, Perlo J, Blümich B (eds) (2011) Single-sided NMR. Springer, Berlin
- Chen W, Liu J, Brue F, Skoczylas F, Davy CA, Bourbon X, Talandier J (2012) Water retention and gas relative permeability of two industrial concretes. *Cem Concr Res* 42(7):1001–1013
- Chen XT, Caratini G, Davy CA, Troadec D, Skoczylas F (2013) Coupled transport and poro-mechanical properties of a heat-treated mortar under confinement. *Cem Concr Res* 49: 10–20, July 2013
- Choinska M, Khelidj A, Chatzigeorgiou G, Pijaudier-Cabot G (2007) Effects and interactions of temperature and stress-level related damage on permeability of concrete. *Cem Concr Res* 37(1):79–88

- Chouteau M, Beaulieu S, Fréchette V, Toe E (2002) Application de la tomographie de résistivité électrique aux infrastructures routières en béton, INFRA 2002, 25 au 27 novembre 2002, Montréal, Québec
- CIB W40 (2012) Heat, air and moisture transfer terminology. Parameters and concepts. de Freitas VP, Barreira E (eds) CIB – W040 heat and moisture transfer in buildings, CIB report 369
- Claissé PA, Ganjian E, Adham TA (2003) A vacuum-air permeability test for in situ assessment of cover concrete. *Cem Concr Res* 33(1):47–53
- Climent MA, de Vera G, López JF, Viqueira E, Andrade C (2002) A test method for measuring chloride diffusion coefficients through nonsaturated concrete. Part I. The instantaneous plane source diffusion case. *Cem Conc Res* 32(7):1113–1123
- Collier NC et al (2008) The influence of water removal techniques on the composition and microstructure of hardened cement pastes. *Cem Concr Res* 38:737–744
- Copeland LE, Hayes JC (1953) The determination of non-evaporable water in hardened Portland cement pastes, PCA, Bulletin 47
- Croney D, Coleman JD, Bridge PM (1952) The suction of moisture held in soil and other porous materials. Road research technical paper no. 24, Her Majesty's Stationery Office, London
- Dana E, Skoczylas F (2002) Experimental study of two-phase flow in three sandstones. II. Capillary pressure curve measurement and relative permeability pore space capillary models. *Int J Multiph Flow* 28(12):1965–1981
- Daniels DJ (ed) (2004) Ground Penetrating radar, 2nd edn. Institution of Electrical Engineers, London (UK), p 726
- Danvind J (2002) Measuring strain and moisture content in a cross section of drying wood using digital speckle photography and computerised X-ray tomography. In: Proceedings of 13th international symposium on nondestructive testing of wood, Berkley, California, 19–21 Aug 2002. Forest Products Society, Madison, Wisconsin
- Danvind J, Morén T (2004) Using X-ray CT-scanning for moisture and displacement measurements in knots and their surroundings. In: Proceedings of the 5th COST ACTION E15: advances in drying of wood, Athens, Greece, 22–24 April
- Dauberschmidt C, Sodeikat Ch, Schießl P, Gehlen Ch (2008) Monitoring von Verkehrsbauten - kontinuierliche Zustandserfassung zur Sicherstellung der Dauerhaftigkeit. In: Tiefbau; Heft 3/2008; Hrsg.: BG Bau - Baugenossenschaft der Bauwirtschaft; Erich Schmidt Verlag GmbH & Co, Berlin
- Davis JL, Chudobiak WJ (1975) In-situ meter for measuring relative permittivity of soils. *Geol Surv Can Pap* 75-1A:75–79
- Davis J, Wells P (1992) Computer tomography measurements on wood. *Ind Metrol* 2(3–4): 195–218
- De Beer FC, Le Roux JJ, Kearsley EP (2005) Testing the durability of concrete with neutron radiography. *Nucl Instrum Methods Phys Res A* 542:226–231
- Debye P (1929) Polar molecules. Dover, New York
- de Cano-Barrita JPF, Marble AE, Balcom BJ, García JC, Masthikin IV, Thomas MDA, Bremner TW (2009) Embedded NMR sensors to monitor evaporable water loss caused by hydration and drying in Portland cement mortar. *Cem Concr Res* 39:324–328
- de Loor GP (1968) Dielectric properties of heterogeneous mixtures containing water. *J Microwave Power* 3(2):67–73
- Denzel W (2015) Feuchte-Messung in Estrichschichten. DNS-Denzel, Börtlingen
- de Sa C, Benboudjema F, Thiery M, Sicard J (2008) Analysis of microcracking induced by differential drying shrinkage. *Cem Concr Compos* 30(10):947–956, Nov 2008. ISSN 0958-9465
- Derluyn H, Griffa M, Mannes D, Jerjen I, Dewanckele J, Vontobel P, Sheppard A, Derome D, Cnudde V, Lehmann E, Carmeliet J (2013) Characterizing saline uptake and salt distributions in porous limestone with neutron radiography and X-ray micro-tomography. *J Build Phys* 36 (4):353–374

- Dérobot X, Iaquina J, Klysz G, Balayssac JP (2008) Use of capacitive and GPR techniques for the non-destructive evaluation of cover concrete. *NDT & E Int* 41:44–52
- de Vera G, Climent MA, Viqueira E, Antón C, Andrade C (2007) A test method for measuring chloride diffusion coefficients through partially saturated concrete. Part II. The instantaneous plane source diffusion case with chloride binding consideration. *Cem Conc Res* 37(5):714–724
- Dewanckele J, De Kock T, Fronteau G, Derluyn H, Vontobel P, Dierick M, Van Hoorebeke L, Jacobs P, Cnudde V (2014) Neutron radiography and X-ray computed tomography for quantifying weathering and water uptake processes inside porous limestone used as building material. *Mater Charact* 88(2):86–99
- Dobmann G, Kroening M, Surkowa N, von Bernus L, Wolter B (2002) The potential of nuclear magnetic resonance (NMR) to non-destructively characterize early-age concrete by an one-sided access (OSA) technique, NDE 2002. Available at: <http://www.qnetworld.de/nde2002/papers/091P.pdf>. Accessed 08 Oct 2013
- Dobson MC, Ulaby FT, Hallikainen MT, El-Rayes MA (1985) Microwave dielectric behaviour of wet soil, II. Dielectric mixing models. *IEEE Trans Geosci Remote Sens* GE-23(1):35–46
- dos Santos WN (2003) Effect of moisture and porosity on the thermal properties conventional refractory concrete. *J Eur Ceram Soc* 23:745–755
- Drungil CEC, Abt K, Gish TJ (1989) Soil moisture determination in gravelly soils with time domain reflectometry. *Trans ASAE* 32(1):177–180
- du Plooy R, Palma Lopes S, Villain G, Dérobot X (2013) Development of a multi-ring resistivity cell and multi-electrode resistivity probe for investigation of cover concrete condition. *NDT&E Int* 54:27–36
- EN 12570 (2013) Hygrothermal performance of building materials and products—Determination of moisture content by drying at elevated temperature (ISO 12570:2013). European Committee for Standardization
- EN 12571 (2013) Hygrothermal performance of building materials and products—Determination of hygroscopic sorption properties (ISO 12571:2013). European Committee for Standardization
- Eriksson J, Johansson H, Danvind J (2007) A mass transport model for drying wood under isothermal conditions. *Drying Technol* 25(3):433–439
- Fabozzi C, Rosina E, Valentini M (1999) Diagnosi sull'umidità: integrazione tra metodo ponderale e termografia [*Moisture detection: integration between gravimetry and thermography*]. *Tema* 2:15–23 (in Italian)
- Fagerlund G (1973) Methods of characterization of pore structure, report 41. Division of Building Materials, Lund Institute of Technology, Lund
- Fagerlund G (2009) Chemically bound water as a measure of degree of hydration—method and potential errors, report TVBM-3150. Division of Building Materials, Lund University, Lund
- Fares M, Fargier Y, Villain G, Derobert X, Palma-Lopes S (2016) Determining the permittivity profile inside reinforced concrete using capacitive probes. *NDT & E Int* 79:151–160
- Faure PF, Rodts S (2008) Proton NMR relaxation as a probe for setting cement pastes. *Magn Reson Imaging*, 1183–1196
- Faure PF, Caré S, Magat J, Chaussadent T (2012) Drying effect on cement paste porosity at early age observed by NMR methods. *Constr Build Mater* 29:496–503
- Fiala L, Pavlíková M, Pavlík Z (2014) Application of TDR method for moisture profiles measurement in cellular concrete. *Adv Mater Res* 982:11–15
- Fieremans E (2008) validation methods for diffusion weighted magnetic resonance imaging in brain white matter. Ph.D. Thesis, Ghent University, 2008. Available at <http://fieremans.diffusion-mri.com/validation-methods-diffusion-weighted-mri-brain-white-matter>. Accessed 14 Feb 2016
- Fischer K (1935) Neues Verfahren zur maßanalytischen Bestimmung des Wassergehaltes von Flüssigkeiten und festen Körpern. *Angew Chem* 48(26):394–396. <https://doi.org/10.1002/ange.19350482605>

- Fischer N, Haerdtl R, McDonald PJ (2015) Observation of the redistribution of nanoscale water filled porosity in cement based materials during wetting. *Cem Con Res* 68:148–155
- Franzoni E (2014) Rising damp removal from historical masonries: a still open challenge. *Constr Build Mater* 54:123–136
- Franzoni E, Sassoni E (2011) Correlation between microstructural characteristics and weight loss of natural stones exposed to simulated acid rain. *Sci Total Environ* 412–413:278–285
- Franzoni E, Sandrolini F, Bandini S (2011) An experimental fixture for continuous monitoring of electrical effects in moist masonry walls. *Constr Build Mater* 25(2011):2023–2029
- Franzoni E, Bandini S, Graziani G (2014) Rising moisture, salts and electrokinetic effects in ancient masonries: from laboratory testing to on-site monitoring. *J Cult Heritage* 15 (2014):112–120
- Franzoni E, Bandini S, Graziani G, Fregni A (2014b) Jointly measuring moisture and salts in old masonry by means of permanent sampling points. In: Lourenço PB, Haseltine BA, Vasconcelos G (eds). Proceedings of 9th international masonry conference, Guimarães (Portugal) 7–9 July 2014, pp 1–8 (cd-rom)
- Fredriksson M, Lindgren O (2012) End grain water absorption and redistribution in slow grown and fast grown Norway spruce (*Picea abies* (L.) Karst.) heartwood and sapwood. *Wood Mater Sci Eng* 8(4):245–252
- Fredriksson M, Claesson J, Wadsö L (2013a) The influence of specimen size and distance to a surface on resistive moisture content measurements in wood. In: Fredriksson M (2013) Moisture conditions in rain exposed wood joints—experimental methods and laboratory measurements, report TVBM-1030. Laboratory of Building Materials, Lund University, Lund, p 12
- Fredriksson M, Wadsö L, Johansson P (2013) Small resistive wood moisture sensors: a method for moisture content determination in wood structures. *Eur J Wood Prod* 71:515–524
- Freyburger C, Longuetaud F, Mothe F, Constant T, Leban JM (2009) Measuring wood density by means of X-ray computer tomography. *Ann For Sci* 66(8):804
- Friedemann K, Kärger J, Stallmach F (2011) NMR-Relaxometrie an hydratisierenden Zementen mit inneren Wasserquellen. *Kurzberichte aus der Bauforschung* 52(3):58–68 in German
- Fukushima E, Roeder SBW (1991) *Experimental Pulse NMR—a nuts and bolts approach*. Addison-Wesley, Boston, Reading
- Gallé C (2001) Effect of drying on cement-based materials pore structure as identified by mercury intrusion porosimetry. *Comp Study Between Oven- Vac- Freeze-drying Cem Concr Res* 31 (2001):1467–1477
- Gardner DR, Jefferson AD, Lark RJ (2008) An experimental numerical and analytical investigation of gas flow characteristics in concrete. *Cem Concr Res* 38:360–367
- Gerdes AH (2001) *Transport und chemische Reaktion siliciumorganischer Verbindungen in der Betonrandzone*. Ph.D.-Thesis, Eidgenössische Technische Hochschule Zürich, Switzerland
- Göller A (2010) MOIST SCAN—Multi layer moisture scans on large areas in practice. In: Kupfer K (ed) *Proceedings of AQUAMETRY 2010*, Bauhaus-Universität Weimar, pp 389–397
- Gorce J-P, Milestone NB (2007) Probing the microstructure and water phases in composite cement blends. *Cem Concr Res* 37(3):310–318
- Granja J, Azenha M, Sousa C, Faria R, Barros J (2014) Hygrometric assessment of internal relative humidity in concrete: practical application issues. *J Adv Concr Technol* 12(8):250–265
- Greenspan L (1977) Humidity fixed points of binary saturated aqueous solutions. *J Res Natl Inst Stan Technol* 81A(1977):89–96
- Guimarães ATC, Climent MA, de Vera G, Vicente FJ, Rodrigues FT, Andrade C (2011) Determination of chloride diffusivity through partially saturated Portland cement concrete by a simplified procedure. *Const Build Mat* 25(2):785–790
- Gummerson RJ, Hall C, Hoff WD, Hawkes R, Holland GN (1979) Unsaturated water flow within porous materials observed by NMR imaging. *Nature* 281:56–57

- Hansen KK (1986) The hygrometric method. Building Materials Laboratory, Technical University of Denmark. Technical Report 161/86 (in Danish)
- Hansen KK, Bentz D (1999) Studies of hydration and drying in cement pastes by scanning X-ray absorptiometry. Workshop on water in cement paste and concrete—hydration and pore structure, Oct 7–8, 1999, Skagen, Denmark. In: Proceedings of the Nordic Concrete Federation, pp 107–114
- Hansen KK, Christensen SL (1998) Drying of concrete. Part I: A comparison of instruments for measuring the relative humidity in concrete structures. In: Proceedings of 'third international symposium on humidity and moisture', National Physical Laboratory, Teddington, UK
- Hansen KK, Jensen S, Gerward L, Singh K (1999) Dual-energy X-ray absorptiometry for the simultaneous determination of density and moisture content in porous structural materials. In: Building physics in the Nordic Countries, proceedings of the 5th symposium, Goteborg, Sweden: Chalmers tekniska högskola, 1999, pp 281–288
- Hansson L, Antti L (2008) Modeling microwave heating and moisture redistribution in wood. *Drying Technol* 26(5):552–559
- Hanzic L, Ilic R (2003) Relationship between liquid sorptivity and capillarity in concrete. *Cem Concr Res* 33:1385–1388
- Hanzic L, Nemeč T, Ilic R (2002) Determination of the capillarity coefficients of distilled water and oil in concrete by neutron radiography. In: Proceedings of 7th world conference of neutron radiography, Rome, Italy: Italian National Agency for New Technologies, 2002, pp 643–650
- Harms AA, Wymann DR (1986) Mathematics and physics of neutron radiography. D. Reidel, Dordrecht
- Haskins JJ (1973) Evaluation of a real time imaging system for neutron radiography. *Gen Electr Rep NEDC* 12512:29
- Hassanein R (2006) Correction methods for the quantitative evaluation of thermal neutron tomography. ETH Zurich, Zurich
- Hassanein R, Lehmann E, Vontobel P (2005) Methods of scattering corrections for quantitative neutron radiography. *Nucl Instrum Methods Phys Res A* 542:353–360
- Hassanein R, Meyer HO, Caiminati A (2006) Investigation of water imbibition in porous stone by thermal neutron radiography. *J Phys D Appl Phys* 39:4284–4291
- Hedenblad G (1995) Drying of excess moisture in concrete. Drying times and moisture measurements (in Swedish), report T12:1995. Swedish Council for Building Research, Stockholm, Sweden, ISBN 91-540-5708-6
- Hedenblad G (1999) Measurement of moisture in high performance concrete. In: 5th international symposium on utilization of high strength/high performance concrete, Sandefjord, Norway, June 20–24 1999
- Hedenblad G, Nilsson L-O (1985) Degree of capillary saturation—a tool for better evaluation of the moisture content in concrete. Contribution to CIB-W40-meeting, 2–5 Sept 1985, Holzkirchen. Report TVBM-7005, Laboratory of Building Materials, Lund University, Lund
- Henderson GD, Basheer PAM, Long AE (2004) Pull-off test and permeation tests. In: Malhotra VM, Carino NJ (eds) Handbook on nondestructive testing of concrete, 2nd edn. CRC Press, Florida
- Hervé E, Care S, Seguin JP (2010) Influence of the porosity gradient in cement paste matrix on the mechanical behaviour of mortar. *Cem Concr Res* 40:1060–1071  
<http://www.magritek.com/products-nmr-mouse>. Accessed 09 Oct 2013
- Hugenschmidt J, Loser R (2008) Detection of chlorides and moisture in concrete structures with ground penetrating radar. *Mater Struct* 41:785–792
- Hunkeler F (1996) The resistivity of pore-water solution—a decisive parameter of rebar corrosion and repair methods. *Constr Build Mater* 10(5):381–389
- ImageJ (2010) (<http://rsbweb.nih.gov/ij/download.html>)
- ISO 11276 (1995) Soil quality—Determination of pore water pressure—tensiometer method

- IUPAC Recommendations (1972) Manual of symbols and terminology for physicochemical quantities and units, Appendix II: definitions, terminology and symbols in colloid and surface chemistry. *Pure Appl Chem* 1972(31):584
- IUPAC Recommendation (1990) Glossary of atmospheric chemistry terms. *Pure Appl Chem* 1990 (62):2169
- IUPAC Recommendations (1990) Glossary of atmospheric chemistry terms. *Pure Appl Chem* 62:2171
- IUPAC Recommendations (1990) Glossary of atmospheric chemistry terms. *Pure Appl Chem* 62:2215
- IUPAC Recommendations (1993) Nomenclature for chromatography. *Pure Appl Chem* 1993 (65):854
- IUPAC Recommendation (2004) Glossary of atmospheric chemistry terms. *Pure Appl Chem* 2004 (76):1985
- Jacobs F (1998) Permeability to gas of partially saturated concrete. *Mag Concr Res* 50(2):115–121
- Johansson P (2005) Water absorption in two-layer masonry systems—properties, profiles and predictions. Ph.D.-thesis TVBM-1024, Laboratory of Building Materials, Lund University, Lund
- Johansson P (2012) Drying of concrete—the laboratory study behind TorKaS3 (in Swedish). Report TVBM-3165, Laboratory of Building Materials, Lund University, Lund
- Johansson P (2014a) Moisture measurement in concrete with low w/c, step 1 (in Swedish). Report TVBM-3178, Laboratory of Building Materials, Lund University, Lund
- Johansson (2014b) Moisture measurement in concrete with low w/c, step 1 (in Swedish), report TVBM-3178. Laboratory of Building Materials, Lund University, Lund
- Johansson J, Kifetew G (2010) CT-scanning and modelling of the capillary water uptake in aspen, oak and pine. *Eur J Wood Wood Prod* 68(1):77–85
- Johansson A, Janz M, Silfwerbrand J, Trägårdh J (2008) Protection of concrete with water repellent agents—What is required to achieve a sufficient penetration depth. *Concrete Repair, Rehabilitation and Retrofitting II*, South Africa, pp 763–768
- Kaczmarek M (2008) Approximate solutions for non-stationary gas permeability tests. *Transp Porous Med* 75:151–165
- Kaczmarek M (2010) Modeling reservoir gas permeability tests for cylindrical and spherical geometry. *Transp Porous Med* 84:95–108
- Kanematsu M, Maruyama I, Noguchi T, Iikura H, Tsuchiya N (2009) Quantification of water penetration into concrete through cracks by neutron radiography. *Nucl Instr Methods Phys Res A* 605:154–158
- Karastathis VK, Karmis PN, Drakatos G, Stavrakakis G (2002) Geophysical methods contributing to the testing of concrete dams, application at the Marathon dam. *J Appl Geophys* 50:247–260
- Kasal B, Lear G (2010) Moisture measurement. In: Kasal B, Tannert T (ed) *In situ assessment of structural timber—state of the art report of the RILEM technical committee 215AST*, Chapter 10, p 6
- Keil A, Orlowsky J, Raupach M (2011) Einsatz eines mobilen NMR-Sensors als zerstörungsfreies Messsystem in der Bauwerkserhaltung: Application of a Mobile NMR Sensor as a Non Destructive Measuring Tool to Conserve Buildings. *Bautechnik* 88, 11, pp 741–748 ISSN 0932-8351
- Khan MI (2002) Factors affecting the thermal properties of concrete and applicability of its prediction models. *Build Environ* 37, Pergamon
- Khelidj A, Bastian G, Baroghel-Bouny V, Villain G (2007) Experimental study of the evolution of heat and moisture transfer parameters of a concrete slab. *Mag Concr Res* 59:377–386
- Kimmich R (1997) *NMR tomography, diffusometry, relaxometry*. Springer, Berlin
- Kington LR, Jones TM (2008) Application for NIR analysis of beverages. In: Burns DA, Ciurczal EW (eds) *Handbook of near-infrared analysis*, 3rd edn. CRC Press, Boca Raton, USA
- Kleinberg RL (1996) Well logging, 1996 In: Grant DM, Harris RK (eds) *Encyclopedia of NMR*. Wiley, New York, pp 4960–4969

- Klysz G, Lataste JF, Fnine A, Derobert X, Piwakowski B, Buyle-Bodin F (2006) Auscultation non destructive du chevêtre du pont de la Marque (59). *Revue Européenne de Génie Civil* 10(1): 1–24
- Kofalk S, Plagge R (1997) Kalibrierung von TDR Messungen zur Erfassung der Bodenfeuchte unter Feldbedingungen. In: Grimmeisen W, Preuhsler T (eds) *Forstliche Forschungsberichte München*, vol 166, pp 104–112
- Kopinga K, Pel L, Brocken H (1998) Moisture transport in masonry observed by NMR. In: *Calcium silicate symposium*, Amsterdam, the Netherlands, 4–5 June
- Koptyug IV (2012) MRI of mass transport in porous media: drying and sorption processes. *Progr Nucl Magn Reson Spectr* 65:1–65
- Korpa A, Trettin R (2006) The influence of different drying methods on cement paste microstructure as reflected by gas adsorption: comparison between freeze-drying (F-drying), D-drying, P-drying and oven-drying methods. *Cem Concr Res* 36:634–649, April 2006
- Kruschwitz S, Niederleithinger E, Trela C, Wöstmann J (2012) Use of complex resistivity tomography for moisture monitoring in a flooded masonry specimen. *J Infrastruct Syst* 18:2–11
- Kullenberg R, Hultnäs M, Fernandez V, Nylinder M, Toft S, Danielsson F (2010) Dual-energy X-ray absorptiometry analysis for the determination of moisture content in biomass. *J Biobased Mater Bioenergy* 4:363–366
- Kuras O, Beamish D, Meldrum PI, Ogilvy RD (2006) Fundamentals of the capacitive resistivity technique. *Geophysics* 71(3):G135–G152
- Larget M (2011) Contribution à l'évaluation de la dégradation du béton : Thermographie infrarouge et Couplage de Techniques. Thèse de l'université Bordeaux 1:204p
- Larsen PK (2014) Determination of water content in solid brick masonry walls using a dielectric probe. In: *Proceeding 9th international masonry conference*, Guimaraes, Portugal
- Lataste JF (2010) Chapter electrical resistivity for the evaluation of reinforced concrete structures. In: Maierhofer Ch, Reinhardt H-W, Dobmann G (eds) *Non-destructive evaluation of reinforced concrete structures: non-destructive testing methods*, vol 2, Woodhead Publishing Limited, Cambridge, UK (ISBN 1 84569 950 5 ISBN-13: 978 1 84569 950 5)
- Lataste JF (2016) Investigations Georadar sur la basilique Saint Seurin de Bordeaux, internal report, Université de Bordeaux, p 111 (in French)
- Lataste JF, Breyse D (2011) Study on the variability of electrical resistivity of concretes, NDTMS 2011, 15–18 May, Istanbul (Turkey), p 8
- Laurens S, Balayssac JP, Rhazi J, Klysz G, Arliguie G (2005) Non destructive evaluation of concrete moisture by GPR: experimental study and direct modeling. *Mater Stuct* 38:827–832
- Lieboldt M, Mechtcherine V (2013) Capillary transport of water through textile-reinforced concrete applied in repairing and/or strengthening cracked RC structures. *Cem Concr Res* 52:53–62
- Lin C-J, Chung C-H, Yang T-H, Lin F-C (2012) Detection of electric resistivity tomography and evaluation of the sapwood-heartwood demarcation in three Asia Gymnosperm species. *Silva Fennica* 46(3):415–424
- Lindgren O (1992) Medical CT-scanners for non-destructive wood density and moisture content measurements. Ph.D. thesis. Luleå University of Technology, Skellefteå Campus, Division of Wood Technology, Report No. 1992:111D
- Lindgren O, du Plessis A, Seifert T (2016) Direct 3D measurements of moisture content in wood using dual energy CT-scanning. *Wood Mater Sci Eng* 11(5)
- Lindsay JT (1983) Development and characterization of a real time neutron radiographic imaging system. University of Missouri, Columbia
- Lion M, Skoczylas F, Ledéret F (2004) Determination of the main hydraulic and poro-elastic properties of a limestone from Bourgogne, France. *Int J Rock Mech Min Sci* 41(6):915–925, Sept 2004. ISSN 1365-1609
- Liu J, Agostini F, Skoczylas F (2013) From relative gas permeability to in situ saturation measurements. *Constr Build Mater* 40:882–890, Mar 2013

- Loke MH, Barker RD (1996) Rapid least-squares inversion of apparent resistivity pseudo-sections using a quasi-Newton method. *Geophys Prospect* 44:131–152
- Loosveldt H, Lafhaj Z, Skoczylas F (2002) Experimental study of gas and liquid permeability of a mortar. *Cem Concr Res* 32(9):1357–1363
- Lopez W, Gonzalez JA (1993) Influence of degree of pore saturation on the resistivity of concrete and the corrosion rate of steel reinforcement. *Cem Concr Res* 23(2):368–376
- Lucero CL, Bentz DP, Hussey DS, Jacobson DL, Weiss WJ (2015) Using neutron radiography to quantify water transport and the degree of saturation in entrained air cement based mortar. *Phys Procedia* 69:542–550
- Lunabba T, Paroll H (2011a) Moisture control in concrete bridges. *n: Proceedings of XXI Nordic concrete research symposium, Hämeenlinna, Finland, May 2011. Nordic Concrete Federation, Publication No. 43. pp 443–446*
- Lunabba T, Paroll H (2011b) Moisture monitoring in concrete bridges 1990–2011. Nordic concrete research, Publication No. 44, 2/2011. Nordic Concrete Federation. Vodskov, Dec 2011, pp 25–44
- Lydon FD (1993) The relative permeability of concrete using nitrogen gas. *Constr Build Mater* 7(4):213–220
- Macedo A, Vaz CMP, Pereira JCD, Naime JM, Cruvinel P, Wei et al (2002) Wood density determination by X- and gamma-ray tomography. *Holzforschung* 56(5):535–540
- Maierhofer C (2008) Combination of non-destructive testing methods for the assessment of masonry structures. In: RILEM international conference, SACOMATIS, Varenna, Italy, pp 715–726
- Maierhofer C, Wostmann J, Trela C, Rollig M (2008) Investigation of moisture content and distribution with radar and active thermography. In: RILEM international conference, SACOMATIS, Varenna, Italy, pp 411–420
- Maierhofer Ch, Reinhardt HW, Dobmann G (eds) (2010) Non destructive evaluation of reinforced concrete structures. CRC Press, Florida, p 624
- Maldague X (2001) Theory and practice of infrared technology for non destructive testing. Wiley, New Jersey, p 684
- Malicki MA, Skierucha WM (1989) A manually controlled TDR soil moisture meter operating with 300 ps rise-time needle pulse. *Irrig Sci* 10(2):153–163
- Malicki MA, Plagge R, Renger M, Walczak RT (1992) Application of Time Domain Reflectometry (TDR) soil measurement microprobe for the determination of unsaturated soil water characteristics from undisturbed soil cores. *Irrig Sci* 13:65–72
- Marble AE, Young JJ, Mastikhin IV, Colpitts BG, Balcom BJ (2007) A small, low cost embedded NMR sensor suitable for bulk measurement of porous materials. In: Proceedings of the eighth international Bologna conference on magnetic resonance in porous media, magnetic resonance imaging, vol 25, pp 572–573
- Margolis SA, Vaishnav K, Sieber JR (2004) Measurement of water by oven evaporation using a novel oven design. *Anal Bioanal Chem* 380:556–562
- Martin GR (1986) A method for determining the relative permeability of concrete using gas. *Mag Concr Res* 38(135):90–94
- Martinho E, Alegria F, Dionisio A, Grangeia C, Almeida F (2012) 3D-resistivity imaging and distribution of water soluble salts in Portuguese Renaissance stone bas-reliefs. *Eng Geo* 141–142:33–44
- Martys NS (1999) Diffusion in partially-saturated porous materials. *Mater Struct* 32:555–562
- Maruyama I, Kanematsu M, Noguchi T, Iikura H, Teramoto A, Hayano H (2009) Evaluation of water transfer from saturated lightweight aggregate to cement paste matrix by neutron radiography. *Nucl Instrum Methods Phys Res Sect A Accelerators, Spectrometers, Detectors Assoc Equip* 605(1/2):159–162
- Massari G, Massari I (1993) Damp buildings, old and new. ICCROM, Rome

- Masschaele B, Dierick M, Cnudde V et al (2004) High-speed thermal neutron tomography for the visualization of water repellents, consolidants and water uptake in sand and lime stones. *Radiat Phys Chem* 71:807–808
- McCann DM, Forde MC (2001) Review of NDT methods in the assessment of concrete and masonry structures. *NDT & E Int* 34:71–84
- McCarter WJ, Garvin S (1989) dependence of electrical impedance of cement based materials on their moisture condition. *J Phys D Appl Phys* 22:1773–1776
- McNair AVF (2015) Assessment of internal deterioration of alkali-silica reaction affected concrete. M.Sc. Thesis, Department of Civil Engineering, Technical University of Denmark, Denmark
- Meier SJ, Wittmann FH (2001) Influence of concrete quality, its age and moisture content, on the penetration depth of water repellent agents. In: Proceedings, hydrophobe III—third international conference on water repellent treatment of building materials, Germany, pp 123–131
- Meziani H, Skoczylas F (1999) An experimental study of the mechanical behaviour of a mortar and of its permeability under deviatoric loading, *Materials and Structures/Matériaux et Constructions*, vol 32, July 1999, pp 403–409, 1359-5997/99, © RILEM SCIENTIFIC REPORTS
- Milachowski C, Lowke D, Gehlen C (2012a) Detection of transport processes during freeze-thaw deicing salt attack using single-sided NMR. In: 2nd international conference “Microdurability”, Amsterdam
- Milachowski C, Lowke D, Gehlen C (2012b) Effect of minimal temperature, salt and moisture content on concrete under freeze-thaw deicing salt attack. In: Proceedings of ICDC 2012, international congress on durability of concrete, Trondheim, Norway, 18–21 June 2012
- Moffitt LR (1964) Time domain reflectometry—theory and applications, *Engineering Design News*, pp 38–44
- Monfore GE (1963) A small probe-type gage for measuring relative humidity. Bulletin No. 160, Portland Cement Association R & D Laboratory, Skokie, USA
- Monfore GE (1968) The electrical resistivity of concrete. *J Portland Cem Assoc Res Dev Lab* 10(2):35–48
- Mujumdar AS (1997) Drying Fundamentals. In: Baker CGJ (ed) *Industrial drying of foods*. Blackie Academic & Professional, London, pp 7–30
- Nestle NC, Zimmermann C, Dakkouri M, Kärger J (2002) Transient high concentrations of chain anions in hydrating cement—indications from spin relaxation measurements. *J Phys D Appl Phys* 35:166–171
- Neville A (2000) *Propriétés des bétons*, éditions Eyrolles, Paris, p 806
- Nielsen EP, Geiker MR (2003) Chloride diffusion in partially saturated cementitious material. *Cem Conc Res* 33(1):133–138
- Nilsson L-O (1976) ‘Moisture investigation of concrete floor slabs on grade, Rydebäck, Vallåkra kommun’ (in Swedish). Lund University, Lund, Laboratory of Building Materials
- Nilsson L-O (1979) Excess moisture in concrete slabs on grade. Drying and measuring methods, part 2: Moisture measurement. Report TVBM-3008, div. of Building Materials, Lund University, Lund
- Nilsson L-O (1980) Hygroscopic moisture in concrete—drying, measurements & related material properties. Ph.D.-thesis, report TVBM-1003. Lund Institute of Technology, Lund
- Nilsson L-O (1988) Moisture transport properties of wood and wooden based boards—a building physics inventory and analysis of knowledge and knowledge needs (in Swedish). Report P-88:4, Department of Building Materials, Chalmers University of Technology, Göteborg
- Nilsson L-O (1997) Assessing moisture conditions in marine concrete structures. In: International conference repair of concrete structures, Svolve, 28–30 May 1997
- Nilsson L-O (1999) Relationship between rate of drying (as measured with the ASTM CaCl<sub>2</sub>-method) and the remaining moisture (as measured with RH at a characteristic depth). FD-calculations. Moisture Engineering Institute, [www.moistengin.com](http://www.moistengin.com), Trelleborg, Nov 1999

- Nilsson L-O (2004) 'Material analysis of samples from the reactor containment B1' (in Swedish). Lund University, Lund, Laboratory of Building Materials
- Nilsson L-O (2006) Moisture effects on materials, critical moisture limits (in Swedish) Formas report T2:2006, Stockholm
- Nilsson L-O (2007) Drying of reactor containment walls of concrete during past and future decades. In: The 19th international conference on structural mechanics in reactor technology (SMiRT 19), 12–17 Aug 2007, Toronto, Canada
- Nilsson L-O, Åhs M (2012) Methods for measuring relative humidity (RH) in concrete floors—development and uncertainties. Aquametry 2010—First European conference on moisture measurement, 5–7 Oct 2010, Weimar, Germany
- Nilsson L-O, Fredlund P (2009) Cast-in probe for measuring drying of concrete—simulation of the effect of the size and orientation of the sensor (in Swedish). Sensobyg D4. Report TVBM-7198, Laboratory of Building Materials, University of Lund, Lund
- Nilsson L-O, Sjöberg A, Togerö A (2006) Moisture measurements in buildings (in Swedish). Formas, Stockholm. ISBN 91-540-5978-X
- Nilsson L-O, Sjöberg A, Togerö Å (2006) Moisture measurements in buildings—an information report. (in Swedish) TVBM-7188, Building Materials, Lund Institute of Technology, Dec 2005
- Nizovtsev MI, Stankus SV, Sterlyagov AN, Terekhov VI, Khairulin RA (2008) Determination of moisture diffusivity in porous materials using gamma-method. *Int J Heat Mass Transf* 51 (2008):4161–4167
- Nokken MR, Hooton RD (2002) Dependence of rate of absorption on degree of saturation of concrete. *ASTM Cem Conc Agg* 24(1):20–24
- NORDTEST (1988) Relative air humidity: calibration of electrical instruments, NT BUILD 340, Nordtest, Espoo, Finland
- Nordtest (1989) Building structures, moisture content: neutron method. NT BUILD 346
- NORMAL 41/93 (1993) Misura locale di umidità superficiale con metodo ponderale, [*Local measurement of surface moisture by the gravimetric method*], Recommendation, ICR, Istituto centrale del restauro, Roma, 1993 (in Italian)
- Ohlsson M, Mikolajewski M (2003) Experimental verification of a new moisture measurement method (in Swedish). Diploma work report, Teknik & Samhälle, Malmö University, Malmö
- Ollivier J-P, Massat M, Parrott LJ (1995) Parameters influencing transport characteristics. In: Kropp J, Hilsforf HK (eds) Performance criteria for concrete durability. E & FN Spon, London, pp 33–96
- Olsson N, Baroghel-Bouny V, Nilsson L-O, Thiery M (2013) Non-saturated ion diffusion in concrete—a new approach to evaluate conductivity measurements. *Cem Conc Comp* 40:40–47
- OmniSense (2010) <http://www.omnisense.com>
- ONSITEFORMASONRY (2006) EUR21696EN Final report, European commission directorate general for research, Brussels
- Orlowsky J (2004) Modeling the long-term behavior of textile reinforced concrete. In: Walraven J, Blaauwendraad J, Scarpas T, Snijder B (eds) 5th international phd symposium in civil engineering, Delft, 16–19 June 2004, vol 1. A.A. Balkema Publishers, Leiden, S 155-16
- Orlowsky J (2011) Mobile NMR—a powerful tool to measure coating thickness in concrete buildings. In: Büyükoztürk O, Tasdemir MA, Günes O, Akkaya Y (eds.) Part I Nondestructive testing of materials and structures, proceedings of NDTMS-2011, Istanbul, 15–18 May 2011, pp 125–130, ISBN 978-94-007-0722-1. 2013
- Orlowsky J (2012) Measuring the Layer thicknesses of concrete coatings by mobile NMR—a study on the influence of steel reinforcements. *Constr Build Mater* 27:341–349. ISSN 0950-0618
- Pang S, Wiberg P (1998) Model predicted and CT scanned moisture distributed in a Pinus radiata board during drying. *Eur J Wood Wood Prod* 56(1):9–14
- Paroll H (1997) Measurement of relative humidity and temperature in new concrete bridges. In: Nordic mini-seminar of the Nordic concrete federation, VTT symposium 174, 22 Aug 1997. Espoo, Finland, pp 51–65

- Paroll H, Nykänen E (1998) Measurement of relative humidity and temperature in a new concrete bridge vs laboratory samples. *Nord Concr Res* 21:103–119
- Parrott LJ (1994) Moisture conditioning and transport-properties of concrete test specimens. *Mater Struct* 27(172):460–468
- Parrott LJ, Chen ZH (1990) Some factors influencing air permeation measurements in cover concrete. *Mater Struct* 24(144):403–408
- Pastrav M (1989) Moisture and temperature measurement in concrete: Risk of erroneous measurements in drilled holes (in Swedish). SP-report 1989:05, Swedish Research and Testing Institute, Borås
- Paulmann K, Molin C (1995) On-site test methods, in RILEM Report 12: Performance criteria for concrete durability, eds. Kropp, J. and Hilsdorf, H.K., E & FN Spon, London, pp 258–279
- Pease B (2010) Influence of concrete cracking on ingress and reinforcement corrosion. Ph.D. thesis, Technical University of Denmark, Kgs. Lyngby, Denmark
- Pease B J, Michel A, Geiker MR, Stang H (2012a) Modelling moisture ingress through simplified concrete geometries. In: Proceedings of ICDC, 17–21 June 2012, Trondheim, Norway
- Pease BJ, Scheffler GA, Janssen H (2012) Monitoring moisture movements in building materials using X-ray attenuation: influence of beam-hardening of polychromatic X-ray photon beams. *Constr Build Mater* 36(2012):419–429
- Pel L, Hazrati K, Kopinga K, Marchand J (1998) Water absorption in mortar determined by NMR. *Magn Reson Imaging*, pp 525–528
- Penner E (1965) Suction and its use as measure of moisture contents and potentials in porous materials. *Humidity Moisture* 4:245, Reinhold Publishing Corporation, NY
- Philippot S, Korb JP, Petit D, Zanni H (1998) Analysis of microporosity and setting of reactive powder concrete by proton nuclear relaxation. *Magn Reson Imaging* 16:515–519
- Phillips MC (1975) Hydration and the stability of foams and emulsions. In: Franks F (ed) *Water in disperse systems—a comprehensive treatise*, vol 5. Springer US, pp 133–172
- Phillipson MC, Baker PH, Davies M, Ye Z, Galbraith GH, McLean RC (2008) Suitability of time domain reflectometry for monitoring moisture in building materials. *Build Serv Eng Res Technol* 29(3):261–272
- Picandet V, Khelidj A, Bastian G (2001) Effect of axial compressive damage on gas permeability of ordinary and high-performance concrete. *Cem Concr Res* 31(11):1525–1532
- Picandet V, Khelidj A, Bellegou H (2009) Crack effects on gas and water permeability of concretes. *Cem Concr Res* 39(6):537–547, June 2009. ISSN 0008-8846
- Pihlajavaara SE, Paroll H (1974) Effect of carbonation on the measurement of humidity in concrete. In: Proceedings of 2nd international CIB/RILEM symposium on moisture problem in buildings, Rotterdam vol. 12(9), pp 5–19
- Plagge R (1991) Bestimmung der ungesättigten hydraulischen Leitfähigkeit im Boden, Ph.D. thesis, *Bodenökologie und Bodengenese*, 3
- Plagge R (2003) Bestimmung von Materialfeuchte und Salzgehalt in kapillarporösen Materialien mit TDR, Kolloquium mit Workshop Innovative Feuchtemessung in Forschung und Praxis, Karlsruhe
- Plagge R, Roth CH, Renger M (1991) Bestimmung the Hysteresis der ungesättigten hydraulischen Leitfähigkeit im Boden, *Mitteilung Deutsche Bodenkundliche Gesellschaft*, 66, pp 201–204
- Plagge R, Roth CH, Renger M (1996) Dielectric soil water content determination using time domain reflectometry (TDR). In: Kraszewski A (ed) *Second workshop on electromagnetic wave interaction with water and moist substances at the 1996 IEEE microwave theory and techniques society international symposium in San Francisco, CA, 17 June*, pp 59–62
- Pleinert H (1998) Determination of moisture distributions in porous building materials—neutron signal transfer analysis. *Build Mater Rep* 14, Aedificatio Publishers, Freiburg
- Pleinert H, Sadouki H, Wittmann FH (1998) Determination of moisture distributions in porous building materials by neutron transmission analysis. *Mater Struct* 31:218–224
- Polder RB (2001) Test methods for on site measurement of resistivity of concrete: a RILEM TC-154 technical recommendation. *Constr Build Mater* 15:125–131

- Powers TC, Brownyard TL (1948) Bulletin 22 of the Research Department of the Portland Cement Association, New York
- Proietti N, Capitani D, Di Tullio V (2014) Applications of nuclear magnetic resonance sensors to cultural heritage. *Sensors* 14:6977–6997
- Radocea A (1992) A study on the mechanism of plastic shrinkage of cement-based materials. Publ. P-92:9, Department of Building Materials, Chalmers university of technology
- Radon J (1917) Über die Bestimmung von Funktionen durch ihre Integralwerte längs gewisser Mannigfaltigkeiten. *Ber Verh Sächsische Akad Wissenschaften* 69:262–277
- Raupach M, Dauberschmidt C, Wolff L, Harnisch J (2007) Monitoring der Feuchteverteilung in Beton—Sensorik und Anwendungsmöglichkeiten. In: *Beton* 57 (2007), Nr. 1
- RBK(2010:6) 6 Routine for drilling of measuring holes (in Swedish), RBK-authorized Moisture Controller, [www.rbk.nu](http://www.rbk.nu)
- RBK(2010:8) 8 Routine for RH-measurement in a drilled hole with the measuring system Humiguard (in Swedish), RBK-authorized Moisture Controller, [www.rbk.nu](http://www.rbk.nu)
- RBK(2010:9) 9 Routine for RH-measurement in a drilled hole (with the measuring system) capacitive sensor Vaisala (in Swedish), RBK-authorized Moisture Controller, [www.rbk.nu](http://www.rbk.nu)
- Rechenberg W (1976) *Zement-Kalk-Gips* 1976, 29, 512–516
- RILEM (1999a) Permeability of concrete as a criterion of its durability. Final report TC 116-PCD: concrete durability—an approach towards performance testing', *Mater Struct* 32:163–173
- RILEM (1999b) Permeability of Concrete as a Criterion of its Durability - Recommendations, RILEM TC 116-PCD. *Mater Struct* 32:174–179, April 1999
- RILEM (2007) Non-destructive evaluation of the penetrability and thickness of the concrete cover—state-of-the-art report of RILEM technical committee 189-NEC, R. Torrent and L. Fernandez Luco, ISBN: 978-2-35158-080-6
- RILEM TC 116-PCD (1999a) Final report: concrete durability—an approach towards performance testing. *Mater Struct* 32:163–173
- RILEM TC 116-PCD (1999b) Recommendations: a preconditioning of concrete test specimens for the measurement of gas permeability and capillary absorption of water. *Mater Struct* 32: 174–176
- RILEM TC 127-MS: Tests for masonry materials and structures
- RILEM TC 177-MDT (2005) Determination of moisture distribution and level using radar in masonry built with regular units, recommendation of the TC177MDT 'Masonry Durability and on site Testing', *Mater Struct* 38:283–288
- RILEM TC 215-AST (2010) In situ assessment of structural timber—state of the art report. Kasal B, Tannert T (ed)—Report vol 7 published by Springer, p 128
- Rittersma ZM (2002) Recent achievements in miniaturised humidity sensors—a review of transduction techniques. *Sens Actuators A Phys* 96(2–3):196–210, 28 Feb 2002. [http://dx.doi.org/10.1016/S0924-4247\(01\)00788-9](http://dx.doi.org/10.1016/S0924-4247(01)00788-9)
- Roels S, Carmeliet J, Hens H, Adan O, Brocken H, Cerny R, Pavlik Z, Ellis AT, Hall C, Kumaran K, Pel L, Plagge R (2004) A comparison of different techniques to quantify moisture content profiles in porous building materials. *J Therm Env Bldg Sci* 27(4):261–276, April 2004
- Rojas G, Hernández RE, Condal A, Verret D, Beauregard R (2005) Exploration of the physical properties of internal characteristics of sugar maple logs and relationships with CT images. *Wood Fiber Sci* 37(4):591–604
- Romer M (2005) Effect of moisture and concrete composition on the torrent permeability measurement. *Mater Struct* 38(2005):541–547
- Roth K, Schulin H, Flüher H, Attinger W (1990) Calibration of time domain reflectometry for water content measurements using a composite dielectric approach. *Water Resour Res* 26 (10):2267–2273
- Roth CH, Malicki MA, Plagge R (1992) Empirical evaluation of the relationship between soil dielectric constant and volumetric water content as the basis for calibrating soil moisture measurements by TDR. *J Soil Sci* 43(1):1–13

- Rucker-Gramm P (2008) Modellierung des Feuchte- und Salztransports unter Berücksichtigung der Selbstabdichtung in zementgebundenen Baustoffen. Ph.D. thesis, Technical University of Munich, German
- Safetyexpress (2016) [www.safetyexpress.com](http://www.safetyexpress.com)
- Sahlén (2016) Private communication about Sahlénsensor 102. FuktCom AB, Lund
- Samaha HR, Hover KC (1992) Influence of micro-cracking on the mass transport properties of concrete. *ACI Mater J* 89(4):416–424
- Sandberg K (2006) Modelling water sorption gradients in spruce wood using CT scanned data. *N Z J For Sci* 36(2/3):347–364
- Sandberg K, Pousette A, Dahlquist S (2011) Wireless in situ measurements of moisture content and temperature in timber constructions. In: XII DBMC, international conference on durability of building materials and components, 12–15 April 2011, Porto, Portugal
- Sandin K (1974) Moisture and temperature investigation in Vadstena Monastery Church (in Swedish), report 50, Department of Building Technology, Lund University, Lund
- Sandrolini F, Franzoni E (2006) An operative protocol for reliable measurements of moisture in porous materials of ancient buildings. *Build Environ* 41:1372–1380
- Sass O (2005) Rock moisture measurements: techniques, results, and implications for weathering. *Earth Surf Process Land* 30:359–374
- Sass O, Viles HA (2010) Wetting and drying of masonry walls: 2D-resistivity monitoring of driving rain experiments on historic stonework in Oxford, UK. *J Appl Geophys* 70(2010): 72–83
- Sbartai ZM, Lataste J-F (2008a) Evaluation non-destructive de l'humidité des matériaux de construction par mesures radar et résistivité électrique en laboratoire. (in French). Rapport interne, Université bordeaux1, US2B, Ghymac, p 50
- Sbartai ZM, Lataste J-F (2008b) Evaluation non-destructive de l'humidité des matériaux de construction par mesures radar et résistivité électrique en laboratoire (in French). Rapport interne, Université Bordeaux1, US2B, Ghymac, p 50
- Sbartai ZM, Laurens S, Rhazi J, Balaýssac JP, Arliguie G (2007) Using radar direct wave for concrete condition assessment: correlation with electrical resistivity. *J Appl Geophys* 62: 361–374
- Sbartai ZM, Laurens S, Rhazi J, Balaýssac JP, Arliguie G (2007) Using radar direct wave for concrete condition assessment: correlation with electrical resistivity. *J Appl Geophys* 62:361–374
- Scheffler GA (2009) Validation of hygrothermal material modelling under consideration of the hysteresis of moisture storage. Ph.D. thesis, Technical University of Dresden, Dresden
- Schießl P, Breit W (1995) Monitoring of the depth-dependent moisture content of concrete using multi-ring-electrodes, concrete under severe conditions—environment and loading, vol 2, Sakai K, Banthia N, Gjorv OE (ed), E&FN Spon., pp 965–973
- Schießl-Pecka A, Gehlen C (2016) The active agent contents in the pre-determined depth, RILEM Week, Copenhagen
- Scholz E (1984) Karl-Fischer-Titration. Springer, Berlin
- Schroefl C, Mechtcherine V, Kaestner A, Vontobel P, Hovind J, Lehmann E (2015) Transport of water through strain-hardening cement based composite applied on top of cracked reinforced concrete slabs with and without hydrophobization of cracks—investigation by neutron radiography. *Constr Build Mater* 76:70–86
- Shang D, Pere P (1997) Wood moisture content measurement by x-ray exposure method. *J For Res* 8(1), Mar 1997
- Shmulsky R, Jones PD (2011) Forest products and wood science: an introduction, 6th edn. Wiley-Blackwell, Chichester
- Siden J, Zeng X, Unander T, Koptyug A, Nilsson HE (2007) Remote moisture sensing utilizing ordinary RFID tags. In: 2007 IEEE Sensors Conference, pp 308–311, Oct 2007

- Siebel et al.: DAFStB Sachstand Siebel E, Bramshuber W, Brandes C, Dahme U, Dehn F, Dombrowski K, Feldrappe V, Frohburg U, Guse U, Huß A, Lang E, Lohaus L, Müller C, Müller HS, Palecki S, Petersen L, Schröder P, Setzer MJ, Weise F, Westendarp A, Wiens U (2005) Sachstandbericht – Übertragbarkeit von Frost-Laborprüfungen auf Praxisverhältnisse. DAFStb-Heft 560, 2005, German
- Sirieux C, Defer D (2005) Méthodes thermiques d'évaluation non destructive, Chapitre B5 de Méthodes d'évaluation non destructive de l'état d'altération des ouvrages en béton, sous la direction de Breysse D., Abraham O., Edition Presses de l'Ecole Nationale des Ponts et Chaussées, Paris, ISBN 2-85978-405-5, pp 253–274
- Sirieux C, Lataste JF, Breysse D, Naar S, Dérobert X (2007) Comparison of non destructive testing: infrared thermography, electrical resistivity and capacity methods in a reinforced concrete structures Tarbes' precast duct. *J Build Appraisal* 3(1):77–88
- Sjöberg A (2004) A method for measuring moisture profiles in concrete structures. Experimental verification of the OE-method. Report TVBM-3122, Building Materials, Lund University, Lund
- Sjöberg A, Nilsson L-O, Rapp T (2002) Moisture measurements in heated concrete floors (in Swedish) P-02:1, Department of Building Materials, Chalmers University of Technology, Göteborg
- Skoczylas F, Henry JP (1995) A study of the intrinsic permeability of granite to gas. *Int Rock Mech Min Sci Geomech Abstr* 32(2):171–179
- Smith DM, Bryant WMD, Mitchell J Jr (1939) Analytical Procedures Employing Karl Fischer's Reagent. I. Nature of the Reagent. *J Am Chem Soc* 61:2407–2412
- Snoeck D, Steuperaert S, Van Tittelboom K, Dubruel P, De Belie N (2012) Visualization of water penetration in cementitious materials with superabsorbent polymers by means of neutron radiography. *Cem Concr Res* 42(8):1113–1121
- Sobczuk H, Plagge R (2007) Time domain reflectometry method in environmental measurements. *Polskiej Akademii Nauk* 39, Lublin, Poland
- Sobczuk H, Plagge R, Walczak R, Roth CH (1992) Laboratory equipment and calculation procedure to rapidly determine hysteresis of some hydrophysical properties under non steady flow conditions. *J Plant Nutr Soil Sci* 155:157–163
- Soutsos MN, Bungey JH, Millard SG, Shaw MR, Patterson A (2001) Dielectric properties of concrete and their influence on radar testing. *NDT&E Int* 34:419–425
- Spanner DC (1951) The Peltier effect and its use in the measurement of suction pressure. *J Exptl Botany* 2:145–168
- Stalnaker JJ, Harris EC (2002) Structural design in wood, 2nd edn. Kluwer academic publishers (in RILEM TC215-AST)
- Strehle N (2009) Bericht Nr. 1220409 Überwachung und Dokumentation der erzielten Messwerte mit dem Feuchtemessgerät DNS Hydrotest G-812 - 2009
- Strømdahl K (1997) Moisture in construction materials—with focus on water binding in the over-hygroscopic range (in Danish). M.Sc. thesis, Department of Structural Engineering and Materials, Technical University of Denmark, Denmark
- Strømdahl K (2000) Water sorption in wood and plant fibres. Department of Structural Engineering and Materials. Technical University of Denmark, R78 (Ph.D. thesis)
- Tang L (2003) A collection of chloride and moisture profiles from the träslövsläge field site—from 0.5 up to 10 years investigations, Publication P-03:3. Chalmers University of Technology, Göteborg
- Tinga WR, Voss WAG, Blossy DF (1973) Generalized approach to multiphase dielectric mixture theory. *J Hydrol* 236:252–258
- Topp GC, Davis JL, Annan AP (1980) Electromagnetic determination of soil water content: measurements in coaxial transmission lines. *Water Resour Res* 16:574–582
- Topp GC, Davis JL, Annan AP (1982) Electromagnetic determination of soil water content using TDR: I. Applications to wetting fronts and steep gradients. *Soil Sci Soc Am J* 46(4):672–678

- Topp GC, Zegelin S, White I (2000) Impacts of the real and imaginary components of relative permittivity on time domain reflectometry measurements in soils. *Soil Sci Soc Am J* 64: 1244–1252
- Torrent RJ (1992) A two-chamber vacuum cell for measuring the coefficient of permeability to air of the concrete cover on site. *Mater Struct* 25:358–365
- Torrent R, Frenzer G (1995) A method for the rapid determination of the coefficient of permeability of the “covercrete”. In: international symposium non-destructive testing in civil engineering, NDT-CE 95, p 8
- Tran NL, Ambrosino R (1972) Mesure de la teneur en eau des sols et des matériaux par une méthode capacitive: III-Applications de la méthode capacitive de la mesure de la teneur en eau, *Bulletin de Liaison des Laboratoires Centrale des Ponts et Chaussées*, 60, pp 173–175
- Tremsin AS, Lehmann EH, McPhate JB, Vallerga JV, Siegmund O, White B, White P, Feller WB, de Beer FC, Kocklmann W (2015) Quantification of cement hydration through neutron radiography with scatter rejection. *IEEE Trans Nucl Sci* 62(3):1288–1294
- Tribius W (2003a) Prüfbericht Nr. 12/742-03 Vergleichende Bestimmung der Feuchtegehalte eines Zementestrich, MFPA Weimar
- Tribius W (2003b) Prüfbericht Nr. 12/741-03 Vergleichende Bestimmung der Feuchtegehalte eines Calciumsulfat-Fliessestrich, MFPA Weimar
- Trtik P, Munch B, Weiss WJ, Kaestner A, Jerjen I, Josic L, Lehmann E, Lura P (2011) Release of internal curing water from lightweight aggregates in cement paste investigated by neutron and X-ray tomography. *Nucl Instrum Methods Phys Res A* 651(1):244–249
- Tsai CM, Cho ZH (1976) Physics of contrast mechanism and averaging effect of linear attenuation coefficients in a computerized transversal axial tomography (CTAT) scanner. *Phys Med Biol* 21:544–559
- Válek J, Kruschwitz S, Wöstmann J, Kind T, Valach J, Köpp C, Lesák J (2010) Non-destructive investigation of wet building material: multimethodical approach. *J Perform Constr Facil*, 462–472. 10.1061/(ASCE)CF.1943-5509.0000056
- Van Tittelboom K, Snoeck D, Vontobel P, Wittmann FH, De Belie N (2013) Use of neutron radiography and tomography to visualize the autonomous crack sealing efficiency in cementitious materials. *Mater Struct* 46(1–2):105–121
- Vaziri M, Orädd G, Lindgren O, Pizzi A (2011) Magnetic resonance imaging of water distribution in welded woods. *J Adhes Sci Technol* 25(16):1997–2003
- Villain G, Lataste JF, Fares M, Balayssac JP, Sbartai ZM, Dérobert X (2016) Comparaison de profils de taux de saturation obtenus par plusieurs méthodes non destructives électriques et électromagnétiques, Congrès Diagnostique, Marrakech (Maroc), 24–25 Mar 2016, p 8
- Villmann B, Slowik V, Wittmann FH, Vontobel P, Hovind J (2014) Time-dependent moisture distribution in drying cement mortars—results of neutron radiography and inverse analysis of drying tests. *Int J Restor Build Monuments* 20(1):49–62
- Walley WR (1993) Considerations on the use of Time Domain Reflectometry (TDR) for measuring soil-water content. *J Soil Sci* 44(1):1–9
- Wang X (1997) Log classification by single X-ray scans using texture features from growth rings. Lecture notes in computer science. Springer, Berlin and Heidelberg. ISSN 0302-9743 pp 1611–3349
- Wang B, Faure P, Thiéry M, Baroghel-Bouny V (2013)  $^1\text{H}$  NMR relaxometry as an indicator of setting and water depletion during cement hydration. *Cem Concr Res* 45:1–14
- Wang W, Liu J, Agostini F, Davy CA, Skoczylas F, Corvez D (2014) Durability of an ultra high performance fiber reinforced concrete (UHPFRC) under progressive aging. *Cem Concr Res* 55(1):1–13, Jan 2014
- Weiland O (2016) Personal message
- Weiss J, Geiker MR, Hansen KK (2015) Using X-ray transmission/attenuation to quantify fluid absorption in cracked concrete. *Int J Mater Struct Integrity* 9(1/2/3)
- WESCOR, INC HR33T Dew Point Microvoltmeter. Instruction/service manual

- Weydert R, Gehlen C (1999) Electrolytic resistivity of cover concrete: relevance, measurement and interpretation. In: Lacasse MA, Vanier DJ (ed) Durability of building materials and components 8. Institute for Research in Construction, Ottawa ON, K1A 0R6, pp 409–419
- Wiberg P, Morén T (1999) Moisture flux determination in wood during drying above fibre saturation point using CT-scanning and digital image processing. *Holz als Roh- und Werkstoff* 57(2):137–144
- Wiebe HH (1971) Measurement of plant and soil water status. Bulletin 484. Utah State University
- Wilkes KE, Atchley JA, Childs PW (2004) Effect of drying protocols on measurement of sorption isotherms of gypsum building materials. In: Performance of exterior envelopes of whole buildings IX international conference, Clearwater, USA
- Williams TL (1988) Industrial and civil applications of thermography in applications of thermal imaging. IOP Publishing Ltd, Philadelphia
- Wolter B, Dobmann G (1995) Nuclear magnetic resonance as a tool for the characterisation of concrete in different stages of its development. In: International symposium on non-destructive testing in civil engineering' (NDT-CE) Proceedings, vol 1, Berlin, Germany, p 181
- Wolter B, Kohl F, Surkowa N, Dobmann G (2003) Practical applications of NMR in civil engineering. In: International symposium non-destructive testing in civil engineering 2003 (NDT-CE 2003). Available at: <http://www.ndt.net/article/ndtce03/papers/v062/v062.htm> Accessed on 20 Aug 2016
- Wu Z, Wong HS, Buenfeld NR (2015) Influence of drying-induced microcracking and related size effects on mass transport properties of concrete. *Cem Concr Res* 68, Feb 2015, ISSN 0008-8846
- Young JJ, Szomolanyi P, Bremner TW, Balcom BJ (2004) Magnetic resonance imaging of crack formation in hydrated cement paste materials. *Cem Con Res* 34:1459–1466
- Zhang P, Wittmann FH, Zhao T, Lehmann EH (2010) Neutron imaging of water penetration into cracked steel reinforced concrete. *Phys B-Condens Matter* 405(7):1866–1871
- Zhang P, Wittmann FH, Zhao TJ, Lehmann EH, Tian L, Vontobel P (2010) Observation and quantification of water penetration into Strain Hardening Cement-based Composites with multiple cracks by means of neutron radiography. *Nucl Instrum Methods Phys Res Sect A* 620 (2/3):414–420
- Zhang P, Wittmann FH, Zhao TJ, Lehmann EH, Vontobel P (2011) Neutron radiography, a powerful method to determine time-dependent moisture distributions in concrete. *Nucl Eng Des* 241(12):4758–4766
- Zintel M, Gehlen C (2012) Epoxy coatings on metallic substrates -Quantitative assessment of the water absorption by use of Single-sided NMR. Proceedings of EUROCORR 2012, The European Corrosion Congress, Istanbul, Turkey, 9–13 Sept 2012